https://doi.org/10.1070/RCR5017

Nanoglobular carbon and palladium – nanoglobular carbon catalysts for liquid-phase hydrogenation of organic compounds

Roman M. Mironenko,[a] Vladimir A. Likholobov,[b] Olga B. Belskaya [a]

[a] *Center of New Chemical Technologies BIC, ul. Neftezavodskaya 54, 644040 Omsk, Russian Federation*
[b] *Boreskov Institute of Catalysis, Siberian Branch, Russian Academy of Sciences, prosp. Akademika Lavrentieva 5, 630090 Novosibirsk, Russian Federation*

The results of studies related to the development of synthesis, determination of formation conditions and elucidation of the mechanism of palladium – carbon catalyst action are integrated and critically analyzed. The attention is focused on Pd/NGC compositions (NGC is nanoglobular carbon). Methods for NGC preparation with an emphasis on its most common form, carbon black, are considered. The following issues are addressed: mechanisms of formation of carbon nanoglobules and their aggregates, methods of varying the size of nanoglobules, functionalization of the NGC surface to make it suitable as a support for palladium nanoparticles, views on the formation mechanism of palladium clusters and nanoparticles on the carbon support surface and effect of the structure and surface chemistry of carbon nanoglobules on the state of palladium sites in Pd/NGC compositions. The published data on selective hydrogenation of organic compounds in the presence of Pd/NGC catalytic compositions are integrated and systematized. The catalytic properties of Pd/NGC are analyzed in comparison with the properties of palladium catalysts supported on other carbon materials (activated carbon, carbon nanotubes). The influence of preparation conditions of NGC-based palladium compositions on their catalytic properties in practically important hydrogenation reactions is discussed. Promising trends for further research on the development of molecular design methods, study of the genesis of Pd/NGC compositions and extension of their applications in hydrogenation processes are considered.
The bibliography includes 623 references.

Contents

1. Introduction 2
2. Methods for production of nanoglobular carbon. Methods for variation of the size of nanoglobules, the size and structure of their aggregates and the composition of functional cover of their surface 4
2.1. Mechanism of formation of nanoglobular carbon upon hydrocarbon pyrolysis in the gas phase 5
2.2. Methods for controlling the structure and properties of nanoglobular carbon as a support for the preparation of supported catalysts 10
2.3. Surface functionalization of nanoglobular carbon as a method to control its ligand properties 15
3. Formation of supported palladium–carbon catalysts 18
3.1. Methods for palladium deposition on the carbon support 18
3.2. Processes of interaction of chloride precursors of palladium with the carbon support and formation of palladium nanoparticles 19
3.2.1. State of the chloride precursor of palladium in aqueous solutions 19
3.2.2. Interactions at the water/carbon interface 20
3.2.3. Fixing of the chloride precursors of palladium on the carbon surface 22
3.2.4. Reduction of palladium chloride compounds attached to the carbon surface. State of the forming clusters and palladium nanoparticles 26
3.3. Role of the structural organization of nanoglobular carbon in the formation of active sites of Pd/NGC 28
4. Selective hydrogenation of organic compounds in the presence of Pd/NGC catalysts 31
4.1. Hydrogenation of alkenes (hydrogen addition to the C=C bonds) 32
4.2. Selective hydrogenation of alkynes (hydrogen addition to the C≡C bonds) 35
4.3. Hydrogenation of the benzene ring in aromatic compounds 39
4.4. Hydrogenation of aromatic aldehydes 42
4.4.1. Hydrogenation of benzaldehyde 45
4.4.2. Hydrogenation of cinnamaldehyde 45
4.4.3. Hydrogenation of furfural 46
4.5. Hydrogenolysis of C–O and C–Cl bonds in organic compounds 49
4.6. Hydrogenation of nitriles 53
4.7. Hydrogenation of nitro compounds 55
5. Conclusion 60
6. Note added in proof 61
7. List of acronyms and designations 61
8. References 62

Received 15 March 2021

© 2022 Uspekhi Khimii, ZIOC RAS, Russian Academy of Sciences and IOP Publishing Limited

1. Introduction

Supported palladium compositions based on porous carbon materials constitute an important group of heterogeneous catalysts.[1–3] They are mainly used in reactions accompanied by transfer of hydrogen atoms or molecules from or to the substrate, *i.e.*, in dehydrogenation, hydrogenation and conjugate hydrogenation–dehydrogenation reactions.[3–6] For example, hydrogenation of organic compounds with molecular hydrogen in the presence of palladium-on-carbon catalysts is a fairly popular reduction method not only in laboratory research, but also in small-scale organic synthesis of fragrances, pesticides, pharmaceuticals and dyes and in large-scale production of intermediates for the manufacture of plastics and synthetic fibres.[3–13] Despite the large range of hydrogenation catalysts based on much less expensive metals (Ni, Cu, Fe, Co, Ru), palladium-on-carbon catalysts are still in high demand. This is indicated, in particular, by the fact that Pd/C catalysts proved to be indispensable for ~75% of hydrogenation reactions (Fig. 1). The trend towards increasing number of publications devoted to the preparation and investigation of Pd/C catalysts (Fig. 2) demonstrates the ever increasing interest in this type of compositions, which is evidently due to expanding scope of their application in chemistry and to the related need to solve arising fundamental and applied problems.

Presumably, the main causes for the high popularity of Pd/C catalysts in both fundamental and applied research are the large diversity of carbon materials that can act as supports [3] and unique chemical properties of palladium metal and ionic species. These properties are, for example, the ease of formation of adducts with hydrogen and complexes with molecules containing carbon–carbon, carbon–nitrogen and carbon–oxygen multiple bonds; high lability of the coordination sphere optimal for the occurrence of ligand rearrangements (oxidative addition, reductive elimination, insertion) within the coordination sphere; abundant chemistry of cluster compounds and nanoparticles (NPs) bound to them, including polymetallic ones, which provides for high mobility of chemisorbed hydrogen.[14–17] The current state of the application of supported (including carbon-supported) palladium catalysts in various liquid-phase reactions is surveyed, for example, in a recent review by Van Vaerenbergh *et al.*[18]

The first experiments on the hydrogenation of organic compounds in the presence of palladium (as palladium black) were performed by Saytzeff[19] back in 1871, but palladium-on-carbon compositions started to be used as hydrogenation catalysts much later. In 1908, Orlow[20] used a coke-supported nickel–palladium catalyst to obtain ethylene from CO and H_2, while in 1914, Mannich and Thiele[21–23] proposed to deposit palladium on a carbon support to prepare a catalyst for hydrogenation of organic compounds. The authors used 2% Pd on animal charcoal as a catalyst for selective hydrogenation of 2-aminoacetophenone and its derivatives to the corresponding amino alcohols[22] and for the preparation of hydrogenated fats from vegetable oils.[23,24] The authors demonstrated better activity and selectivity of the compositions they used compared to bulk (not supported) palladium catalysts, which were used previously. The procedure they proposed for the preparation of the Pd/C catalyst,[22,23] which consisted in the impregnation of the carbon material with a $H_2[PdCl_4]$ solution followed by hydrogen treatment,

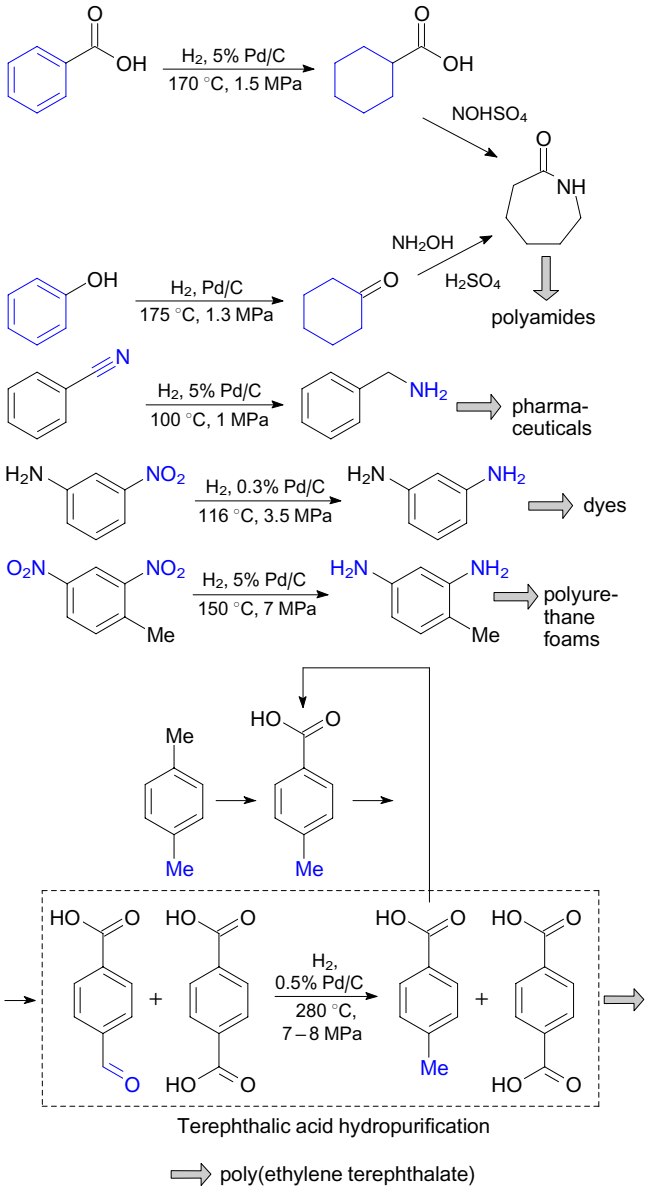


Figure 1. Examples of industrial processes of Pd/C-catalyzed hydrogenation of organic compounds.

R.M.Mironenko. Ph.D, Senior Researcher at CNCT BIC SB RAS.
E-mail: mironenko@ihcp.ru
Current research interests: Synthesis and physicochemical studies of supported metal catalysts, catalytic organic synthesis.
V.A.Likholobov. Doctor of Sciences, Professor, Chief Researcher at BIC SB RAS.
E-mail: likholobov47@mail.ru
Current research interests: catalytic organic synthesis, targeted synthesis of catalytically active sites, mechanisms of catalytic reactions, development and synthesis of nanostructured carbon materials, activation of small molecules, hydrogen energy production, chemical processes of hydrocarbon processing.
O.B.Belskaya. Ph.D, Leading Researcher at CNCT BIC SB RAS.
E-mail: obelska@ihcp.ru
Current research interests: chemistry of complex compounds of noble metals, synthesis and physicochemical studies of supported metal catalysts.

Translation: Z.P.Svitanko

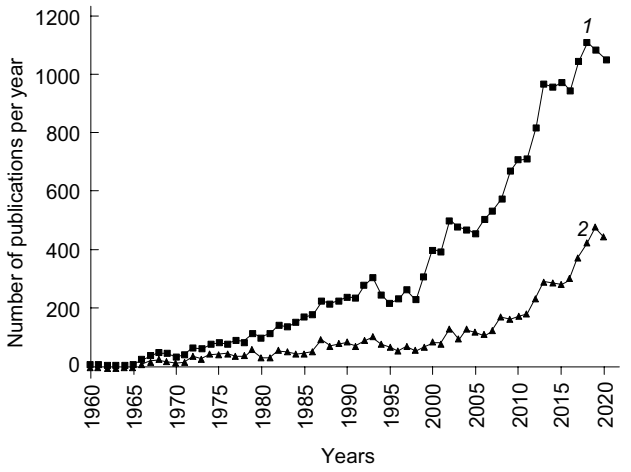


Figure 2. Increase in the number of publications dealing with the preparation, investigation and application of Pd/C catalysts (*1*); out of these, publications related to intellectual property (*2*). Analysis was performed by the authors using SciFinder® database (Chemical Abstracts Service).

became basic and has been used in various versions for many years not only in laboratory practice, but also on an industrial scale.[6, 8, 9, 25–33]

The Pd/C catalysts used in industrial hydrogenation processes are prepared by deposition of, most often, 0.3 to 5 wt.% palladium on special types of activated carbon (AC), which are obtained by carbonization of wood, fruit shells of some plants (for example, nuts), fossil coals, synthetic polymers, *etc*.[5–8, 26, 33] In addition, a frequently used support for palladium catalysts is Sibunit™, a nanostructured carbon–carbon composite material, which has a mesoporous structure (specified by its template synthesis[34]) with virtually no micropores and thus combines high specific surface area, extensive pore space and chemical inertness to strong acids, bases, halogens, *etc*.[35–37]

In recent years, studies dealing with the synthesis, structure and properties of mesoporous carbon materials received a new impetus due to vigorous progress in the design of materials for the energy conversion and storage. The most intensive studies along this line are related to the development of ordered mesoporous carbon (OMC) materials.[3, 38] The studies involve variation of materials used to form the template (matrix) such as carbon, silica, alumina, organic polymers and aerogels, *etc*. and development of methods for deposition on the template of carbon, the future OMC framework material (catalytic or non-catalytic decomposition of carbon compounds) and methods for the removal of the template from the obtained carbon–carbon or carbon–mineral composite to give OMC.

Currently, carbon nanomaterials, such as fullerenes, graphene, nanotubes (CNTs), nanofibres (CNFs), nano-onions, carbon nanohorns, nanocones, nanospheres and so on, are of particular interest as supports for palladium catalysts.[3, 12, 38–48] Note that the term carbon spheres was proposed by Inagaki[49] in a discussion of formation pathways of the nanotexture in spherical carbon particles. Later, Serp *et al*.[50] introduced the term carbon nanospheres to designate solid products of decomposition of hydrocarbons in the gas phase, with the size of spheres ranging from 50 nm to 1 μm, thus differentiating them from carbon nano-onions (particle size of 2–20 nm) and carbon nanobeads (particle size of > 1 μm). In our opinion, from the geometric standpoint, the term carbon nanospheres correctly applies only to fullerenes, which have carbon atoms on the sphere surface rather than in the bulk. Probably, that is why, the fact that carbon atoms are present in the bulk was reflected by phrases solid carbon nanospheres,[50] bulk carbon nanospheres and filled carbon nanospheres.[51] In essence, all these phrases describe globular carbon NPs, which can be simply designated by the common term carbon nanoglobules (CNGs), or nanoglobular carbon (NGC) introduced by Kryazhev *et al*.[52] Note that globular NPs, in the general case, are not necessarily perfectly spherical and completely filled inside, as they may be formed by structural units that cannot be closely packed. As an example, recall that the coils formed by some polymer molecules are also called globules, while due to specific features of coiling of these molecules (which often have bulky substituents), these globules can contain voids and channels that connect voids with the globule surface; therefore, they can be called hollow nanoglobules.

Among the above carbon nanomaterials nanoglobular carbon (below referred to as NGC) is one of most abundant. For example, globular carbon particles are present in aerosols that are formed upon incomplete combustion of organic compounds. However, if the combustion is uncontrolled (*e.g*., occurs as open flame in which the contact area of the burning region with air varies with time under the action of uncontrolled external factors), the physicochemical properties of the resulting carbon aerosol (which is called soot in this case) may change during the formation and, therefore, they are not characteristic, *i.e*., they do not have a stable and reproducible set of parameters. Note that in the fullerene synthesis by electric arc method, the primary product of evaporation of graphite is fullerene soot, which then serves as the raw material (carbon charge) to isolate individual fullerenes C_{60} and C_{70} by extraction and adsorption separation methods.[53, 54]

Special procedures for mechanical and chemical treatment of the carbon soot resulting from thermal and thermocatalytic pyrolysis of hydrocarbons are also used to isolate CNTs[55–57] and carbon nanospheres.[58–60] Unlike particles of single fullerenes, which are composed of identical molecules, the CNT and NGC particles are mixtures of structuring macromolecules (single nanotubes and nanoglobules, respectively) of various dimensions (length and diameter). Therefore, the properties of CNTs and NGC as nanomaterials depend (by analogy with synthetic polymers) on the width of the particle size distribution of these macromolecules; the narrower the distribution, the more pronounced a particular feature of CNTs or NGC. It is more expedient to attain narrowing of the size distribution not only during the mechanical and chemical treatment of the carbon soot, but also (primarily) during the synthesis (generation) by selecting the optimal composition of the carbon-containing feedstock, treatment conditions and (especially) by the design of appropriate process equipment. This concept is implemented, for example, in the synthesis of the carbon material known as carbon black,† which is formed upon thermal or thermo-oxidative pyrolysis of

† Since the carbon black particles are composed of carbon nanoglobules, in what follows, unless otherwise specified, NGC stands particularly for commercially produced carbon black, one of the most readily available and inexpensive nanomaterials (in 2018, its global output was ~13 million tons[64]).

hydrocarbon feed of strictly controlled composition under strictly controlled conditions. The degree of narrowing of the distribution of the properties of this material attained owing to the well-developed production processes makes it possible to manufacture more than 100 varieties (grades) of carbon black.[61–63]

We would like to emphasize that carbon black is not the same as soot (black carbon). A detailed analysis of structural and physicochemical differences between carbon black and black carbon can be found in the literature.[65,66] Watson and Valberg[66] give particular examples of chemical compositions of carbon black and soot to demonstrate differences between them. For example, a furnace black sample contained 98% carbon and ~1% organic compounds, which could be extracted with solvents, and ~1% ash, whereas these characteristics for soot resulting from diesel engine operation were 61, 30 and 1%, respectively (the rest was a group of unidentified compounds, possibly oxygen-, nitrogen- and sulfur-containing tars).

A very important requirement to NGCs meant for the use as supports for catalysts containing noble metals, especially in very low amounts (< 1 wt.%), is chemical purity. The preparation and physicochemical studies of highly pure NGC (with > 99% carbon), in particular, solid carbon nanospheres mentioned above, have been considerably intensified in recent years.[58] This is done by oxygen-free pyrolysis of single hydrocarbons, *i.e.*, heating of hydrocarbon vapour up to temperatures of decomposition of hydrocarbon molecules to carbon and hydrogen: chemical vapour deposition (CVD) method using either external[67,68] or internal source of heating (*e.g.*, plasma discharge through the gas phase[69]) and solution plasma process based on plasma discharge passed through liquid hydrocarbons.[70]

All known types of NGC are characterized by average size of globules, the degree of aggregation (so-called structure index, which depends on the average number of CNGs grown together into the aggregate and the aggregate shape; see Section 2.2), the specific surface area, electrical conductivity and chemical (acid-base and redox) properties of the functional groups on the surface of CNGs. The listed characteristics depend on the method of NGC preparation. For example, types of NGC obtained by thermal process (non-oxidative pyrolysis of natural gas) have an average diameter of nanoglobules in the 150–500 nm range, a specific surface area of not more than 15 $m^2 g^{-1}$ and a low structure index, whereas NGC types produced by the furnace method (oxidative pyrolysis of liquid hydrocarbon feedstock followed by treatment) consist of nanoglobules with a diameter of 10–80 nm, have a specific surface area of 100–1500 $m^2 g^{-1}$ and may have very high structure indices.[9,61] The chemical purity (carbon content) of commercial carbon blacks is relatively high and varies depending on the production method: > 97% for furnace grades and > 99% for thermal grades.[63] These values and NGC structural features in combination with the physicochemical characteristics of the surface (composition of the functional cover) allow nanoglobular carbon to be considered as a promising support for catalytic components. Apparently, the first studies in which the Pd/NGC catalysts were used for hydrogenation of organic compounds were published in the 1950s.[71–73] In practice, a catalyst consisting of Pd (0.77 wt.%) and some Pt and Fe supported on Shawinigan Black® NGC (see Section 4.7) was developed for industrial production of 2,4-diaminotoluene by hydrogenation of 2,4-dinitrotoluene in the liquid phase.[9]

In the vast majority of modern reviews devoted to the genesis, structure and applications of various carbon materials in catalysis, little attention is paid to NGC, while preference is given to other nanomaterials such as graphene, CNTs, fullerenes, *etc.*,[3,33,41,44] with NGC being mentioned mainly in relation to the development of electrocatalysts for fuel cells and photoactive compositions.[3,33] In addition, analysis of papers summarizing the results of studies of Pd/C catalysts [6,33,41,44] indicates that most publications consider mainly the structure (including modelling) and catalytic properties of palladium–carbon compositions, while much less attention is devoted to the details of formation of palladium active sites, role of the carbon support in this process (structure of the surface and especially the bulk of its primary NP macromolecules) and the effect of these factors on the catalytic properties. Relevant papers concerning NGC-supported palladium catalysts are very rare, although the trend towards increasing interest in the synthesis and studies of these systems has already appeared.[42,43,63,74,75]

This review is an attempt to fill these gaps by integration and critical analysis of available data on the synthesis, regularities of formation and elucidation of functioning mechanisms of palladium-on-carbon catalysts. The attention is focused on Pd/NGC compositions, especially regarding their use as catalysts of liquid-phase hydrogenation of organic compounds. The review addresses the following issues:

— general information about the preparation methods of NGC; carbon black as a representative of NGC, mechanism of formation and structure of nanoglobules; methods for varying the size of carbon black nanoglobules, sizes and structures of their aggregates, functionalization of carbon nanoglobules in order to endow them with properties necessary for successful use as a support for the dispersed metal particles;

— methods of palladium deposition on carbon supports; established views on the mechanism of formation of palladium clusters and NPs on the carbon support; effect of the structure and surface chemistry of CNGs on the state of palladium sites in Pd/NGC compositions; models of palladium sites;

— selective hydrogenation of organic compounds in the presence of Pd/NGC catalysts; effect of Pd/NGC preparation conditions on the state of supported palladium and its catalytic properties in practically important hydrogenation reactions; possibility of producing intermediate partial hydrogenation products upon variation of the structure and physicochemical characteristics of NGC; comparison with other Pd/C catalytic compositions.

2. Methods for production of nanoglobular carbon. Methods for variation of the size of nanoglobules, the size and structure of their aggregates and the composition of functional cover of their surface

The main approach to the production of carbon nanoglobules is based on thermal or thermo-oxidative decomposition (pyrolysis) of hydrocarbons. The key step of pyrolysis is conversion of hydrocarbon molecules to nanosized carbon spheres, which are formed in the bulk of a gas or in a gas flow as an aerosol. Depending on the nature of the initial hydrocarbons and the technique of pyrolysis (type of the reactor), six main types of the produced NGC (carbon black) are distinguished: channel, gas, thermal,

acetylene, lamp and furnace types of carbon black, the names of which reflect the production technique.

Historically, the first one was the lamp method based on combustion of vegetable oils in lamps under clay pots on the inner surface of which dispersed carbon particles were deposited (China, 3rd century BCE). Beginning from the 15th century, the lamp technique has been further developed in Europe (in Germany, France and the Netherlands) for industrial production of black pigments for paints from camphor resin or crude oil.[76–78]

In the channel technique developed in the late 19th century in the USA, carbon particles are deposited from the flame of burning natural gas onto a cooling surface that moves above or through the flame.[77–81] High variability of production conditions (for example, the height above the burner base at which carbon particles are sampled from the flame) and significantly simpler composition of the hydrocarbon feed (natural gas instead of crude oil or mineral oil) in the channel technique made it possible to produce a certain range of grades of dispersed carbon for various purposes (production of pigments, toners, gunpowders, rubber fillers, *etc.*).

The thermal technique patented in 1916[82] and deployed on an industrial scale in 1922 in the USA[78,81,83] is based on the pyrolysis of natural gas in the reaction zone preheated to 900–1400 °C in the absence of air. As a result, an aerosol of carbon particles is produced in the reaction zone and further directed to a separation system. A specific feature of the carbon produced in this way is that up to 25% of its particles are single globules the size of which may be as large as 500 nm. This type of dispersed carbon was primarily used in the tyre rubber industry, which was rapidly developing at that time.

The rapid growth of demand in rubber-based technical products for machine building stimulated intensive research aimed at the creation of large-scale, high-performance, flexible and cost-effective processes for the production of dispersed globular carbon, which resulted in the development of the furnace production technique in 1922–1945.[78,81] The conceptual difference of this technique from alternative methods is that pyrolysis of hydrocarbons takes place in a high-velocity flow of fuel (preferably natural gas) combustion gases at ~1700 °C. To this end, the hydrocarbons are fed into the gas flow, while aerosol carbon particles are subsequently isolated from the flow using cyclones and filters. Owing to the record-high specific productivity, broad variety of options for process control and automation, flexibility of production conditions and availability of hydrocarbon feed (natural gas and accompanying crude oil and coal refining products), this process of NGC production has rapidly become a leader in the global output of carbon black. According to the data of 2012, the NGC produced by the furnace technique from gaseous or liquid hydrocarbon feed, with the product range consisting of ~120 grades, accounted for >95% of its global production.[61] A more detailed discussion of these issues can be found in specialized monographs.[62,84] This Section is primarily focused on the formation regularities and structural features of NGC particles produced by any method described above (*i.e.*, pyrolysis of hydrocarbons that occurs in the gas phase under the action of internal or external heating sources) and also the ways to functionalize the particles and endow them with properties favourable for their use as supports in the catalytic Pd/NGC compositions (*i.e.*, the properties of a functional macroligand).

2.1. Mechanism of formation of nanoglobular carbon upon hydrocarbon pyrolysis in the gas phase

Before proceeding to the discussion of the formation mechanism of nanoglobular carbon, note once again that the production techniques mentioned above are based on both the processes in which carbon particles are produced upon combustion of hydrocarbons with air deficiency, *i.e.*, hydrocarbon molecules thermally decompose due to the heat released upon their combustion (the lamp and channel techniques) and the processes in which hydrocarbons do not burn in the limiting case, *i.e.*, they do not react with oxygen, but thermally decompose into carbon and hydrogen in designed hot zones in a batch (thermal technique) or continuous flow process (the furnace technique in which the hydrocarbons are fed into the zone of gases produced by complete combustion of a special fuel, primarily methane, under the conditions when gases do not contain residual oxygen.) Thus, in all the techniques considered above, the carbon particles are produced *via* thermal decomposition of gas hydrocarbons into carbon and hydrogen.‡

Study of the mechanism of formation of carbon particles upon combustion of hydrocarbons, which apparently was first formulated as a research problem by M.Faraday more than 150 years ago,[85] still remains one of the least resolved problems. The reason is the complex nature of the process comprising a multitude of stages, the non-equilibrium, non-isothermal and non-stationary nature of the process, the necessity to use high temperatures and ensuing difficulties related, for example, to the use of research equipment. Due to the experimental difficulty of investigating the combustion of hydrocarbons, the mechanism of the process still remains unclear despite numerous studies in this field. Therefore, the transformations of hydrocarbons in the flame still may be interpreted in different ways. Quantitative data on the production of dispersed carbon in the flame and the views on the mechanism of this process published before 1970 were integrated and discussed in a monograph by Tesner,[86] while later results were summarized in reviews[87–97] and in more recent publications.[98–100]

Without going into discussion of the degree of substantiation of each particular version of the dispersed carbon production mechanism, among those proposed during almost fifty years that have passed since the publication of Tesner's monograph,[86] we would like to note that all of them assume the key role of polycyclic aromatic hydrocarbons (PAHs) in this process and the necessary stage of formation of a CNG seed (growth nucleus; GN), as a nanosized (1–2 nm) cluster of carbon atoms bound together (for details, see below). The composition, structure and concentration relationship of PAHs and GN and the profiles of their variation with time appreciably depend on the nature of hydrocarbons (the ratio of carbon and hydrogen) and characteristics of the reaction space (reactor) in which the carbon particles are produced. The most critical parameters are the process temperature and time.[101,102] Thus, it should not be expected that the detailed mechanism (sequence of steps) of the formation of carbon particles in a diffuse flame with a pyrolysis zone temperature of ~1200 °C (the lamp technique) will be identical to that for turbulent combustion of hydrocarbons in a high-velocity gas flow with a flame temperature of ~1700–1800 °C (the

‡ The total mass balance equations of these production processes should include oxygen (as a consumable reactant) and CO, CO_2 and H_2O, apart from C and H_2 as the products.

furnace technique); this similarity is even less probable for the detonation production of NGC from acetylene, which occurs at a higher temperature and over a shorter time.

Beginning the 1990s, the fullerene model of the CNG formation, which assumes that fullerene is the CNG growth nucleus, has gained popularity.[103–109] This model is based on experimental observation of the production of various carbon clusters in the gas phase at high temperatures[110,111] and the detection of fullerenes C_{60} and C_{70} (Refs 112, 113) and even larger fullerenes, up to C_{116}, in benzene extracts of carbon black.[114] It is of interest that, according to Mansurov,[92] the $C_{70}:C_{60}$ ratio in the aerosol product formed upon benzene combustion in oxygen is 0.26–8.8, while in solid products of graphite evaporation in an electric arc it is only 0.02–0.18, which may point to another mechanism of fullerene production in the hydrocarbon combustion flame. The same study[92] reports a detailed analysis of the fullerene production and transformation in the flames.

Owing to the enhancement of computational capacity, recent years witnessed a significant growth of activity in the use of molecular dynamics methods to calculate the formation of carbon clusters containing several thousand atoms; these calculations made it possible to assess the feasibility of pathways to particular PAHs and formation of GNs from these PAHs.[115–119] For example, Pineau *et al.*[115] modelled the formation of carbon clusters starting from single carbon atoms at a temperature of 2000 K (Fig. 3). The simulation has shown that carbon atoms are bound into clusters of two types: low-atomic closed chains (apparently, polyynes) and polyatomic (fullerene-like) spheroids; the latter can attach chain clusters (Fig. 3 *a*). An increase in the number of atoms in the box results in a significant increase in the relative content of spheroidal clusters aggregated into secondary clusters (Fig. 3 *b*).

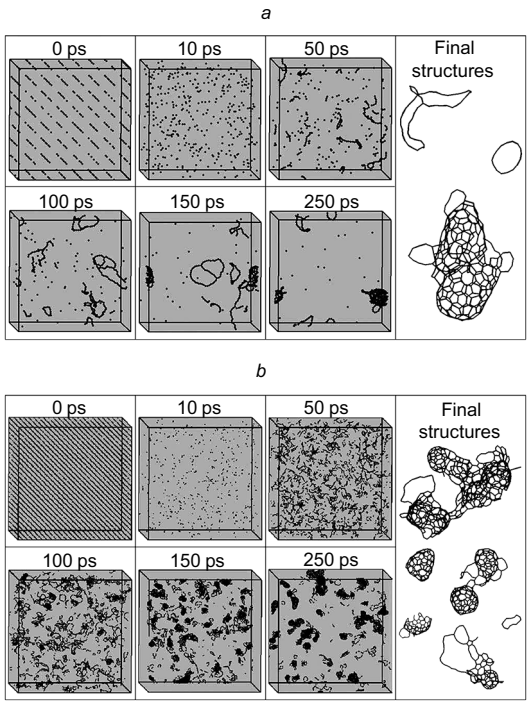


Figure 3. Results of simulation of carbon cluster formation from single atoms for boxes containing 400 (*a*) and 10800 (*b*) carbon atoms. The temperature was 2000 K in both cases. The total simulation time was 2 ns.[115] Published with permission from AIP Publishing.

It is of interest that no planar clusters (graphenes) are produced in any of the cases. This is in line with the data[120] indicating that at high temperatures, the graphene sheet,

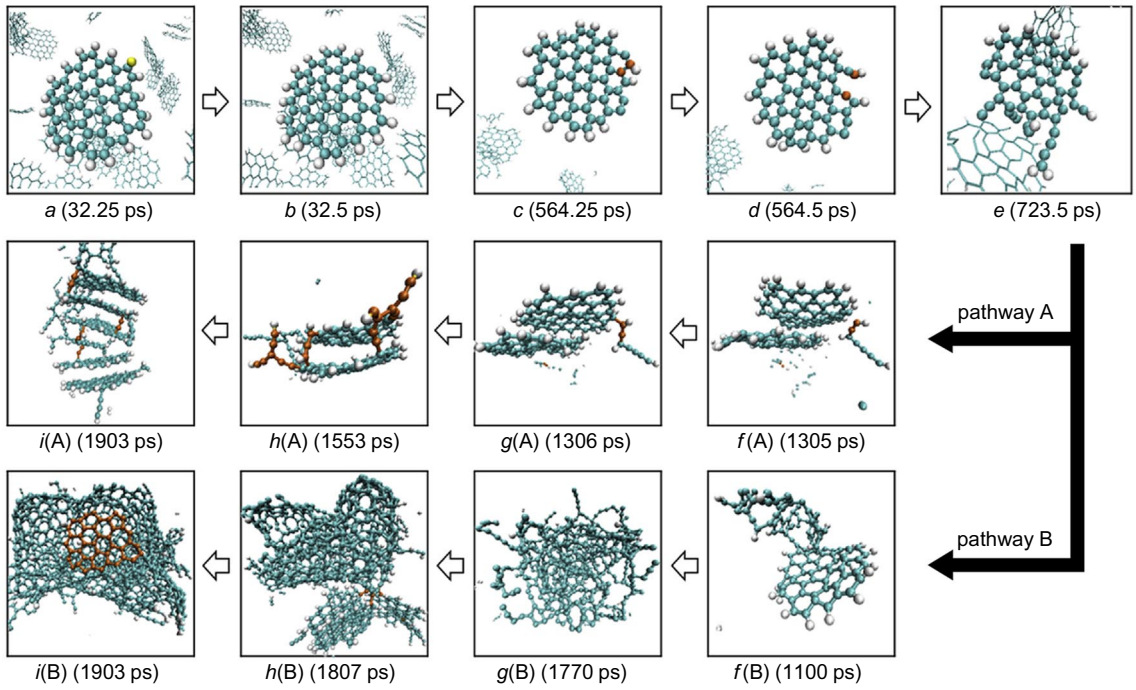


Figure 4. Snapshots of the key stages of fragmentation of circumcoronene along paths A and B at 2500 K and emergence of corresponding carbon clusters (see the text). Turquoise and white spheres represent carbon and hydrogen atoms, respectively; the carbon and hydrogen atoms important for the transformations are shown in brown and yellow.[116] Published with permission from Elsevier.

which contains coordinatively unsaturated carbon atoms (graphene, unlike PAHs, lacks peripheral hydrogen atoms), is crumpled and corrugated tending to a coil, due to the formation of defects.

Mao *et al.*[116] modelled the formation of clusters at 2500 K starting from a large PAH molecule such as circumcoronene $C_{54}H_{18}$ (Fig. 4 *a*). The modelling has shown (Fig. 4) that transformation of this molecule begins with dehydrogenation *via* thermal dissociation of a C–H bond to give the relatively stable (due to the resonance with the aromatic system) $C_{54}H_{17}^{\bullet}$ radical (Fig. 4 *b*), and this is followed by partial destruction of the molecule periphery to give flat-curved (bowl-shaped) structures that contain C_5-C_7 rings and C_2-C_6 alkyne groups (Fig. 4 *e*). In the subsequent transformations, the latter can attach the planar molecules of starting circumcoronene and the bowl-shaped fragments of its partially broken molecules to form packages (see Fig. 4, path A).

Another path of transformations (see Fig. 4, path B) is related to direct reactions of bowl-shaped fragments with each other and the $C_{54}H_{17}^{\bullet}$ radicals (formed in early steps) with the formation of a clot with fullerene-like parts of the surface. Actually the package [see Fig. 4 *i*(A)] and the clot [see Fig. 4 *i*(B)] can be regarded as GNs of different density, with their further linking giving growth to CNGs. It is important to emphasize that, due to the presence of a dipole moment (and, hence, dipole–dipole interaction), the bowl-shaped molecular structures are more prone to the formation of a package than the planar structures (containing only C_6 rings and no dipole moment); this self-assembly results in the formation of ball-shaped particles.[121]

The presented version of the CNG formation mechanism, which was published in 2018,[122, 123] is currently believed to be the most realistic, since it provides an explanation to most of the experimental observations and is supported by the results of the most recent studies. For example, atomic force microscopy (AFM) was used[124] to study for the first time the products of ethylene combustion in laminar flame, which were sampled at various heights above the burner and purified from soot particles by sublimation. The AFM study showed that the sublimation products primarily consisted of PAH molecules containing several tens of carbon atoms (Fig. 5).

Some similarity should be noted between the $C_{52}H_{26}$ molecule (which is a $C_{29}H_{14}+C_{23}H_{12}$ dimer two parts of which have a bowl shape; see Fig. 5 *a*) and the dimer simulated by Mao *et al.*[116] [see Fig. 4 *f*(B)]. Some aspects of the mechanism of CNG formation upon combustion of hydrocarbons, which was called HACA (hydrogen-abstraction carbon-addition) were recently explored by Davis *et al.*[125] and Baldelli *et al.*[126]

The views on the formation mechanism and structures of nanoglobule GN are primarily based on studies of hydrocarbon combustion in the diffusion or laminar flame with a pyrolysis zone temperature of ~1200–1500 °C (*i.e.*, under conditions corresponding to the lamp or channel technique of NGC production). In the higher temperature techniques of NGC production (for example, furnace technique in the turbulent flame with a pyrolysis zone temperature of ~1500–1800 °C), chain HACA mechanism is facilitated (due to acceleration of the endothermic steps of formation of aromatic radicals). However, the GN will tend to acquire a spherical rather than the elongated stacked

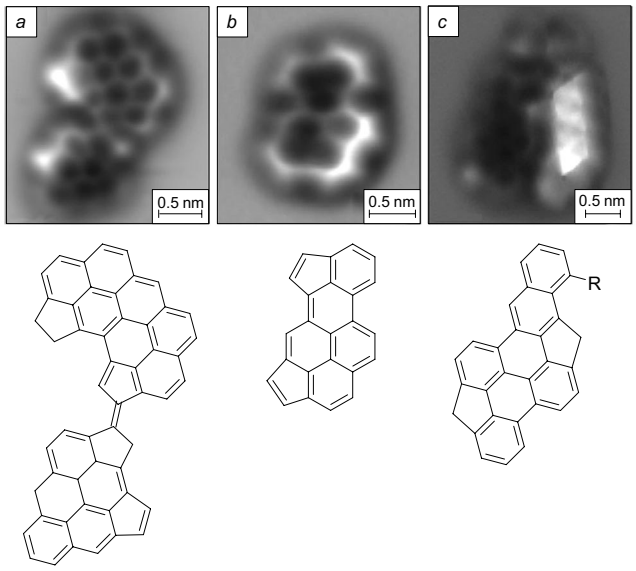


Figure 5. AFM images and chemical structures of molecules $C_{52}H_{26}$ (*a*), $C_{24}H_{12}$ (*b*) and $C_{30}H_{15}R$, where $R = C_xH_{2x+1}$ (*c*) isolated by sublimation from solid products of ethylene combustion in a laminar flame.[124] Published with permission from Elsevier.

geometry formed by means of *rim*-binding,§ due to the large contribution of PAH *syn*-binding¶ (Fig. 6 *a*). According to Ozawa and Ōsawa,[94] this will lead to spiroids and, subsequently, to fullerenes. This approach is considered to be fairly productive for the synthesis of fullerenes.[128, 129] Di- and oligomerization reactions *via rim*- and *syn*-binding occur more easily for PAHs with broken aromaticity (if aromaticity is defined by the $4n+2$ Hückel rule), which include not only hydrocarbons with destroyed peripheral C_6 rings, but also some starting compounds such as pyrene ($C_{16}H_{10}$) and coronene ($C_{24}H_{12}$). In the latter hydrocarbon, the central part of the molecule is aromatic, whereas the reactivity of six peripheral C=C bonds is rather similar to that of olefins.[130]

The mechanism of aggregation of spherical NGC particles during the pyrolysis of hydrocarbons consists of the following steps:

— PAH formation from initial hydrocarbons *via* dehydrogenation, pyrolysis, cracking and aromatization reactions, in which a significant role is played by intermediately formed acetylene;

— GN formation from PAHs by chain oligomerization *via* the formation of C_5 and/or C_6 rings;

— GN growth due to coalescence, coagulation and grafting of various hydrocarbon fragments to the GN surface followed by dehydrogenation, increase in the C : H atomic ratio and CNG formation;

— CNG aggregation and carbonization of aggregates into particles that form the NGC texture.

This mechanism, depicted in Fig. 6 *a*, is reflected in the electron microscopic images of NGC particles (Fig. 6 *b*). It can be seen that the CNG structure contains a disordered core surrounded by packages of graphene layers (graphite-

§ Formation of the intermolecular C–C bond across the radical centre in a peripheral C_5 ring of the PAH molecule.[127]

¶ Zipping mechanism means step-by-step formation of several intermolecular C–C bonds beginning from the radical centre in a peripheral C_6 ring.

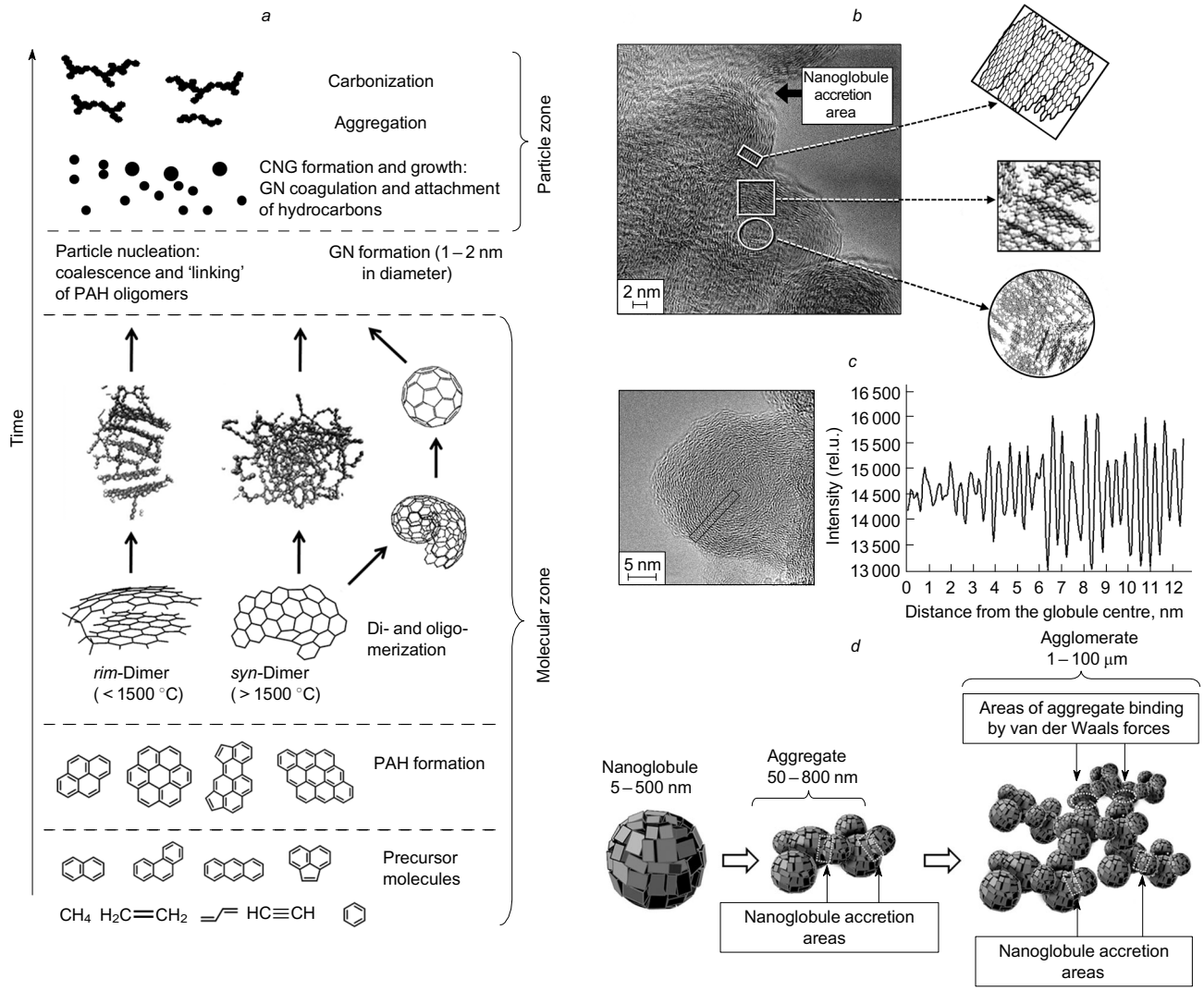


Figure 6. Key stages (mechanism) of the formation of NGC particles (according to Ref. 131 with allowance for the discussions reported in other papers [62, 92, 94, 116, 122 – 126]), separated into low- and high-temperature regions with a conventional boundary at 1500 °C (*a*); structure of a nanoglobule of P277 NGC according to high-resolution TEM data (JEM-2100, JEOL, instrument) and models of the carbon structures of enclosed areas (using the data of Refs 132, 133), which correspond to some stages of CNG formation (*b*); TEM image and radial profile of the layered structure of CNG, demonstrating the continuous increase in the structural ordering of carbon layers from the centre to the periphery (results obtained on a JEM-2100, JEOL, instrument; see also Ref. 134) (*c*); model of the structural organization of a CNG in NGC particles (*d*). Figures *a* and *b* are published with permission from Elsevier; the micrographs in Fig. *b* and *c*, made by Dr. M.V.Trenikhin, researcher at the Center of New Chemical Technologies BIC, were taken from authors archive for Ref. 134.

like crystallites; GLCs), and the degree of ordering of layer packing in the packages increases from the core to the periphery (Fig. 6 *c*).

The chart in Fig. 6 *a* reflects the above-discussed data on the possible effect of temperature on the GN structure and the role played by fullerenes, which are detected in NGC synthesis, in the GN formation. Thus, it may be hypothesized that if NGC is formed at temperatures below 1500 °C, the GN structure is primarily formed by *rim*-binding of PAH molecules and is a package, while at temperatures above 1500 °C, *syn*-binding mainly occurs, and the GN structure is a clot. In the latter case, in the initial stage of GN formation, its precursor, PAH dimer or trimer, can be transformed into fullerene *via* intramolecular dehydrogenation and rearrangement reactions, analogous to *rim*- and *syn*-binding. Subsequently, this fullerene can disappear by being involved in GN enlargement and CNG growth as a raw material,[135] together with other PAH clusters.

A detailed experimental study of CNG nucleation was recently performed by Vitiello *et al.*[136] They used EPR and Raman spectroscopy to examine particles of ethylene combustion products (temperature of ~1450 °C) sampled at various heights of this flame. Considering the gas mixture feed rate, this enabled determination of the time during which these products were formed. A special aerosol analyzer was used to determine particle size and size distribution. The first observable 2 – 3 nm particles of combustion products were detected after ~16 ms. EPR and Raman spectral data suggested that these particles were ensembles of stacked aromatic radicals with a ~1.1 – 1.2 nm lateral dimension. In our opinion, this description of the first detected particles and their size are quite applicable, for example, to the structures shown in Fig. 6 *a* as linked PAH packages (*rim*-oligomers) containing, on average, ~5 layers of PAH molecules in the package, with the flat part containing, on average, ~10 fused benzene rings. In

accordance with this model, the particles observed by Vitiello *et al.*[136] with sizes of 2–3 nm contain, on average, ~2000 carbon atoms.

The GN formation time and size can be quantitatively estimated by studying decomposition of hydrocarbons in the front of a reflected shock wave generated in a shock tube (attained temperatures of 2100–3700 K at times of 10^{-4}–10^{-2} s).[137–143] For example, Shaitanov and Surovikin[137] found that the onset of CNG formation, *i.e.*, the GN formation accompanied by the transition of the system from the molecular zone to the particle zone in Fig. 6 *a* (which is detected by the emergence of a continuous emission spectrum with a maximum at 750 nm typical for black body) is preceded by an induction period the duration of which depends on the process temperature and hydrocarbon type. The larger the number of carbon atoms in the aromatic hydrocarbon molecule, the shorter the induction period. For example, the induction period for the naphthalene molecule is 12 μs at 2560 K,[137] with the estimated GN diameter being 2 nm.

High-precision experimental studies and simulation of the processes related to the particle zone (see Fig. 6 *a*) are yet not numerous compared to those for the moleculear zone; however, their number has significantly increased lately. Analysis of the data presented in monograph[62] and in earlier summarizing publications[84, 94, 95, 144, 145] demonstrated that GN generation is the slowest step, since for this process to occur during PAH oligomer formation, cleavage of C–H bonds with energies of ~450 kJ mol^{-1} is required.[146] Meanwhile, increasing the GN surface *via* grafting of PAH oligomers and acetylene does not require C–H or C–C bond cleavage, while the conformational changes of PAH oligomer molecules needed for this grafting have activation energies an order of magnitude lower than the C–H bond energy. By varying the starting hydrocarbon type and initial concentration in the gas phase, the process temperature and the temperature profile along the length (height) of the reaction zone, it is possible to affect not only the GN formation rate and size, but also the ratio of volume concentrations of GN and PAH oligomers as a starting parameter before the onset of the growth stage. For example, if the number of the produced GNs exceeds the number of remaining PAH oligomer molecules, primary nanoglobules will mainly grow *via* coalescence of several GNs to give one or more GN of larger size (Fig. 7 *a*, coalescence) or a GN cluster (Fig. 7 *b*,*c*, coagulation). This process shifts the (GN + GN cluster): PAH oligomer concentration ratio in favour of oligomers, which serve to complete the increase in the surface area of GNs and GN clusters and, as a result, the formation of primary CNGs. It is noteworthy that the differences in the bulk structure of the primary CNGs grown with participation of either GN clusters or single GNs are clearly identified using high-resolution transmission electron microscopy (Fig. 7).[147, 148]

An important feature of GN particles involved in the coalescence process should be plasticity (liquid-like state); the critical parameters for the appearance of this state are the GN size (the smaller the size and larger the surface curvature, the lower the temperature at which plasticity is attained), the molecular mass of the PAHs that constitute the GN and the temperature of the GN as a particle. If the growth nucleus features some plasticity (*i.e.*, the mobility of separate parts of PAH oligomer molecules forming the GN relative to one another), it will have a spherical shape irrespective of the structure (package or clot; see Fig. 6 *a*) of its precursor (although the packing densities of such spheroids will be different). Recently, GN formation steps and structural features have received considerable attention in both experimental and theoretical studies that use various model reactions and computational models.[149–155]

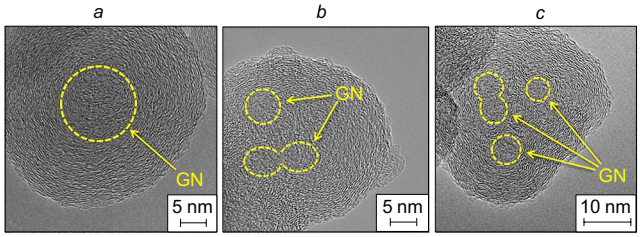


Figure 7. TEM images of the central part (interiors) of NGC particles formed from various hydrocarbons under various conditions: furnace carbon black (the grade is not specified) (*a*);[147] diesel-engine soot (*b*);[148] P267-E carbon black (the image was obtained on a JEM-2100, JEOL, instrument) (*c*). The dashed circles enclose the structures in the carbon nanoglobule that were presumably formed upon primary GN coalescence (*a*) or coagulation (*b*, *c*). Figure *a* is published with permission from MDPI, Figure *b* is published with permission from the American Chemical Society; Figure *c*, made by Dr. M.V.Trenikhin, researcher at the Center of New Chemical Technologies BIC, were taken from authors archive for Ref. 134.

In contrast to coalescence, coagulation results not in the complete merging of colliding particles into a single particle but to the formation (in the order of decreasing degree of mutual penetration) of clusters, bunches or aggregates. The formation of aggregates is most typical of the CNGs that lost their plasticity. An important role in aggregation starts to be played by nanoparticle electric charging, which occurs upon thermoelectron emission, friction and collisions of particles with one another or with gas phase ions.[156] General issues of coagulation (aggregation) of aerosol particles in different types of flow (laminar and turbulent) and the role in this process of the relationship between the electric (Coulomb) and kinetic energies of colliding particles are considered in detail in specialized monographs and reviews.[157–159]

Since, in addition to the size of primary nanoglobules, the extent of their aggregation and the shape of the aggregates are among the most important characteristics that dictate the physicochemical (including ligand) properties of NGC, understanding of regularities in the formation of these aggregates is important. Primary attention should be concentrated on the aggregation of nanoglobules (see Fig. 6 *b*,*d*), as the layered structure of an aggregate may indicate that it has formed as a result of deposition of pyrolytic carbon at the sites of contact between the nanoglobules where the surface has a large negative curvature and apparently acts as a template. The issues related to the pyrolysis of hydrocarbons on carbon matrices are explored in more detail in a monograph.[160] In the case of furnace process, it is also important to consider the reaction of the produced carbon particles with oxygen-containing products of thermo-oxidative pyrolysis, *i.e.*, CO_2, H_2O and CO, and the post-reactor contact of the particles with air in the process units where they are isolated, which result in the modification (functionalization) of the CNG surface, in particular, in the formation of oxygen-containing groups on the surface. These issues are considered in more detail below.

2.2. Methods for controlling the structure and properties of nanoglobular carbon as a support for the preparation of supported catalysts

The properties of NGC as a catalyst support are determined by physicochemical characteristics of its surface, which depend primarily on its functional composition, structural features, the electronic state of surface and sub-surface layers of its particles and, to some extent, by the bulk structure of particles (most frequently, the presence of defects). One of characteristics of the particle structure of carbon materials is the degree of three-dimensional ordering (g) of carbon atoms in a carbon crystallite, which is found from powder X-ray diffraction (XRD) data using the formula

$$g = \frac{d_{\text{disord}} - d_{002}}{d_{\text{disord}} - d_{\text{graph}}} \quad (1)$$

where d_{002}, d_{disord} and d_{graph} are the distances between graphene layers in the carbon material being considered, in the disordered carbon structure and in the graphite structure, respectively.[161, 162] The parameter g characterizes the three-dimensional structure of carbon material particles (being an integral characteristic of the degree of perfection of packing of graphene layers in the crystallite, which is found using TEM data; see Fig. 8 *a*). Therefore, the knowledge of this parameter is needed, for example, for understanding of the properties of carbon materials in reductive adsorption processes, *i.e.*, processes that occur with participation of weakly bound (not involved in the formation of covalent C–C bonds) electrons of graphite-like crystallites (GLCs) (see Section 3.2.3 below). The average size of the ordered part of crystallites (coherent scattering region, CSR) can be determined based on XRD data by calculating the length (L_a), the thickness (L_c) and interplanar distance

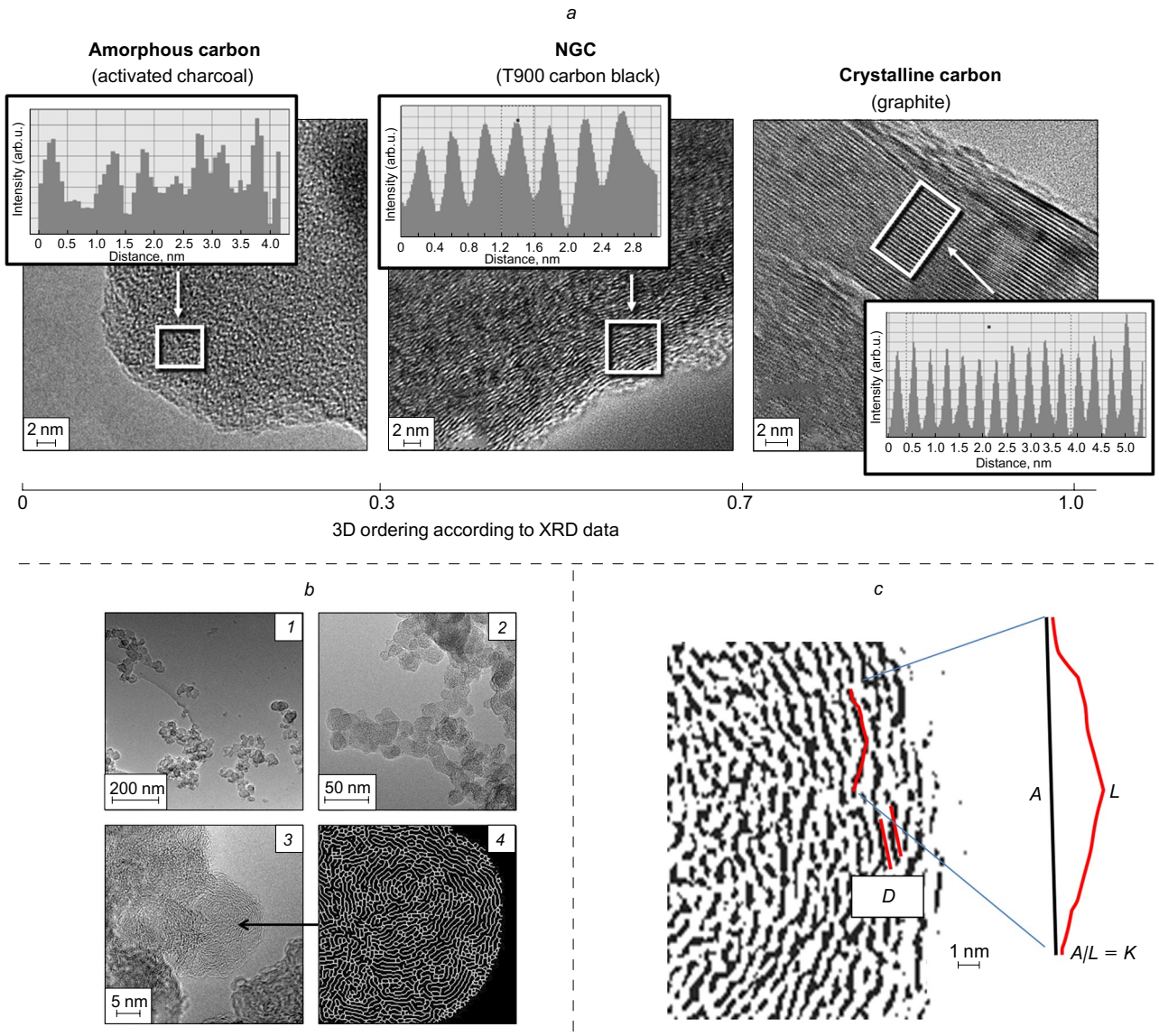


Figure 8. Position of the T900 thermal nanoglobular carbon in the concept of structural organization of carbon materials (*a*); TEM image of furnace NGC particles (P236 grade) under various magnifications (*1*–*3*) and image of a section of CNG (*4*) obtained by digital processing of the TEM image (*b*); methods for determination of the layer length (L) and curvature (K) and the distance between layers (D) (*c*).[163] The TEM images were obtained using a JEM-2100 (JEOL) electron microscope and processed using the DigitalMicrograph™ software (Gatan) (see also Refs 134, 164). Figures *a* and *b*, made by Dr. M.V.Trenikhin, researcher at the Center of New Chemical Technologies BIC, were taken from authors archive for Ref. 163.

(d_{002}) in a graphite-like package averaged over the entire volume of the carbon particle.

The surface-exposed graphene crystallites, in addition to being carriers of weakly bound electrons, would also determine, to a large extent, the ligand properties (coordination chemistry) of the CNG surface. The formation of these properties is closely related to the real nanostructure of the carbon particle bulk, which consists of carbon layers of various length and with various curvatures located at various distances from each other (Fig. 8 *b*, panel *4*). These characteristics can be determined by examining NGC by high-resolution TEM methods including special programs for digital processing of images, for example, DigitalMicrograph™ distributed by Gatan (Fig. 8 *c*).[126, 134, 163–165]

One of the ways to vary ligand properties of NGC is to change the nanoglobule size (diameter): if the diameter diminishes, the surface curvature increases and, hence, the contribution of shorter and more curved carbon layers to the microstructure increases. This change in the NGC texture can be accomplished during its synthesis; for example, in the furnace method, it can be done by varying the temperature and time of synthesis, with the gas flow velocity in the reactor being controlled (Table 1).[62] An increase in the synthesis temperature not only decreases the size of primary nanoglobules but, which is of utmost importance, narrows the particle size distribution, *i.e.*, the CNG uniformity is enhanced (Fig. 9).[95]

The CNG size can be varied during the synthesis also by changing the pressure of the gas phase in which carbon aerosol is formed. Special equipment is needed for such an experiment that enables, for example, measurement of colour parameters and temperature and sampling of carbon particles from the flame that burns in a closed space at an excess pressure.[166] Such complicated experiments have shown that if pressure increases from 0.5 to 2.0 MPa, the average diameter of the CNGs sampled at the flame centre increases from 33 to 45 nm. Upon the pressure increase, the flame temperature at the sampling point also increases (on average, from 1600 to 1900 K). A recent publication[167] reports the effect of pressure on the parameter L_a, which increases from 1.17 to 1.21 nm as pressure increases from 0.2 to 0.8 MPa. The authors explained this phenomenon by the earlier emergence of GNs at higher pressure.

Table 1. Effect of the parameters of furnace synthesis of NGC on the size of primary nanoglobules (anthracene fraction as the feed).[62]

Temperature, °C	Gas flow velocity in the reactor, m s^{-1}	Synthesis time, s	CNG diameter, nm
1800	400–500	0.008	27
1650	300–500	0.010	32
1550	180–300	0.031	46
1450	30–50	1.0	93
1400	30–40	1.5	109
1350	10–20	2–5	124

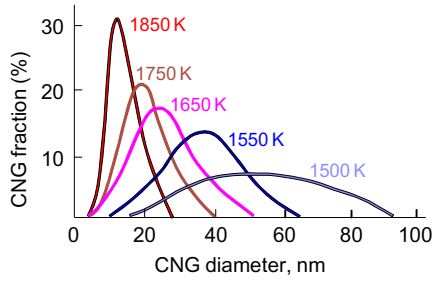


Figure 9. Size distribution of primary nanoglobules for the NGC samples obtained at various temperatures.[95]

The NGC nanostructure parameters can also be controlled by varying the type (composition) of the starting hydrocarbons. For example, Botero *et al.*[168] have found that the average diameter of NGC nanoglobules sampled from the top of the flame generated by combustion of heptane or toluene is larger in the case of toluene (18 and 38 nm, respectively). Also, in the case of toluene, the carbon layers that compose the nanoglobule have a greater length (0.91 and 0.99 nm, respectively), smaller curvature and a smaller distance between layers (0.468 and 0.449 nm, respectively). Verma *et al.*,[169] who studied soot production under high-temperature shock compression conditions, found that if the amount of organic oxygen-containing additives in the base hydrocarbon fuel is increased up to a certain concentration (from 0 to 12 wt.% oxygen), CNG diameter decreases (from 20 to 16 nm), the curvature of layers increases and the distance between layers also increases (from 0.38 to 0.43 nm). Although the data reported in the cited studies enable determination of only general trends in the variation of CNG bulk nanostructure following variation of the CNG formation conditions, the knowledge of these trends may prove to be very useful for understanding how changes in nanostructure affect the ligand properties of CNG surface.

It was noted above (see Fig. 6) that CNG coagulation and chemical aggregation give, in most cases, secondary structures (aggregates), while the latter are converted to agglomerates (that usually exist as powders) as a result of weak interactions between particles (for example, electrostatic interactions between a charged site of the surface of one particle and the charge induced on a surface site of another particle).[157] If an NGC powder is mixed with other substances (*e.g.*, solvents), agglomerates can be disintegrated to aggregates. This means that when NGC is used as a catalyst support for suspension processes, it should be borne in mind that suspension particles, being CNG aggregates, can have internal porosity and, to compare properties of catalysts supported on different NGC grades, one should take into account not only the size distribution of primary nanoglobules but also the size and shape distributions of their aggregates (an example of using electron microscopy for this purpose was described by Grulke *et al.*[170]).

Thus, apart from the size and bulk nanostructure parameters of primary CNGs, the degree of their aggregation and the shape of aggregates are among important physicochemical characteristics of NGC particles [they are included in the structure index represented by so-called specific oil number (M_a) equal to the ratio of the volume of liquid dibutyl phthalate (DBP) absorbed by an NGC sample to the sample mass (cm^3 g^{-1}) or surface area (cm^3 m^{-2})]. By now, several empirical rules have been derived to control this value in the production of carbon black,[62] and understanding of basic regularities of CNG aggregation is in progress.

The size and structure of CNG aggregates as well as the size of primary nanoglobules (see Table 1) can also be varied during NGC synthesis. The most important parameter that affects aggregation is the relationship between the electric (Coulomb) and kinetic energies of interaction between colliding particles, called coagulation structuring parameter (ψ), which takes into account concentration, average diameter (average mass) and average charge of

particles before coagulation. As ψ increases, the structure index of NGC particles increases (Fig. 10 *a*). This issue is analyzed in more detail in a monograph;[62] here, we would only like to note that the particle concentration and average diameter before coagulation can be affected not only by changing the reactor temperature but also by varying the initial concentration of the hydrocarbon feed in the reactor (C_0) and by changing the number of aromatic rings in the average molecule of the feed (N_a). An increase in C_0 and N_a results in increasing structure index of NGC particles.

The average charge of particles can be changed both by varying the regime of their motion in the flow (charging by friction), *i.e.*, by modifying the reactor design, and by feeding to the reactor, along with the starting hydrocarbon, other chemical compounds (additives) that can thermally dissociate in flame under the conditions of oxidative pyrolysis to give charged particles. This behaviour is inherent, for example, in alkali metal compounds MX (M = Li, Na, K, Rb, Cs; X = OH, Cl). When they are added to the CNG generation zone, CNGs capture M^+ ions and, as a result, the nanoglobule coagulation rate diminishes (due to the appearance of Coulomb repulsion) and, hence, the structure index of NGC particles diminishes as well. This effect is enhanced with increasing amount of added MX, and, in the case of equal MX amounts, in the order Li < Na < K < Rb < Cs, *i.e.*, it is inversely correlated with the ionization energy of the corresponding alkali metal atom (Fig. 10 *c*).[62]

The effect of addition of alkali metal compounds described above can be explained by considering data on the structure and properties of K^+ adducts with bowl-shaped dipole corannulene molecules (Fig. 10 *d*).[155] Since, as was noted above, the bowl-shaped fragments of PAH oligomer molecules play a decisive role in the formation of GNs, the their complexation with K^+ hampers (due to electrostatic repulsion) the aggregation of both the GNs and the nanoglobules they form.

Consideration of the ligand properties of the surface of native CNGs (*i.e.*, those obtained in the synthesis without additional treatment) may be based on the assumption that these properties are determined by the nature of the structural groups (elements) exposed on the CNG surface, that is, GLC basal and edge planes protruding above the surface, fragments of inclusions of intercrystallite amorphous carbon and various oxygen-containing groups that are formed in the final stages of isolation of NGC aerosol particles due to contact with air. All these groups can be reliably identified using modern methods of electron microscopy, X-ray photoelectron spectroscopy (XPS) and IR and NMR spectroscopy.[3]

To understand the nature of the ligand properties of particular structural groups, it is expedient to consider specific properties of the surface structure of carbon materials that can serve as models of these groups. For example, fullerene, carbon nanotubes, graphene and the basal plane of crystalline graphite[41, 120] with implanted defects can be used as models of the basal layer of GLC (Fig. 11 *a*). Similarly, a defective edge plane of crystalline graphite can serve as a model of the GLC edge plane; the surface of a carbon filament (fibre) in which graphene layers are arranged in a fishbone pattern (see Fig. 11 *b*, panel *1*) or a card deck pattern (see Fig. 11 *b*, panel *2*) can also be employed as such a model.[172, 173, 175, 176]

Quite a few studies published to date (including reviews[41, 120, 177]) analyze the defective states of various carbon nanostructures; the results of this analysis can be used to describe localization and chemical nature of the ligand functions of these structures on the NGC surface. For example, high-resolution TEM data show that the surface of native graphite crystal, which looks like oncoming sea waves (see Fig. 11 *c*, panel *1*),[174] primarily consists of

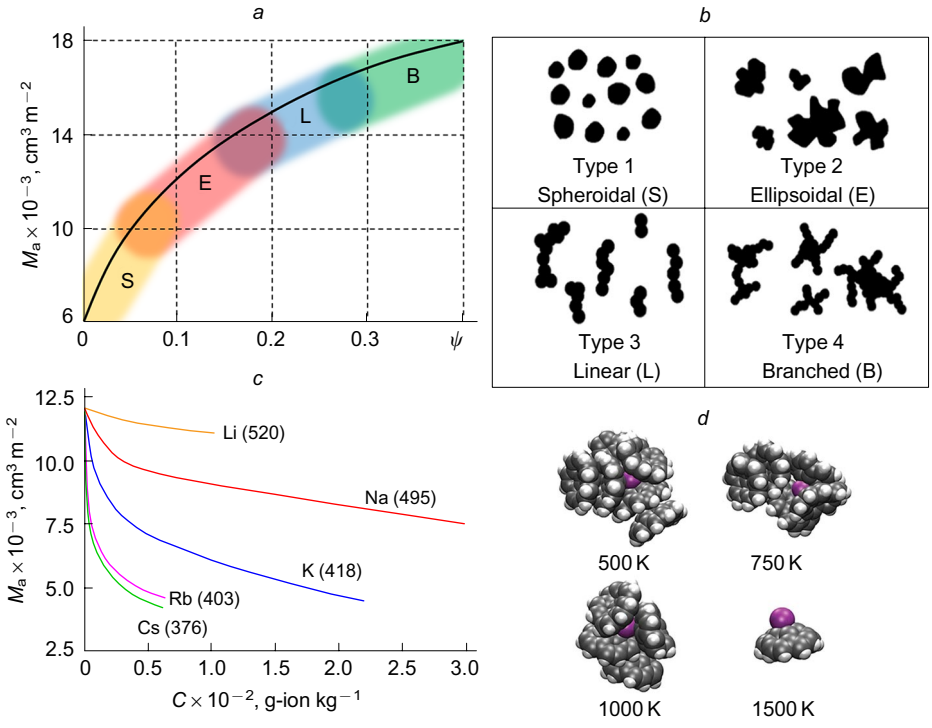


Figure 10. Basic dependence of the specific oil number of carbon black, characterizing the structuring, on the coagulation parameter ψ (following the discussion reported by Gyulmisaryan *et al.*[62] based on the data collected in pilot and industrial plants using various hydrocarbon feedstock); the letters S, E, L, B denote the parameters M_a and ψ characteristic of NGC particles shapes shown in Fig. *b* (*a*); various shapes of carbon black aggregates according to the classification proposed by Herd *et al.*[171] (*b*); reduced oil number of N234 grade carbon black as a function of the concentration of alkali metal ions in the feedstock (the values in parentheses are ionization energies of corresponding atoms in kJ mol^{-1}) based on the data of Gyulmisaryan *et al.*[62] (*c*); models of the K^+ ion clusters with corannulene molecules at various temperatures (*d*).[155] Figure *d* is published with permission from Taylor & Francis.

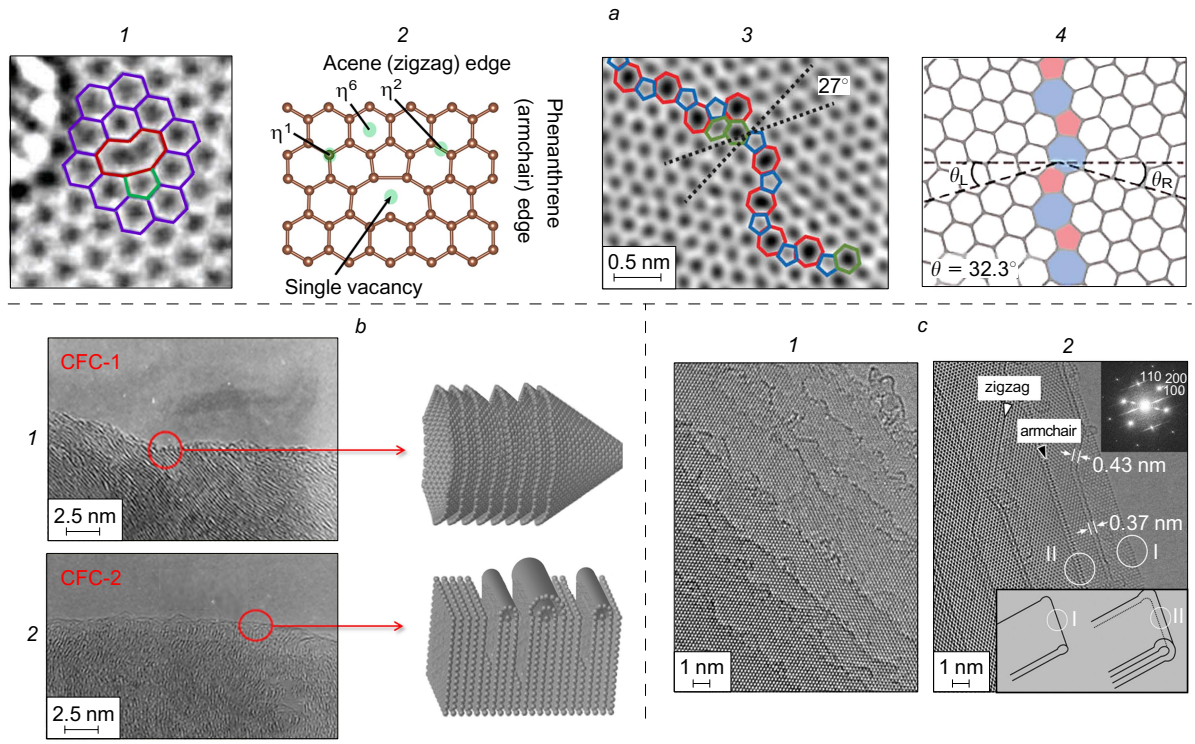


Figure 11. Location sites and chemical nature of some carbon structures acting as ligands on NGC surface. (*a*) GLC basal plane, graphene as the model [(*1*) high-resolution TEM image of a single vacancy on the graphene surface,[120] (*2*) model of a vacancy with other locations of the adsorption sites,[41] (*3*) dark-field image obtained by scanning transmission electron microscopy (STEM) for a linear dislocation: line of linking of graphene layers that contact at an angle of 27°,[120] (*4*) dislocation model for the symmetrical linking of acene and phenanthrene edges; $\theta = \theta_L + \theta_R$ is the disorientation angle ($0° < \theta < 60°$) that describes the mutual orientation of two crystalline domains and is related to the density of dislocations: the larger this angle, the higher the dislocation density [120]]; (*b*) GLC edge plane, filamentary carbon as the model [TEM images of CFC-1 and CFC-2 samples with fishbone (*1*) and card deck (*2*) arrangements of layers; [172] to the right of the images, there are the corresponding idealized models of the encircled carbon structures of the surface,[173] taking account of the breaks in the graphene layer, slits (*1* and *2*), and connections of the graphene layers with each other (*2*)]; (*c*) high-resolution TEM images of graphite powders [(*1*) native sample prior to thermal treatment; the edges resemble sea waves; (*2*) sample after the vacuum thermal treatment at 2000 °C for 3 h, which resulted in annealing of most of defects and formation of closed structures of graphene edges upon connection of two (structure I) and four (structure II) layers].[174] Figure *a*, panel *2* is published with permission from the American Chemical Society, panels *1*, *3*, *4* are published with permission from Taylor&Francis; Figures *b*, *c* are published with permission from Elsevier and the American Physical Society, respectively.

basal planes that form steps with a height of several graphene layers, while the basal planes themselves and their breaks contain defects the surface concentration of which is the highest in the corners of the graphene layer breaks and in the corners where the step adjoins the basal plane. Given this structure, the surface can exhibit both hydrophilic (oxygen-containing groups on the graphene layer edges) and hydrophobic (graphene layer below the step) properties. An example is the adsorption of palladium complexes, which are adsorbed on graphite from dilute solutions either in water [palladium(II) polynuclear hydroxo complexes, PHCs [178]] or in organic solvents [palladium(0) complex with dibenzylideneacetone [179]] exclusively in the sites indicated above and replicate the geometrical shape of the steps.

High-temperature treatment of graphite in a vacuum results both in the removal of oxygen-containing groups from the surface and annealing of most of structural defects located at the steps, some of which are, for example, edge non-aromatic structures have appeared during annealing (before annealing, they were stabilized by the oxygenated groups). Therefore, the stepped structures become nearly perfect, with their geometric shape being specified by the bulk crystal structure (acene, or zigzag edge, and phenanthrene, or armchair edge; see Fig. 11 *c*, panel *2*),[174] while only thermally stable defects persist on the graphene layer surface, such as point defects (the absence of a carbon atom; see Fig. 11 *a*, panels *1* and *2*) or topological defects (an atomic structure of the edge linking of graphene layers other than hexagonal; see Fig. 11 *a*, panels *3* and *4*). [120]

It was noted above that the GLC edge plane is adequately modelled by the surface of carbon filaments that are produced upon catalytic decomposition of methane on mono- or bimetallic crystallites (Al_2O_3-supported Fe, Co, Ni with addition of Cu). On the faces of these filaments, oriented growth of graphene layers occurs as a card deck or fishbone or as nested coaxial cylinders (if the number of cylinders is small, such a carbon material is better known as a multiwalled CNT). Since the filament aspect ratio may be as large as several tens, the surface of the first two types of packing mainly consists of the edges of graphene layers and that of the last-mentioned type represents graphene basal planes, like in CNTs. Electron microscopy examination of the filament surface of the fishbone and card-deck structural types showed [172] that the graphene layer edges are, in most cases, not broken but rather contact each other (like in

annealed graphite;[174] see Fig. 11 *c*, panel *2*) and form structures similar to CNT parts or carbon nanoonions, which can be separated by slits with a width equal to the thickness of a single graphene layer, *i.e.*, 0.34–0.35 nm (see Fig. 11 *b*, panel *2*). The presence of such slit-like pores has been experimentally confirmed by Fenelonov *et al.*,[180] who studied adsorption of planar C_6H_5X molecules, where X = F, Cl, Br, I, with a suitable (for penetration into the pore) thickness of the benzene ring. The presence of slit-like surface defects is more typical of carbon filaments of the card-deck type. It should be noted that the ^{129}Xe NMR chemical shift for xenon atoms adsorbed on carbon materials the surface of which is composed of graphene layers increases with increasing angle between these layers and filament longitudinal axis.[181,182] As a whole, the GLC adsorption potential depends not only on the nature of surface defects, which can be determined using data on the adsorption of various probe molecules, but also on the degree of defectiveness (structure disruption) of GLC bulk, which can be determined using data provided by structural methods. For example, it was shown [183] that the equilibrium constant of adsorption of Pd^{II} chlorides from aqueous solutions of $H_2[PdCl_4]$ on strong adsorption sites (which are primarily located on carbon crystallite edges) depends on the set of parameters L_a, d_{002} and g, which are related, in turn, to the curvature and the length of graphene layers and the thickness of their packages.

A significant contribution to the NGC ligand properties can be made by amorphous carbon, which is mainly located at the sites of GLC junction (merging) in the primary CNG; probably, the appearance of amorphous carbon is associated with the formation of GLC itself. For example, according to XPS and IR and ^{13}C NMR spectroscopy data, the amorphous carbon formed upon the pyrolysis of light hydrocarbons on the surface of various inorganic matrices mainly consists of sp^2-hybridized carbon atoms (and has some sp^3-hybridized carbon atoms).[184–186] As follows from model *ab initio* calculations,[187] this amorphous carbon is a low-density coil of randomly connected linear, low-nuclearity ring and bowl-shaped carbon clusters resembling the carbon structure formed at CNG inception (see Fig. 6 *a*). Simulation of the graphene amorphization also yields a similar structure.[188]

An atomic resolution for the structure of the amorphous carbon formed upon pyrolysis of gaseous methane was attained only recently, owing to the development of a production process of this carbon as a film made of several atomic monolayers, selection of a film area representing an atomically thick monolayer and application of most recent advances in electron microscopy (Fig. 12).[189]

It can be seen from the image that the obtained film is completely disordered in any direction and consists of chaotically connected ring-shaped structures composed of five to eight carbon atoms with significantly variable C–C bond lengths and bond angles. This is an indication that the C–C bonds that form the rings may be single or double bonds and can also be involved in various types of conjugation: allylic, diene, aromatic, *etc*. It should be noted that this structure of the amorphous carbon surface follows from model density functional theory (DFT) calculations, which were carried out by Caro *et al.*[190] The calculations showed that to describe the surface of amorphous carbon as a chaotic combination (binding) of sp-, sp^2- and sp^3-hybridized carbon atoms, it is necessary to introduce some additional intermediate states (sp^{1+n} and sp^{2+m} types,

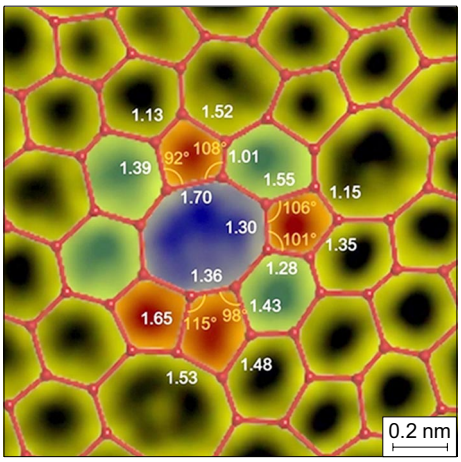


Figure 12. Magnified high-resolution TEM image of a monolayer of amorphous carbon grown from methane by laser CVD.[189] The numbers are bond lengths in ångströms. Published with permission from Springer Nature.

where n and $m < 1$) that would form carbon structures with intermediate C–C bond lengths and bond angles. Analysis of the distribution histograms of C–C bond lengths and bond angles for clusters in a structure made of such clusters, reported by Caro *et al.*,[190] and comparison of the results with the values measured experimentally for an amorphous carbon monolayer (see Fig. 12) indicates that, in terms of physicochemical description, its surface has a clear-cut sp^2 character with some contribution of sp^3-hybridization and an insignificant contribution of sp-hybridization. Thus, it should be expected that the ligand properties of the surface of the amorphous carbon formed in NGC synthesis by gas-phase pyrolysis of hydrocarbons would not differ qualitatively from these properties of a defective surface of graphene. However, there is a quantitative difference consisting in a larger surface concentration of adsorption sites formed by carbon rings containing more than six

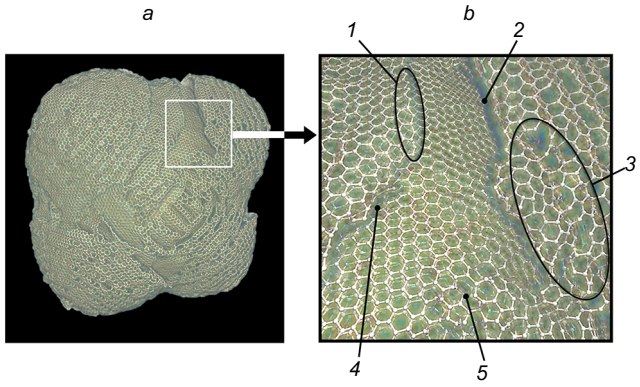


Figure 13. Images of the three-dimensional CNG model obtained by LAMMPS (*a*) and a fragment of the model (*b*).[192] On the model surface, one can detect all types of the considered adsorption sites (some of them are marked in the indicated part of the globule surface) and fragments representing amorphous carbon. (*1*) zigzag (acene) edge; (*2*) micropore containing slit-like pores; (*3*) amorphous carbon; (*4*) slit-like pore; (*5*) vacancy. Published with permission from I.Wald.

carbon atoms and non-aromatic multiple C—C bonds in the case of amorphous carbon.

A view on the type of adsorption sites formed by the defects of a real surface of a nanoglobule as a three-dimensional macroligand can be drawn from the results of large-scale atomic/molecular massively parallel simulation (LAMMPS) of this system.[191, 192] The 3D model of CNG shown in Fig. 13 contains 740,000 carbon atoms; its average diameter is ~20 nm.[192]

2.3. Surface functionalization of nanoglobular carbon as a method to control its ligand properties

The above consideration of the ligand properties of the NGC surface refers to the case where the ligand groups were composed of only carbon atoms. However, during the NGC synthesis, other atoms can also be incorporated into the CNG surface and, in some cases, also into the bulk. Most often, this is oxygen, which appears, for example, when the NGC particles at the outlet of the high-temperature zone contact with water and air while being separated from aerosol (filtered, granulated, *etc*.) The oxidation of NGC surface depends on the NGC production technique. For example, the content of oxygen in furnace blacks does not exceed 1–2 wt.%, while in channel blacks, it may be as high as 5–6 wt.%.[62] The carbon atoms located at the graphene step edges of crystallites and at numerous defects of the amorphized phase are most reactive towards oxygen.

The content of oxygen-containing groups on the NGC surface can be increased by subsequent treatment of carbon nanoparticles prior to or after their separation from aerosol. In a practically important large-scale process, the additional introduction of oxygen (up to 15 wt.%) is accomplished by treating stirred carbon granules with ozonized air at room temperature or with air mixed with NO_2 (oxygen carrier) at 200–300 °C, or with aqueous nitric acid during granulation and subsequent drying of carbon black at 150–250 °C.[62] In all cases, the oxidation duration and the amount of oxygen introduced into NGC substantially depend on the degree of dispersion (size) of primary CNGs, which may be a consequence of the influence of the degree of three-dimensional ordering (*g*) of carbon atoms on the oxidation. In this regard, worth mentioning is a study by Grzyb *et al*.,[193] who showed that varying the source of carbon injected into plasma (styrene, methane, acetylene NGC), with the NGC production process being the same (cracking in plasma), the reactivity of the produced NGC towards oxidation with nitric acid (at 90 °C followed by drying at 120 °C) to give surface oxygen-containing groups significantly increases in the following order: NGC from styrene < NGC from methane < fullerene soot produced from acetylene NGC. According to TEM data, the contribution of disordered carbon not arranged into graphene stacks to the CNG nanostructure increases in the same order (Fig. 14).[193]

More selective incorporation of oxygen atoms into the surface of carbon particles is accomplished by low-temperature (~0 °C) treatment with ozone or oxygen containing singlet molecular oxygen ($^1O_2$) generated *in situ*.[194–199] These oxidants are known to react, first of all, with olefinic C=C bonds and aromatic C—H bonds to afford, first, ketone and phenol groups and, later, upon cleavage of adjacent C—C bonds, also hydroxycarboxy and dicarboxy groups.[200–202] In addition, singlet oxygen ($^1O_2$) can add to aromatic rings, for example, in positions 1 and 4 of the benzene ring, which results in the formation of *p*-benzoquinone.[203, 204] In polyaromatic compounds, zigzag (acene) edges feature higher reactivity towards ozone and produce ketone groups upon oxidation, while armchair (phenanthrene) edges are less reactive and are oxidized with cleavage of aromatic C—C bonds. For example, biphenyl-2,2′-dicarboxylic acid is formed from phenanthrene.[201] The data of Liu *et al*.[205] indicate that the reactivity of the zigzag edges of carbon crystallites towards chemisorption of oxygen molecules is higher than that of armchair edges.

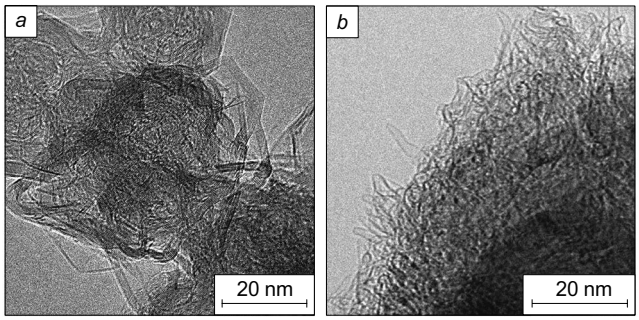


Figure 14. TEM images of NGC obtained by plasma cracking of styrene in a nitrogen atmosphere (*a*) and fullerene soot obtained after plasma treatment of acetylene NGC (Y50A grade) in a helium atmosphere (*b*).[193] Published with permission from Taylor & Francis.

The functional groups that contain nitrogen atoms are formed during post-treatment of the carbon particles with ammonia at elevated temperatures (~400 °C).[206, 207] The functional groups that contain sulfur and phosphorus atoms are added in a similar way at temperatures of 200–600 °C. The modification agents used for this purpose include elemental sulfur, hydrogen sulfide or sulfuric acid, phosphorus, phosphine or phosphoric acid.[208–211] Among the most recent achievements in functionalization of NGC surface with nitrogen-containing groups, mention should be made of a study by Leistenschneider *et al*.,[212] in which the mechanical activation of carbon black powder with ammonia was used for modification (with simultaneous increase in the surface area) at room temperature. The composition and properties of heteroatomic functional groups located on the surface of carbon nanomaterials (fullerenes, CNTs, graphene, *etc*.) have been explored in detail in numerous studies and discussed, for example, in a review.[177] The composition and location of these functional groups are depicted in Fig. 15. Taking into account the knowledge of the coordination and organometallic chemistry of palladium,[213, 214] it may be concluded that the following functional groups with ligand properties can be of interest for stabilizing the ionic states and small palladium clusters: olefinic (C=C), ester, anhydride, pyrone, ketone, quinone, diene sequence (C=C—C=C) in defective C_7—C_8 rings or terminal carbon atom (radical or carbene) (Fig. 15 *a*); pyridine, amine, imine, nitrile, nitrosyl and pyrrole (Fig. 15 *b*); sulfide, thiophenol, disulfide and thiolactone groups (Fig. 15 *d*). If the surface of carbon nanomaterials is functionalized with phosphorus compounds, of most interest are ligand groups containing the phosphorus atom in −3 (phosphines) or +3 (phosphites) oxidation state, but they are very reactive towards oxygen and are rapidly transformed into phosphorus compounds in +5 oxidation state (Fig. 15 *c*), which are of no significant value for the formation of complexes with palladium.

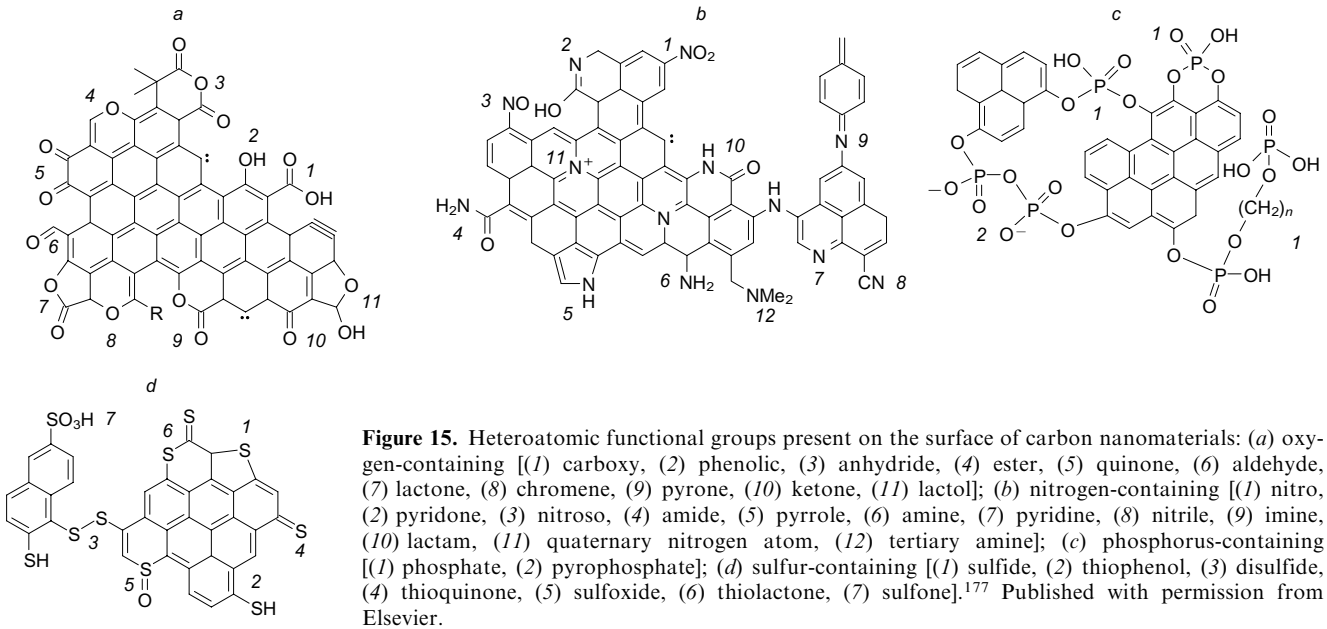


Figure 15. Heteroatomic functional groups present on the surface of carbon nanomaterials: (*a*) oxygen-containing [(*1*) carboxy, (*2*) phenolic, (*3*) anhydride, (*4*) ester, (*5*) quinone, (*6*) aldehyde, (*7*) lactone, (*8*) chromene, (*9*) pyrone, (*10*) ketone, (*11*) lactol]; (*b*) nitrogen-containing [(*1*) nitro, (*2*) pyridone, (*3*) nitroso, (*4*) amide, (*5*) pyrrole, (*6*) amine, (*7*) pyridine, (*8*) nitrile, (*9*) imine, (*10*) lactam, (*11*) quaternary nitrogen atom, (*12*) tertiary amine]; (*c*) phosphorus-containing [(*1*) phosphate, (*2*) pyrophosphate]; (*d*) sulfur-containing [(*1*) sulfide, (*2*) thiophenol, (*3*) disulfide, (*4*) thioquinone, (*5*) sulfoxide, (*6*) thiolactone, (*7*) sulfone].[177] Published with permission from Elsevier.

During the last decade, the so-called anchoring method has gained popularity for surface functionalization of carbon nanomaterials. According to this method, the ligand groups of a carbon support are formed by the reaction of its native functional groups (*i.e.*, carbon- and/or oxygen-containing surface groups) with molecules that contain both the desired ligand group and an anchoring group, which is linked to the native one. Conceptually, this approach can be considered to be a further development of the studies carried out in the 1970s–1980s to elaborate functionalization methods for the surface of inorganic oxides (primarily, SiO_2) in order to obtain heterogenized homogeneous transition metal catalytic compositions.[215–217] The opportunities provided by anchoring techniques for varying the composition and structure of ligand groups and properties of the corresponding metal complexes on the surface of fullerenes, CNTs and graphene were discussed in recent reviews by Serp and co-workers.[3,41] It is worth noting that in this case, no influence of the carbon surface type on the ligand group properties should be expected. This is a significant difference from the case considered above (see Figs 14 and 15), where the functionalization of the carbon nanoparticle surface resulted in the formation of a ligand group involving one or more carbon atoms that belong to the carbon nanocrystallite surface; in addition, due to the presence of non-bonded electrons in the crystallite, the change in the physicochemical state of the crystallite bulk will affect the properties of the surface ligand function. Even a tighter interaction between a heteroatomic group and surface carbon atoms can be attained by involving unsaturated surface carbon atoms into various polymerization processes with heteroatomic monomers and by performing subsequent special chemical or thermal treatment of the anchored polymer (this results in cross-linking and/or partial decomposition) to make it non-volatile and non-leachable. This is exemplified by Qian *et al.*[218] and Xie *et al.*,[219] who created polymer islands consisting of melamine (thermal polymerization *via* deamination) and 3,4-ethylenedioxythiophene (oxidative polymerization) on Vulcan®XC-72R grade NGC. The carbon materials modified in this way exhibited significant advantages regarding the electrical conductivity and stability of electro-oxidation catalysts based on them.

The targeted modification of the ligand properties of carbon crystallite surface by changing the bulk properties of the material may become a new trend in the design of metal-on-carbon catalytic compositions. The following key techniques can be mentioned:

— selective chemical and/or energy treatment of the intraglobular amorphized (core) and peripheral graphite-like (shell) CNG regions;

— implantation of heteroatoms into the CNG core.

The former type of methods includes either the removal of the core by gasification reaction of NGC with oxidants (O_2, H_2O and CO_2 at appropriate temperatures) or increase in the core density by NGC graphitization *via* high-temperature treatment at 1500–2500 °C, or carrying out both procedures in some order. Among the most recent key results obtained in this area, note the study by Toth *et al.*,[220] who used a modern electron microscopy technique (spherical aberration-corrected environmental transmission electron microscopy, SAC-ETEM) with a point-to-point resolution of 0.1 nm to investigate the mechanism of CNG gasification by molecular oxygen. Nanoglobular carbon of N990 grade was used as an example to show that at a temperature of 600 °C and O_2 pressure of 1 Pa, the reaction of oxygen with the external surface layers of CNGs begins at the edge of a graphene lamella, which results in its gradual flaking, bending and formation of a fullerene-like structure (the so-called fullerenation of the surface). The fullerene-like surface structure possesses some mobility on the surface, gradually burns and breaks into fragments; apparently, some of the fragments finally burn out in the gas phase. An increase in the oxygen pressure up to 10 Pa increases the rate of oxidation of GLC lamella edges. Therefore, the oxidation also develops into the depth and reaches the inner part of the CNG, which is composed of more reactive weakly ordered carbon, that is, graphene structures of smaller size and larger curvature (see Fig. 6 *b*,*c*), thus providing for more rapid burning out of the lamella and possible collapse of the remaining thin lamellar shell. Thus, variation of temperature, oxidizing

gas pressure and duration of thermo-oxidative treatment may give a variety of intermediate structures (Fig. 16 *a*).[220] In our opinion, among these structures, CNGs with a fullerened external layer of lamellae[221] (blue area in Fig. 16 *a*; see also Fig. 16 *b*) and thin-walled hollow carbon spheres[222, 223] (yellow area in Fig. 16 *a*; see also Fig. 16 *c*) are of most interest as three-dimensional ligands.

A study[224] of N990 NGC (both original and pre-heated for graphitization in an argon flow) using atomic oxygen (a mixture of O_2 and O generated *in situ* in the electron microscope chamber) for gasification demonstrated that at a temperature of 800 °C and O_2 pressure of 1 Pa, molecular oxygen reacts, first of all, with carbon atoms of the amorphous core, diffusing through pores of the shell (which, in principle, agrees with the results of Toth *et al.*[220] discussed above), while atomic oxygen, which is very reactive, rapidly reacts with shell carbon atoms and, therefore, it does not have enough time to diffuse towards the core. The latter circumstance can even lead to an ordering of the graphene crystallites of the core as a result of removal of disordered carbon (burning out) from the periphery of these crystals. To summarize, provided that the optimal conditions have been chosen for graphitization and that gasification is carried out by selective burning out of the amorphous carbon contained both in the core and in the intercrystallite space of the shell, it is possible to obtain perforated hollow carbon spheres, with their inner cavity being connected with the interglobular space *via* the pores that pass through the shell.[225]

Since gasifying agents such as H_2O and CO_2 are less reactive than O_2, they are more selective towards the reaction with the amorphous core and weakly ordered carbon. Therefore, it is possible to obtain hollow nanoglobules with shell thickness of several graphene layers, which leads to a significant increase in the surface area in parallel with an increase in electrical conductivity.[226] This option is important, for example, if porous thin-wall nanoglobules are used to create supercapacitors and electrochemical formulations.[225] As regards the use of such nanoglobules as palladium catalyst supports, an important feature is the change in the D and G bands in the Raman spectra observed during the thermo-oxidative modification of NGC;[223, 227, 228] as the degree of modification determined by the sample mass loss increases, these bands are narrowed and the ratio of their intensities decreases from 1.6 to 1.4. This result attests to increasing the degree of perfection of graphene layers and, as a result, to an effect of this modification on the NGC ligand functions: a decrease in the contribution of the adsorption sites located in amorphous structures and an increase in the contribution of the adsorption sites located on graphene lamella edges (see Fig. 13).

The shell thickness can be increased by either preliminary graphitization of the core part adjacent to the shell or preliminary coating of the shell by more ordered carbon than that in the core, for example, pyrolytic carbon. A sequence of carbonization and gasification treatments of carbon black granules underlies the production process of Sibunit™, a carbon material that consists of accreted hollow CNGs, the walls of which have numerous burnt spots.[34] This material combines high strength, chemical inertness (resembling in this way pyrolytic carbon) and a large surface area with no micropores (resembling in this way highly dispersed carbon black). The application of Sibunit™ as a support for palladium particles has been described in detail[35–37] and, to our knowledge, the production of this carbon material is the first and still the only one example of using bulk modification of carbon black in industrial catalysis.

The high-energy treatment of carbon materials consists in exposure of the materials to electron, ion, photon and other particle beams, the deceleration of which in the material bulk gives rise to very high temperatures (~4000–6000 °C), which change the material structure. In the case of NGC, these changes are primarily related to graphitization, affecting not only the amorphous core but also the more structurally ordered shell.[52, 164, 222, 229] Studies along this line revealed an important feature: an effect of carbon nanoglobule size (diameter) on graphitization induced by high-energy beams. If nanoglobule size is small, hollow spheres with an onion-like shell consisting of several layers are formed, but as the globule diameter increases and reaches some critical value, graphite sheets consisting of a dozen of ordered graphene layers are formed instead of hollow spheres (Fig. 17).[163] This result can be explained under the assumption that if the globule size is small, the outer shell of the CNG withstands the pressure of the carbon 'broth' that appears within the globule, while in the case of a larger size, the shell fails to withstand such a pressure; hence, it collapses and disintegrates to give graphene packages shaped like elongated bars (Fig. 17 *b*,*c*).

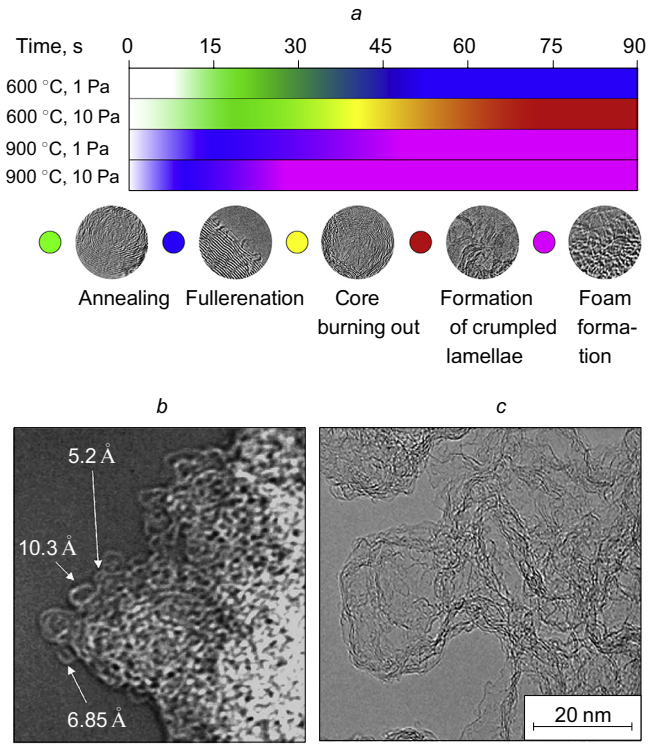


Figure 16. Results of studies of thermo-oxidative gasification of CNGs: oxygen-induced qualitative changes of N990 grade NGC arising upon variation of O_2 pressure and treatment temperature and time (*a*);[220] TEM image of the fullerened surface of the soot obtained upon combustion of benzene in an oxygen–argon mixture at the O : C atomic ratio close to 1 and a pressure of 5.3 kPa; the numbers indicate the diameters of the fullerene structures marked by arrows (*b*);[221] TEM image of thin-walled hollow CNGs (crumpled lamellae) obtained by thermo-oxidative treatment of furnace type P145 NGC with steam at 900 °C (*c*).[223] Figures *a*, *b* are published with permission from Elsevier.

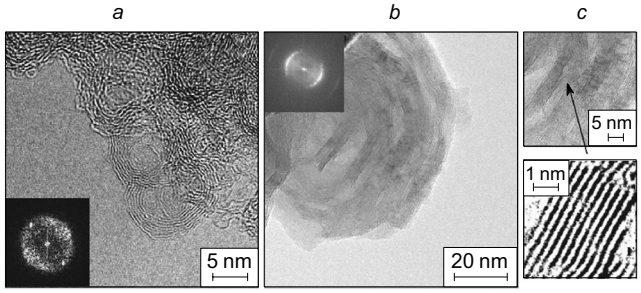


Figure 17. Changes in the NGC structure under the action of pulsed laser radiation (Nd : YAG laser, radiation wavelength of 1064 nm, pulse duration of 16 ns) depending on globule diameter. (*a*) Highly dispersed NGC with CNG diameter of 10 – 30 nm; (*b*, *c*) low-dispersed NGC with a globule diameter of 100 – 300 nm. The interplanar spacings d_{002} are 0.360 – 0.370 nm for onion-like structures and 0.345 – 0.365 nm for graphite sheets.[163]

Hollow CNGs with a graphitized shell can be obtained by laser irradiation of a suspension of NGC particles in the liquid phase. Moreover, it turned out that if the liquid phase contains soluble platinum compounds, for example $H_2[PtCl_6]$, along with NGC particles, the irradiation results in the formation of hollow CNGs with platinum metal nanoparticles inside (Fig. 18).[230]

Development of the other trend of NGC functionalization mentioned above, namely, implantation of heteroatoms into the CNG core, started only recently and is primarily focused on the creation of carbon materials that can be used in supercapacitors or electrocatalytic devices. Since the strength of the bonds of carbon with heteroatoms such as nitrogen or sulfur is lower than the carbon – carbon bond strength, attempts to obtain a heteroatomic NGC by thermal gas-phase decomposition of appropriate heteroatomic aromatic compounds (for example, pyridine or thiophene instead of benzene) failed: the C – N and C – S bonds cleaved to give NH_3 (N_2/H_2) and H_2S (S/H_2), respectively, at temperatures that were significantly lower than the temperatures required to cleave C – C and C – H bond in an aromatic ring and to start chain oligomerization of the aromatic rings to give PAHs, key precursors of CNGs. Therefore, to obtain bulk-modified carbon particles, a so-called *in situ* solution plasma process has been proposed quite recently; the process is based on generation of a plasma discharge in the liquid phase of an organic compound.[231,232] In particular, heteroatomic *N*-methyl-2-pyrollidone[233] and thioanisole[234] were used to produce the corresponding carbon nanostructures bulk-doped with nitrogen and sulfur, which provided for enhanced electrical conductivity and thermal stability of the dispersed platinum particles deposited on these structures.

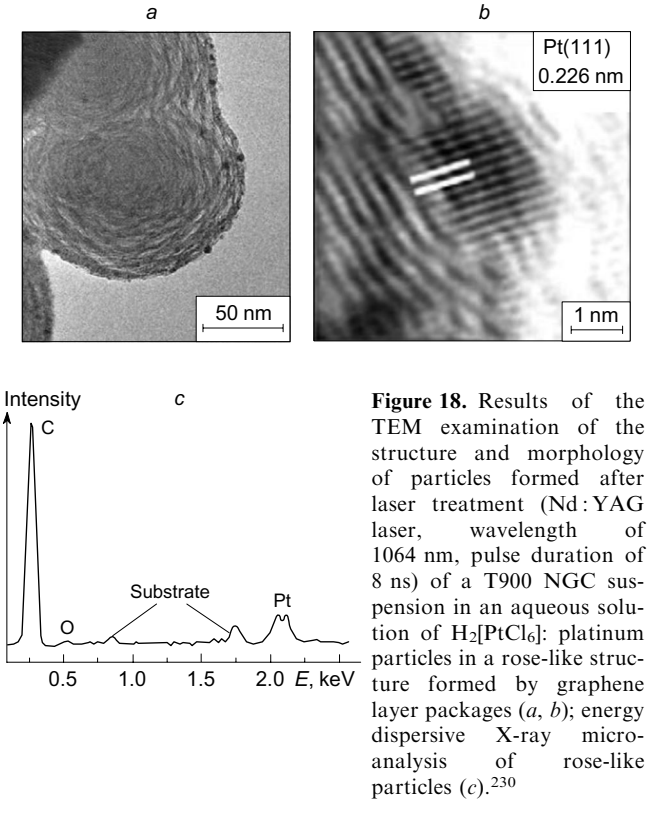


Figure 18. Results of the TEM examination of the structure and morphology of particles formed after laser treatment (Nd : YAG laser, wavelength of 1064 nm, pulse duration of 8 ns) of a T900 NGC suspension in an aqueous solution of $H_2[PtCl_6]$: platinum particles in a rose-like structure formed by graphene layer packages (*a*, *b*); energy dispersive X-ray microanalysis of rose-like particles (*c*).[230]

3. Formation of supported palladium–carbon catalysts

3.1. Methods for palladium deposition on the carbon support

Currently, numerous methods have been developed for the preparation of supported Pd/C catalysts; these methods are surveyed in reviews.[31,33] Most widely used are impregnation, deposition – precipitation and deposition – reduction methods. The impregnation process, which is traditionally used to prepare Pd/C catalysts, was recognized as most facile and readily available. According to this process, the particles or granules of the carbon support are mixed with a solution of a palladium compound. Depending on the volume ratio between the impregnating solution and the support pores, impregnation may be either dry (according to the water uptake) or wet (using an excess of impregnating solution).[31,33,235–237] The compounds proposed as palladium precursors include the acid $H_2[PdCl_4]$ and its salts, $Pd(NO_3)_2$, palladium(II) ammonia complexes, $Pd(OAc)_2$, palladium(II) acetylacetonate and other palladium compounds.[6,8,9,28–33,235,238–240] The impregnation of carbon supports with aqueous solutions of $H_2[PdCl_4]$ or its salts is used most often. In some cases, palladium is also deposited from non-aqueous solutions as coordination compounds with organic ligands.[29,31–33,239–241] After deposition, the palladium compound is reduced to give dispersed particles of palladium metal on the carbon support surface. The reduction is carried out either by treatment with solutions of various reducing agents such as HCO_2Na, $NaBH_4$, N_2H_4, formaldehyde, ethylene glycol (liquid-phase reduction) or by passing hydrogen gas at high temperature through the pre-dried catalyst.[28–33,242] Note that on contact with a carbon support, palladium chloride complexes can be spontaneously reduced (by weakly bound GLC electrons) to give palladium metal particles (see below, Section 3.2.3). The reduction may not be needed if the palladium precursor is unstable and decomposes on contact with the carbon surface to give palladium metal, for example, as in the case of impregnation of a carbon support with a solution of palladium(0) complex $[Pd_2(dba)_3]$ (dba is dibenzylideneacetone).[241]

The deposition – precipitation method consists in the transformation of the dissolved molecular precursor into a highly dispersed poorly soluble compound which is very slowly converted to a precipitate in solution, but is rapidly

deposited on the extensive surface of the support.[29–33,235,237,242] Usually this is attained by a change in the pH of the precursor solution upon slow addition of an appropriate precipitation agent. Then, using the same procedures as in the case of impregnation method, the deposited palladium compounds are converted to palladium metal. As an example of using deposition–precipitation technique for the preparation of supported Pd/C catalysts, consider the approach developed by Simonov, Troitskii and co-workers,[30,243] according to which $H_2[PdCl_4]$ dissolved in water is subjected to hydrolysis (*e.g.*, with an alkali metal carbonate) in a narrow pH range (from 4 to 6)

$$H_2[PdCl_4] + M_2CO_3 \rightarrow M_2[PdCl_4] + H_2O + CO_2 \quad (2)$$

M = Li, Na, K

$$m\,M_2[PdCl_4] + 2m\,H_2O \rightarrow \quad (2a)$$

$$\rightarrow \{M_n[Pd(OH)_2]_m\}^{n+} + (2m-n)\,M^+ + 2m\,H^+ + 4m\,Cl^-$$

This results in the formation of palladium PHCs $\{M_n[Pd(OH)_2]_m\}^{n+}$, which retain their colloidal state for a long period of time in solution, owing to the presence of a charge; however, when a carbon support is added, they lose M^+ cations and are rapidly deposited on the support surface. Thus, by varying pH and the nature of the M^+ cation in the precipitation agent, it is possible to control the size of palladium PHCs and particles that are subsequently formed.[244] Most often, the particle size of the palladium PHCs (mainly 3.5 nm, according to small-angle X-ray scattering, SAXS, data) exceeds the diameter of the support micropores (< 2 nm), which prevents the formation of palladium metal particles in micropores and increases the accessibility of the palladium particle surface to reactants. One more advantage of this approach is the ability of palladium PHCs to be reduced with hydrogen at lower temperature than palladium chloride complexes; owing to this, enlargement (sintering) of the newly formed palladium particles can be minimized if necessary.

In the deposition–reduction method, a solution of a reducing agent (HCO_2Na, $NaBH_4$, N_2H_4, CH_2O) is added to a carbon support suspended in a solution of a palladium compound.[29,31,33,236] The reduction of this compound in solution gives palladium clusters and NPs attached to the carbon surface. This approach also rules out the insertion of palladium NPs into the narrow pores of the support, since the reduction and NP formation processes in the solution bulk occur much faster than diffusion of the reactants into micropores. A drawback of the method is the possible contamination of the ready catalyst, when adsorbed components of reducing agents and their transformation products have not been completely removed.

Supported Pd/C catalysts are also prepared by so-called metal colloid method, which has lately become especially popular (although it has been known for ~100 years[245]). The essence of this method is immobilization, on the carbon support, of colloidal palladium particles that are first formed and stabilized in solution; this is done using various complex forming additives, organic solvent extraction and other approaches.[29,33,236,237,246–249] The metal colloid method is attractive because the resulting catalysts are composed of metal NPs with a specified size and shape uniformly distributed on the support.

An interesting approach combining the deposition–reduction and metal colloid methods is the successive growth method proposed by Zamaraev *et al.*[250–252] This approach is based on the following observation: palladium(II) acetate, existing as the trimer $[Pd(OAc)_2]_3$, is reduced with formic acid in toluene after an induction period, apparently caused by the necessity for the formate anion to enter the inner coordination sphere of palladium by displacing the acetate anion. The appearance of the first palladium metal clusters attached to the carbon support switches the reduction of most of remaining palladium acetate to a pathway involving surface palladium hydrides formed upon the decomposition of formic acid to H_2 and CO_2 on the palladium metal surface. This switching leads to palladium-on-palladium growth. Thus, by gradual addition of formic acid, it is possible to grow palladium crystallites with a desired narrow size distribution on the support surface.

All of the methods listed above are also utilized to prepare NGC-supported palladium catalysts.[33] However, to prepare catalysts for practical use, preference is given most often to the methodically simple, well-elaborated and, therefore, the most common method, namely, support impregnation with aqueous solutions of $H_2[PdCl_4]$ or its salts (below referred to as chloride precursors of palladium). Therefore, in what follows, the attention is focused on this method. Data on the formation of Pd/C compositions (including NGC-based ones) using other palladium precursors, *e.g.* $Pd(NO_3)_2$, palladium(II) ammonia complexes, palladium(II) PHCs, $Pd(OAc)_2$, palladium(II) π-allyl complexes, $[Pd_2(dba)_3]$ and so on, for deposition from appropriate solvents (including organic solvents) can be found in the literature.[29–32,42,43,235,238–241]

3.2. Processes of interaction of chloride precursors of palladium with the carbon support and formation of palladium nanoparticles

When dihydrogen tetrachloropalladate is deposited from aqueous solutions on a carbon support, the components ($H_2[PdCl_4]$ and carbon particles) interact with each other when occur in the aqueous phase. Therefore, we would briefly analyze the state-of-the-art studies of the reactions of these components with water, including formation of inner- and outer-sphere Pd^{II} aqua and hydroxo complexes and the nature of water/carbon particle interface, in order to evaluate its effect on the distribution of adsorbed palladium compounds over the particle surface and the possible changes of this distribution during drying.

3.2.1. State of the chloride precursor of palladium in aqueous solutions

The thermodynamic and kinetic regularities of the complex formation in the $Pd^{II}–OH^––Cl^––H_2O$ system have been very well studied to date, and their qualitative and quantitative characteristics (structures of complexes, complex formation constants, rate constants of ligand substitution) were reported and discussed in the reference literature,[253] review publications[14,254–256] and original articles.[257,258] In all inner-sphere aqua chloro hydroxo complexes, palladium has a square ligand environment, which corresponds to d^8 electron configuration in the dsp^2-hybridization. The replacement of inner-sphere ligands in these complexes mainly follows the S_N2 mechanism involving a dsp^3-hybridized transition state (trigonal bipyramid). Due to small difference between the *trans*-effects of Cl, OH and H_2O

ligands, clearly defined positions (*cis* or *trans*) are not manifested when they replace one another. The Pd^{II} coordination sphere is highly labile and, when the concentrations of the Cl^- and OH^- (or H^+) ions in the solution change, a new equilibrium is established very rapidly, within several minutes. In acid medium at pH < 4, the main ligands competing for the inner coordination sphere of Pd^{II} are Cl and H_2O, while at pH > 4, these are Cl and OH groups. According to Cruywagen and Kriek,[258] the logarithms of the formation constants (β_n or β_{pq}) of these complexes have the following values (at 25 °C):

for $[PdCl_n(H_2O)_{4-n}]^{2-n}$

$\log\beta_1$	$\log\beta_2$	$\log\beta_3$	$\log\beta_4$
4.47	7.80	10.18	11.53

for $[PdCl_p(OH)_q]^{2-}$

$\log\beta_{31}$	$\log\beta_{22}$	$\log\beta_{13}$	$\log\beta_{04}$
16.48	20.63	24.02	26.23

Since the equilibria in the formation of these complexes are established very rapidly, the knowledge of these constants can help to assess the composition of the complexes that exist in the adsorption equilibrium with a solution and to separately study the subsequent transformations of the adsorbed precursor (by monitoring the variation of the solution pH and concentration of Cl^- ions during the adsorption of complexes on the support). Such a detailed investigation is hardly possible, for example, for Pt^{II} complexes with a structurally similar coordination sphere, which are 10^5 times less labile than Pd^{II} complexes;[254] for this reason, the course of adsorption of platinum(II) chloride complexes is rate-limited by the substitution of inner-sphere ligands, while the composition of the adsorbed precursors is controlled by the adsorption time. The ratio of the number of Cl atoms and H_2O molecules in the Pd^{II} coordination sphere also affects the potential of the redox transition

$$Pd^{II} + 2e \rightarrow Pd^0 \qquad (3)$$

which increases with increasing number of inner-sphere water molecules, from +0.591 V for $[PdCl_4]^{2-}$ to +0.951 V for $[Pd(H_2O)_4]^{2+}$, but sharply decreases on passing to pH > 7 and with increasing number of inner-sphere OH ligands (down to +0.10 V for $[Pd(OH)_4]^{2-}$).[259,260] Since the carbon support is a potential reducing agent, the possibility of controlling the emf of the Pd^{II}/C pair is also exceptionally valuable for studying the mechanisms of formation and the nature of the points of attachment of palladium sites on the carbon material surface.

The preparation procedure of impregnation catalysts always includes the stage of drying at elevated temperature; therefore, it is also necessary to know the thermal stability of the Pd^{II} aqua chloro complexes in aqueous solutions. It was shown [261] that aqueous solutions of these complexes are homogeneous during autoclave treatment up to a temperature of 125 °C; however, at 200 °C, they lose homogeneity due to the formation of insoluble products of hydrolysis. In conformity with the complex formation constants, as the temperature increases in the range from 5 to 125 °C, the thermodynamic stability of the aqua chloro complexes dissolved in water increases, while that of the tetrachloride complex decreases. The aqua complex $[Pd(H_2O)_4]^{2+}$ is hydrolyzed even in very acidic solutions (although very slowly) to give initially oligomeric oxo hydroxo complexes, *e.g.*, the $[Pd_{10}O_4(OH)_8(H_2O)_{12}]^{4+}$ cluster, the structure of which has been proposed on the basis of EXAFS and SAXS studies of these solutions.[262] Since the volume of this cluster is only 1 nm^3, it is of obvious interest as a precursor of highly dispersed palladium particles.

Studies of the composition and structure of the outer-sphere Pd^{II} aqua complexes resorting to advanced physical methods and model calculations started not long ago.[263–265] It was found that the outer sphere of the $[PdCl_4]^{2-}$anion contains eight water molecules that are structurally ordered as a square prism, with the O···O distance at the base of the prism being 0.332 nm and a packing density of water molecules being 75% higher than that for liquid water under ambient conditions. The enhanced attachment of water molecules that form the outer sphere of the $[PdCl_4]^{2-}$anion may result in that the palladium chloride complexes adsorbed on the support would exist in the hydrated state during drying even at temperatures above 100 °C (roughly 120–130 °C); this may induce their further transformations (hydrolysis, redistribution among the adsorption sites, *etc.*). It is of interest that in the case of $[Pd(H_2O)_4]^{2+}$ aqua complex, coordination of two water molecules above and below the square plane gives rise to the $[Pd(H_2O)_4(trans\text{-}H_2O)_2]^{2+}$ complex cation with the geometry of a square bipyramid, which additionally has an outer coordination sphere, like $[PdCl_4]^{2-}$, composed of eight H_2O molecules.[266] It can be expected that breaking the $\{[Pd(H_2O)_6](H_2O)_8\}^{2+}$ hydrate and removing the inner-sphere water molecules would require even a higher drying temperature, which may induce more profound changes in the adsorbed complexes — precursors of the palladium sites. These thermal modifications of the adsorbed precursors are difficult to control; therefore, development of methods for their reduction without preliminary drying, *i.e.*, the use of dissolved reducing agents, becomes very important for the production of Pd/C catalytic compositions with reproducible desired properties.

3.2.2. Interactions at the water/carbon interface

The studies of interaction of liquid water with a surface of carbon particles have been carried out for a relatively long time, first of all, in relation to development of efficient systems for the recovery of valuable organic compounds, such as flotation agents, from water. Lately, studies along this line have been intensified due to the interest in the application of certain carbon nanomaterials (graphene, CNTs and NGC) in electrocatalytic oxidation and reduction of organic compounds in aqueous solutions and in energy storage systems (supercapacitors).[267] Regarding the investigation area considered in this review, it is important to understand the nature of interactions that arise in the carbon particle/aqueous HCl system and their influence on the formation of palladium-on-carbon compositions; however, to our knowledge, there are no publications directly addressing this topic. In a review devoted to analysis of the role of interactions at the liquid/solid support interface in the genesis of supported catalysts, Bourikas *et al.*[268] noted that currently it is almost impossible to describe the interactions at the carbon/electrolyte solution interface as applied to the catalyst preparation in terms of a fundamental approach. In view of this fact, we attempted to address the important issue of interactions in the $NGC-H_2O_{(liq)}-HCl$ system by drawing analogy to the trends found for some model or related systems (H_2O/NGC,[269,270] H_2O/AC,[271] H_2O/mesoporous car-

bon,[272] $HCl_{(g)}$/defective graphene[273]) and by analyzing review papers.[274, 275]

It was noted above (see Sections 2.2 and 2.3) that the CNG surface contains various carbon and carbon–oxygen groups giving rise to hydrophobic and hydrophilic areas, respectively. Since the oxygen functional groups are mainly concentrated at the periphery (breaks) of graphene layer packages (GLCs), these areas exhibit hydrophilic properties and exactly they are responsible for adsorption binding of water molecules to give clusters, which are subsequently transformed into islands, which, in turn, coalesce into mono- and polylayers and fill the intercrystallite space (Fig. 19 *a*,*b*).[276]

The adsorption binding of water on the ideal basal plane of a graphite crystal has an exceptionally low energy and is manifested only at temperatures below the freezing point of water. However, when there are defects on this plane, the adsorption is possible; furthermore, the location of such defects near the periphery of the layer facilitates adsorption due to the possible stabilization of the adsorbed state by hydrogen bonds formed between water molecules and oxygen groups on the GLC edge and basal planes. Therefore, enhancement of the disorder of graphene layers caused by a decrease in their size (parameter L_a) and their number in the package (parameter L_c) and also increase in the content of oxygen-containing groups would be favourable for more pronounced and uniform wetting of the carbon surface; hence, a hydrophilic palladium precursor would be adsorbed on a greater number of sites and this would give rise to a catalyst with smaller and more uniformly distributed palladium particles. High disorder of carbon atoms on the amorphized part of CNG surface (see Fig. 13) and a greater content of oxygen groups on this surface indicate that upon the introduction of water, these parts of CNG surface would be the first to be wetted.

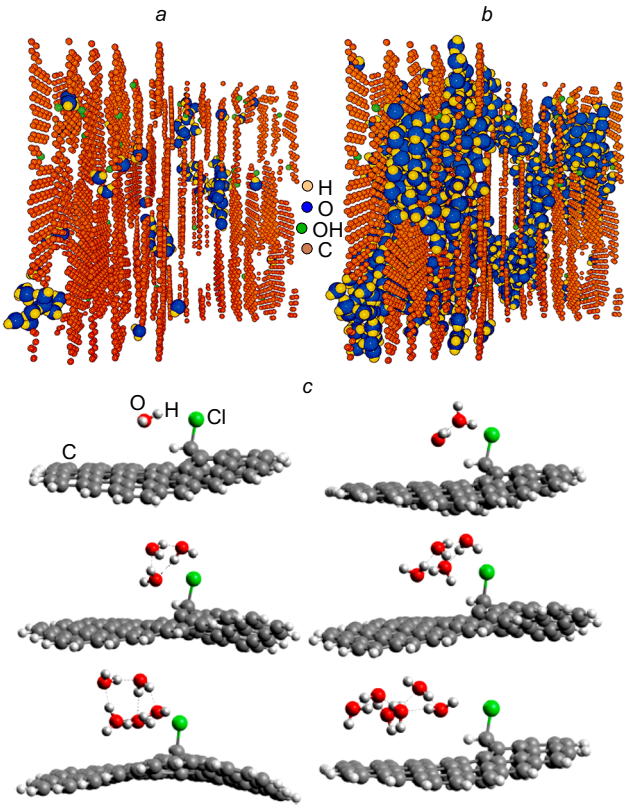


Figure 19. Results of Monte Carlo simulation of the adsorption of water on a disordered carbon crystallite (the surface density of adsorption sites is 0.65 nm^{-2}) at a temperature of 300 K and relative water vapour pressure P/P_0 of 0.05 (*a*) and 0.2 (*b*);[276] results of DFT and *ab initio* molecular dynamic calculations of the formation and growth of clusters of water molecules around the chlorine atom located at a graphene layer defect (*c*).[273] The simulation was performed using the Vienna *ab initio* simulation package (VASP); the step was 1 fs. Figures *a*, *b* are published with permission from the American Chemical Society, Figure *c* is published with permission from Elsevier.

The addition of hydrogen chloride into the aqueous phase considerably affects the interaction processes at the water/carbon interface. As the HCl concentration increases, *i.e.*, the medium becomes more acidic, more and more ligand groups of the carbon surface are protonated, starting with basic oxygen groups (chromene, pyrone, ketone and quinone groups)[277, 278] and proceeding to the regions containing olefinic groups and aromatic rings (complexes of H^+ with these groups were reported[279–281]). The surface carboxy groups are not protonated even in highly acidic aqueous solutions.[278] As a result of protonation, the CNG surface in an acid medium is positively charged, with a significant part of the charge being concentrated in the edge planes of GLCs, and only a minor part of the charge being located in the basal planes, at the sites of structural defects. Note that the addition of HCl to basal plane defects enhances the wettability of the surface because of aggregation of water molecules around the chlorine atom (see Fig. 19 *c*).[273] The surface distribution of the positive charge is repeated (reproduced) by Cl^- anions, thus giving rise to an electrical double layer (EDL), the capacitance of which is many times higher at the edge plane than at the basal plane of GLC. The difference between these capacitances can be derived from results of Yuan *et al.*,[282] who showed that in a potassium chloride-containing phosphate buffer, the electrical capacitance of the EDL formed at the edge of a graphene sheet is more than 4 orders of magnitude higher than the EDL capacitance for the basal plane of the same sheet (1.0×10^5 and 4 μF cm^{-2}, respectively), which is attributable to the presence of a large number of structural defects and dangling bonds of carbon at the edge.

The formation of EDL plays a crucial role in the subsequent adsorption interactions and reactions of palladium complexes.

First, the negatively charged chloride complexes $[PdCl_4]^{2-}$ and $[PdCl_3(H_2O)]^-$, being involved in the formation of EDL, would be concentrated near the most positively charged sites of the GLC surface (*i.e.*, mainly near the protonated basic ketone and quinone groups).

Second, since the orientational structuring of the H_2O dipoles around a charged surface site near a water layer adjoining the surface leads to a sharp decrease in the dielectric constant (ε) (from $\varepsilon \approx 80$ for the liquid water phase to $\varepsilon \approx 5$ for water in the EDL inner Helmholtz layer), the Coulomb interaction of anions with protonated surface sites increases with decreasing distance between them; this increase is more characteristic of the double-charged $[PdCl_4]^{2-}$ anion.

Third, because of identical charges of graphene layer edges, low dielectric constant and the presence of defects that bend graphene layers (vacancies, C_5-C_7 rings, *etc.*), the carbon crystallite would undergo layer separation with

insertion of some of the adsorbate into the interlayer space along the periphery of the nanocrystallite.

Fourth, the difference between the degrees of protonation of the edge and basal planes of the carbon crystallite gives rise to an electric field in its bulk, which promotes redistribution of weakly bound electrons (conduction electrons) towards more positively charged areas, thus determining the sites of possible redox transformations of the adsorbed palladium compounds.

Thus, deliberate variation of the EDL structure considerably affects the adsorption interaction of palladium complexes with the carbon material surface and the nature of the adsorbed precursor; it is most efficient to vary pH, ionic strength and temperature of the solution (especially on going to the >100 °C region) and to generate and vary an electrical potential on the carbon support.[30, 235]

The above analysis gives only the conceptual grounds for taking account of the effects of aqueous phase on the physicochemical state of the adsorption interaction participants. The details will be discussed below in relation to particular stages of formation of the palladium–carbon catalytic composition. Note that the CNGs is a challenging investigation object, due to the fact that the edge planes (steps) of crystallites have very low height (1–3 layers; see Fig. 13) and apparently they are not the edges of broken layers, because these layers can be partly connected, thus forming low-ordered areas with a large curvature and C=O, C−OH and C=C groups able to be protonated and form an EDL.

3.2.3. Fixing of the chloride precursors of palladium on the carbon surface

Unlike oxide supports, carbon supports have a markedly more abundant surface chemistry bearing both hydrophilic and hydrophobic areas, defective structures, olefinic groups and various oxygenated functional groups, the concentration of which can be varied over a broad range.[177] In addition, the carbon surface can contain nitrogen and sulfur groups formed upon functionalization of the carbon support with appropriate heteroatomic compounds (see Fig. 15). The modern views on the physicochemical processes that take place upon the contact of $H_2[PdCl_4]$ with graphite-like carbon materials in water[31, 32, 242, 283–286] are mainly based on pioneering studies of Simonov and co-workers.[30, 235, 287–290] Since the $[PdCl_4]^{2-}$ anion is rapidly hydrolyzed in aqueous solutions even at room temperature to give mixed palladium aqua chloro complexes (as indicated above; see also Refs 291 and 292)

$$[PdCl_4]^{2-} + x\,H_2O \rightleftarrows [PdCl_{4-x}(H_2O)_x]^{x-2} + x\,Cl^- \qquad (4)$$

$x = 0, 1, 2$

in the subsequent discussion of $H_2[PdCl_4]$ adsorption from aqueous solutions and transformations on the carbon support surface, we will imply not only the tetrachloropalladate ion, but its labile aqua forms that are present in equilibrium in the impregnation solution.

According to Simonov and co-workers,[30, 235, 287–290] trapping of palladium from aqueous solutions of $H_2[PdCl_4]$ on a carbon support proceeds according to two competing pathways: redox and coordination ones.

According to redox mechanism, Pd^{II} is reduced with the electron gas of GLCs to give palladium metal particles

$$[PdCl_4]^{2-} + 4\,C_{(s)} \rightarrow Pd^0/2\,C_{(s)} + 2\,[Cl^-/C^+_{(s)}] + 2\,Cl^- \qquad (5)$$

where $C^+_{(s)}$ is the positively charged adsorption site, which appears upon the transfer of electrons located in the carbon support crystallites to Pd^{II} (the letter s indicates that the carbon atoms belong to the GLC surface). As noted above, this process is made possible by the formation of EDL on the carbon crystallite surface, which gives rise to an electric field within the crystallite bulk and, hence, induces redistribution of weakly bound conduction electrons towards more positively charged parts of the surface. The capacitance of the EDL formed at the GLC edge plane is several orders of magnitude higher than the capacitance of the basal plane EDL. Thus, the spontaneous reduction of palladium compounds deposited on the carbon material may be very significant for carbon supports that combine high specific surface area with a large contribution of edge planes of GLCs forming the carbon material.

The width of the band gap (E_g) separating the valence band of localized $2p_z$ electrons (π band) from the conduction band (π^* band), in which electrons can move through the GLC bulk towards the surface and participate in reduction reactions, depends on the degree to which GLC is similar to a graphite crystal. In graphite, the valence band and the conduction band almost meet ($E_g \approx 0$), but as the three-dimensional ordering (CSR) of the crystallite decreases, the width of the band gap increases to reach $\sim 0.2–0.5$ eV for graphite-like materials with CSR of ~ 2 nm.[293] Since the experimental value of the electron work function of graphitized carbon black (as a representative of highly ordered graphite-like materials) is ~ 4.5 eV,[290] while the calculated absolute potential of the standard hydrogen electrode is 4.43 V,[294] that is, the difference between the chemical potentials is only ~ 0.1 V, it can be taken that the reduction potential of GLC π-electrons in electrochemical processes would be mainly determined by the band gap. Thus, even if $E_g = 0.5$ eV, these GLC electrons would be thermodynamically able to reduce the $[PdCl_4]^{2-}$ complex to Pd^0 [the standard redox potential of the $[PdCl_4]^{2-}/Pd^0$ pair in acid medium is 0.591 V (Ref. 259)]. The transfer of two electrons from carbon to Pd^{II} gives a Gibbs free energy benefit of ~ 0.2 eV. A two-electron reduction of $[PdCl_4]^{2-}$ as a result of chemical reaction with graphite (with crystal destruction) is also possible; however, this reaction is thermodynamically less favourable than reaction (5). For example, the redox potential of the two-electron oxidation of carbon atoms in graphite

$$C + H_2O \rightarrow CO + 2\,H^+ + 2\,e \qquad (6)$$

amounts to 0.518 V. The four-electron oxidation of carbon to CO_2

$$C + 2\,H_2O \rightarrow CO_2 + 4\,H^+ + 4\,e \qquad (7)$$

with a potential of 0.12 V would be thermodynamically more favourable than reaction (5); however, implementation of this reaction requires simultaneous transfer of four electrons from one surface carbon atom to two Pd^{II} atoms, for example, *via* the formation of the hypothetical $C_{(s)}\cdots\{2\,[PdCl_4]^{2-}\}$ adduct. Meanwhile, this is unlikely, due to spatial and Coulomb restrictions.

Reaction (5), which is similar to the cathodic electrodeposition of metals,[295, 296] proceeds much faster than the diffusion of complex anions into pores and, hence, if the carbon support is made of granules in which the electron-

conductive carbon NPs can tightly contact with one another (*i.e.*, a granule acts as a common container of free electrons), then the reduction of Pd^{II} would mainly take place on the external surface of the granules and would give very large Pd particles (from 10 nm to several micrometres in size). When a granule is broken in the adsorption system, the number of particles increases (the number of potential Pd^{II} reduction sites increases, but their size and container electron capacity decrease). On the one hand, this leads to decreasing size of the palladium crystallites being formed, while on the other hand, their number is greater. Highly dispersed palladium particles of medium size of < 3 nm can be formed upon the reduction of $[PdCl_4]^{2-}$ by the carbon support and if the carbon surface was preliminarily enriched with oxygen groups.[297, 298] This effect can be explained by assuming that palladium(II) reduction sites (below referred to A_R) are carbon islands located at the graphene layer steps and separated from one another by C–OH and C=O groups. This assumption about the role of surface oxygen was confirmed by Oliveira *et al.*,[299] who ascertained that oxygen-containing groups (especially basic ones such as pyrone, ketone and quinone groups) facilitate the two-electron electrochemical reduction of benzyl bromide to toluene on the carbon cathode.

It is noteworthy that the coupled two-electron Pd^{II} to Pd^0 reduction pathway is kinetically more favourable than the pathway comprising two single-electron steps. At least, attempts to detect Pd^I compounds in the electrochemical reduction of the Pd^{II} chloride complex on a carbon cathode were not a success.[300] Analysis of the results of studies of the Pd^0–*p*-benzoquinone–Pd^{II}–hydroquinone redox composition (known in homogeneous catalysis) and electroreduction of other compounds of this class,[301–303] studies on identification of quinone groups on the surface of carbon materials [304] and studies of the electrochemical properties of specially synthesized carbon materials with increased content of quinone groups [305–308] suggest that the coupled transfer of two electrons proceeds *via* the formation of Pd^{II} adduct with the catechol groups of the phenanthrene edge of the graphene layer (Fig. 20).

In the context of the considered issue, that is, the nature of sites of spontaneous reduction of palladium(II) on the carbon crystallite surface, it is appropriate to take into account the data on nanographites obtained by Ziatdinov.[309, 310] According to X-ray diffraction data, nanographites consist of 3–4 graphene layers with the average in-plane dimension $L_a \approx 2$ nm and ~ 0.4 nm distance between the planes, *i.e.*, with the package thickness $L_c \approx 2$ nm (which is close to the CSR size of nanocrystallites of high-temperature NGC samples). For these nanographites at low temperature, EPR signals of localized spins and spin resonance of conduction electrons are observed simultaneously, with the intensity of the latter being proportional to the density of states of charge carriers at the Fermi level. According to measurements, the density of states of charge carriers at the Fermi level for nanographite crystallites is more than an order of magnitude higher than the corresponding parameter of the ordered three-dimensional graphite.

According to calculations, the electronic structure of nanographite particles critically depends on the edge shape. In the case of acene edges, up to 2% of the total number of π-electrons are concentrated near the Fermi level (for comparison, for bulk graphite, this is only $\sim 10^{-3}$% of their total number). The insertion of phenanthrene areas

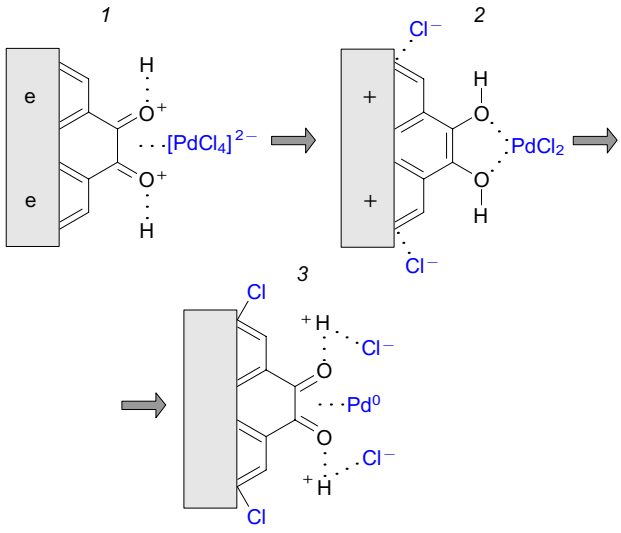


Figure 20. Presumptive steps of two-electron reduction of palladium(II) chloride complex taking place at the A_R sites of the carbon crystallite in acidic aqueous solutions: (*1*) adduct of the $[PdCl_4]^{2-}$ anion with the protonated *o*-quinone groups of the phenanthrene edge of the graphene layer (e are conduction electrons); (*2*) palladium(II) chloride adduct with catechol groups arising upon reduction of the *o*-quinone groups by conduction electrons; (*3*) Pd^0 adduct with *o*-quinone groups as the product of oxidation of catechol groups by palladium(II).

reduces the influence of acene edges on the electron state density, but in the case of crystallite that are several nanometres in size, this influence is still retained. If the armchair edge of the graphene layer has a defect, there is a local peak of the electron state density near the defect, with the peak energy being ~ 30 meV lower than the Fermi level. These data may be indicative of the fact that the sites of location of charge carriers, *i.e.*, the reducing function, are associated particularly with these defects, which, on contact with H_2O and O_2, can form C=O and C–OH groups, needed for the two-electron reduction of Pd^{II} with charge carriers. Data of several publications [311–314] suggest that the A_R site of CNGs is located at the protruding edge plane of the GLC and has a size of $\sim 1.5–2$ nm. This size corresponds to a step $\sim 4–6$ layers in height (because d_{002} of most NGCs is 0.35–0.37 nm), which is higher than the usual steps of 1–3-layer height. With the assumption that all π-electrons concentrated near the Fermi level are involved in the reduction of Pd^{II} to Pd^0, the amount of reduced palladium for a 2×2 nm GLC will be ~ 4 wt.%.

Considering the results of Zhang *et al.*,[315] it can be assumed that the Pd atoms formed in the A_R sites fill the defects of this site and thus form islands of amorphous palladium metal similar to A_R in size. This islands subsequently act as palladium cathodes on which larger particles of palladium metal may grow (as a result of the same Pd^{II} electroreduction with electrons of the crystallite). In view of the results of studies on the mechanism of palladium electrodeposition on graphite, gold and platinum cathodes [316–321] and assuming that the palladium-on-palladium deposition follows the same regular patterns, one can accept that this process involves the formation of the bridging structure $A_R(Pd^0)_n \cdots Cl \cdots Pd^{II}$, where $A_R(Pd^0)_n$ is an island of palladium atoms located on the

A_R site and providing fast inner-sphere two-electron transfer from A_R to Pd^{II}.

The Cl^- anions formed in amounts equivalent to the number of electrons spent by the carbon material for the $Pd^{II} \rightarrow Pd^0$ reduction are first adsorbed at those sites that have become electron-deficient to give $Cl^- - C^+_{(s)}$ ion pairs; some of them are rapidly converted to covalent-bonded $Cl - C_{(s)}$ pairs *via* charge transfer, *i.e.*, the surface of carbon crystallites is chlorinated at the sites of defects, in particular near Pd^0 atoms (see Fig. 20). However, some of the adsorbed Cl^- ions can be replaced by $[PdCl_4]^{2-}$ ions (ion exchange). The latter, being involved in equilibrium

$$2\,[Cl^-/C^+_{(s)}] + [PdCl_4]^{2-} \rightleftarrows [PdCl_4]^{2-}/2\,C^+_{(s)} + 2\,Cl^- \qquad (8)$$

can participate in the coordination binding of palladium.

In the case of coordination mechanism, $PdCl_2$ forms π-complexes with parts of the GLC surface containing C=C bonds,

$$[PdCl_4]^{2-} + C_\pi \rightleftarrows C_\pi \cdots PdCl_3^- + Cl^- \qquad (9)$$

$$C_\pi \cdots PdCl_3^- \rightleftarrows C_\pi \cdots PdCl_2 + Cl^- \qquad (10)$$

Reactions (9) and (10) occur on non-oxidized parts of the carbon surface and involve so-called C_π, or A_π sites (the sites of Pd^{II} coordinative anchoring), which can be differentiated in terms of the strength of their interaction with palladium chloride, estimated by treatment with various eluents. According to this characteristic, Simonov and coworkers [30, 235, 322] distinguished three types of these sites: weak (A_1), strong (A_2) and irreversible (A_3) adsorption sites. Presumably, type A_1 site is a hexagon located in the GLC basal plane; type A_2 site is a combination of C=C moieties belonging to both basal and edge planes that form a step; and type A_3 site is located in micropores formed by packing defects, *e.g.*, in slit-like pores (Fig. 21). Determination of the concentrations of these sites is based on the following fact: after saturation (attainment of the adsorption equilibrium) of the carbon support with the palladium chloride, $PdCl_2$ complexes with the A_1 sites occurring in equilibrium with $[PdCl_4]^{2-}$ are desorbed with water, complexes with the A_2 sites are desorbed with HCl ($1-5$ mol L^{-1}), while complexes with the A_3 sites are stable to these eluents. It was shown that for most graphite-like carbon materials (including NGC), the concentration of the weak adsorption sites A_1 is approximately equal to the sum of concentrations of the A_2 and A_3 sites.[322]

According to Simonov *et al.*,[30, 235, 290] the $PdCl_2$ molecules attached to the A_1 and A_2 sites *via* reactions (9) and (10) may interact with each other during water desorption (drying), thus forming three-dimensional $(PdCl_2)_n$ clusters, structurally resembling the orthorhombic α-$PdCl_2$, as a result of epitaxial interaction with the steps of the GLC edge plane. The epitaxy is possible owing to the similarity of the interatomic distances in the carbon support and α-$PdCl_2$ structures. It was also found that the highly dispersed state of supported palladium chloride (including clusters) is mainly maintained by the A_2 sites, which play the key role in the formation of Pd/C catalysts containing 0.5 to 5% palladium, because the surface concentration of the A_2 sites is usually an order of magnitude higher than the surface concentration of the A_3 sites.[235] It is noteworthy that the ligand strength of the A_2 sites, which are characterized by K_2 value, determined from the isotherm of $[PdCl_4]^{2-}$ adsorption on a carbon material, is related to their structural characteristics such as d_{002}, L_a (they together determine CSR) and g.

Due to low adsorption constants of the palladium chloride complexes on the A_1 sites and low content of the A_3 sites on the surface, the natures of the palladium compounds adsorbed on these sites have been barely studied experimentally. However, considering the achievements in the synthesis and studies of the formation mechanism and structure of the palladium complexes and clusters with arene ligands, it is possible to make some substantiated assumptions about the nature of these adsorbed states. A study of the crystals obtained from solutions containing Pd_6Cl_{12} and aromatic hydrocarbons (benzene, 1,3,5-trimethylbenzene, 1,2,4,5-tetramethylbenzene, hexamethylbenzene) showed that an arene and a palladium chloride cluster react in such a way that the arene molecule is arranged parallel to the plane of the $\{PdCl_4\}$ moiety of the cubic Pd_6Cl_{12} cluster with distances from 0.325 to 0.338 nm between the planes, depending on the nature of the arene (Fig. 22 *a*,*b*).[323] Spisak *et al.*[324] found that even stronger adducts with Pd_6Cl_{12} are formed by corannulene $C_{20}H_{10}$, which, unlike methyl-substituted benzenes, is oriented by a carbon atom of the C_5 ring, which leads to a shorter Pd···C distance (Fig. 22 *c*).

Complexes of one more type that is of interest for understanding the structure of palladium chloride clusters adsorbed on the carbon support are formed upon the reaction of arenes with palladium compounds in an oxidation state between 0 and +2. One of the first such compounds, $[Pd_2Cl_2(C_6H_6)_2(AlCl_3)_2]$, obtained by Allegra *et al.*[325] by the reaction of $PdCl_2$ with Al (reducing agent) and $AlCl_3$ in benzene, had a sandwich structure, with the Pd_2^{II} dimer sandwiched between two benzene molecules. Subsequently, attempts were made to prepare structures containing more than two palladium atoms in the sandwich filler. Murahashi *et al.*[326] obtained a sandwich consisting of the linear Pd_4^{II} cluster and two perylene molecules by the reaction of $[Pd_2(MeCN)_6][BF_4]_2$ and

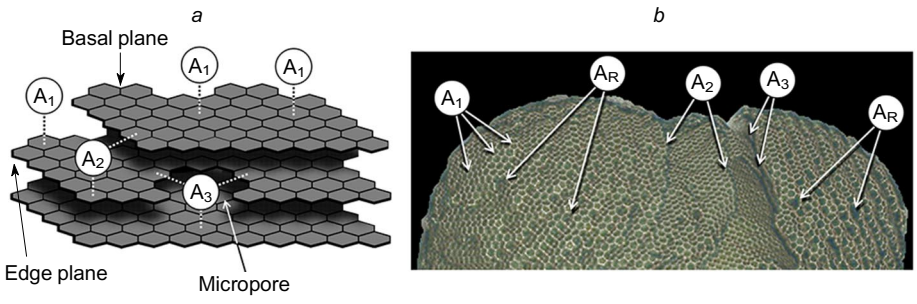


Figure 21. Conceptual model of positions of A_π sites for weak (A_1), strong (A_2) and irreversible (A_3) adsorption of $H_2[PdCl_4]$ on the surface of carbon supports and character of Pd^{II} chemical binding in these sites (*a*);[30, 290, 322] example of positions of the same sites and also A_R sites (Pd^{II} reduction sites) on the surface of a three-dimensional model of CNG obtained by LAMMPS [192] (see Section 2.2, Fig. 13) (*b*). Figure *b* is published with permission from I.Wald.

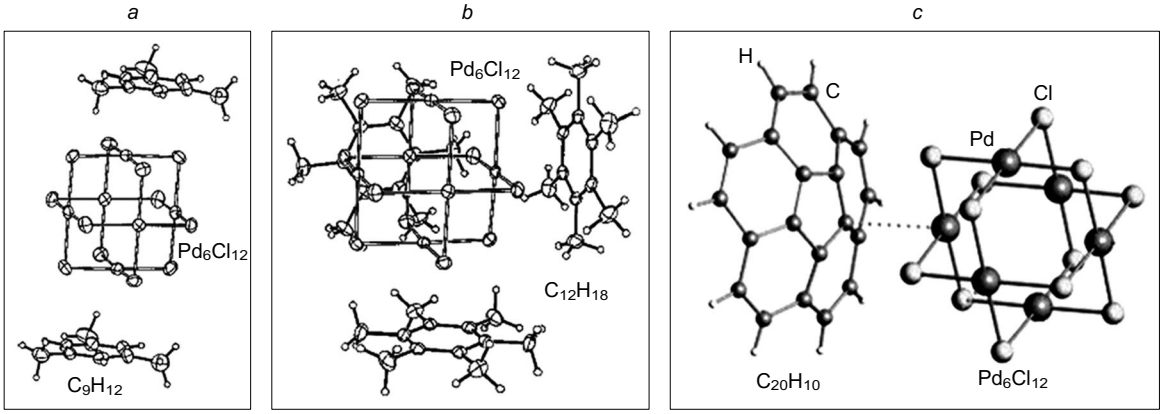


Figure 22. Relative positions of molecules: 1,3,5-trimethylbenzene and Pd_6Cl_{12} in the $[Pd_6Cl_{12}(C_9H_{12})]$ adduct (*a*), hexamethylbenzene and Pd_6Cl_{12} in the $[Pd_6Cl_{12}\cdot 1.5(C_{12}H_{18})]$ adduct (*b*),[323] corannulene and Pd_6Cl_{12} in the $[Pd_6Cl_{12}(C_{20}H_{10})]$ adduct (*c*).[324] Figures *a*, *b* are published with permission from the American Chemical Society, Figure *c* is published with permission from Elsevier.

$[Pd_2(dba)_3]$ dissolved in perylene ($C_{20}H_{12}$) (Fig. 23); the distance between the perylene planes was 0.42 nm, the Pd–C bond length was on average 0.22 nm; the line connecting the centres of palladium atoms was not strictly straight but arc-shaped, in line with the arrangement of carbon atoms located most closely to palladium atoms.

Thus, going back to discussing the nature of palladium compounds located in the A_1 and A_3 sites of the carbon support surface, with allowance for the above data, it can be assumed that the palladium chloride species adsorbed on the A_1 sites may represent single or associated Pd_6Cl_{12} molecules formed during drying, which are stabilized on the basal plane areas with bending defects (modelled by the adduct of Pd_6Cl_{12} with corannulene). Palladium compounds adsorbed on the A_3 sites (related to the presence of micropores) should evidently be modelled by sandwich complexes, as exactly these complexes can form in micropores due to the presence of closely spaced graphene layers (0.4–0.5 nm slits) and dangling C–C bonds, *i.e.*, carbon atoms with reducing properties needed for the partial reduction of Pd^{II} chloride complexes adsorbed from solution.

According to the model proposed by Simonov *et al.*,[30, 235, 290] oxygen-containing groups on the carbon support surface do not directly participate in the chemical binding of palladium(II) chloride complexes from acidic aqueous solutions, which was established experimentally by studying the structure of the supported chloride precursor of palladium by XPS[235, 288, 290] and EXAFS.[283] This is the basic distinction from binding of palladium chloride complexes to the surface of oxide supports, in which the key role is played by the functional OH groups, which directly chemically react with palladium complexes (ligand exchange).[31, 32, 242] Meanwhile, as noted above, oxygen-containing groups on the carbon surface can participate in the formation of EDL and thus affect the reduction potential of the support electrons. In addition, oxygen-containing groups, being the molecular structures of GLC edges, can also affect the ability of C=C moieties of the carbon surface to coordinate $[PdCl_4]^{2-}$ ions, which determines the stability of $C_\pi\cdots PdCl_2$ π-complexes. The data of several studies[327–329] suggest that oxygen functional groups located near A_π sites would increase the stability of π-complexes; hence, these group indirectly participate in the attachment of the chloride precursor of palladium to the support surface and thus affect the dispersion of the deposited palladium particles formed afterwards.

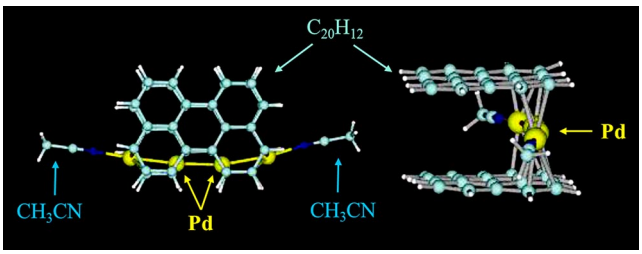


Figure 23. Model of the structure of the $[Pd_4(C_{20}H_{12})_2(MeCN)_2]^{2+}$ complex.[326] Published with permission from the American Chemical Society.

Thus, binding of $H_2[PdCl_4]$ to the carbon support from acidic aqueous solutions gives rise to the following deposited palladium species:

— palladium metal particles formed upon spontaneous reduction of the chloride precursor with the electron gas of the carbon crystallite in the A_R sites;

— various palladium(II) complex species formed upon complex formation of Pd^{II} chlorides with the A_π sites, represented by basal plane hexagons, edge plane C=C groups and defective structures of the GLC surface.

The predominance of a particular way of fixing palladium chloride complexes on the carbon surface and, hence, the quantitative relationship between various deposited palladium species depend on both the physicochemical state of the carbon support, determined by the preparation conditions and subsequent treatment of the material, and on the procedure and conditions of $H_2[PdCl_4]$ adsorption. The undesirable reduction of the adsorbed precursor by the carbon support, resulting in the formation of relatively large particles of palladium metal, would be suppressed if the Pd^{II}/Pd^0 oxidation potential is decreased (this can be done, for example, by decreasing the acidity and increasing the Cl : Pd atomic ratio in the solution) and the solution contains an oxidant (*e.g.*, H_2O_2 or O_2), which competes with palladium(II) for the electron gas of the carbon support.

Another approach used to prevent the reduction of Pd^{II} is based on carbon support treatment to decrease the surface concentration of the A_R sites associated with rough-

ness or the presence of relatively high (with a height of 5–6 graphene layers) surface steps (see below).

3.2.4. Reduction of palladium chloride compounds attached to the carbon surface. State of the forming clusters and palladium nanoparticles

Simonov *et al.*[30, 235, 288, 290] reported a detailed discussion of the formation of palladium nanoparticles on the carbon support upon the reduction of the deposited precursors by hydrogen. Note that the coarsely dispersed palladium particles concentrated at the periphery of carbon granules (that will be called primary Pd^0), which result from the chemical reaction of palladium chloride complexes with carbon ($Pd^{II} \rightarrow Pd^0$ reduction with electron gas; see Fig. 20), do not change by themselves under the action of hydrogen. Meanwhile, primary Pd^0 particles can grow as a result of reduction of surrounding $[PdCl_4]^{2-}$ anions adsorbed in holes; these anions can remain in the hydrated state even in the absence of liquid water phase (*i.e.*, after drying at 120–150 °C),[330] presumably as associates (clusters) of outer-sphere aqua complexes $\{m[PdCl_{4-x}(H_2O)_x] \cdot n H_2O\}^{m(x-2)}$, where $0 < x < 2$ and $m < n$. The structure of hydrated complex anions of platinum metal chlorides has been considered by theoretical methods.[263–265] The n value can be estimated using the data of Naidoo *et al.*,[264] who demonstrated that the outer coordination sphere (or the hydration shell) of the $[PdCl_4]^{2-}$ anion contains eight water molecules, which occupy the vertices of a square prism (see Section 3.2.1). In these aqua clusters, the outer-sphere water molecules connected by hydrogen bonds can generate a microliquid medium in the hydrophilic areas of the carbon support surface. In this medium, the $[PdCl_{4-x}(H_2O)_x]^{x-2}$ complexes are transferred to a primary Pd^0 particle and then reduced by hydrogen adsorbed on Pd^0. The palladium atoms or clusters thus formed, being bound to the metal phase at its boundary with carbon, can coalesce with primary Pd^0 to a single particle, which thus grows. The possible mechanism of this low-temperature coalescence was reported by Grammatikopoulos *et al.*[331]

The secondary Pd^0 particles are formed only upon reduction of $C_\pi \cdots PdCl_2$ π-complexes and $(PdCl_2)_n$ clusters. It is known from the chemistry of palladium complexes that the formation of colloidal palladium black on treatment of solutions of $H_2[PdCl_4]$ with hydrogen has an induction period, involving heterolytic activation of hydrogen to give unstable palladium(II) hydride, which occurs in equilibrium. The hydride is then converted to low-nuclearity ionic palladium clusters, starting with the Pd_2^{II} dimer (containing Pd–Pd bonds, to which homolytic addition of hydrogen takes place),[332–334] presumably, according to the following equations:

$$[PdCl_4]^{2-} + H_2 \rightleftarrows [(H^-)Pd^{II}Cl_3]^{2-} + H^+ + Cl^- \quad (11)$$

$$[HPdCl_3]^{2-} + [PdCl_4]^{2-} \rightleftarrows \quad (12)$$

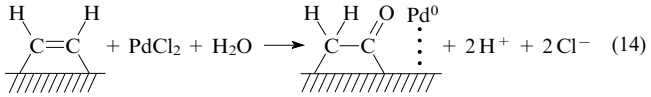
$$\rightleftarrows [Cl_2Pd^I - Pd^ICl_2]^{2-} + H^+ + 3\,Cl^-$$

$$[Cl_2Pd^I - Pd^ICl_2]^{2-} + H_2 \rightarrow \quad (13)$$

$$\rightarrow [Cl_2(H)Pd - Pd(H)Cl_2]^{2-} \rightarrow \cdots \rightarrow [Pd_nH_mCl_k]^{x-}$$

When $[Pd_nH_mCl_k]^{x-}$ type clusters appear, the induction period is completed, and the reduction of the remaining palladium(II) complex occurs rapidly by a mechanism similar to the successive growth mechanism, which is discussed above (see Section 3.1). Note that hydride species are formed much faster if the inner coordination sphere of palladium contains a hydroxy group that binds H^+ ions; as a result, equilibria (11) and (12) shift to the right. Palladium(II) chloro hydroxo complexes can be formed during drying of the $H_2[PdCl_4] \cdot n H_2O/C$ system upon insertion of the outer-sphere water molecules into the Pd^{II} inner coordination sphere and subsequent inner-sphere deprotonation, which is facilitated at higher temperatures.[261]

It is known that ethylene, propylene, butenes, *etc.*, readily reduce Pd^{II} chloride complexes in protic solvents (water, alcohols, acetic acid) to give palladium metal, and this reaction proceeds *via* the intermediate formation of inner-sphere π-olefinic Pd^{II} complexes (*e.g.*, $[Cl_2Pd(\pi\text{-}C_2H_4)OH]^-$, which then decomposes to Pd^0, acetaldehyde, H^+ and Cl^-).[327] Therefore, presumably, the hydrogen reduction of the adsorbed $(PdCl_2)_n$ oligomer may start with the formation of the first palladium clusters at the site of Pd^{II} π-binding to non-aromatic C=C structures (defects of the GLC edge plane or inclusions of amorphous carbon), *i.e.*, with a reaction like



(14)

However, it cannot be ruled out that inclusions of –Pd–(OH)–Pd– units can act as such sites for the onset of reduction. Apparently, palladium chloro hydroxyl moieties are most reactive towards hydrogen. Indeed, it was found[335, 336] that freshly precipitated palladium hydroxide is rapidly converted to palladium black on treatment with hydrogen even at room temperature. The product formed upon $PdCl_2$ hydrolysis by boiling water is converted to palladium black even on treatment with cyclohexane, which is simultaneously dehydrogenated to benzene.[213] The above indicates that in the synthesis of palladium–carbon compositions *via* palladium PHCs, the step of hydrogen reduction is relatively fast, and the palladium NP size distribution is specified by the corresponding distribution of supported PHC particles. When chloride precursors are used, the slower reduction step determines the size distribution of palladium NPs by affecting the distribution width and modality.

Thus, the co-existence of the two major pathways of interaction of the palladium chloride precursors with the carbon surface gives rise, upon hydrogen reduction, to a broad (in some cases, bimodal) size distribution of the resulting palladium NPs and to non-uniform distribution of the active component over the carbon support granule.[30, 235, 288, 290] The main cause for the lower dispersion of palladium in Pd/C catalyst is the formation of primary Pd^0 particles and $[PdCl_4]^{2-}/2\,C_{(s)}^+$ ionic species. The adsorbed palladium compounds as mononuclear $C_\pi \cdots PdCl_2$ π-complexes and epitaxial $C_\pi \cdots (PdCl_2)_n$ clusters are precursors of highly dispersed secondary Pd^0 NPs. If the adsorption conditions result in the formation of only these palladium species on the carbon support, the apparent dispersion of palladium NPs (determined by the chemisorption of probe molecules) does not depend on the Pd content in the Pd/C catalyst in the range where it is lower than that required to form a monolayer of palladium atoms on the surface of carbon crystallite. It was shown[290] that the catalysts with a

palladium content varying over a broad range (0.1 – 1.4 μmol m^{-2}), obtained by deposition of Pd^{II} chloride complexes on the carbon material Sibunit®, are characterized by similar and relatively high apparent dispersion (0.6 – 0.7), which corresponds to an average palladium NP size of 1.6 – 1.9 nm.

It was noted above that the supported precursor of palladium can be reduced either by treatment of dried sample with hydrogen gas at elevated temperature or by placing the sample into a solution of reducing agents (HCO_2Na, $NaBH_4$, CH_2O, N_2H_4, *etc.*).[28 – 33, 242] The method and conditions of reduction of the adsorbed chloride precursor of palladium have a considerable effect on the dispersion of the resulting palladium NPs.[31, 33, 237, 337 – 339] Neri *et al.*,[337] who studied the 1% Pd/C catalysts obtained by impregnation of active carbon with palladium(II) chloride complexes, found that the reduction of deposited chloride precursors by introduction of a solution of sodium formate into a suspension of $PdCl_2$/C composition gives rise to palladium NPs with an average size (~3 nm according to CO chemisorption and TEM) more than two times smaller than that in the samples obtained by treatment of the isolated and dried particles of this composition with hydrogen gas at 200 °C. In the latter case, an increase in the reduction temperature from 200 to 600 °C leads to a more than 7-fold increase in the average size of the formed Pd particles. Gurrath *et al.*[338] identified a non-monotonic dependence of the palladium dispersion in Pd/AC catalysts on the temperature at which hydrogen reduction took place.

Alcohols can also be used as reducing agents in the liquid-phase reduction of the deposited palladium precursors. In this respect, mention should be made of a study by Wang *et al.*,[340] who used ethanol, ethylene glycol and glycerol for this purpose. The authors found that the nature of the alcohol has an effect on not only the step of reduction of the adsorbed precursor, but also on the precursor formation from the palladium chloride complex and subsequent adsorption (Fig. 24). It was found that increasing number of hydroxyl groups (and the template properties of the alcohol) in the series ethanol < ethylene glycol < glycerol leads to higher dispersion of the resulting palladium metal NPs and, as a consequence, higher activity of the resulting catalyst towards the oxidation of benzyl alcohol to benzaldehyde.[340]

The liquid-phase reduction of supported palladium chloride complexes can be used to obtain palladium NPs of a smaller size than those obtained from the same precursor by hydrogen reduction without a solvent. Moreover, it was shown in a number of publications (*e.g.*, Ref. 339) that attempts to carry out additional hydrogen reduction of the catalysts reduced in the liquid phase lead to the formation of larger palladium particles. A possible explanation to this phenomenon follows from the assumption that palladium NPs obtained by liquid-phase reduction contain an increased proportion of charged $Pd^{\delta+}$ species that link Pd_n to defective structures of the carbon crystallite surface and thus decrease the probability of agglomeration.

According to the modern views,[41, 341 – 343] palladium NPs and clusters resulting from the reduction of a carbon-supported precursor form Pd – C bonds with various sites of the carbon surface. Model DFT calculations demonstrated that two types of bonds between Pd and C atoms are possible in the palladium/carbon system:

— donor-acceptor bonds resulting from the electron transfer from the carbon $2p_z$ orbitals to the vacant 5s orbitals of Pd and also in the opposite direction, from Pd 4d orbitals to C 2s orbitals;

— covalent Pd – C σ-bonds formed without participation of the π-electron system of the carbon support.[341, 342]

The length and strength of Pd – C bonds depend on the size of the attached cluster (or palladium NP) and on the nature of the surface site that retains the cluster (or palladium NP). According to published data,[41, 343 – 345] on going from a single atom to a palladium NP, the Pd – C distance increases and interaction with the support is weakened. For example, DFT calculations demonstrated that for the Pd_4 clusters attached to a smooth CNT surface, the Pd – C bond length is in the range of 0.194 – 0.211 nm,[344] whereas for the Pd_9/CNT system, this value is somewhat greater and can reach 0.244 nm.[345] The surface curvature of the graphene layer on which clusters are formed also affects the strength of the Pd – C bonds: binding of Pd clusters was found to be stronger on a curved surface (such as CNTs) than on a flat surface (such as graphite-like surface).[345] However, the strength of interactions in the palladium-on-carbon system is affected most appreciably by the microstructure of the carbon surface (degree of its inhomogeneity arising due to different configurations of the graphene edges, structure of the basal plane

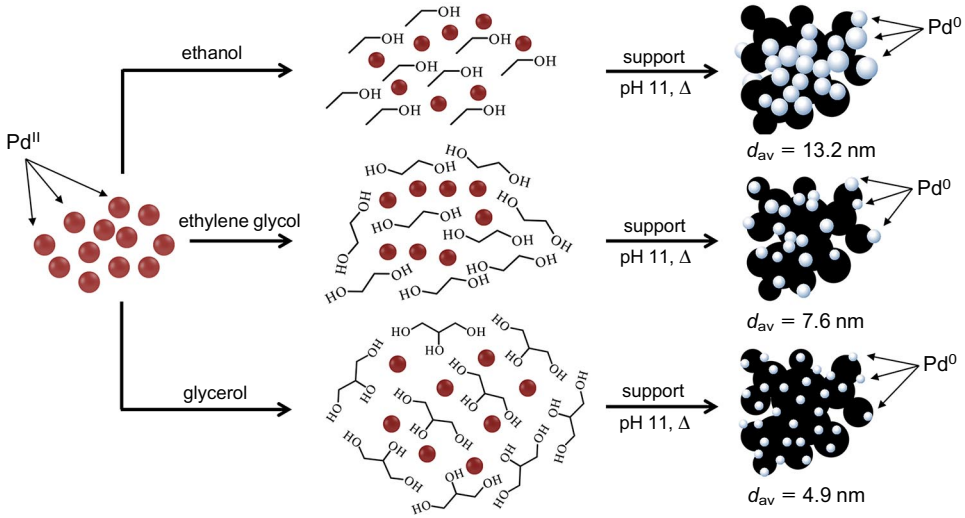


Figure 24. Scheme of the possible mechanism of formation of Pd/C catalysts (with Vulcan®XC-72 NGC as the support) by reduction of the chloride precursor of palladium by ethanol, ethylene glycol and glycerol.[340] d_{av} is the average size of metallic Pd NPs according to TEM data.

defects of GLCs and so on) and the physicochemical state of the surface (*e.g.*, GLC oxidation state or the nature of oxygen functional groups). The surface defects of the carbon support (such as various types of carbon vacancies in the graphene layers and heteroatoms) are beneficial for stronger binding of palladium. This prevents aggregation of palladium clusters and provides for higher dispersion of the supported metal.[41, 179, 341, 344, 346] For example, according to DFT calculations,[344] the reaction of Pd_4 clusters with oxygen-containing groups of the CNT surface gives rise to Pd—O bonds, which promotes stronger interactions in the palladium-on-carbon system.

Experimental studies of the metal—support interactions in the Pd/C compositions are described in numerous publications (see, for example [31, 32, 41, 290, 347–349]). In general, it was shown that several types of interactions are possible between the palladium NPs formed upon the reduction and the carbon surface. The types of interaction are determined by the nature of the carbon support (in particular, surface microstructure and physicochemical state) and conditions of catalyst preparation, including reduction conditions. The strong metal–support interactions (SMSI), which were first investigated and traditionally considered for oxide-supported metal catalysts,[350] was also found for the supported palladium–carbon compositions.[41] For example, it was shown [31, 41, 290, 348, 349] that SMSI in the Pd/C system induce changes in the structure, geometry and size of palladium NPs accompanied by charge transfer. Under certain conditions (*e.g.*, as a result of penetration of NPs into micropores), Pd nanoparticle can be completely or partially encapsulated into the support; in this case, it is coated by a carbon layer. The penetration of carbon into the NP and formation of carbide inclusions (as a result of chemical reaction) cannot be ruled out. An even more extensive interaction was found by Kochubey *et al.*,[347] who studied low-percentage palladium catalysts obtained by deposition of palladium chloride complexes on carbon nanofibres with a card deck structure (see Fig. 11 *b*, *2*) followed by the reduction by hydrogen at 250 °C. By means of TEM, EXAFS and model DFT calculations, it was shown that deposited palladium in concentrations of <0.2 wt.% mainly occurs in the catalyst as single atoms (in the atomic dispersed state), which penetrate between graphene layers of the support and are located near the surface (Fig. 25).

Perhaps, slit-like pores, which are type A_3 sites (see above) can provide for intercalation of palladium atoms into carbon crystallites. The intercalation of palladium atoms may increase the distance between the graphene layers in the carbon crystallite (at the palladium location points) from 0.335 to 0.375 nm.

The indicated SMSI in the Pd/C system lead to either partial or complete blocking of palladium clusters (nanoparticles); as a result, they may become inaccessible to the reactant molecules during the catalytic reaction. For the same reason, Pd/C catalysts often show deviations between the average Pd particle sizes determined by chemisorption of probe molecules (CO), on the one hand, and by TEM and XRD methods, on the other hand.[348] A number of approaches are used to minimize blocking of palladium particles to make them accessible to reactant molecules. One of these approaches is to transform the precursor into small and readily reduced aggregates. For this purpose, Simonov *et al.*[30, 290] proposed a fairly convenient method in which palladium chloride complexes were first hydrolyzed under strictly controlled conditions, which ensured the formation of colloid particles of PHCs [see reactions (2) and (2a) in Section 3.1].

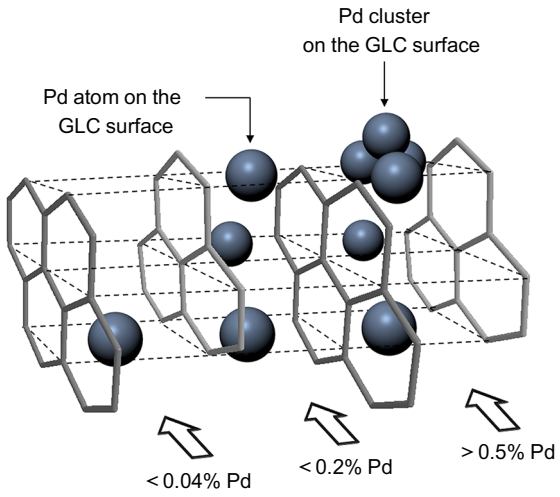


Figure 25. Possible positions of palladium atoms and clusters in the Pd/CNF catalysts depending on the palladium content.[347]

3.3. Role of the structural organization of nanoglobular carbon in the formation of active sites of Pd/NGC

Numerous studies [181, 351–359] demonstrated that the surface of CNGs that constitute a NGC particle is heterogeneous, *i.e.*, it is structurally and energetically non-uniform, which is due to the presence of structurally different adsorption sites (see above). Some sites differ little in the structure and they are expected to show minor differences in the energy of adsorption interactions (several kilojoules per mole); for other sites, this difference can reach tens of kilojoules per mole. Schröder *et al.*[351–354] studied the adsorption properties of NGC samples differing in the preparation method and morphology towards gases such as ethane and ethylene. The results allowed the authors to propose a model according to which they distinguished at least four types of CNG surface elements acting as adsorption sites:

— type I sites represent basal planes of GLCs;

— type II sites are amorphized carbon areas (composed of sp^2- and sp^3-hybridized atoms, see Section 2.2) as transient structures between neighbouring crystallites;

— type III sites are lateral faces (edges) of crystallites;

— type IV sites are slit-like voids between neighbouring crystallites.

The binding strengths of these surface elements with adsorbate (ethylene) molecules (adsorption energies) differ by 4–5 kJ mol^{-1} and increase in the order I < II < III < IV (Fig. 26). The ratio of the listed types of sites depends on the preparation method and structural organization of NGC (Table 2). In the grades of NGC prepared by the thermal method and consisting of relatively large single CNGs (150–500 nm), type I sites predominate almost completely (96% for N990 nanoglobules), while the percentage of strong adsorption sites is very low. Carbon nanoglobules that make up the furnace grades of NGC are highly aggregated, and their much smaller diameters (10–80 nm) give rise to high surface curvature and, as a consequence, high content of defects; therefore, for these materials, the percentage of strong adsorption sites (II, III and IV types) can exceed 30%.

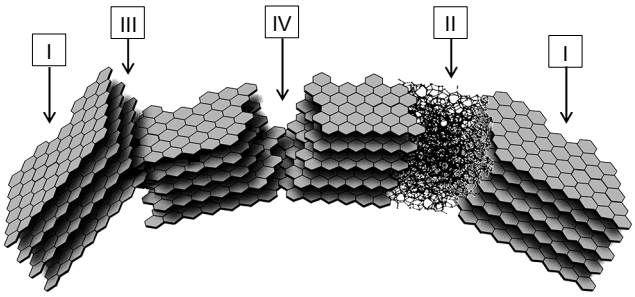


Figure 26. Model of the structure and positions of the adsorption sites for a part of CNG surface. For I–IV, see the text. The figure was created by the authors using published data.[351–354]

The CNG microstructure and, hence, the ratio of surface adsorption sites of various types are appreciably affected by high-temperature treatment (graphitization) of NGC at 2500–3000 °C; as a result of this treatment, the initially chaotically arranged GLCs grow along directions L_a and L_c (as a result of annealing of atomic vacancies in graphene layers) and become ordered, while the CNG size remains invariable.[3, 9, 322] According to Schröder *et al.*,[351–354] graphitization of the grade N220 furnace carbon at 2500 °C makes the CNG surface highly uniform: 99% of all adsorption sites occur in the basal planes of carbon crystallites (type I); type II sites disappear upon graphitization, while type III and IV sites remain only in trace concentrations (see Table 2). A similar result was reported by Simonov *et al.*,[181] who compared the surface microstructures for the initial and graphitized furnace NGC (Corax® 3) using high-resolution TEM and ^{129}Xe NMR spectroscopy.

The above data indicate that the structural and energetic surface non-uniformity of CNGs, first, plays an important role in fixing of palladium chloride complexes, thus determining the final state of the resulting palladium particles and, second, considerably depends on the preparation method, preparation conditions and pretreatment of NGC. Generally, this creates the scientific and technological basis for varying the properties and expanding the scope of applicability of Pd/NGC catalytic compositions.

The interaction of $H_2[PdCl_4]$ with the CNG surface and formation of Pd/NGC compositions are commonly studied using the model of A_π sites considered above,[31, 235, 289] although in some most recent studies,[360–362] preference is given to the structure model of NGC adsorption sites proposed by Schröder *et al.*[351–354] Comparison of these two models (*cf.* Figs 21 and 26) suggests that, upon attachment of $H_2[PdCl_4]$ to NGC, the adsorption sites of type I on the CNG surface correspond to weak adsorption sites (A_1), type II and III sites correspond to strong adsorption sites (A_2), and type IV sites correspond to irreversible adsorption sites (A_3). However, it should be borne in mind that this correlation is rather arbitrary, because the concentrations of adsorption sites in these models were determined by different methods and, what is more important, using chemically different adsorbates (ethylene in the case of Schröder model and $[PdCl_4]^{2-}$ in the case of the Simonov model). According to Romanenko and Simonov,[322] the concentration of the A_1 adsorption sites in many grades of NGC is, most often, approximately equal to the sum of concentrations of the A_2 and A_3 sites (Table 3); meanwhile, according to Schröder *et al.*,[351–354] the content of weak sites (type I) on the CNG surface is substantially higher than the total content of strong adsorption sites (types II, III and IV) (see Table 2). This difference may be attributable to the fact that type II (A_2) sites are more selective to the adsorption of Pd^{II} chloride complexes than type I (A_1) sites.

A detailed investigation of the interaction between $H_2[PdCl_4]$ and NGC and the state of the deposited palladium precursor were studied by Simonov and co-workers.[235, 289] It was shown that the palladium chloride precursor is attached to the surface of NGC by the coordination mechanism according to reactions (9) and (10). Under deposition conditions used by the authors, the reduction of chloride precursor with carbon, which should

Table 3. Specific surface area (S_{BET}) and relative content of A_π adsorption sites of palladium(II) chloride complexes on the surface of some NGC grades.[322]

NGC sample	S_{BET}, $m^2\,g^{-1}$	Proportion of A_π sites (%)		
		A_1	A_2	A_3
Elftex® 285	36	47	53	0
P245	105	49	49	2
Vulcan® XC-72	210	50	48	2
Ketjenblack® DJ-600	1284	52	46	2
Black Pearls® 2000	1505	53	44	3

Table 2. Structure characteristics and proportions of various surface adsorption sites for some grades of NGC.[145, 354]

NGC sample	Production method	Average CNG diameter according to TEM data, nm	Structure index based on the DBP absorption, $cm^3\,(100\,g)^{-1}$	S_{BET}, $m^2\,g^{-1}$ (see [a])	Proportion of surface sites differing in the ethylene adsorption energy (Q, kJ mol^{-1}) (%)			
					type I ($Q \approx 16$)	type II ($Q \approx 20$)	type III ($Q \approx 25$)	type IV ($Q \approx 30$)
N115	Furnace	17	113	143	69	13	15	3
N220	Furnace	21	114	118	84	7	7	2
N220g	Graphitization (2500°C, N_2)	–	–	88	99	0	< 1	< 1
N550	Furnace	56	122	44	93	6	1	< 1
N990	Thermal	285	43	9	96	0	3	1

Note. Here and in other Tables, dash means that this value is not reported in the published source. [a] Specific surface area determined by the Brunauer–Emmett–Teller method using nitrogen adsorption.

give rise to palladium metal particles, does not take place. These conditions of $H_2[PdCl_4]$ deposition on NGC (low temperature, excess of HCl, the presence of atmospheric oxygen) and the physicochemical state of the support (small grain size, relatively small specific surface area, the presence of oxygen functional groups) are used in the vast majority of cases to prepare Pd/NGC catalysts for practical use. They are favourable for fixing the chloride precursor on the CNG surface mainly or exclusively as palladium chloride. Simonov and co-workers[235,289] used X-ray diffraction method to determine the radial electron density distribution and demonstrated that the deposition of $H_2[PdCl_4]$ on NGC (PME-800 carbon black) and drying on the CNG surface gives rise to small $(PdCl_2)_n$ clusters with an average size of 1.8 nm and a structure resembling the structure of orthorhombic α-$PdCl_2$. Approximately 60 wt.% of the whole amount of NGC-supported $PdCl_2$ existed as these clusters. The rest of $PdCl_2$ remained in the molecular dispersed state, for example, as Pd_6Cl_{12} molecules. The key role in maintaining the highly dispersed state of NGC-supported palladium chloride [including $(PdCl_2)_n$ clusters] belonged to the C=C groups of the GLC edge steps on the CNG surface, that is, A_2 adsorption sites. In view of the moderate size of the steps of graphene packages (1–3 layers) and relatively small spatial length of their planes (1–3 nm) (see Figs 13 and 21 *b*), it can be assumed that the subsequent reduction of the palladium chloride clusters formed on them gives rise to palladium NPs bound to a combined $\{A_2 + A_1\}$ site.

Albers and co-workers,[360–362] who studied a 5% Pd/NGC sample (Evonik Industries catalyst; a type of NGC and its characteristics were not reported), found that the GLC edge sites on the CNG surface (type III sites corresponding to the A_2 sites) play a key role in the formation, growth and aggregation of palladium NPs. According to TEM data (Fig. 27),[360] highly dispersed palladium NPs (average diameter of 2.1 nm) are not randomly distributed over the CNG surface (as in the case of AC-supported catalysts), but form linear chains (aggregates), according to the arrangement of type III sites. In other words, the CNG surface acts as a template and specifies a definite arrangement (relative positions) of the deposited palladium NPs. Albers and co-workers[360] ascertained that in the 5% Pd/NGC catalyst they studied, ~90% of the whole amount of palladium supported on NGC occurred as organized aggregates, while the rest of palladium existed as isolated NPs.

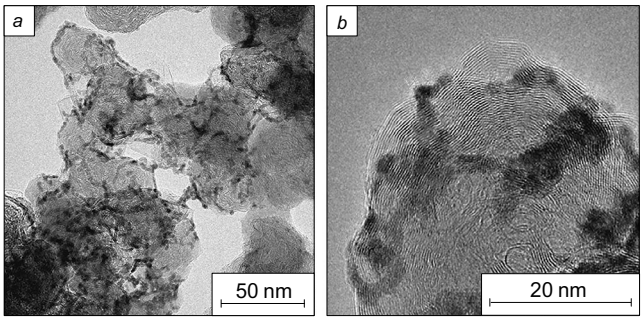


Figure 27. TEM images of the 5% Pd/NGC catalyst (Evonik Industries), in which positions of palladium NPs and their aggregates can be seen on the CNG surface.[360] Published with permission from Elsevier.

A recent study[363,364] addresses the formation of 1% Pd/NGC catalysts with carbon black samples of P145, P278-E and T900 grades being chosen as NGC. The samples differed in the method and conditions of preparation and, consequently, in the aggregate morphology and texture (Table 4). Despite the fact that the chosen supports had similar microstructure characteristics (d_{002}, L_c and L_a), they considerably differed in other characteristics such as the CNG diameter, average size of aggregates and the degree of aggregation (the number of nanoglobules in an aggregate). For example, the particles of the T900 grade NGC consisted of large single or slightly aggregated CNGs with an average diameter of 170 nm, while the same characteristics of P145 and P278-E were 22 and 31 nm, respectively. The number of nanoglobules in an aggregate reached tens or hundreds. Although Mironenko *et al.*[363,364] did not study the microstructure of the CNG surface, the results of Schröder *et al.*[351–354] suggest that the CNG surface of the T900 sample was fairly smooth and the percentage of the strong adsorption sites (types II, III and IV) was very low (< 10%). The furnace NGC types, P145 and P278-E, had markedly nonuniform CNG surface (defective and rough surface; this was especially characteristic of P278-E and accounted for its high specific surface area; see Table 4). The fractions of type III and IV sites for these materials were apparently higher than that for T900.

According to the results of temperature-programmed reduction (TPR) with hydrogen and to TEM data,[363,364] palladium chloride complexes supported on T900 were reduced in a narrow temperature range (not higher than at 98 °C) to give highly dispersed palladium NPs (average diameter of 2.5 nm) with a very narrow size distribution (Fig. 28). The TPR peaks for the supported precursor for samples based on P145 and P278-E were markedly broader and were shifted to higher temperatures (the maxima were at 120 and 139 °C, respectively), while the formed palladium NPs had a broad size distribution with an increased contribution of larger particles (especially in the case of 1% Pd/P145).

These results can be interpreted in the following way. As noted above, the surface of the T900 support is rather uniform in the type of adsorption sites (mainly type I); therefore, the supported palladium complexes have similar stability, are reduced at roughly the same temperature and form palladium NPs with similar sizes. The P145 and P278-E supports are characterized by higher fractions of

Table 4. Characteristics of NGC samples used to prepare 1% Pd/NGC catalysts.[363,364]

Characteristics	NGC sample		
	P145	P278-E	T900
Production method	Furnace	Furnace	Thermal
d_{002}, nm (see [a])	0.369	0.363	0.363
L_c, nm (see [a])	1.73	1.99	1.97
L_a, nm (see [a])	4.61	4.74	4.96
Average CNG diameter, nm (see [b])	22	31	170
Average aggregate size, nm (see [b])	205	197	700
S_{BET}, $m^2\ g^{-1}$ (see [c])	103	415	10

[a] XRD data; [b] TEM data; [c] data on nitrogen adsorption at −196 °C.

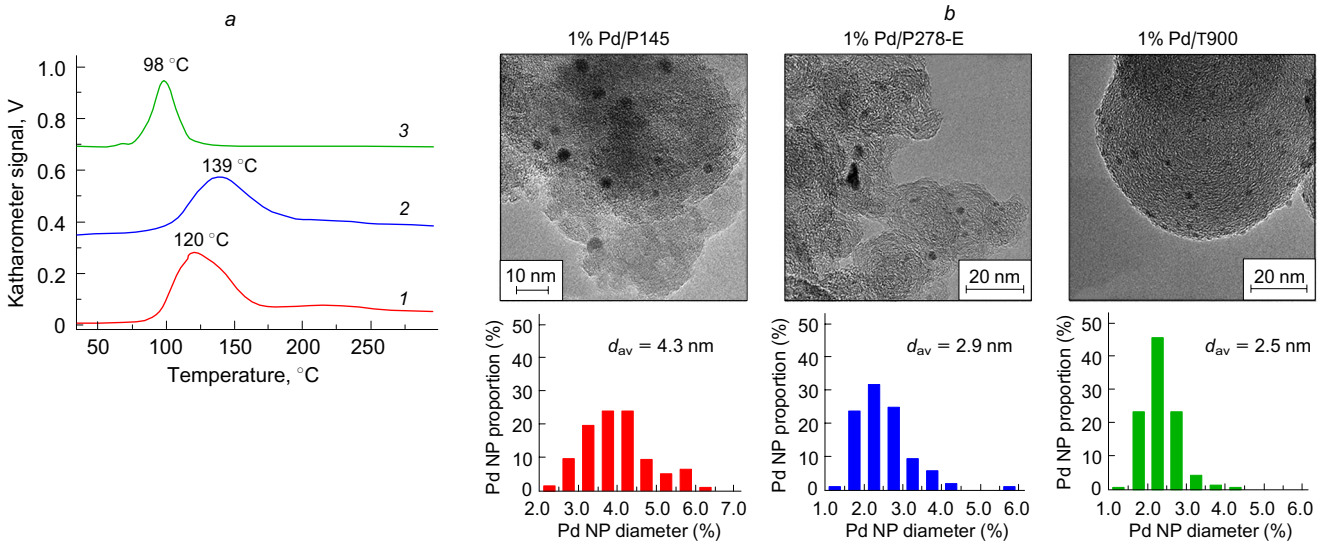


Figure 28. Profiles of TPR of the chloride precursor of palladium deposited on P145 (*1*), P278-E (*2*) and T900 (*3*) NGC in amounts corresponding to 1 wt.% palladium (*a*); TEM images and Pd particle size distribution histograms for these 1% Pd/NGC catalysts after reduction (*b*).[363, 364] Figure *b* is published with permission from Springer Nature.

strong adsorption sites (types II, III and IV), which strongly hold palladium chloride complexes, which are, therefore, reduced at higher temperatures (especially those adsorbed on type IV sites). Due to high constants of adsorption of palladium chloride complexes on these adsorption sites, the sites are indistinguishable towards these complexes, *i.e.*, they act as a common II + III + IV site.† Therefore, the adsorbed palladium(II) compounds bound to these sites are non-uniform, in particular, regarding their susceptibility for reduction; therefore, hydrogen consumption during the TPR takes place over a broad temperature range. For this reason, palladium NPs formed on P145 and P278-E supports have less uniform size distribution and a higher content of larger particles compared to 1% Pd/T900. These circumstances can account for the absence of increase in the degree of dispersion of supported metal particles with increasing specific surface area of the support, which is expected for low-percentage metal/support catalytic compositions.

4. Selective hydrogenation of organic compounds in the presence of Pd/NGC catalysts

It was noted above that the supported Pd/C catalysts represent the most important type of heterogeneous catalysts for hydrogenation of organic compounds (see Fig. 1); most often, special types of activated carbon are used as supports in these catalysts. The use of NGC (*i.e.*, carbon black) for this purpose is not popular so far, despite many experimental results that attest to high efficiency of Pd/NGC catalysts in liquid-phase hydrogenation reactions: depending on the catalyst preparation and reaction conditions, their catalytic characteristics (activity, selectivity and stability) may be not inferior or even superior to those of palladium catalysts based on other (oxide, carbon) supports.[365] Moreover, in some of modern studies, Pd/NGC catalysts are considered to be most promising for attaining high performance of selective hydrogenation of polyfunctional organic compounds. The interest in these catalytic compositions, which has increased lately, is also related to the possibility of more flexible and subtle control over structural characteristics, physicochemical properties of the surface, electronic and dispersion characteristics of supported palladium and, finally, the catalytic properties of the whole composition is possible for NGC than for other carbon materials.

Currently, the contribution of the support to the formation of structure and properties of deposited metal clusters and particles is the subject of intensive research in the field of catalysis. The morphology and dispersion of the deposited palladium particles and the type and strength of interaction between the palladium particles and the carbon support (up to the appearance of SMSI effects) are largely determined by the microstructure and physicochemical properties of the carbon surface (see above). If the catalytic reaction that takes place in the presence of a particular Pd/C catalyst is structure-sensitive,[366, 367] the size and structure of the supported palladium particles have a crucial effect on the catalyst activity and selectivity. This is also completely true for Pd/NGC systems. However, unlike other, more widely used Pd/C catalysts (which are conventionally prepared using AC and, lately, also CNTs and CNFs), the Pd/NGC systems are still little studied regarding the relationship between the structural and physicochemical characteristics of the support, which are determined by conditions of its synthesis, storage and post-treatment and by the catalytic properties of palladium active sites formed on the catalyst surface. In addition, the electronic structure of the deposited active metal clusters and particles has a significant effect on reactant adsorption and subsequent transformations on the catalyst surface. However, in the case of Pd/NGC catalysts, data concerning the relationship between the catalytic characteristics and the electronic state of the supported palladium, which is specified, among other factors, by the NGC surface chemistry, are very scarce.

† However, they can be distinguished by elution of the complexes (see above).

Apart from the effect of the support, the presence of other metals in the compositions can have more pronounced influence on the geometry and electronic structure of active sites. Bi- and polymetallic catalysts often show synergistic effect, due to the interaction of supported metals with one another; this is manifested as a pronounced enhancement of the catalyst performance in comparison with the same characteristics of monometallic catalysts.[368–373] This can account for the interest in bi- and polymetallic compositions, which has been lately expressed also in relation to Pd/NGC catalysts.

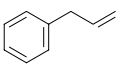
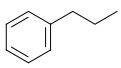
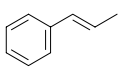
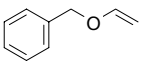
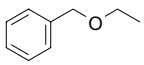
This part of the review addresses the applications of Pd/NGC systems in practically important hydrogenation reactions of organic compounds of various classes. The discussion is focused on the studies that pay some attention to the dependence of the catalytic properties of Pd/NGC on structural features of NGC and catalyst preparation conditions. The mechanisms of the considered reactions and the engineering aspects of modern processes are not discussed, but the list of references includes references to some publications that report detailed information on these issues.

4.1. Hydrogenation of alkenes (hydrogen addition to the C=C bonds)

Hydrogenation of the C=C bonds in organic compounds in the presence of supported palladium catalysts is a thoroughly studied and probably the most widespread hydrogenation reaction, which is carried out both in laboratory research and on an industrial scale.[7, 8, 11, 27, 374, 375] Among industrially important processes of hydrogen addition to C=C bonds in hydrocarbons that are conducted in the presence of Pd/C type catalysts, mention should be made of selective hydrogenation of cyclodienes and cyclotrienes to the corresponding cycloalkenes.[376–382] It is also noteworthy that Pd/Sibunit catalysts with a low palladium content were proposed for the large-scale hydrogenation of vegetable oils to obtain food products (so-called hardening of oil), instead of the conventional nickel systems, which serve as the source of hydrogenated fat contamination by toxic nickel.[383–386] Hydrogenation of polyfunctional organic compounds in fine organic synthesis often has be highly chemoselective to hydrogenation of C=C bonds in the presence of other functional groups able to add hydrogen (*e.g.*, carbonyl groups) in the substrate molecule. This requirement is met by the Pd/C catalysts, which are used, for example, for the selective hydrogenation of unsaturated carbonyl compounds in the synthesis of vitamins E and B_7.[11, 387, 388]

Experimental studies[235, 241, 389–394] showed the applicability of NGC-supported palladium catalysts for the hydrogenation of alkenes (Table 5). In some cases, these catalysts were not inferior or even superior to catalysts on other supports (oxide and carbon supports) in the characteristics (activity, selectivity).

Table 5. Examples of using Pd/NGC catalysts in the hydrogenation of alkenes (hydrogen addition to the C=C bonds).

Catalyst	Substrate	Hydrogenation conditions [a]	Substrate conversion (%)	Products	Selectivity (%)	Ref.
1.1% Pd/PM-105		EtOH, 0 °C, 0.1 MPa	–	–	–	235
Pd/Black Pearls® 2000		MeOH, 40 °C, 0.5 MPa, 0.5 h	100		–	389
Pd/Black Pearls® 2000		40 °C, 0.5 MPa, 0.25 h	82.3		–	390
0.73% Pd/NGC (NGC manufactured by Micromeritics)		No solvent, 75 °C, 0.4 MPa H_2	10–30		> 99	391
2.1% Pd/Vulcan® XC-72, coated by SiO_2 (7%)		MeOH, 21 °C, 0.2 MPa H_2, ~3.8 h	100		–	392
0.73% Pd/NGC (NGC manufactured by Micromeritics)		No solvent, 75 °C, 0.4 MPa H_2	> 99		81	391
					19	
1%Pd/P145		EtOH, 30 °C, 0.1 MPa, 1.5 h [b]	98		99	241
5% Pd/graphitized NGC (grade not indicated)		Hexane, 20 °C, 0.1 MPa	–		> 74.5	393
					< 25.5	
2% Pd/T900		MeOH, 22 °C, 1.0 MPa of H_2, 2 h	> 99		> 99	394

[a] The hydrogenation conditions indicated here and in other Tables include: solvent, temperature, pressure (the original sources do not always indicate whether this is hydrogen pressure or total pressure) and duration of the process; some parameter can be missing if they are not given in the cited source; [b] formic acid is used as the hydrogenating agent.

Ali *et al.*[391] showed advantages of the 0.73% Pd/NGC catalyst obtained by the magnetron sputtering of palladium NPs on NGC (the NGC type was not indicated, S_{BET} = 30 $m^2 g^{-1}$) over a 5% Pd/AC commercial catalyst (E101 NO/W, Degussa) in cyclohexene hydrogenation: under identical reaction conditions (batch process without a solvent; 75 °C, 0.4 MPa of H_2), the NGC-based sample had an almost 2.5-fold higher turnover frequency (TOF) than the activated carbon-based sample (35.1 and 13.4 s^{-1}, respectively).The authors noted that the TOF value of the 0.73% Pd/NGC catalyst they prepared in the hydrogenation of cyclohexene was 10 times higher than the activity of palladium-containing compositions based on oxide supports. Also, this catalyst demonstrated high selectivity to cyclohexene (81% for substrate conversion of >99%) in the hydrogenation of cyclohexa-1,3-diene. The selectivity was retained when the reaction was repeated many times. The simple and fast (0.5–12 min) magnetron sputtering method made it possible to vary the palladium content in the catalyst by varying the time of sputtering; the method always provided high shape and size homogeneity of the resulting palladium nanoparticles (according to TEM data, spherical NPs with an average diameter of 3.7–3.9 nm were formed, irrespective of the sputtering time).

Dubois *et al.*[392] showed that the supported palladium catalyst prepared using furnace NGC (Vulcan® XC-72) as the support was more efficient towards hydrogenation of cyclohexene than the palladium catalysts based on various types of activated carbon (DARCO® G60 and Norit® SX Plus). All catalysts were produced by impregnation using $H_2[PdCl_4]$ as the precursor followed by high-temperature reduction in a hydrogen flow. In order to prevent agglomeration (sintering) of the deposited palladium NPs during high-temperature treatment (up to 800 °C), the catalysts were coated with SiO_2 by deposition of organosilicon compounds followed by hydrolysis. The results demonstrated the advantage of the 2.1% Pd/NGC catalyst in the hydrogenation of cyclohexene: under identical conditions (batch process, MeOH, 21 °C, 0.2 MPa of H_2), the NGC-based sample showed an almost 50 times higher catalytic activity (1.062 mol g_{Pd}^{-1} min^{-1}) than samples based on activated carbon (not more than 0.021 mol g_{Pd}^{-1} min^{-1}). The authors noted that in the AC-based catalysts, palladium NPs were located within micropores of the support; this effect was enhanced by the deposition of SiO_2, thus additionally decreasing the accessibility of palladium for reactant molecules and, hence, decreasing also the catalyst activity. Meanwhile, the type of NGC used by Dubois *et al.*[392] did not have a clear-cut system of micropores; therefore, the palladium NPs were mainly located on the external surface of CNGs and were thus accessible to reactant molecules. In the Pd/NGC sample, supported silica did not block palladium NPs (as was the case for AC-based samples), but formed walls on the CNG surface, which physically prevented the agglomeration of NPs.

Yakukhnov *et al.*[241] developed a fast and simple approach to the synthesis of the Pd/NGC catalyst, which was highly efficient in the C=C bond hydrogenation. The preparation procedure, which lasted for <5 min, included stirring of an NGC suspension (P145 furnace NGC was used) in a solution of $[Pd_2(dba)_3]$ in $CHCl_3$ at 80 °C, filtering, washing and drying of the ready catalyst. It is noteworthy that this approach does not require reduction or other pretreatment of the catalyst, as the $[Pd_2(dba)_3]$ precursor decomposes after deposition on the carbon surface to give highly dispersed metallic palladium NPs (average size of 2.1 nm according to TEM data). The authors compared the activity of the 1% Pd/P145 catalyst prepared in this way in the hydrogenation of styrene to ethylbenzene (using formic acid as hydrogenating agent, EtOH, 30 °C, 1.5 h) with the activities of similar samples based on AC, graphite and CNTs in the same reaction. According to the results, the 1% Pd/P145 sample provided 98% conversion of styrene, whereas the catalysts prepared using other carbon supports did not ensure complete conversion of the substrate (Fig. 29 *a*). In addition, the 1% Pd/P145 sample demonstrate high activity and selectivity in the hydrogenation of a number of other substrates containing C=C bonds, either isolated or conjugated with a carbonyl group (Fig. 29 *b*).

The enhanced activity of this catalyst could be attributed, according to the authors,[241] to high dispersion and accessibility of palladium supported on NGC; in this case, palladium NPs were formed on the external surface of the support (in the case of AC, the particles were located in micropores) and were not agglomerated (unlike those in the graphite-based sample). Evidently, the carbon support structure plays the crucial role in the catalytic properties of the palladium–carbon composition. Owing to the globular morphology, the chosen type of NGC demonstrated the optimal combination of structural characteristics,

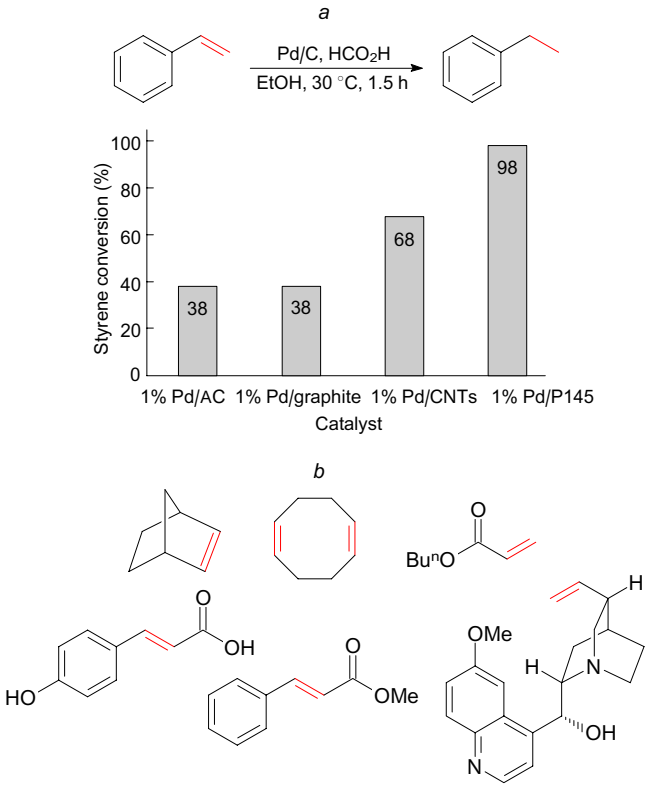


Figure 29. Comparison of 1% Pd/C catalysts regarding the styrene conversion during hydrogenation (*a*) and substrates that were used in hydrogenation (HCO_2H, EtOH, 50 °C, 2 h) to test the 1% Pd/P145 catalyst (*b*). The C=C bonds that undergo hydrogenation are highlighted in red. According to GC/MS and ^1H NMR data, the substrate conversion and selectivity were >99% in all cases.[241]

including the presence of defects on the CNG surface, which contributed to stabilization of palladium in the highly dispersed state, and an extensive system of interglobular pores needed for fast transport of reactant and product molecules.

Kim *et al.*[389, 390] demonstrated that the catalytic performance of the Pd/NGC compositions in the C=C bond hydrogenation can be varied over a broad range depending on the conditions of pretreatment of the support and conditions of the catalyst preparation. It was noted[390] that the oxidative pretreatment of NGC (Black Pearls® 2000 furnace NGC, Cabot, was used) with aqueous solutions of a $HNO_3-H_2SO_4$ mixture (1 : 1) with various acid concentrations (2, 4 and 8 mol L^{-1}) influenced the degree of dispersion of palladium particles in the reduced Pd/NGC catalysts and their activity in the liquid-phase hydrogenation of cyclohexene (batch process, 40 °C, 0.5 MPa). It was shown (see also Refs 389 and 395) that upon oxidative treatment, the NGC microstructure becomes more disordered (the intensity ratio of the D- and G-bands in the Raman spectra increases), its surface becomes enriched with oxygen-containing groups (according to IR spectroscopy data, mainly carboxy groups) and, in addition, the fraction of micropores markedly decreases. Study of the reduced Pd/NGC catalysts (prepared by deposition from a solution of $H_2[PdCl_4]$ using sodium citrate and sodium hydroxide and subsequent reduction in a solution of $NaBH_4$) demonstrated that the oxidative pretreatment of the support increases the dispersion of Pd particles in the catalyst and the cyclohexene conversion; the highest values are attained when the acid concentration is 4 mol L^{-1} (Fig. 30). Considering the views on the interactions in the Pd/C system (see Section 3.2.4), it can be assumed that the oxygen-containing groups, the concentration of which on the NGC surface increases upon the oxidative treatment, stabilize palladium in the highly dispersed state, thus creating a barrier against their agglomeration, and that the decrease in the content of micropores upon the pretreatment led to lower proportion of palladium particles located within these pores. However, as the concentration of the acids was further increased (8 mol L^{-1}), the authors[390] observed a considerable decrease in both the dispersion of the deposited palladium particles and the conversion of cyclohexene (see Fig. 30), which may be attributable to the destruction of the defective structures of the CNG surface layer — the centres of formation of highly dispersed palladium particles.

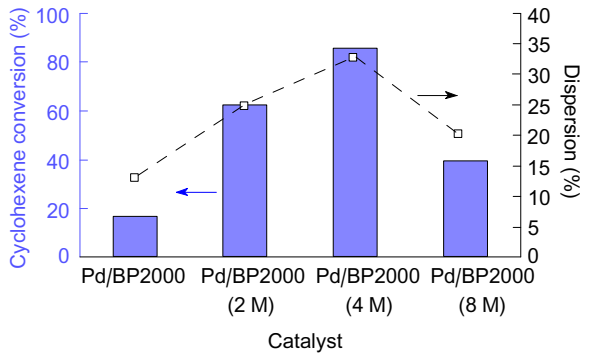


Figure 30. Comparison of palladium catalysts based on the pristine and pretreated Black Pearls® 2000 NGC samples (Cabot) in the dispersion of deposited palladium particles (CO chemisorption data) and the cyclohexene conversion during hydrogenation (batch process, 40 °C, 0.5 MPa). The concentrations of solutions of $HNO_3-H_2SO_4$ mixture used for oxidative pretreatment of the support are given in parentheses below the designations of catalysts. The figure was created by the authors using published data.[390]

Kim *et al.*[389] investigated the effect of preparation conditions of the Pd/NGC catalysts on their activity towards cyclohexene hydrogenation and on the dispersion state of palladium. The catalysts were prepared using the following approaches:

— deposition – precipitation from a $H_2[PdCl_4]$ solution with sodium carbonate (at 30 °C and pH 6) followed by reduction at 60 °C in a formaldehyde solution;

— deposition – precipitation from a $H_2[PdCl_4]$ solution using sodium citrate and sodium hydroxide (at 5 °C and pH 7) followed by reduction in a solution of $NaBH_4$;

— deposition – reduction using a $H_2[PdCl_4]$ solution as the palladium precursor and ethylene glycol as the reducing agent (polyol method).

In all cases, the same type of furnace nanoglobular carbon (Black Pearls® 2000, Cabot) was used as the support. According to the results, the dispersion of palladium particles and the activity of Pd/NGC catalysts (which was evaluated from conversion of the substrate) considerably depended on the preparation method. Both deposition methods based on precipitation gave catalysts containing highly dispersed palladium particles (2 – 5 nm according to TEM data), which ensured high activity of the catalysts in the hydrogenation of cyclohexene (batch process, MeOH, 40 °C, 0.5 MPa, 0.5 h). In the presence of most active of these catalysts (prepared using sodium citrate and sodium hydroxide and subsequent reduction with a $NaBH_4$ solution), complete conversion of cyclohexene was attained. The catalyst sample obtained by the polyol method contained rather large palladium particles (~20 nm according to TEM data), and the cyclohexene conversion in the presence of this sample was only 26% for the same reaction time.

Recently, Mironenko *et al.*[394] demonstrated that monometallic 2% Pd/NGC catalysts are very efficient in the hydrogenation of C=C bonds in vinyl derivatives such as benzyl vinyl and nonyl vinyl ethers, dodecyl vinyl sulfide and 9-vinylcarbazole. The supports used to prepare catalysts included multiwalled CNTs and P278-E (furnace type) and T900 (thermal type) nanoglobular carbons. The catalysts were prepared by deposition of $H_2[PdCl_4]$, $[Pd(OAc)_2]$, $[Pd_2(dba)_3]$ and palladium PHCs on these carbon supports and subsequent reduction to palladium metal. The authors demonstrated that the catalytic performance of the samples used in this reaction (in MeOH or benzene, 22 °C, 1.0 MPa H_2, 2 h) depended on both the type of NGC and the chemical nature of the palladium precursor. Many of the studied Pd/NGC catalysts were more active than the sample prepared using CNTs and provided a high selectivity (> 95%) to the corresponding ethyl derivatives (benzyl ethyl and nonyl ethyl ethers, dodecyl ethyl sulfide, 9-ethylcarbazole). Especially high performance was found for samples based on the T900 support. The results obtained by Mironenko *et al.*[394] suggest that this could be due, in particular, to the optimal structural characteristics of T900 (see Table 4), which apparently ensured high accessibility of palladium sites to the reactant molecules (see also other studies by Mironenko *et al.*[363, 364]).

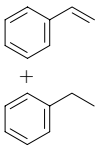
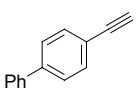
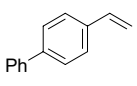
4.2. Selective hydrogenation of alkynes (hydrogen addition to the C≡C bonds)

The partial hydrogenation of the C≡C bonds in organic compounds in the presence of supported palladium catalysts is of particular interest as an efficient method for the synthesis of alkenes. Traditionally, alkynes are hydrogenated in the presence of palladium catalysts supported on oxides; the well-known Lindlar catalyst composed of palladium supported on $CaCO_3$ and partially poisoned by some lead salt and quinoline to increase the selectivity is often used.[8, 27, 374, 396, 397] The drawbacks of the Lindlar catalyst (fast deactivation, the presence of toxic lead compounds, the necessity to add quinoline) stimulated the search for other catalytic systems for alkyne hydrogenation that would be not inferior in selectivity, but simultaneously more cost effective and environmentally benign. Quite a few recently published experimental and review papers consider various aspects of partial hydrogenation of the C≡C bonds in organic compounds, including the synthesis and investigation of new highly selective catalysts for this reaction.[10, 11, 375, 397–404] Note that the main approach used to attain high yields of alkenes upon the catalytic hydrogenation of alkynes is optimization of the structure and physicochemical properties of the active surface of the catalyst with the goal to increase the thermodynamic selectivity, which is sensitive to these characteristics (the adsorption of alkyne on the catalyst should be much stronger than the adsorption of the corresponding alkene that is formed upon hydrogenation).[375, 404]

Currently, among the supported catalysts of partial hydrogenation of alkynes, considerable interest is aroused by mono- and bimetallic palladium-containing compositions supported on carbon materials that demonstrate high activities at low contents of the expensive metal and simultaneously meet the modern requirements imposed on selective catalysts for organic synthesis reactions. Among the industrially important C≡C bond hydrogenation reactions for which selective Pd/C catalysts were proposed, mention should be made of the partial hydrogenation of acetylene impurity present in ethylene produced by pyrolysis of hydrocarbon feedstock[405–408] and stereoselective hydrogenation reactions in organic synthesis: but-2-yne-1,4-diol to *cis*-but-2-ene-1,4-diol in the production of vitamin B_6 and insecticide endosulfan[11, 409–412] and hex-3-yn-1-ol to *cis*-hex-3-en-1-ol — a fragrance widely used in perfumery and food industry.[413–415]

The results of experimental studies[71, 240, 416–422] attest to a high efficiency of NGC-supported palladium (mono-, bi- and polymetallic) catalysts in the selective hydrogenation of various alkynes to the corresponding alkenes (Table 6). Furthermore, as will be shown below, modern achievements and approaches of nanochemistry are now used more and

Table 6. Examples of using Pd/NGC catalysts in the hydrogenation of alkynes (hydrogen addition to the C≡C bond).

Catalyst	Substrate	Hydrogenation conditions	Substrate conversion (%)	Products	Selectivity (%)	Ref.
1% Pd/NGC (NGC manufactured by Nihon Kasei)	HC≡CH	Static conditions, 30 °C, ~0.3 h	–	$H_2C{=}CH_2$ + H_3C-CH_3	–	71
1% Pd/Vulcan® XC-72R	HC≡CH in excess ethylene (1 : 70)	Gas-phase continuous flow hydrogenation at 35–125 °C	100 (at 105–125°C)	$H_2C{=}CH_2$	–	416
0.88% Pd/CD6026 (NGC manufactured by Columbian Chemicals)		MeOH, 50 °C, 0.1 MPa of H_2, ~7 h	100		96.9	417
9.1% Pd/Vulcan® XC-72		DMF, 25 °C, 0.1 MPa of H_2	–		–	418
9.1% Pd/Vulcan® XC-72R		DMF, 25 °C, 0.1 MPa of H_2, 0.25 h	100		89–92	240
Pd/Vulcan® XC-72		CH_2Cl_2, 30 °C, 0.1 MPa of H_2, 5 h	98		94	419
Pd/Ketjenblack®		CH_2Cl_2, 30 °C, 0.1 MPa of H_2, 8 h	95		95	419
Pd_3Fe/Vulcan® XC-72R		EtOH, 30 °C, 0.6 MPa of H_2, 5 h	100		~92	420
$Pd_3P_{0.95}$/Vulcan® XC-72		MeOH – H_2O, 25 °C, 0.1 MPa of H_2, 0.58 h	>99		96	421
$Pd_{33}Cu_{11}Ni_{29}P_{27}$/ Vulcan® XC-72		MeOH – H_2O, 45 °C, 0.1 MPa of H_2, 3.2 h	>99		>99	422

more often in the synthesis of Pd/NGC catalysts to provide high selectivity of the partial hydrogenation of alkynes (especially for the creation of controlled nanoarchitecture of the catalyst [423, 424]).

Benavidez *et al.*[416] compared the properties of palladium catalysts in the gas-phase hydrogenation of acetylene in excess ethylene. The supports were MgO, γ-Al_2O_3 and a furnace NGC (Vulcan® XC-72R). All catalysts contained 1% Pd and were prepared by deposition–reduction under identical conditions: the chosen supports were impregnated with a solution of palladium acetate in methanol; this did not require separate reduction of the precursor, because methanol acted simultaneously as the solvent and as the reducing agent. According to the obtained results, all of the tested catalysts provided complete conversion of acetylene under the same reaction conditions (continuous flow gas-phase hydrogenation, 70-fold excess of ethylene, 74–125 °C). In the presence of the Pd/NGC catalyst, no undesirable conversion of ethylene present in excess to ethane took place until the acetylene conversion approached 100%, whereas in the case of samples based on oxide supports, hydrogenation of excess ethylene started already when the acetylene conversion was <60%. The average diameter of the deposited palladium NPs differed little for the three samples (in the 0.7–1.0 nm range according to TEM data); however, according to XANES data, palladium in the Pd/NGC catalyst was completely reduced (Pd^0), whereas in the samples based on MgO and γ-Al_2O_3, the fraction of palladium in the oxidized state reached 15% (in terms of PdO). Therefore, the authors suggested that the low activity of Pd/NGC in the ethylene hydrogenation could be due to increased electron density on palladium for this sample (caused by the palladium–carbon interaction with electron donation by the support) and, hence, to decreasing hydrogen solubility in the material, which reduced the probability of undesirable exhaustive hydrogenation to ethane.

Domínguez-Domínguez *et al.*[417] studied the effect of the nature of carbon support on the dispersion of the supported palladium and catalytic properties of Pd/C compositions in the liquid-phase hydrogenation of phenylacetylene to styrene. As catalyst supports, carbon materials of various origin were used: AC obtained by chemical activation of anthracite possessing pronounced microporosity (S_{BET} = 2879 $m^2\,g^{-1}$) and also CNTs (NanoBlack™, Columbian Chemicals Co.) and NGC (CD 6026, Columbian Chemicals Co.) with predominantly mesoporous structure (S_{BET} = 253 and 214 $m^2\,g^{-1}$, respectively). All catalysts were prepared by the metal colloid method, *i.e.*, by deposition of Pd nanoparticles formed preliminarily in solution on the chosen support. According to the CO chemisorption and TEM data (Table 7), the Pd nanoparticles in CNT- and NGC-based catalysts were in the highly dispersed state (average size of 2.5 and 2.6 nm), whereas the Pd/AC sample contained much larger palladium NPs (average size of 5.6 nm) with a broad size distribution. Furthermore, for the last-mentioned sample, the average NP size calculated from CO chemisorption data proved to be markedly greater than the average size derived from TEM data, which may be indicative of location of palladium nanoparticles in AC micropores.

According to the results of comparative experiments (see Table 7), the obtained catalysts differed in the activity in the hydrogenation of phenylacetylene, but nevertheless they provided complete conversion of the substrate under mild reaction conditions (MeOH, 50 °C, 0.1 MPa). The Pd/NGC and Pd/CNTs catalysts demonstrated high selectivity to styrene (~97% at complete conversion of the substrate) and surpassed, in this characteristic, the AC-supported catalyst, which had the lowest activity with the greatest average size of palladium NPs.

Table 7. Effect of the nature of the carbon support on the average diameter of palladium NPs and catalytic properties of Pd/C samples in the liquid-phase hydrogenation of phenylacetylene to styrene (MeOH, 50 °C, 0.1 MPa).[417]

Catalyst	Average diameter of Pd NPs, nm		TOF, s^{-1} (see [a])	*X* (%) (see [b])	*S* (%) (see [c])
	CO chemisorption data	TEM data			
0.66% Pd/CNTs	2.7	2.5	0.96	100	97.4
0.88% Pd/NGC	2.9	2.6	0.86	100	96.9
0.65% Pd/AC	10.0	5.6	0.81	100	95.3

[a] TOF values were found as the ratio of the phenylacetylene hydrogenation rate to the palladium dispersion (based on TEM data); [b] phenylacetylene conversion based on gas chromatography (GC) data; [c] selectivity to styrene based on GC data.

Al-Wadhaf *et al.*[240] studied Pd/NGC catalysts in the partial hydrogenation of phenylacetylene and observed a similar trend towards decrease in the catalyst activity with increasing average size of palladium NPs. In this study, catalysts containing 9.1% Pd were prepared by impregnation of the same furnace NGC support (Vulcan® XC-72R). In order to vary the size of supported Pd nanoparticles in the ready catalysts, the authors used palladium precursors of various composition (η^3-allyl complexes) and various temperatures of hydrogen reduction. According to the results (Table 8), the deposition of the η^3-allyl palladium complex containing acetate ligands gave more dispersed palladium NPs after the subsequent reduction than the deposition of palladium allyl chloride complexes (for the same temperature of reduction).

The influence of the composition of η^3-allyl palladium complexes on the size of palladium NPs formed upon reduction is probably due to different reactivities of these

Table 8. Effect of the composition of the palladium precursor and the temperature of hydrogen reduction on the average diameter of palladium NPs and catalytic properties of 9.1% Pd/Vulcan® XC-72R samples in the liquid-phase hydrogenation of phenylacetylene to styrene (DMF, 25 °C, 0.1 MPa, 15 min).[240]

Palladium precursor	Reduction temperature, °C,	Average diameter of Pd NPs, nm (see [a])	Activity (see [b])	*S* (%) (see [c])
$[Pd(\eta^3\text{-}C_3H_5)Cl]_2$	120	4.0	70	96.8
$[Pd(\eta^3\text{-}C_3H_5)Cl]_2$	300	6.3	29	95.7
$[Pd(\eta^3\text{-}C_3H_5)(OAc)]_2$	120	3.1	87	97.0
$[Pd(\eta^3\text{-}C_3H_4CH_2OMe)Cl]_2$	120	8.0	58	96.5

[a] According to the data of electrochemical method based on O_2 adsorption;[425] [b] the activity was found as the ratio of the phenylacetylene hydrogenation rate to the amount of palladium in the catalyst ($mol\,g_{Pd}^{-1}\,s^{-1}$); [c] initial selectivity to styrene according to GC data (for phenylacetylene conversion of 20–30%).

complexes towards hydrogen.[238] In the case of Pd/NGC samples obtained from allyl palladium chloride, it was found that the higher the temperature of reduction of the deposited precursor, the larger the palladium NPs (generally, this is in line with the results obtained earlier for other Pd/C catalysts [337, 338]).

All Pd/NGC catalysts studied by Al-Wadhaf *et al.*[240] showed high (and similar) initial selectivity values (96–97%) in the partial hydrogenation of phenylacetylene (see Table 8). The increase in the substrate conversion induced a decrease in the styrene selectivity down to 89–92% for complete conversion of phenylacetylene. Meanwhile, the activities of the catalysts were markedly different, with the highest activity being inherent in the sample with the smallest average size of palladium NPs.

In some studies (see, for example Refs 426 and 427), hydrogenation of phenylacetylene to styrene in the presence of supported palladium catalysts was shown to be a structure-sensitive reaction, with higher TOFs and styrene selectivities being observed for greater average size (lower dispersion) of palladium NPs (most often, this is also true for hydrogenation of other alkynes [375, 397, 398, 404]). However, as can be seen from the above examples, this dependence does not necessarily hold for Pd/C catalysts. Also, it is known that the activity and selectivity of supported palladium catalysts in the partial hydrogenation of alkynes appreciably depend not only on the size of deposited palladium NPs, but also on their electronic state, the type (strength) of interaction with the support and the presence of modifying agents or admixtures.[398, 400, 403, 404, 427]

The publications discussed above [240, 417] do not present data on the electronic state or type of interaction of palladium NPs with the carbon support in the Pd/C catalysts. However, presumably, the electronic factor plays an important role for these catalysts by influencing the dependence of the activity on the average size of palladium NPs. The AC used by the authors [417] as supports were markedly structurally different from CNT and NGC supports; apparently, the disordered AC surface was enriched with oxygen-containing groups, which could decrease the electron density on palladium NPs, thus affecting the strength of interaction of the NPs with reactant molecules and, hence, the activity and selectivity of the catalyst. It was shown [419] that oxygen-containing groups, which are present in a higher concentration on the AC surface than on the NGC surface, have an unfavourable effect on the catalytic properties of Pd/C composition in the partial hydrogenation of phenylacetylene; for high selectivity to styrene, it is desirable that the electron density on palladium be increased,[428] which corresponds to lower binding energy of palladium $3d_{5/2}$ electrons in the X-ray photoelectron spectrum. Al-Wadhaf *et al.*[240] suggested that, after the reduction of NGC-supported allyl palladium chloride complexes, the ready catalysts can contain residual surface-bound chlorine, which changes the electronic state of palladium (decreases the electron density of palladium) and, hence, affects the catalytic properties of Pd/NGC.

Approaches directed towards restriction of the accessibility of the catalyst active surface to reactant molecules are often used to attain high selectivity in the partial hydrogenation of alkynes. In recent years, metal colloid methods in which ligands are anchored to Pd nanoparticles gained popularity for the preparation of supported palladium catalysts. The ligands not only retain NPs on the support surface, but also hamper the access of reactant molecules of a certain size.[399, 400, 404] In this respect, consider a study by Yoshii *et al.*,[419] who proposed an approach to the synthesis of Pd/NGC catalysts that were highly selective in the partial hydrogenation of phenylacetylene. The approach was based on immobilization of palladium NPs preliminarily formed in solution on a support (widespread furnace NGC such as Vulcan® XC-72 and Ketjenblack® were used). Before immobilization, the support surfaces were decorated with 11-[4-(1-pyrenyl)phenoxy]undecane-1-thiol ($PyC_{12}SH$) ligand molecules. According to XAFS and XPS data, immobilization of Pd($PyC_{12}SH$) was due to π–π-interactions (π-stacking) between the carbon surface and the pyrene groups of the ligand (Fig. 31 *a*). This approach ensured a high dispersion of the immobilized palladium NPs (according to high-angle annular dark-field STEM, the average diameter was 2.1 nm at a fairly narrow size distribution, Fig. 31 *b*), which was preserved during the catalytic reaction.

According to the results of comparative experiments (hydrogenation in CH_2Cl_2, 30 °C, 0.1 MPa of H_2), Pd($PyC_{12}SH$)/NGC catalysts were superior in the selectivity of styrene formation from phenylacetylene to the samples obtained by immobilization of palladium NPs on AC or pyrogenic SiO_2 (Aerosil) using the same approach and to the conventional Lindlar catalyst and 5% Pd/AC. For example, the sample based on Vulcan® XC-72 provided a selectivity to styrene of up to 94% for almost complete conversion of phenylacetylene (98% after 5 h of the reaction), while during further hydrogenation, the selectivity decreased to 75% due to the formation of ethylbenzene. The Lindlar catalyst and samples based on AC and SiO_2 were substantially active under the same conditions in the exhaustive hydrogenation to ethylbenzene; as a consequence, the selectivity to styrene sharply decreased during the reaction (in the case of Pd/AC samples, down to zero) due to the subsequent transformation of styrene.[419]

According to model DFT calculations, high selectivity of the Pd($PyC_{12}SH$)/NGC catalysts in the partial hydrogenation of phenylacetylene is due to the steric effect of pyrene groups of $PyC_{12}SH$, which form hydrophobic pores (average size of 0.35 nm, Fig. 31 *c*), thus restricting the access of styrene molecules to the NP surface and preventing styrene hydrogenation. (It is of interest that varying the solvent polarity allowed the authors to change the orientation of these pyrene groups and the distance between them and thus to control the activity and selectivity of the catalyst.) In addition, strong π-stacking between the carbon surface and Pd($PyC_{12}SH$) nanoparticles provides high stability and prevents leaching of palladium NPs from the support surface or agglomeration of NPs during the catalytic reaction (this was observed in the case of SiO_2-based sample); this is also favourable for high selectivity of the reaction.[419]

Having compared the structural characteristics of catalysts obtained using carbon supports [Pd($PyC_{12}SH$)/Vulcan® XC-72, Pd($PyC_{12}SH$)/Ketjenblack® and Pd($PyC_{12}SH$)/AC], Yoshii *et al.*[419] concluded that the strength of binding between decorated NPs and the carbon surface was enhanced with increasing degree of ordering (degree of graphitization) of the carbon support, which was the highest for Vulcan® XC-72. In the authors opinion, the absence of clear-cut defects on the smooth CNG surface was one of the causes why this type of catalysts provided a higher selectivity in the partial hydrogenation of phenylacetylene.

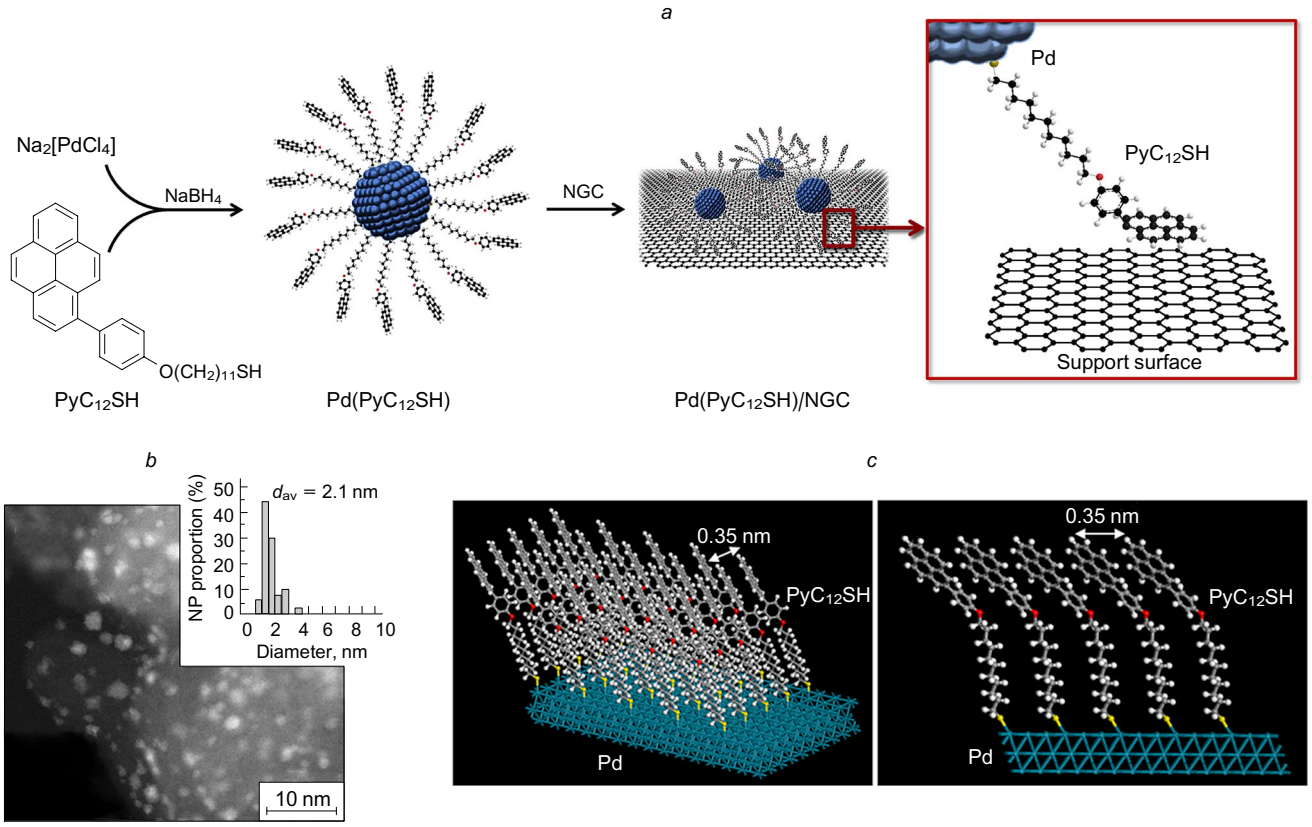
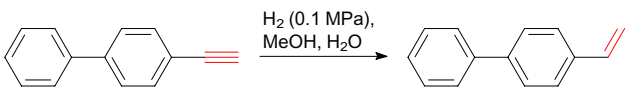


Figure 31. Scheme of formation of Pd($PyC_{12}SH$)/NGC catalysts in which palladium NPs are immobilized on the carbon surface *via* anchored $PyC_{12}SH$ ligand molecules (*a*); high-angle dark-field STEM image of Pd($PyC_{12}SH$)/Vulcan® XC-72 sample and NP size distribution histogram (*b*); optimized configuration of the $PyC_{12}SH$ molecules anchored to the Pd(111) surface, according to model DFT calculations (*c*).[419] Published with permission from the American Chemical Society.

A popular approach used to attain high activity and selectivity of supported palladium catalysts in the partial hydrogenation of alkynes is the introduction of other chemical elements (modification agents, promoters) into the catalytically active component. These additives can strongly influence the nature of metal – support interaction and the size and electronic state of deposited NPs and, hence, the binding strength between the reactant molecules and active sites.[397, 398, 400, 403, 404] In this regard, consider the data of Zhao *et al.*,[421, 422] who showed high efficiency of phosphorus-modified (mono-, bi- and polymetallic) palladium catalysts based on furnace NGC (Vulcan® XC-72) in the partial hydrogenation of various alkynes to alkenes. The catalysts were prepared using the metal colloid method, *i.e.*, by deposition of palladium-containing NPs (Pd–P, Pd–Cu–P, Pd–Cu–Ni–P), preliminarily formed and stabilized in solution, on the carbon support. The NPs were synthesized in one step from acetylacetonates $M(acac)_2$ (M = Pd, Cu, Ni) and triphenylphosphine (modifying agent) using a surfactant (trioctylphosphine oxide), reducing agent (borane adduct with *tert*-butylamine) and a stabilization agent (oleylamine). According to the authors,[421] the modified monometallic Pd–P/NGC catalyst (6.5% Pd) obtained in this way contained well-crystallized spherical $Pd_3P_{0.95}$ NPs with an average diameter of 4.8 nm and proved to be highly selective in the partial hydrogenation of phenylacetylene and other alkynes ($MeOH-H_2O$, quinoline, 25 °C, 0.1 MPa of H_2), providing almost complete conversion (Fig. 32). Furthermore, hydrogenation of alkynes with internal C≡C bond (1,2-diphenylacetylene, 1-phenylpropyne, ethyl 3-phenylpropiolate) resulted in highly stereoselective formation of *Z*-alkenes ($Z:E > 99\%$).

Zhao *et al.*,[422] while studying bi- and polymetallic palladium-containing systems (Pd–Cu–P, Pd–Cu–Ni–P) by XRD and high-resolution TEM, ascertained that at a copper content of <40 mol.%, the active component is formed as amorphous spherical NPs of relatively uniform size (average diameter of 10 nm). The polymetallic $Pd_{33}Cu_{11}Ni_{29}P_{27}$/Vulcan® XC-72 catalyst containing such NPs had very high performance in the partial hydrogenation of 4-ethynylbiphenyl ($MeOH-H_2O$, 45 °C, 0.1 MPa of H_2, 3.2 h): the substrate was completely converted to 4-phenylstyrene, which was not hydrogenated to 4-ethylbiphenyl (Scheme 1, Table 9). This catalyst showed a slightly higher performance than the $Pd_{26}Cu_{47}P_{27}$/NGC and $Pd_2Cu_{83}P_{15}$/NGC samples, in which the NPs were well crystallized due to increased copper content. In addition, considerable advantages of the NGC-based polymetallic catalyst were demonstrated over similar SiO_2-based catalyst, the $Pd_{75}Cu_{25}$/NGC catalyst obtained by impregnation

Scheme 1



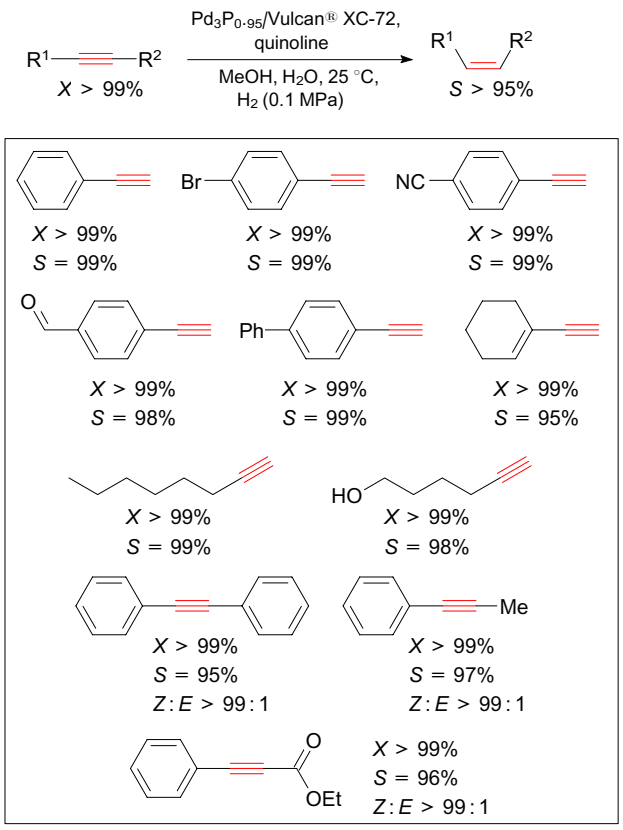


Figure 32. Alkynes used in the hydrogenation to test the $Pd_3P_{0.95}$/Vulcan® XC-72 catalyst.[421] *X* is alkyne conversion, *S* is selectivity to alkene (according to GC/MS and ^{1}H NMR data). Stereoselectivity is characterized by the ratio of selectivities to *Z*(*cis*)- and *E*(*trans*)-isomers (*Z*:*E*). The figure was created by the authors using published data.[421]

and containing no phosphorus, and conventional Lindlar catalyst.

In the authors' opinion,[422] high activity and selectivity of the polymetallic $Pd_{33}Cu_{11}Ni_{29}P_{27}$/NGC catalyst were attained owing to the amorphous morphology of the deposited NPs, which prevented the undesirable formation of palladium hydrides in the catalytic reaction, and owing to the synergistic effect of the metals, related to their interaction and formation of a nanoalloy, which was accompanied by a change in the electronic state of palladium. This study did not address the effect of NGC as a support for

Table 9. Catalytic properties of modified palladium compositions obtained using furnace type NGC (Vulcan® XC-72) as the support in the hydrogenation of 4-ethynylbiphenyl to 4-phenylstyrene.[422]

Catalyst [a]	Pd content (see [a])	Temperature, °C	Time, h	*X* (%) (see [b])	*S* (%) (see [c])
$Pd_{72}P_{28}$/NGC	3.92	25	2.5	99	97
$Pd_{26}Cu_{47}P_{27}$/NGC	7.23	45	3.5	95	96
$Pd_2Cu_{83}P_{15}$/NGC	0.68	45	3.5	99	97
$Pd_{33}Cu_{11}Ni_{29}P_{27}$/NGC	4.03	45	3.2	> 99	> 99

[a] Catalyst composition determined by ICP MS; [b] conversion of 4-ethynylbiphenyl according to ^{1}H NMR data; [c] selectivity to 4-phenylstyrene according to ^{1}H NMR data.

polymetallic NPs; however, the results reported in this paper (and in other papers) suggest that the physicochemical state of the NGC surface (defects acting as ligands) was an important factor, determining the size, morphology and composition of deposited NPs. For example, considering published data,[403, 405, 429–431] it cannot be ruled out that the interaction of palladium-containing NPs with the defective structures of NGC surface is accompanied by their contamination with carbon (see Section 3.2.4); this suppresses the formation of palladium hydrides (or dissolved hydrogen species) that are active towards non-selective hydrogenation of alkynes to alkanes.

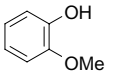
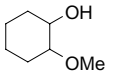
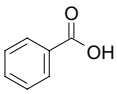
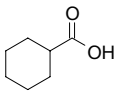
4.3. Hydrogenation of the benzene ring in aromatic compounds

The catalytic hydrogenation of benzene and its derivatives is an important and widely used method for the preparation of various alicyclic compounds, cyclohexane derivatives. The carbon-supported palladium catalysts were recognized to be highly efficient in arene hydrogenation [7, 8, 432, 433] and currently they are employed in large-scale production processes of cyclohexanone by hydrogenation of phenol,[7, 434–437] cyclohexanecarboxylic acid by hydrogenation of benzoic acid [7, 243, 434, 437] and dicyclohexylamine by hydroamination of phenol with aniline.[438, 439] A challenging issue of modern organic synthesis is to ensure high chemoselectivity of the hydrogenation of benzene ring when the substrate molecule contains other functional groups capable of adding hydrogen.[433, 440, 441] This is a complicated task, especially for the hydrogenation of polyfunctional aromatic compounds: due to the high stability of the benzene ring, the hydrogenation of which in the presence of heterogeneous catalysts usually requires relatively drastic conditions, more reactive functional groups (C=C, C=O, C–Cl, *etc*.) are the first to undergo hydrogenation or hydrogenolysis. However, it was shown [433, 440] that this task can be successfully solved, for example, in the case of chemoselective hydrogenation of phenols, using Pd/C catalysts modified by Lewis acids ($ZnCl_2$, $AlCl_3$).

A number of experimental studies [243, 429, 430, 442–446] demonstrated the applicability of Pd/NGC catalysts for the hydrogenation of benzene ring in aromatic compounds (Table 10); it was found that in some cases, these catalysts are not inferior and even superior in some performance characteristics (activity and/or selectivity) to palladium catalysts based on other carbon supports. Chen *et al*.[445] showed that a catalyst based on NGC (Alfa Aesar acetylene NGC, specific surface area of 75 $m^2\ g^{-1}$) containing 10% Pd is comparable in the catalytic performance in the chemoselective hydrogenation of phenol to cyclohexanone with analogous 10% Pd/C catalysts obtained using CNT and CNF supports and surpasses AC-based catalysts. In the synthesis of these catalysts, all carbon supports were preliminarily functionalized with polyaniline (PANI) by polymerization of aniline on the support surface in the presence of $(NH_4)_2S_2O_8$ as an oxidant (matrix polymerization method [447]). Then, $K_2[PdCl_4]$ was deposited from a THF–H_2O solution on the supports prepared in this way; the subsequent addition of an aqueous solution containing Na_2CO_3 and $NaBH_4$ induced the formation of supported palladium NPs.

Using IR spectroscopy and XPS, Chen *et al*.[445] found that PANI strongly immobilized on the carbon surface through π-stacking stabilizes palladium NPs by forming Pd–N bonds. Owing to its electrical conductivity,[447, 448]

Table 10. Examples of using Pd/NGC catalysts for hydrogenation of benzene ring in aromatic compounds.

Catalyst	Substrate	Hydrogenation conditions	Substrate conversion (%)	Products	Selectivity (%)	Ref.
5% Pd/NGC (NGC grade is not specified)		Cyclohexane, 150 °C, 5.0 MPa, 0.5 h	–	–	–	442
2.1%Pd/Black Pearls® 2000		Continuous flow gas-phase hydrogenation, 140 °C, 6.7 kPa of benzene, 90.7 kPa of H_2	< 10	–	–	429, 430
(1 – 10%)Pd/Vulcan® XC-72R		Continuous flow gas-phase hydrogenation, 60 – 230 °C, 4 kPa of benzene, 66.6 kPa of H_2	In a broad range		100	443
5.82% Pd/Black Pearls® 2000		Liquid phase, no solvent, 100 °C, 5.0 MPa, 1 h	12.1		100	444
5.79% Pd – 5.96% Ni/ Black Pearls® 2000		Liquid phase, no solvent, 100 °C, 5.0 MPa, 1 h	20.1		100	444
2.94% Pd – 3.08% Ru/ Black Pearls® 2000		Liquid phase, no solvent, 100 °C, 5.0 MPa, 1 h	17.6		100	444
3.10% Pd – 3.06% Ru – 5.60% Ni/Black Pearls® 2000		Liquid phase, no solvent, 100 °C, 5.0 MPa, 1 h	35.7 (100 after 6 h)		100	444
Pd/PANI-functionalized acetylene NGC (NGC manufactured by Alfa Aesar)		H_2O, 80 °C, 0.1 MPa of H_2, 9 h	> 99		> 99	445
5% Pd/Vulcan® XC-72R (support was treated with HNO_3)		Decane, 250 °C, 4.0 MPa of H_2, 1 h	54		76	446
5% Pd/NGC (NGC grade is not specified)		No solvent, 170 °C, 1.8 MPa of H_2	> 99.5		> 98	243

PANI provides for electron transfer between the carbon support and deposited palladium NPs. According to the results of comparative experiments, the Pd/PANI – NGC catalyst demonstrated very a high performance in the chemoselective hydrogenation of phenol (H_2O, 80 °C, 0.1 MPa of H_2, 9 h): the substrate was almost completely converted to cyclohexanone, while its subsequent hydrogenation to cyclohexanol was suppressed (Table 11).[445] Under the same reaction conditions, this catalyst was not inferior to the Pd/PANI – CNTs and Pd/PANI – CNFs samples in the catalytic performance and considerably surpassed the Pd/PANI – AC samples. According to the authors,[445] the higher activity of the Pd/PANI – NGC catalyst (as well as Pd/PANI – CNTs and Pd/PANI – CNFs) in the phenol conversion could be attributable to the electrical conductivity of PANI, which accelerated the reduction reactions and provided almost complete conversion of phenol.

Table 11. Catalytic properties of palladium compositions (10% Pd) based on PANI-functionalized NGC, CNTs, CNFs and AC in the hydrogenation of phenol to cyclohexanone (H_2O, 80 °C, 0.1 MPa of H_2, 9 h).[445]

Catalyst	*X* (%) (see [a])	*S* (%) (see [b])	
		cyclohexanone	cyclohexanol
Pd/PANI – NGC	> 99	> 99	< 1
Pd/PANI – CNTs	> 99	> 99	< 1
Pd/PANI – CNFs	> 99	> 99	< 1
Pd/PANI – AC	60	> 99	< 1
Pd/AC	55	89	11
Pd/CNTs	98	87	13

[a] Phenol conversion according to GC data; [b] selectivity to hydrogenation products according to GC data.

It is noteworthy that the palladium catalyst in which the carbon support was functionalized with nitrogen-containing, but non-conductive polyvinylimidazole was significantly less active under the same reaction conditions; the conversion of phenol with this catalyst was only 73%. Therefore, according to the hypothesized mechanism of phenol hydrogenation catalyzed by Pd/PANI – C (Fig. 33), phenol molecules adsorbed on the catalyst interact with PANI through the formation of strong OH···N hydrogen bonds and the hydrogen molecules are activated on the palladium sites. This is followed by hydrogenation reaction with destruction of the conjugation system of the benzene ring in phenol and isomerization of the resulting enol to cyclohexanone. Since the interaction of PANI with cyclohexanone is weak, the latter is easily displaced from the surface by the substrate (more acidic phenol), which prevents further hydrogenation of cyclohexanone to cyclohexanol.

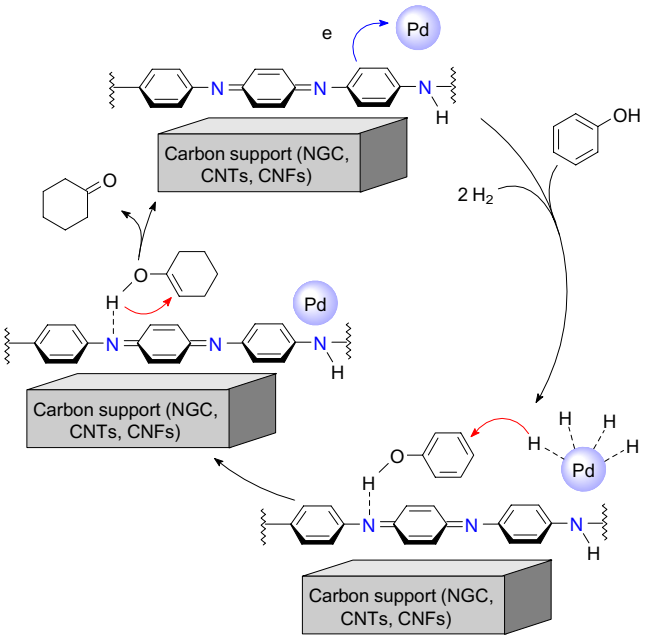


Figure 33. Mechanism of phenol hydrogenation to cyclohexanone in the presence of palladium catalysts based on PANI-functionalized carbon materials. The figure was created by the authors using published data.[445]

Lee *et al.*[446] compared the supported palladium catalysts based on γ-Al_2O_3, $Al_2O_3-SiO_2$ and NGC (Vulcan® XC-72R furnace black pretreated with nitric acid) containing 5% Pd in the liquid-phase hydrogenation of guaiacol (decane, 250 °C, 4.0 MPa of H_2, 1 h) and found that the Pd/NGC sample, although did not ensure complete conversion of the substrate, but still provided a relatively high chemoselectivity to the product of benzene ring hydrogenation, 2-methoxycyclohexanol, the subsequent hydrodeoxygenation of which was suppressed (Fig. 34). Meanwhile, the

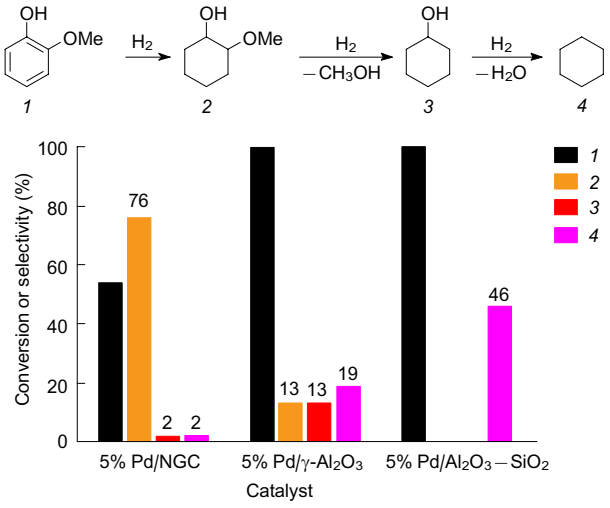


Figure 34. Conversion of guaiacol (*1*) upon hydrogenation in the presence of supported palladium catalysts and selectivity to 2-methoxycyclohexanol (*2*), cyclohexanol (*3*) and cyclohexane (*4*). Reaction conditions: decane as solvent, 250 °C, 4.0 MPa of H_2, 1 h; the products were analyzed by GC. The figure was created by the authors using published data.[446]

catalyst samples based on oxide supports, which had a much higher surface concentration of acid sites than NGC (according to the data of temperature-programmed desorption of ammonia), were highly active in the hydrodeoxygenation under the same conditions; therefore, cyclohexane was the predominant product (out of the products identified by the authors) of complete conversion of guaiacol in the presence of these catalysts.

A number of studies (for example, Refs 374, 440, 449) showed that the catalytic hydrogenation of the benzene ring in aromatic compounds in the presence of supported palladium catalysts is a structure-insensitive reaction, *i.e.*, specific activity of the catalyst (TOF) does not depend on the size and surface structure of the deposited palladium NPs. Meanwhile, it is known that the activity of supported palladium catalysts in the hydrogenation of aromatic compounds is considerably affected by factors related to interaction of palladium with the support surface, which depend both on the chemical nature of the support and physicochemical properties of the support surface and on the conditions of catalyst preparation and post-treatment.[449] In the case of palladium–carbon systems, this effect was demonstrated[429,430,443] in relation to the Pd/NGC catalysts, which were tested in the gas-phase hydrogenation of benzene. Krishnankutty and Vannice[429,430] studied the catalysts prepared by impregnation of a furnace NGC (Black Pearls® 2000, Cabot) with a solution of $Pd(acac)_2$ in THF followed by the reduction of deposited precursor in a hydrogen flow at 300 °C and demonstrated (see also Refs 450 and 451) that the appearance of carbon on the Pd NP surface and in their bulk (*e.g.*, palladium carbide inclusions) not only decreases the proporion of palladium accessible to adsorbed molecules, but also suppresses the formation of palladium β-hydride on contact with hydrogen, and this is a cause for decreasing catalyst activity in benzene hydrogenation. The part of carbon impurities resulting from the destruction of supported palladium acetylacetonate during high-temperature reduction was removed during the oxidative treatment of the catalyst in a flow of 4% O_2 and helium mixture at 300 °C and the repeated reduction in hydrogen, which induced a 2–3-fold increase in the catalyst activity (Table 12). The other carbon impurities that were not removed during the above procedure were due to the interaction of palladium with the carbon support surface. Only oxidation–reduction cycles repeated many times made it possible to completely clean the surface of palladium NPs and thus markedly increase the activity.

Jen *et al.*[443] used a set of physical methods (EXAFS, TEM, CO chemisorption, thermal analysis) to identify the causes for deactivation of Pd/NGC catalysts during the gas-phase hydrogenation of benzene (60–230 °C, 4 kPa of benzene, 66.6 kPa of H_2 and balance helium). The catalysts were prepared using a furnace NGC (Vulcan® XC-72R, Cabot), which was impregnated with an aqueous solution of $H_2[PdCl_4]$ or $Pd(NO_3)_2$ and then reduction was carried out by adding a solution of $NaBH_4$. The authors established, in particular, that the nature (strength) of interaction of palladium NPs with the carbon surface depends on the composition of the palladium precursor and considerably affects the adsorption and catalyst performance (activity and stability) of the Pd/NGC system. For example, in the case of 10% Pd/NGC catalyst obtained from $Pd(NO_3)_2$, the interaction with the carbon support was weaker than in the case of sample of the same composition, but prepared using $H_2[PdCl_4]$. In the latter case, stronger binding of palladium

Table 12. Activity of supported palladium catalysts obtained using a furnace NGC (Black Pearls® 2000) as the support and differing in the pretreatment conditions in the gas-phase hydrogenation of benzene (140°C, 6.7 kPa of benzene, 90.7 kPa of H_2).[430]

Catalyst	Support pretreatment conditions	Catalyst pretreatment conditions	Activity, 10^{-4} μmol g_{Pd}^{-1} s^{-1} (see [a])	TOF, 10^{-4} s^{-1} (see [b])
2.6% Pd/NGC	No pretreatment	Reduction in H_2 flow at 300°C	4	4
2.8% Pd/NGC	H_2 flow at 950 °C for 16 h	Reduction in H_2 flow at 300°C	454	360
2.8% Pd/NGC	H_2 flow at 950 °C for 16 h	Oxidative treatment in a flow of 4% O_2 and He mixture at 300°C followed by cooling in the mixture down to 27°C, then purging with He flow and reduction in H_2 flow at 100°C	927	1000

[a] The activity was found as the ratio of benzene hydrogenation rate to the weight of palladium in the catalyst; [b] TOF values were found with allowance for palladium dispersion from CO chemisorption data.

to the support provided higher stability of the deposited NPs against sintering during high-temperature treatment and five times higher activity in the hydrogenation of benzene (2.067 μmol g^{-1} s^{-1} at 90 °C) compared to the catalyst prepared by deposition of palladium nitrate (0.414 μmol g^{-1} s^{-1} at 90 °C). Having noted the important role played by the metal–support interaction in the formation of catalytic properties of Pd/NGC, the authors also admitted that the cause for the influence of the composition of palladium precursor on this interaction is still unclear.

One approach to increasing the performance of supported palladium catalysts in arene hydrogenation is to introduce other metals into catalysts.[374, 440, 452, 453] The interaction of the deposited metal NPs with one another (often to give a nanoalloy) may produce a synergistic effect, *i.e.*, the activity (selectivity) of bi- or polymetallic catalyst may by higher by a large factor than those of monometallic analogues.[368–373] In this connection, mention should be made of a study by Pei *et al.*,[444] who showed a high activity of the Pd–Ru–Ni trimetallic catalyst based on a furnace NGC (Black Pearls® 2000, Cabot) in the liquid-phase hydrogenation of ethylbenzene to ethylcyclohexane. This catalyst, containing 3.10 wt.% Pd, 3.06 wt.% Ru and 5.60 wt.% Ni, was prepared by replacing a part of nickel in the 11.78% Ni/NGC sample [obtained by deposition of a specified amount of $Ni(OH)_2$ on the chosen support and subsequent reduction with hydrazine hydrate] by adding $(NH_4)_2[PdCl_4]$ and $RuCl_3$ solutions to an aqueous suspension of the catalyst. Study of the ready catalyst structure using a set of spectral and microscopic methods showed that bimetallic clusters or highly dispersed Pd–Ru nanoparticles (nanoalloy) are distributed over the surface of $Ni/Ni(OH)_2$ composite nanoparticles (mainly <10 nm in size according to TEM data) deposited on NGC and that nickel is not included in the nanoalloy. As a result of interaction between the deposited metals, the relative content of electron-deficient palladium and ruthenium species in the trimetallic catalyst (XPS data) turns out to be higher than that in mono- and bimetallic samples (Pd/NGC, Ru/NGC, Pd–Ru/NGC, Pd–Ni/NGC, Ru–Ni/NGC).

According to the results of Pei *et al.*,[444] the Pd–Ru–Ni/NGC trimetallic catalyst proved to be fairly active in the hydrogenation of ethylbenzene (batch process without a solvent, 100 °C, 5.0 MPa, 1 h) and, under the same reaction conditions, it was markedly superior to not only monometallic, but also bimetallic catalysts in the yield of ethylcyclohexane and TOF (Fig. 35). An increase in the hydrogenation time in the presence of a trimetallic catalyst to 6 h (with other reaction conditions being unchanged) resulted in complete conversion of ethylbenzene to ethylcyclohexane (100% yield).

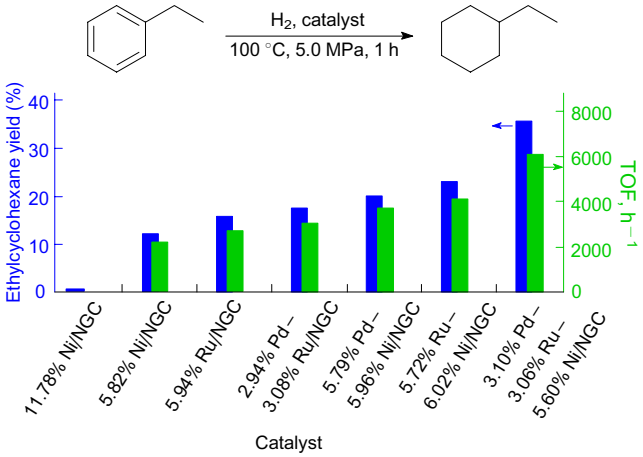


Figure 35. Comparison of the trimetallic Pd–Ru–Ni catalyst with mono- and bimetallic catalysts based on furnace type NGC (Black Pearls® 2000, Cabot) regarding TOF and the yield of ethylcyclohexane upon ethylbenzene hydrogenation. The catalyst compositions were established by ICP MS; the yield of ethylcyclohexane was calculated from GC data; TOF values were found as the ratio of the ethylbenzene conversion rate to the palladium dispersion (TEM data). The figure was created by the authors using published data.[444]

Considering their own results and published data, Pei *et al.*[444] suggested that the increased activity of the trimetallic catalyst was caused, in particular, by easy activation of the hydrogen molecules on highly dispersed Pd–Ru nanoalloy particles. The $Ni/Ni(OH)_2$ composite nanoparticles participated in the adsorption and activation of ethylbenzene molecules and, furthermore, stabilized Pd–Ru bimetallic clusters and nanoparticles on the surface, thus preventing them from being washed away during the catalytic reaction. This ensured the retention of high catalyst activity upon reuse.

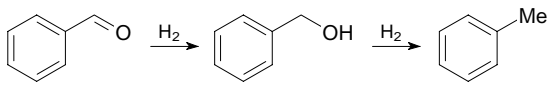
4.4. Hydrogenation of aromatic aldehydes

The hydrogenation of aldehydes with molecular hydrogen in the presence of heterogeneous catalysts is used most

widely in the practice of organic synthesis for the preparation of corresponding alcohols.[4, 8, 27, 454, 455] Out of the wide range of catalysts proposed for the selective hydrogenation of aldehydes to alcohols, preference is given, most often, to supported compositions containing noble metal NPs (especially Pd, Pt, Rh or Ru). As was emphasized in a monograph by Sheldon and van Bekkum,[4] supported palladium catalysts are most appropriate for liquid-phase hydrogenation of aromatic aldehydes, because their high activity under mild reaction conditions (5–100 °C, 0.1–1 MPa) provides for high yields of target alcohols, whereas, for example, ruthenium catalysts prove to be less active under the same conditions, and in the case of platinum and rhodium catalysts, side hydrogenation of the benzene ring in the aromatic substrate may take place.

The catalytic hydrogenation of aromatic aldehydes is of high practical importance for particularly benzaldehyde, cinnamaldehyde (3-phenylpropenal) and furfural. Benzaldehyde hydrogenation catalyzed by supported metal catalysts is used in the production of benzyl alcohol, which serves as a solvent for varnishes and resins and as the starting compound for the industrial production of a number of fragrances.[7, 456–458] This reaction can be accompanied by hydrogenolysis of the C–O bond to give toluene (Scheme 2); this decreases the yield of the target benzyl alcohol. Therefore, according to the data of modern publications (see, for example, a review by Bhanushali *et al.*[458]), the goal of developing catalysts for highly selective hydrogenation of benzaldehyde to benzyl alcohol is still relevant.

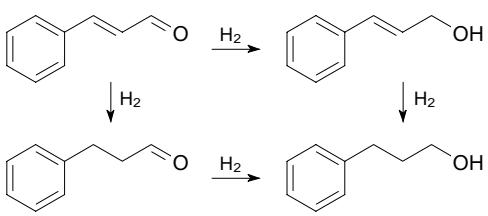
Scheme 2



Cinnamaldehyde is one of the most important representatives of α,β-unsaturated aldehydes containing an aromatic group. The catalytic hydrogenation of cinnamaldehyde can occur both as the addition of hydrogen to the C=C bond and as hydrogenation of the aldehyde group (Scheme 3). Therefore, despite different reactivities of the C=C and C=O bonds towards hydrogen, the attainment of high chemoselectivity in the hydrogenation of cinnamaldehyde, *i.e.*, the preparation of predominantly one of the possible intermediates (either 3-phenylpropanal or cinnamyl alcohol) is a challenging task.

Quite a number of recent experimental and review publications[402, 403, 459–462] are devoted to various aspects

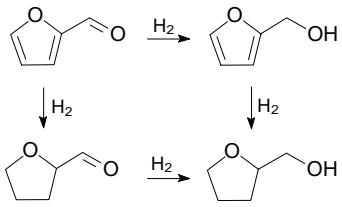
Scheme 3



of selective hydrogenation of cinnamaldehyde and especially the synthesis and investigation of new highly selective catalysts for this process. The high interest in these issues is related to the practical significance of hydrogenation of cinnamaldehyde, which is used to produce cinnamyl alcohol, 3-phenylpropanal and 3-phenylpropyl alcohol for perfumery.[4, 7, 456] In addition, cinnamaldehyde is a representative model substrate the hydrogenation of which is used to study the structure–activity (selectivity) relationships of supported metal catalysts.

Even more challenging is to attain high selectivity in the catalytic hydrogenation of furfural,[462–468] because in this case, first, hydrogen can add to not only the aldehyde group, but also to the C=C bonds of the furan ring (Scheme 4) and, second, hydrogenation can be accompanied by hydrogenolysis of C–O bonds, including furan ring opening reactions, which are especially intense at elevated temperatures and involve solvents. When furfural is hydrogenated in water under hydrothermal conditions, water participates in the hydrolytic furan ring opening reaction and in rearrangements to produce a broad range of various chemical products (Scheme 5), many of which are of interest.[466–471]

Scheme 4



In particular, this method can be used to convert furfural to cyclopentanone, which is widely employed in organic synthesis, for example, in the production of the fungicide pencycuron,[472, 473] the drugs cyclopentobarbital and cyclopentolate[472, 474] and jasmonic acid esters for perfumery.[456, 472]

Scheme 5

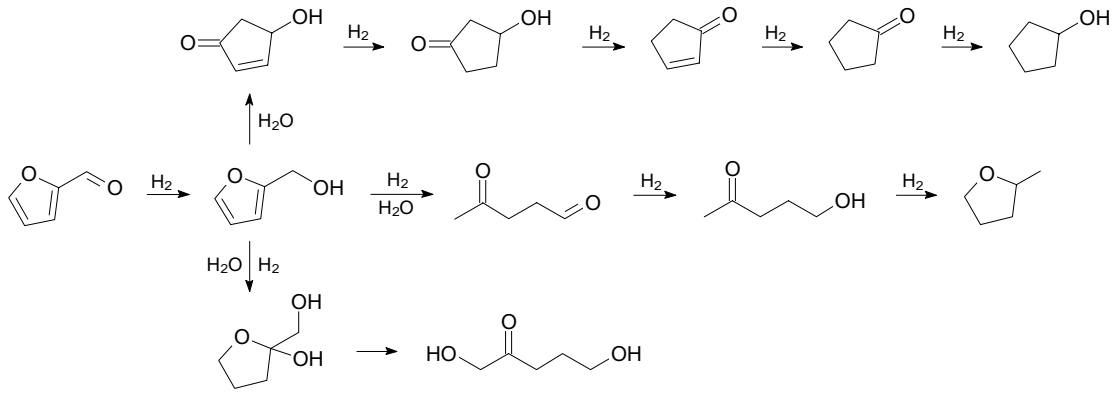


Table 13. Examples of using Pd/NGC catalysts in the liquid-phase hydrogenation of benzaldehyde (EtOH, 40 °C, 0.5 MPa of H_2).

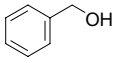
Catalyst	Time, h	Benzaldehyde conversion (%)	Selectivity (%)		Ref.
					
1.0% Pd/P278-E	2	100	84	8	475
1.5% Pd/P278-E	1	99	42	52	476
0.8% Pd–0.8% Ru/P278-E	1	100	86	10	476
0.5% Pd–1.2% Ru/P278-E	1	100	90	8	476

Table 14. Examples of using Pd/NGC catalysts in the liquid-phase hydrogenation of cinnamaldehyde.

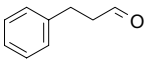
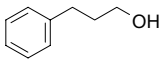
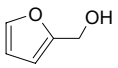
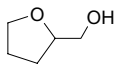
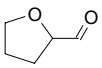
Catalyst	Hydrogenation conditions	Cinnamaldehyde conversion (%)	Selectivity (%)		Ref.
					
5% Pd/NGC (NGC manufactured by Wako Pure Chemical)	1,4-Dioxane, 30 °C, 0.1 MPa, 3 h	>99	95	5	477
2%Pd/Vulcan® XC-72	Toluene, 22 °C, 0.1 MPa, 0.8 h	100	60	30	478
2% Pd–7.8% Au/Vulcan® XC-72	Toluene, 22 °C, 0.1 MPa, 2.7 h	100	30	60	478
Pd–Co/Printex® U (N-doped support)	Cyclohexane, 50 °C, 0.3 MPa, 5 h	95	89	–	479

Table 15. Examples of using Pd/NGC catalysts in the liquid-phase hydrogenation of furfural.

Catalyst	Hydrogenation conditions	Furfural conversion (%)	Selectivity (%)						Ref.
									
1.5% Pd/P278-E	H_2O, 50 °C, 2.0 MPa of H_2	46	98	<1	0	0	0	0	480, 481
1.0% Pd/P145	H_2O, 50 °C, 3.0 MPa of H_2, 1 h	71	85	6	5	0	0	1	482
1.0% Pd/P145	H_2O, 150 °C, 3.0 MPa, 1 h	>99	0	3	0	18	48	22	482
1.0% Pd/P278-E	H_2O, 150 °C, 3.0 MPa, 1 h	72	0	4	0	21	58	3	470
1.0% Pd/T900	H_2O, 150 °C, 3.0 MPa, 1 h	98	0	1	0	22	57	6	470
8% Pd/Vulcan® XC-72	H_2O, 20 °C, 0.1 MPa of H_2, 8 h	>99	0	65	18	–	–	17	483
2% Pd/Vulcan® XC-72	Pr^iOH, 35 °C, 0.6 MPa of H_2	60	49.2	5.8	–	–	–	–	484
2% Pd/Vulcan® XC-72 (the support was oxidized with H_2O_2 and modified with SO_3H)	Pr^iOH, 35 °C, 0.6 MPa H_2	60	34.5	5.3	–	–	–	–	484
2% Pd/Vulcan® XC-72 (the support was oxidized with HNO_3 and modified with SO_3H)	Pr^iOH, 35 °C, 0.6 MPa H_2	60	34.0	10.8	–	–	–	–	484
3.0% Pd/Black Pearls® 2000	EtOH, 100 °C, 5.0 MPa, 1 h	97.6	0	10.8	–	–	–	–	485
3.0% Pd–2.1% Ni/$Ni(OH)_2$/Black Pearls® 2000	EtOH, 10 °C, 5.0 MPa, 2 h	100	90.7	1.9	–	–	–	–	485
1% Pd/Vulcan® XC	Pr^iOH, 180 °C, 2.0 MPa H_2, 5 h	46.7	24.3	7.2	–	–	–	–	486

Analysis of recent publications indicates that mono- and bimetallic palladium-containing compositions based on carbon materials can be considered as highly promising for selective hydrogenation of aromatic aldehydes. In particular, according to published data,[470, 475–486] Pd/NGC catalysts, depending on their preparation conditions and structure and physicochemical properties of NGC, can exhibit high activity and/or selectivity in the liquid-phase hydrogenation of benzaldehyde (Table 13), cinnamaldehyde (Table 14) and furfural (Table 15).

4.4.1. Hydrogenation of benzaldehyde

According to the results of Mironenko and co-workers,[475, 476] palladium catalysts obtained using a furnace NGC (P278-E) as the support were highly active in the liquid-phase hydrogenation of benzaldehyde (EtOH, 40 °C, 0.5 MPa of H_2). In the presence of 1.5% Pd/P278-E, almost complete conversion of benzaldehyde was attained, whereas the use of a similar sample based on CNTs resulted in only 32% conversion of benzaldehyde (Fig. 36).[476] However, the catalyst based on the P278-E support did not provide a high selectivity to benzyl alcohol (42%), since the product was further hydrogenated to toluene.

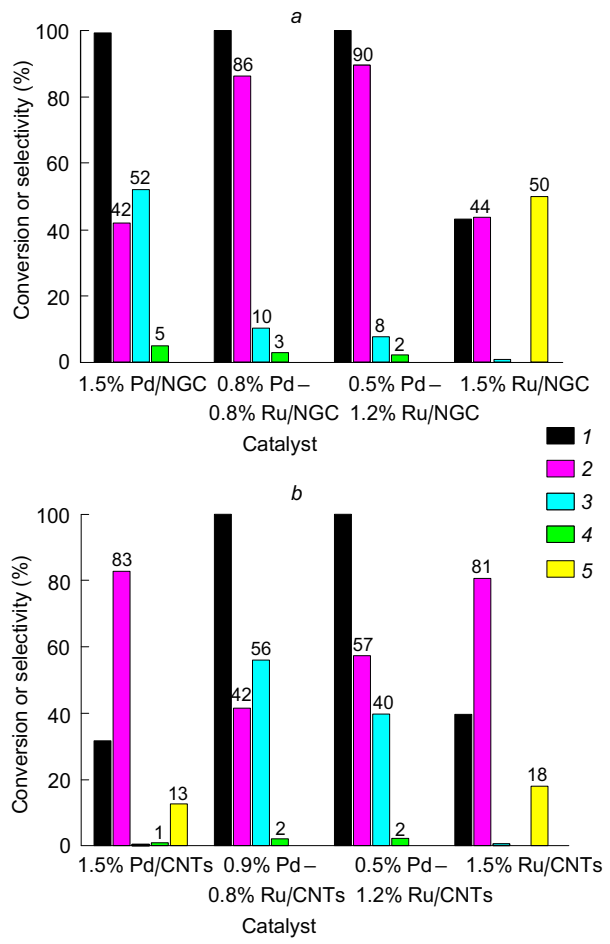


Figure 36. Benzaldehyde conversion (*1*) and selectivity to benzyl alcohol (*2*), toluene (*3*), (ethoxymethyl)benzene (*4*) and (diethoxymethyl)benzene (*5*) during hydrogenation catalyzed by palladium, ruthenium and palladium–ruthenium supported on P278-E NGC (*a*) and CNTs (*b*). Reaction conditions: EtOH as the solvent, 50 °C, 0.5 MPa of H_2, 1 h. The products were analyzed by GC. The figure was created by the authors using published data.[476]

With the goal to minimize the undesirable hydrodeoxygenation during the hydrogenation of benzaldehyde and, hence, to increase the selectivity to benzyl alcohol, Mironenko *et al.*[476] studied bimetallic Pd–Ru/C catalysts, which were prepared using the same supports, but differed in the Pd : Ru atomic ratio (1 and 0.4), with the total metal content in the catalysts being close to the palladium and ruthenium contents in monometallic catalysts (1.5 wt.%). Using TEM and XPS methods, it was shown that the deposited metals in the bimetallic catalysts form NPs of a highly dispersed palladium–ruthenium alloy with an increased proportion of electron-deficient palladium species, which can act as electrophilic sites for benzaldehyde adsorption and activation. The authors found that hydrogenation of benzaldehyde in the presence of bimetallic catalysts proceeds at a much higher rate than that with monometallic catalysts, with complete conversion of the substrate being reached within an hour under mild reaction conditions (EtOH, 50 °C, 0.5 MPa) (see Fig. 36).[476] However, the Pd–Ru/CNTs catalysts exhibited high activity not only in the hydrogen addition to the aldehyde group of benzaldehyde, but also in the hydrogenolysis of the C–O bond; as a result, the selectivity to benzyl alcohol was markedly lower than in the case of monometallic Pd/CNTs and Ru/CNTs samples (see Fig. 36 *b*). The Pd–Ru/P278-E catalysts surpassed both monometallic Pd/P278-E and Ru/P278-E samples and analogous bimetallic catalysts based on CNTs. They ensured complete conversion of benzaldehyde with high selectivity (up to 90%) to benzyl alcohol (see Fig. 36 *a*).

4.4.2. Hydrogenation of cinnamaldehyde

Harada *et al.*[477] carried out a comparative study of 5% Pd/C catalysts, differing in the nature of the carbon support and conditions of deposition of palladium precursor, in the selective hydrogenation of cinnamaldehyde to 3-phenylpropanal. As catalyst supports, the authors used AC (S_{BET} = 1500 $m^2 g^{-1}$) and NGC (the type or grade were not indicated, S_{BET} = 80 $m^2 g^{-1}$) manufactured by Wako Pure Chemical and also mesoporous carbon material CMK-3, which was obtained by sucrose carbonization using mesoporous silica (SBA-15) as a template. Each catalyst was prepared by adding an aqueous solution of $Na_2[PdCl_4]$ to a suspension of carbon support in aqueous NaOH followed by reduction of the deposited precursor by KBH_4. The authors varied the molar ratio γ = [NaOH] : [$Na_2[PdCl_4]$] during the synthesis in the 0 to 20 range, which allowed them to control the size of palladium NPs and the uniformity of their distribution in the ready catalysts.

According to XRD and TEM data, it was shown that deposition of the palladium precursor on the carbon support without addition of NaOH (γ = 0) and the subsequent reduction gave rise to rather large palladium NPs (Fig. 37 *a*) highly non-uniform in size. The addition of NaOH (γ = 2–10) led to hydrolysis of the chloride precursor to palladium hydroxo complexes, which were reduced to give dispersed and size-uniform palladium NPs (average diameter < 5 nm). However, if NaOH was present in a large excess (γ = 20), colloidal $Pd(OH)_2$ particles were formed; their subsequent reduction resulted in the formation of large aggregates of palladium particles. It is noteworthy that this trend was clearly pronounced when AC or CMK-3 support was used, whereas in the case of NGC, the average size of palladium NPs in the ready catalysts varied over a narrow range and did not exceed 8 nm over the whole wide range of

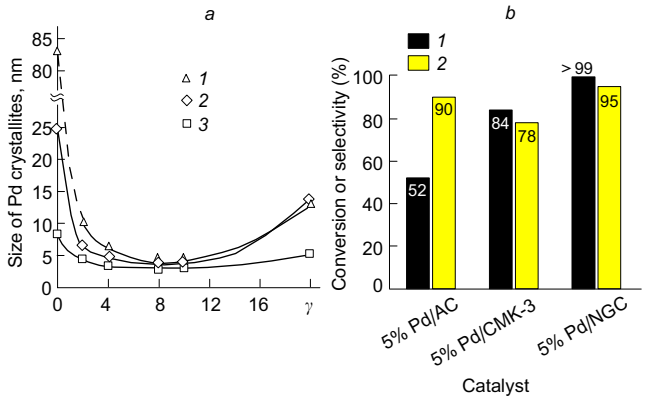


Figure 37. Crystallite size of palladium particles (XRD data) deposited on AC (*1*), CMK-3 (*2*) and NGC (*3*) *vs.* molar ratio of NaOH and $Na_2[PdCl_4]$ used for palladium deposition (*a*); conversion of cinnamaldehyde (*1*) and selectivity to 3-phenylpropanal (*2*) in the hydrogenation in the presence of 5% Pd/C catalysts prepared for $\gamma = 4$ (*b*).[477] Figure *a* is published with permission from Elsevier; Figure *b* was created by the authors using published data.[477]

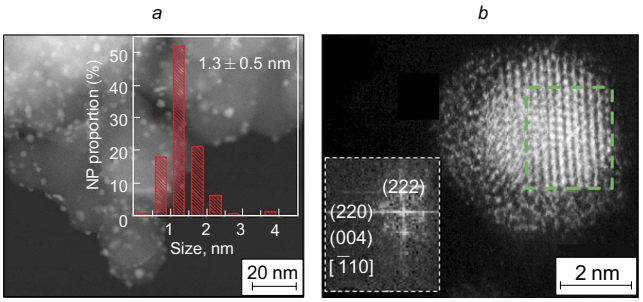


Figure 38. High-angle dark-field STEM image and size distribution histogram of bimetallic NPs for the Pd–Co/N-NGC sample (*a*) and aberration-corrected STEM image demonstrating the core/shell type structure for one of the deposited Pd–Co nanoparticles >2 nm in diameter (*b*).[479] Published with permission from Elsevier.

γ (see Fig. 37 *a*). This could be caused by structural features of the CNG surface, which prevent coarsening of the deposited palladium particles, in particular by the presence of defects on the carbon surface; these defects, acting as macroligands, stabilized palladium in the highly dispersed state.

The use of the synthesized 5% Pd/C catalysts in the hydrogenation of cinnamaldehyde (1,4-dioxane, 30 °C, 0.1 MPa, 3 h) demonstrated that the NGC-based sample prepared at $\gamma = 4$ was most efficient, since it ensured a selectivity to 3-phenylpropanal at 95% level with almost complete substrate conversion (see Fig. 37 *b*). Under the same conditions, in the presence of Pd/CMK-3 and Pd/AC, also characterized by $\gamma = 4$, hydrogenation of cinnamaldehyde was incomplete and had a lower selectivity to 3-phenylpropanal, which was converted to 3-phenylpropyl alcohol. The authors demonstrated that the variation of γ has a more pronounced effect on the catalyst activity than on the selectivity. Indeed, the Pd/NGC catalysts obtained without ($\gamma = 0$) or with a large excess of NaOH ($\gamma = 20$), *i.e.*, containing large palladium particles, did not provide complete conversion of cinnamaldehyde; however, the selectivity to 3-phenylpropanal was relatively high in both cases (at least 85%).

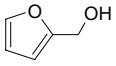
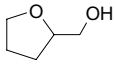
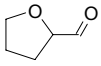
In recent years, the synthesis and study of supported bimetallic catalysts with the goal to attain high selectivity in the cinnamaldehyde hydrogenation has attracted a lot of interest of researchers.[402,403,459–462] In this regard, note the paper by Hu *et al.*,[479] who proposed highly efficient palladium–cobalt catalysts supported on a channel type NGC (Printex® U, Orion Engineered Carbons) pre-doped with nitrogen (by calcination with urea) for the selective hydrogenation of cinnamaldehyde to 3-phenylpropanal. Catalysts containing 1.1 wt.% Pd and Pd : Co = 1.7 (atomic ratio) were prepared by joint impregnation of the support with aqueous solutions of $Na_2[PdCl_4]$ and $Co(NO_3)_2$ and subsequent drying and reduction in an H_2 flow at various temperatures. It was shown that increase in the reduction temperature leads to increasing size of the deposited NPs. According to electron microscopy data, one catalyst obtained in this way (reduced at 200 °C) contained spherical NPs of palladium – cobalt alloy, relatively uniform in size, with an average diameter of 1.3 nm (Fig. 38 *a*). The NPs >2 nm in diameter consisted of a palladium core surrounded with a shell of a cobalt-enriched alloy (Fig. 38 *b*), while bimetallic NPs of a smaller diameter had a disordered structure. The authors emphasized the important role of nitrogen atoms on the surface of doped NGC for stabilization of the bimetallic NPs in a highly dispersed state. To confirm this statement, they studied a sample obtained using pristine, nitrogen-undoped NGC as the support and showed that in this case, large palladium, cobalt and Pd–Co alloy particles were formed on the carbon surface.

According to the data of Hu *et al.*,[479] Pd–Co/N-NGC catalysts differing in the average size of bimetallic NPs showed a high efficiency in the liquid-phase hydrogenation of cinnamaldehyde (cyclohexane, 50 °C, 0.3 MPa, 5 h); in the formation of 3-phenylpropanal, they were markedly superior to commercial 5% Pd/C (Ventron Alfa Products) in the activity, substrate conversion and selectivity. As the average size of NPs decreased from 2.3 to 1.3 nm, the activity of bimetallic catalysts increased almost twofold (from 0.24 to 0.5 mol g_{Pd}^{-1} min^{-1}), with the deposited metal contents being equal. This is generally consistent with the results of other studies[478,487] and attests to the structure sensitivity of this reaction. In the case of the most active Pd–Co/N-NGC catalyst, the selectivity to 3-phenylpropanal reached ~90%, with the cinnamaldehyde conversion being 95%. In addition, this catalyst showed stability in this reaction (high substrate conversion and selectivity were retained when the catalyst was reused many times).

4.4.3. Hydrogenation of furfural

Mironenko *et al.*[480–482] demonstrated that the Pd/NGC catalysts are rather active and selective in the liquid-phase hydrogenation of furfural to furfuryl alcohol and surpass analogous palladium systems based on CNTs. The authors used catalysts containing 1 or 1.5 wt.% Pd, which were prepared by impregnation of Baytubes® C 150 HP CNTs (Bayer MaterialScience AG) and furnace type NGC (P145 and P278-E) with aqueous solutions of $H_2[PdCl_4]$ followed by high-temperature reduction in H_2 flow. The furfural hydrogenation in an aqueous solution at a temperature of 50 °C and a hydrogen pressure of 0.5 MPa catalyzed by 1.5% Pd/P278-E afforded furfuryl alcohol with 99% selectivity, while the 1.5% Pd/CNTs catalyst proved to be inactive under the same conditions (Table 16).

Table 16. Average size of palladium NPs in Pd/C catalysts obtained using CNTs and P145 and P278-E NGC as supports and the performance of the catalysts in furfural hydrogenation in aqueous solution at a temperature of 50 °C.[480–482]

Catalyst	d_{av}, nm (see [a])		P_{H_2}, MPa (see [b])	X (%) (see [c])	S (%) (see [d])		
	CO chemisorption data	TEM data					
1.5% Pd/P278-E	6.9	–	0.5	29	99	< 1	0
1.5% Pd/CNTs	3.1	2.3	0.5	0	–	–	–
1.5% Pd/P278-E	6.9	–	2.0	46	98	< 1	0
1.5% Pd/CNTs	3.1	2.3	2.0	40	97	< 1	0
1.0% Pd/P145	3.4	4.3	3.0	71	85	6	5
1.0% Pd/CNTs	1.9	2.3	3.0	52	70	11	13

[a] Average size of palladium nanoparticles; [b] hydrogen pressure in the hydrogenation process; [c] furfural conversion according to GC data; [d] selectivity to furfuryl alcohol, tetrahydrofurfuryl alcohol and tetrahydrofurfural according to GC data.

As the hydrogen pressure is increased to 2 MPa, the conversion of furfural increased, with the high selectivity to furfuryl alcohol being retained for both catalysts. Further pressure increase (up to 3 MPa) resulted in hydrogenation of furfuryl alcohol to tetrahydrofurfuryl alcohol (see Scheme 4). The use of 1%Pd/P145 resulted in a much higher conversion of furfural (71%) and a selectivity to furfuryl alcohol (85%) compared to those observed for 1% Pd/CNTs (70% selectivity and 52% conversion).

While conducting a comparative study of 1.5% Pd/CNTs and 1.5% Pd/P278-E catalysts, Mironenko *et al.*[480] suggested that the noticeable difference between their behaviours in furfural hydrogenation may be attributable to different dispersions of deposited palladium NPs. It is known that hydrogenation of furfural is a structure-sensitive reaction, *i.e.*, the reaction rate and the transformation pathway depend on the metal NP size and surface structure.[467,488] The 1.5% Pd/P278-E catalyst was more active (led to a higher conversion of furfural) than 1.5% Pd/CNTs and contained larger palladium particles (see Table 16). Similarly, the 1.0% Pd/P145 catalyst, in which the palladium dispersion was lower than that in 1.0% Pd/CNTs, proved to be more active in this reaction. Furfural adsorption on highly dispersed palladium particles mainly occurs through C=C bonds of the furan ring, while an increase in the palladium particle size is accompanied by an increase in the size of the Pd(111) surface, on which furfural adsorption preferably occurs through C=O bonds.[449,467] As a consequence, P145-based catalyst with larger palladium NPs was more selective in the hydrogenation to give furfuryl alcohol than 1.0% Pd/CNTs (see Table 16).

It was indicated above that during catalytic hydrogenation of furfural under hydrothermal conditions, water participates in the hydrolytic furan ring opening reactions and rearrangements; this, as a rule, produces a broad range of products. It was shown[470,471,482] that Pd/C-catalyzed hydrogenation of furfural in water under drastic conditions (> 150 °C, > 1 MPa) follows predominantly two parallel pathways, one of which ends in cyclopentanone *via* rearrangement of the intermediate furfuryl alcohol involving water and acid sites. The other pathway includes hydrolytic conversion of furfuryl alcohol to 4-oxopentanal, which is converted to 5-hydroxypentan-2-one and 2-methyltetrahydrofuran upon further hydrogenation (see Scheme 5).

It was found[470,482] that the activity and selectivity of Pd/C catalysts in these reactions considerably depend on the nature of the carbon support. In the presence of Pd/CNTs catalyst, hydrogenation of furfural under hydrothermal conditions (H_2O, 150 °C, 3.0 MPa, 1 h) predominantly led to cyclopentanone; the selectivity to cyclopentanone (at least 48%) was much higher than the selectivity to products of the parallel reaction pathway (Fig. 39 *a*). Conversely, in the presence of palladium catalysts based on an NGC (P278-E), the selectivity to 4-oxopentanal was nearly 60%, whereas the selectivity to cyclopentanone was ~20% (Fig. 39 *b*).

Higher selectivity (up to 63%) of the furfural conversion to 4-oxopentanal and an almost three times lower selectivity

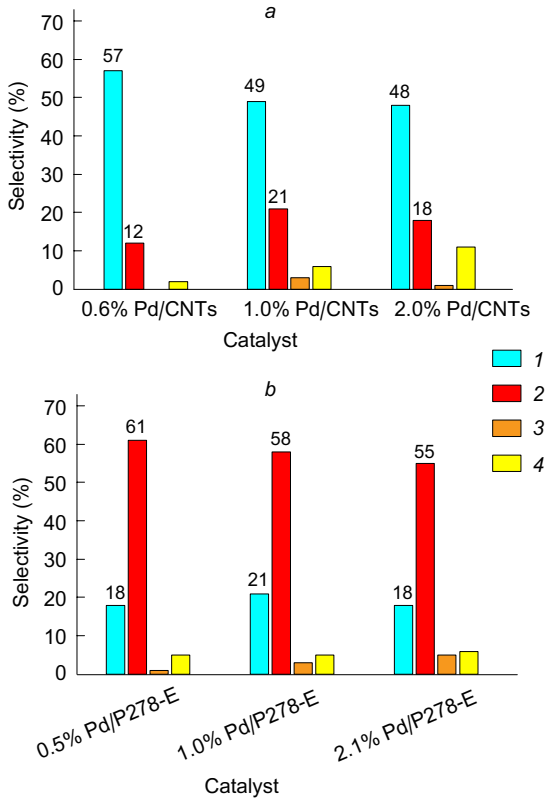


Figure 39. Selectivity to cyclopentanone (*1*), 4-oxopentanal (*2*), 5-hydroxypentan-2-one (*3*) and 2-methyltetrahydrofuran (*4*) in the hydrogenation of furfural in the presence of palladium catalysts supported on CNTs (*a*) and P278-E NGC (*b*). Reaction conditions: H_2O as solvent, 150 °C, 3.0 MPa, 1 h; the products were analyzed by GC. The figure was created by the authors using published data.[470]

to cyclopentanone were also inherent in palladium catalysts obtained using other NGC grades (P145, T900).[470, 482] It was noted[471] that the formation reactions of 4-oxopentanal and cyclopentanone require participation of not only metal sites, but also acid sites; in Pd/C catalysts, oxygen-containing groups on the carbon support surface can act as such acid sites. The results of IR spectroscopy studies of the composition of functional cover of the surface of the support used by the authors[364, 470, 480] and the results of determination of the palladium dispersion in the catalysts based on these supports[470, 482] indicate that the selectivity difference between Pd/CNTs and Pd/NGC catalysts could be attributable to the increased concentration of the oxygen-containing groups (*e.g.*, hydroxy groups) on the surface of the given NGC types *versus* almost complete absence of these groups on the CNT surface and also to much lower dispersion of palladium NPs in Pd/NGC in comparison with Pd/CNTs. Apparently, selective formation of cyclopentanone by Pd/C-catalyzed hydrogenation of furfural under hydrothermal conditions requires a low content of oxygen-containing groups on the support surface and a high dispersion of supported palladium NPs. Highly dispersed palladium NPs contain an increased fraction of electron-deficient $Pd^{\delta+}$ species,[480] which can themselves act as acid sites in the hydrolytic transformations of furan compounds.[471] Conversely, in order to direct the reactions towards the formation of 4-oxopentanal, large palladium particles in the catalyst and increased concentration of acid functional groups on the support surface are required.

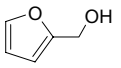
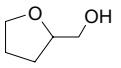
It was shown above in relation to cyclohexene and benzene hydrogenation that modification of the functional cover of the CNG surface with the goal to change its acid-base properties is an efficient method to control the activity of the Pd/NGC catalysts. In this regard, note the study by Kosydar *et al.*,[484] who showed that catalytic performance of Pd/NGC compositions in the liquid-phase hydrogenation of furfural considerably depends on the composition and concentration of functional groups on the support surface. The catalysts were prepared using a furnace NGC (Vulcan® XC-72) as the support. The support was modified, first, by oxidative treatment with a 30% solution of H_2O_2 or a 60% solution of HNO_3 at room temperature and, next, by treatment with fuming sulfuric acid (also at room temperature) to functionalize the oxidized sample surface with sulfonic acid groups. A comparative study of supports demonstrated that modification insignificantly affected the NGC structure and morphology, but markedly increased the concentration of functional groups. According to IR spectroscopy data, modified NGC samples had a higher content of oxygen functional groups (hydroxyl and carboxyl groups) than the pristine support; the highest content of these groups was attained upon the oxidative treatment with nitric acid. Since nitric acid is a stronger oxidant than H_2O_2, treatment with nitric acid induced much more intense oxidation and formation of surface defects; therefore, during the subsequent sulfonation, the surface of the nitric acid-oxidized sample was enriched with SO_3H groups to a greater extent than that of the H_2O_2-treated sample according to XPS data.

Palladium catalysts based on non-modified and modified NGC samples and containing 2 wt.% Pd were prepared by the metal colloid method using $Na_2[PdCl_4]$ as the palladium precursor, an aqueous solution of N_2H_4 (reducing agent) and an isooctane solution of sodium dioctyl sulfosuccinate (surfactant). The authors showed that modification of the support had little effect on the average size of palladium NPs, which was 5–6 nm (XRD data) for all prepared catalysts. Meanwhile, according to XPS data, the oxidation and sulfonation of NGC surface resulted in a considerable increase in the content of electron-deficient palladium species with Pd $3d_{5/2}$ electron binding energies of 338.4 and 339.1 eV, which was especially pronounced for a sample based on NGC treated with nitric acid and enriched with sulfonic acid groups.

Testing of the resulting Pd/NGC catalyst in the liquid-phase hydrogenation of furfural under mild conditions (Pr^iOH, 35 °C, 0.6 MPa of H_2) demonstrated considerable effect of the support modification, in particular, on the reduction pathways (see Table 15). For furfural conversion being the same (60%), the catalyst based on non-modified NGC had a markedly higher selectivity to furfuryl alcohol (49%) than the catalysts prepared using modified support samples (34%). In the presence of the catalyst containing an increased fraction of electron-deficient palladium species (NGC pretreated with nitric acid and enriched with sulfonic acid groups), the selectivity to tetrahydrofurfuryl alcohol was almost two times higher than for catalysts based on non-modified and H_2O_2-treated NGC samples. Among furfural hydrogenation products obtained in isopropyl alcohol, the authors detected, in particular, 2-(diisopropoxymethyl)furan (furfural diisopropyl acetal), which resulted from the reaction of furfural with the solvent on the acid sites of the catalyst. In the case of modified catalysts with a support enriched with acidic functional groups, the highest selectivity to 2-(diisopropoxymethyl)-furan was attained (up to 80% for furfural conversion of 30%), whereas in the presence of Pd/NGC in which the support was not modified, the selectivity to this product was almost two times lower, with the furfural conversion being the same.

An approach to attaining high catalyst performance in hydrogenation of organic compounds that was repeatedly mentioned above implies the introduction of other metals into the palladium catalyst, *i.e.*, the use of bi- and polymetallic supported compositions. In this regard, mention should be made of a recent publication by Ruan *et al.*,[485] who proposed a highly efficient Pd–Ni bimetallic catalyst based on a furnace NGC (Black Pearls® 2000, Cabot) for the selective hydrogenation of furfural to furfuryl alcohol under mild conditions. This catalyst, containing 3.0 wt.% Pd and 2.1 wt.% Ni, was prepared by substituting palladium for a part of nickel in Ni/NGC [prepared by deposition of a specified amount of $Ni(OH)_2$ onto the chosen support followed by reduction with hydrazine hydrate]. This was done by adding a solution of $(NH_4)_2[PdCl_4]$ to an aqueous suspension of Ni/NGC. Exploration of the sample structure with a set of spectral and microscopic methods showed that the dispersed palladium NPs were distributed on the surface of NGC-supported $Ni/Ni(OH)_2$ composite particles (with an average size of 7.83 nm according to TEM data); nickel was present on the surface of these particles mainly as NiO, NiOOH and $Ni(OH)_2$ and did not form an alloy with palladium. Meanwhile, according to XPS data, as a result of interaction of palladium with nickel-containing composite particles, the relative content of electron-deficient $Pd^{\delta+}$ species (Pd $3d_{5/2}$ electron binding energy of 337.5 eV) was much higher in the bimetallic catalyst than in the monometallic Pd/NGC sample, in which palladium metal predominated (Pd^0; Pd $3d_{5/2}$ electron binding energy of 335.6 eV).

Table 17. Catalytic properties of 6.7% Ni/NGC, 3.0% Pd/NGC and 3.0% Pd – 2.1% Ni/NGC samples in liquid-phase hydrogenation of furfural (EtOH, 5.0 MPa).[485]

Catalyst	Reaction time, h	Temperature, °C	TOF, h^{-1} (see [a])	X (%) (see [b])	S (%) (see [c])		
							other products
Ni/NGC	1	100	0	0	–	–	–
Pd/NGC	1	100	1788	97.6	0	10.8	89.2
Pd – Ni/NGC	1	100	1830	100	10.0	34.1	55.9
Pd – Ni/NGC	1	25	1830	100	40.6	22.3	37.1
Pd – Ni/NGC	1	10	1494	81.5	92.4	2.4	5.2
Pd – Ni/NGC	2	10	936	100	90.7	1.9	7.4

[a] TOF was calculated as the ratio of furfural conversion rate (mol h^{-1}) to the amount of palladium (mol) and palladium dispersion according to TEM data; [b] the conversion of furfural was determined from GC data; [c] the selectivities to furfuryl alcohol, tetrahydrofurfuryl alcohol and other products (not indicated in Ref. 485) were determined from GC data.

According to the results obtained by Ruan *et al.*,[485] the bimetallic Pd – Ni/NGC catalyst was more efficient in the liquid-phase hydrogenation of furfural to furfuryl alcohol than monometallic Pd/NGC and Ni/NGC samples (Table 17). It was also shown that the activity and selectivity of the bimetallic sample in the formation of furfuryl alcohol depended on the reaction conditions. As the temperature was lowered from 25 to 10 °C, with the reaction time remaining the same (1 h), the TOF and furfural conversion decreased, but simultaneously the selectivity to furfuryl alcohol increased more than twofold. Conduction of the reaction in the presence of bimetallic Pd – Ni/NGC catalyst at low temperature (10 °C) for two hours ensured complete conversion of furfural and high (~91%) selectivity to furfuryl alcohol. In addition, this catalyst was stable in this reaction (high levels of substrate conversion and selectivity were retained after reuse).

On the basis of their results and published data, Ruan *et al.*[485] suggested that during hydrogenation of furfural in the presence of bimetallic Pd – Ni/NGC catalyst, hydrogen is dissociatively adsorbed on highly dispersed palladium NPs, while on the surface of $Ni(OH)_2$ particles, electrophilic activation of furfural molecules takes place with participation of the C=O bonds. Due to spillover effect, adsorbed hydrogen migrates to the $Ni(OH)_2$ surface and adds to the activated C=O bond of adsorbed furfural; this provides for high selectivity to furfuryl alcohol. In addition, presumably, the $Ni(OH)_2$ particles in the bimetallic catalyst strongly bind palladium NPs, thus preventing them from being washed away during the catalytic reaction. This accounts for the high stability of the catalyst.

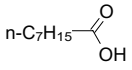
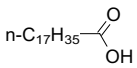
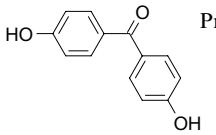
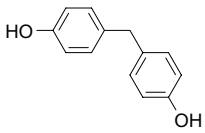
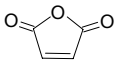
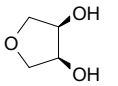
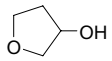
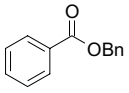
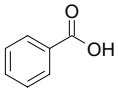
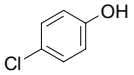
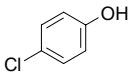
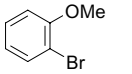
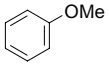
4.5. Hydrogenolysis of C – O and C – Cl bonds in organic compounds

The selective hydrogenation of organic compounds in the presence of palladium catalysts can be accompanied, even under mild conditions, by hydrogenolysis, *i.e.*, cleavage of bonds in organic molecules with hydrogen being added to the resulting fragments. In the above discussion of selective hydrogenation of benzaldehyde, it was noted that hydrogenolysis of the C – O bond lowers the yield of the product of selective hydrogenation (benzyl alcohol); therefore, it is an undesirable reaction. Meanwhile, hydrogenolysis of heteroaromatic organic compounds is used rather widely in organic synthesis.[4, 7, 8, 27] For example, hydrogenolysis of fatty acid esters (in particular, methyl esters of coconut and palm fatty acids) is a well-known process of industrial production of $C_6 – C_{22}$ monohydric saturated alcohols (higher fatty alcohols), which are used, for example, to obtain anionic and non-ionic surfactants, plasticizers and lubricating materials.[7, 489 – 492]

The hydrogenolysis of C – O bonds (and other deoxygenation reactions) in plant-based oxygen substrates have been attracting (especially in the last decade) considerable interest since it can be used to obtain valuable chemicals and environmentally benign motor fuels from renewable raw materials.[493 – 502] Type Pd/C catalysts often exhibit high performance characteristics, for example, in hydrodeoxygenation of plant biomass pyrolysis tar (so-called bio-oil),[497, 500, 502] various single aromatic compounds, bio-oil components[497, 498, 501] and furan derivatives formed upon cellulose hydrolysis.[497] The Pd/C-catalyzed hydrodebenzylation is widely used in the practical organic synthesis, in particular, in the synthesis of some biologically active compounds and pharmaceuticals, in order to remove benzyl-types groups, which are introduced to protect the reactive oxygen- and nitrogen-containing functional groups at a certain step of synthesis.[5, 8, 10, 27] One more practically important hydrogenolysis reaction is hydrodechlorination, that is, hydrogen-induced C – Cl bond cleavage in organochlorine compounds accompanied by C – H bond formation and elimination of HCl molecule (replacement of Cl atoms by H atoms). The catalytic hydrodechlorination reactions are considered to be most promising for the processing and deactivation of toxic organochlorine wastes; therefore, these reactions and development of efficient catalyst for them (including Pd/C) attract a lot of attention.[503 – 506] It was shown[72, 507 – 515] that Pd/NGC compositions are applicable for deoxygenation (including hydrogenolysis of C – O bonds) and hydrogenolysis of C – Cl bonds of organic compounds (Table 18); some interesting examples are considered in detail and analyzed below.

Sun *et al.*[507, 508] studied the influence of the support nature in supported palladium catalysts on the deoxygenation of higher fatty carboxylic acids, in particular octanoic (caprylic) acid. They used commercial catalysts based on AC (E117 of Evonik-Degussa and AA38300 of Alfa Aesar) and SiO_2 (Escat 1351 of BASF) and also catalysts prepared by impregnation of acetylene NGC (grade was not indicated, Strem Chemicals) and SiO_2 (Aerosil® 300) with an

Table 18. Examples of using Pd/NGC catalysts in hydrogenolysis of C–O and C–Cl bonds in organic compounds.

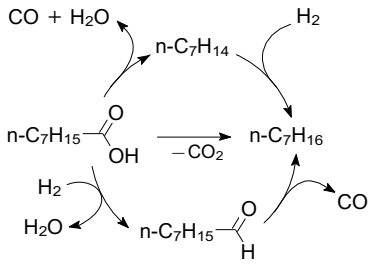
Catalyst	Substrate	Hydrogenation conditions	Substrate conversion (%)	Products	Selectivity (%)	Ref.
5% Pd/acetylene NGC (NGC manufactured by Strem Chemicals)		Gas-phase hydrogenation in a flow regime, 260 °C, 0.1 MPa, 1 h	75	n-C_7H_{16}	> 97	507, 508
5% Pd/acetylene NGC (NGC manufactured by Strem Chemicals)		Dodecane, 300 °C, 1.5 MPa of H_2	70	n-$C_{17}H_{36}$	–	508
5% Pd/NGC (manufactured by Baker and Co.)		Pr^iOH, 25 °C, 5 h	–		95 (see [b])	72
5% Pd/Vulcan® XC-72		Supercritical CO_2, 200 °C, 20 MPa (4 MPa of H_2), 2 h	100		81	509
Pd–WO_x/ Vulcan® XC-72		1,4-Dioxane, 220 °C, 8 MPa of H_2, 8 h	> 95		72	510, 511
					14	
1% Pd/Vulcan® XC-72		EtOH, KOH, 70 °C, 0.1 MPa, 1 h (see [a])	99		99 (see [b])	512, 513
0.5% Pd/acetylene NGC (NGC manufactured by Alfa Aesar)		H_2O, 30 °C, 0.1 MPa, 4 h	100		> 97	514
1% Pd/acetylene NGC (NGC manufactured by Alfa Aesar)		H_2O, 30 °C, 0.1 MPa, 4 h	> 99.5		92	515
					8	
1% Pd/Vulcan® XC-72		EtOH, KOH, 70 °C, 0.1 MPa, 1 h (see [a])	100		–	512, 513

[a] Formic acid as the hydrogenating agent; [b] isolated yield.

aqueous solution of $Pd(NO_3)_2$ followed by high-temperature reduction in a hydrogen flow. All catalysts contained 5 wt.% palladium.

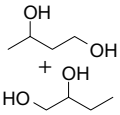
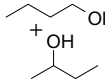
The gas-phase deoxygenation of octanoic acid to n-heptane in the presence of palladium catalysts (flow process, 235–300 °C, atmospheric pressure) followed several parallel pathways (Scheme 6). The contribution of a particular pathway depends on the nature of the catalyst support.

Scheme 6



In the presence of 5% Pd/SiO_2, deoxygenation of octanoic acid to n-heptane proceeded either *via* decarbonylation to hept-1-ene followed by hydrogenation (direct decarbonylation pathway) or *via* the formation of octanal (indirect decarbonylation pathway). The 5% Pd/AC catalysts showed enhanced activity in both decarbonylation and decarboxylation reactions; therefore, the use of these catalysts results in high yields of CO_2. The 5% Pd/NGC catalyst was not inferior to SiO_2-based samples in the activity towards deoxygenation of octanoic acid and provided high selectivity to n-heptane (> 97%), which changed little with time (~15 h; continuous flow process). It is important that reactions with this catalyst mainly proceeded as direct decarbonylation (octanoic acid → hept-1-ene → n-heptane). Relying on their data on catalyst characterization, the authors suggested that high selectivity of 5% Pd/NGC

Table 19. Catalytic properties of the Pd – WO_x system (molar ratio Pd : W = 0.25) based on various supports in the liquid-phase hydrogenation of *cis*-1,4-anhydroerythritol (1,4-dioxane, 180 °C, 8 MPa of H_2, 16 h).[510]

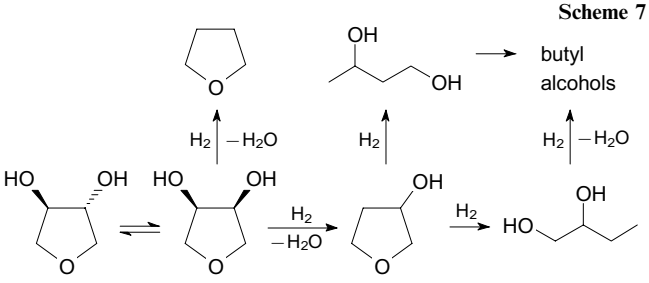
Catalyst	Activity, mmol g_{cat}^{-1} h^{-1}	*X* (%) (see [a])	*S* (%) (see [b])				
							
Pd – WO_x/ZrO_2	0.3	7	71	3	5	< 1	< 1
Pd – WO_x/SiO_2	1.4	36	69	2	< 1	5	< 1
Pd – WO_x/Al_2O_3	0.9	22	65	8	8	5	1
Pd – WO_x/TiO_2	1.2	30	51	19	3	< 1	1
Pd – WO_x/CeO_2	1.0	25	47	9	30	2	< 1
Pd – WO_x/MgO	0.1	3	45	3	31	< 1	< 1
Pd – WO_x/NGC	1.8	44	69	8	1	7	< 1

[a] Conversion of *cis*-1,4-anhydroerythritol according to GC data; [b] selectivity to tetrahydrofuran-3-ol, tetrahydrofuran, *trans*-1,4-anhydroerythritol, butane-1,3- and butane-1,2-diols (sum), butan-1- and butan-2-ols (sum) according to GC data.

towards this reaction pathway could be attributed to the absence of micropores in NGC and low concentration of oxygen functional groups on the surface of this carbon support (unlike AC).[507, 508]

Tomishige and co-workers[510, 511] showed that the Pd – WO_x/NGC composition is highly efficient in the hydrogenation of *cis*-1,4-anhydroerythritol (the product of dehydration of erythritol resulting from glucose fermentation) to tetrahydrofuran-3-ol. This catalyst, containing 1.4 wt.% Pd and 9.9 wt.% W (molar ratio Pd : W = 0.25), was prepared by impregnation of a furnace NGC (Vulcan® XC-72) first with an aqueous solution of $(NH_4)_6[H_2W_{12}O_{40}]\cdot n\,H_2O$ and then with an aqueous solution of $Pd(NO_3)_2$. After each deposition step, the sample was dried and calcined in air (500 °C). For the liquid-phase hydrogenation of *cis*-1,4-anhydroerythritol (1,4-dioxane, 180 °C, 8 MPa of H_2, 16 h), the obtained Pd – WO_x/NGC catalyst was not only superior to analogous samples prepared with oxide supports in the activity and substrate conversion, but also provided high selectivity (69%) of hydrogenolysis of only one C – O bond in the *cis*-1,4-anhydroerythritol molecule to give tetrahydrofuran-3-ol (Table 19, Scheme 7). Furthermore, at higher temperature (220 °C), the Pd – WO_x/NGC catalyst provided complete conversion of *cis*-1,4-anhydroerythritol, while the selectivity to tetrahydrofuran-3-ol did not decrease (72%).

Scheme 7



A comparative study of the catalyst structure by a set of physical methods showed that palladium nanoparticles in Pd – WO_x/NGC are uniformly distributed over the surface of dispersed WO_3 particles deposited on NGC (according to XRD and TEM data).[510] During the reaction, hydrogen activated in the palladium sites partially reduces WO_3 to W^{IV} oxide species. The activation of substrate molecules and hydrogenolysis of C – O bonds take place on W^{IV} oxide species, which are thus oxidized again to W^{VI} oxide. The enhanced activity of the Pd – WO_x/NGC catalyst in this reaction could be attributable, in the authors opinion, to more extensive porosity of NGC (S_{BET} = 254 m^2 g^{-1}) compared with the porosity of oxide supports (S_{BET} < 133 m^2 g^{-1}, except for SiO_2) and to the fact that WO_3 occurs on the NGC surface in the dispersed or amorphous state and is rather reactive under the reaction conditions, *i.e.*, it can be partially reduced at temperatures below 180 °C (TPR data). An inactive WO_3 phase is formed, for example, on the SiO_2 surface; however, the activity of the catalyst with this support was close to the activity of Pd – WO_x/NGC (see Table 19), apparently, owing to the extensive porosity of SiO_2 (S_{BET} = 535 m^2 g^{-1}).

Yakukhnov and Ananikov[512] (see also Ref. 513) established a high efficiency of low-percentage Pd/NGC catalyst in *O*- and *N*-debenzylation reactions under mild conditions (formic acid as hydrogenating agent, EtOH, KOH, 70 °C, 1 h). Traditionally, supported catalysts with relatively high palladium contents (5 – 20 wt.%), which are active in hydrogenolysis, are used for hydrodebenzylation reactions.[5, 8] It was shown[512] that the Pd/Vulcan® XC-72 catalyst containing only 1 wt.% palladium, prepared by a fast and simple procedure developed previously (stirring a NGC suspension in a solution of $[Pd_2(dba)_3]$ in $CHCl_3$ at 80 °C, filtration, washing and drying[241]), showed high performance in the hydrodebenzylation of a broad range of organic substrates (Fig. 40) and was more active than a similar catalyst based on CNTs and a number of commercial 5% Pd/C catalysts.

Baeza *et al.*[514] investigated the effect of the preparation conditions of 0.5% Pd/NGC on the catalytic activity and selectivity in the hydrodechlorination of 4-chlorophenol. The catalysts were prepared using the same acetylene NGC (Alfa Aesar; S_{BET} = 76 m^2 g^{-1}) as the support and three methods for the deposition of palladium:

— mixing of NGC with aqueous solutions of $H_2[PdCl_4]$ (precursor), methanol (reducing agent) and polyvinylpyrrolidone (PVP, stabilizing agent) and refluxing of the obtained mixture for 3 h; as a result, palladium NPs were formed in the presence of a support (series of samples *A*);

— reduction of $H_2[PdCl_4]$ with methanol in solution and subsequent stabilization of the obtained palladium NPs

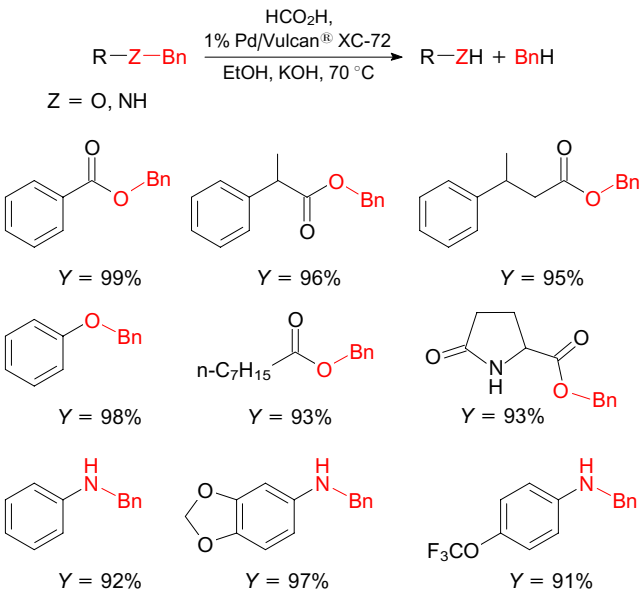


Figure 40. Formulae of some substrates that were used in hydrodebenzylation to test the 1% Pd/Vulcan® XC-72 catalyst.[512] The substrate conversion was 99% in all cases, according to ^{1}H NMR data; *Y* is yield. The figure was created by the authors using published data.[512]

with PVP and fixing of Pd–PVP on NGC (series of samples *B*);

— impregnation of NGC with a solution of $H_2[PdCl_4]$, subsequent calcination at 200 °C and reduction in a hydrogen flow at 100 °C (sample *C*).

While preparing the catalysts, the authors used various types of the metal colloid method (series *A* and *B*) and varied the PVP : Pd molar ratio in the range from 5 to 35. It was shown that the methods and conditions of the preparation of Pd/NGC catalysts considerably affected the size and morphology (shape) of deposited Pd NPs (according to STEM data). When the conventional impregnation method was used followed by hydrogen reduction (catalyst *C*), dispersed palladium NPs with an average size of 3 nm were formed on the NGC surface, whereas the use of metal colloid methods (catalysts of series *A* and *B*) resulted, most often, in the formation of much larger palladium NPs with a broad size distribution. The average NP size considerably depended on the PVP : Pd molar ratio. The procedure in which the palladium precursor was reduced with methanol in the presence of the support (series *A*) afforded palladium NPs shaped like distorted polyhedra, with their average size increasing from 12 to 42 nm upon the increase in the PVP : Pd molar ratio from 5 to 35 (Fig. 41).[514]

All of the obtained 0.5% Pd/NGC catalysts provided complete conversion of 4-chlorophenol under mild reaction conditions (H_2O, 30 °C, 0.1 MPa, 4 h); however, they markedly differed in the catalytic activity and selectivity. Indeed, the catalyst obtained by the conventional impregnation method (sample *C*) showed high activity in the hydrodechlorination of 4-chlorophenol to phenol, while the subsequent hydrogenation reactions did not take place in the presence of this catalyst sample (Fig. 42).[514] Meanwhile, catalysts of series *A* obtained by one of the variants of metal colloid method were less active under the same conditions, and the selectivity to phenol was lower due to the subsequent hydrogenation of phenol to cyclohexanone and cyclohexanol.

Since palladium-catalyzed hydrodechlorination of 4-chlorophenol is a structure-sensitive reaction,[516] the differences between the catalytic properties of 0.5% Pd/NGC samples were attributed to different sizes of the deposited palladium NPs. In addition, the use of stabilizing agent (PVP) in the synthesis of catalysts by various metal colloid

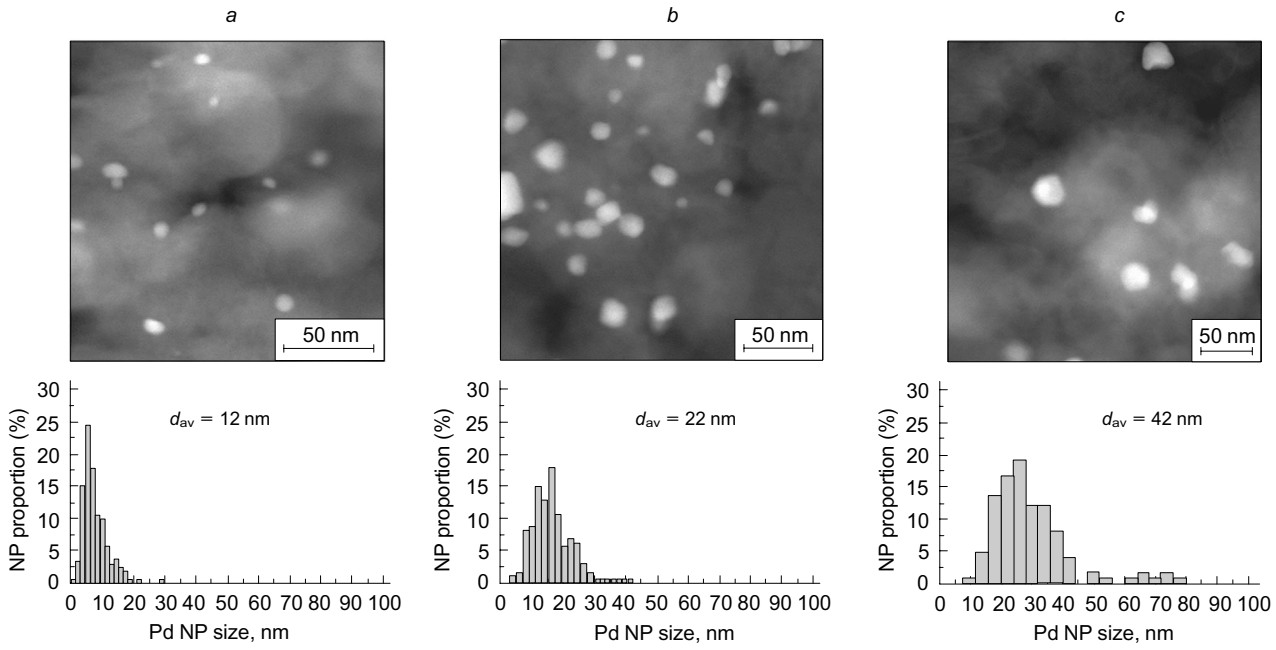


Figure 41. STEM images and size distribution histograms of palladium NPs for 0.5% Pd/NGC samples prepared by method *A* (see text): *A*-5 (*a*), *A*-20 (*b*), *A*-35 (*c*). The numbers 5, 20 and 35 in the designations of catalysts correspond to the PVP : Pd molar ratio; d_{av} is the average size of palladium NPs.[514] Published with permission from Elsevier.

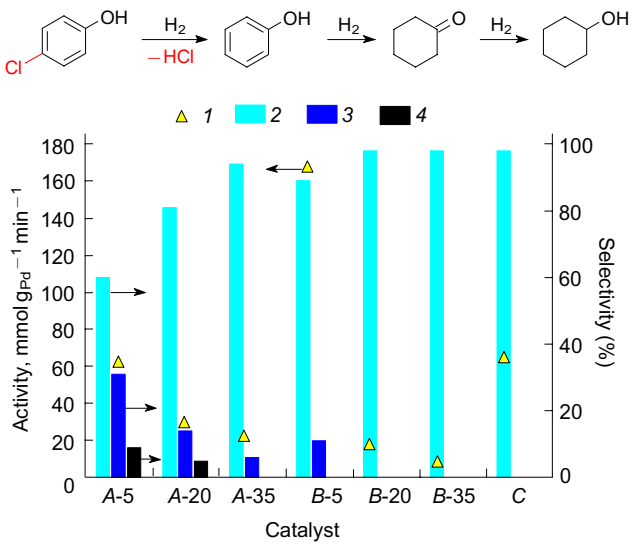


Figure 42. Activity of 0.5% Pd/NGC catalysts in the hydrogenation of 4-chlorophenol (*1*) and selectivity to phenol (*2*), cyclohexanone (*3*) and cyclohexanol (*4*) for complete conversion of 4-chlorophenol. Reaction conditions: H_2O, 30 °C, 0.1 MPa, 4 h. In the catalyst designation, the letter stands for the preparation method (see text) and the number means the PVP : Pd molar ratio. The figure was created by the authors using published data.[514]

procedures also had a considerable effect on the catalytic properties: an increase in the PVP : Pd molar ratio (for the same synthetic procedure) resulted in decreasing activity (see Fig. 42). In the authors opinion, PVP hampered the access of reactants to the catalyst active sites, *i.e.*, as the amount of PVP increased, the active sites became less accessible, with the content of palladium remaining the same.

Another study by Baeza *et al.*[515] addresses the effect of preliminary graphitization of NGC on the electronic and dispersion state of the deposited palladium NPs and on the catalytic properties of the Pd/NGC compositions in the hydrodechlorination of 4-chlorophenol. The catalysts were prepared using acetylene NGC (Alfa Aesar; S_{BET} = 76 $m^2\ g^{-1}$). Graphitization was carried out at 2800 °C in a helium flow for 30 min. Catalysts containing 1 wt.% Pd were prepared by impregnation of the pristine or graphitized NGC (GNGC) with an aqueous solution of $H_2[PdCl_4]$ followed by calcination at 200 °C and reduction in a hydrogen flow at 100 °C. According to the results of a comparative study of the catalysts by a set of physical methods (Table 20), the average size of palladium NPs was the same in both samples (STEM data); however, a considerable difference between the electronic states of NPs was found (XPS data): the catalyst obtained using pristine NGC contained a higher content of electron-deficient palladium species ($Pd^{\delta+}$: Pd^0 = 2.0), whereas in the GNGC-based sample, the atomic ratio of electron-deficient and metallic species was close to unity. The lower fraction of charged Pd species in the sample prepared using GNGC as a support was attributed to the fact that graphitization, which was accompanied by structure ordering and annealing of defects, resulted in increasing electron mobility in the nanoglobular carbon; this facilitated the subsequent reduction of the deposited palladium compounds by hydrogen.

Both catalysts provided complete conversion of 4-chlorophenol under mild reaction conditions (H_2O, 30 °C, 0.1 MPa, 4 h); however, their activity and selectivity were considerably different (see Table 20). The activity of the GNGC-based sample was more than 2.5-fold higher than that for the catalyst obtained using non-graphitized NGC. In addition, the Pd/GNGC sample was more active in the subsequent hydrogenation of phenol; as a result, the selectivity to cyclohexanone increased (~14%). Since the catalysts did not differ in the palladium NP size, the authors attributed their different activities to different electronic states of deposited palladium. Probably, the GNGC-based catalyst contained palladium in the optimal electronic state (balanced ratio of $Pd^{\delta+}$ and Pd^0), which accounted for the high catalyst activity in this reaction.

Table 20. Results of studying palladium catalysts supported on pristine and graphitized NGC by STEM and XPS methods and performance of the catalysts in the liquid-phase hydrogenation of 4-chlorophenol (H_2O, 30 °C, 0.1 MPa, 4 h).[515]

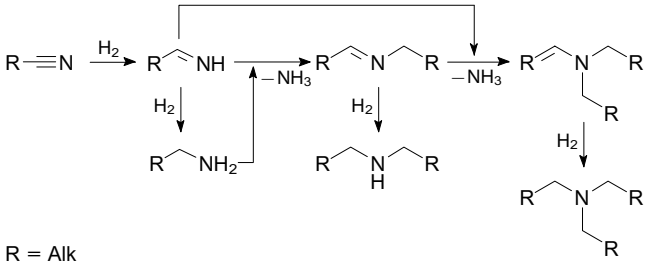
d_{av}, nm (see [a])	$Pd^{\delta+}$: Pd^0 (see [b])	Activity (see [c])	*S* (%) (see [d])	
				
		1% Pd/NGC		
3	2.0	63.7	92	8
		1% Pd/GNGC		
3	0.9	173.5	86	~14

[a] Average size of palladium nanoparticles according to STEM; [b] atomic ratio of electron-deficient and metallic palladium species according to XPS; [c] in mmol $g_{Pd}^{-1}\ min^{-1}$; [d] selectivity to phenol and cyclohexanone (according to GC) at complete conversion of 4-chlorophenol.

4.6. Hydrogenation of nitriles

The catalytic hydrogenation of nitriles, in addition to the hydrogenation of nitro compounds, is an important method for the preparation of amines in practical organic synthesis.[7,8,517–519] Hydrogen addition to the C≡N bond in the nitrile molecule occurs rather easily; however, the reaction is not limited to the formation of a primary amine, because intermediate aldimine, which is highly reactive, undergoes condensation reactions that give secondary and tertiary amines (Scheme 8). In addition, hydrogenation of nitriles may be accompanied by side decyanation, transamination and polymerization reactions.[518] Therefore, to attain high selectivity to a particular product of nitrile hydrogenation is a challenge, and the selectivity is often determined by the choice of the catalyst.[519–522] The selective hydrogenation of aliphatic nitriles to primary amines is mainly carried out using cobalt, nickel

Scheme 8



and ruthenium catalysts,[8, 521] while secondary and tertiary aliphatic amines are preferably prepared using rhodium and palladium catalysts, including Pd/C compositions.[8, 523] Among industrially important processes of nitrile hydrogenation in the presence of supported palladium catalysts, it is worth mentioning 5% Pd/C-catalyzed hydrogenation of benzonitrile to benzylamine,[7] which is rather widely used, for example, to prepare some pharmaceutical drugs [474] and hexanitrohexaazaisowurtzitane, a component of explosive compositions.[524, 525]

The catalytic hydrogenation of nitriles is much less studied than, for example, hydrogenation of nitro compounds,[518] and information about the use of NGC-supported palladium catalysts is scarce (Table 21).

According to a patent,[526] the selectivity of bimetallic Pd–Au/NGC catalysts in the hydrogenation of valeronitrile considerably depends on the formation conditions and the state of deposited metals. The catalysts containing 25 wt.% Pd and 5 wt.% Au were prepared by joint impregnation of acetylene NGC (the grade and manufacturer were not indicated) with aqueous solutions of $Na_2[PdCl_4]$ and $H[AuCl_4]$ followed by reduction of the deposited precursors by an aqueous solution of formaldehyde with the addition of KOH. The relative content of the Pd–Au alloy in the series of obtained 25% Pd–5% Au/NGC bimetallic catalysts was found to depend on the pH of the solution of the reducing agent, which was varied by changing the KOH concentration (Table 22). According to XRD data, the proportions of Pd–Au alloy in the catalysts obtained by reduction at pH of 8 and 13 were < 13% (the rest was monometallic Pd and Au particles) and 96%, respectively.

When hydrogenation of valeronitrile (AcOH, 50 °C, 0.15 MPa of H_2, 3 h) was carried out over the Pd–Au/NGC catalyst in which the deposited metals occurred almost completely as the Pd–Au alloy, the selectivity to pentylamine was markedly higher than that with the monometallic 30% Pd/NGC catalyst (see Table 22). In the opinion of the authors, this could be due to the change in the electronic state of palladium alloyed with gold (however, no data on the electronic state of deposited metals were given in the publication). Meanwhile, when the bimetallic catalyst obtained by reduction at pH 8 with a low fraction of alloy particles was used in the reaction, the selectivity to pentylamine was only 29%, *i.e.*, almost 2.5 times lower (see Table 22). The authors suggested that in this sample, gold particles, which were inactive in this reaction (since no transformation of valeronitrile took place with the monometallic Au/NGC sample), blocked the active palladium and palladium–gold alloy particles, which resulted in lower hydrogenation rate, higher contribution of side condensation reactions of the intermediate pentanimine (see Scheme 8) and, hence, in a lower selectivity to pentylamine.

One more example of the use of NGC-supported palladium catalyst in nitrile hydrogenation is the DuPont patented production process of 1,3- and 1,5-dimethyl-2-piperidones from 2-methylglutaronitrile (by-product of the synthesis of adiponitrile by hydrocyanation of buta-1,3-diene) catalyzed by bimetallic 4.5% Pd–0.5% Pt/NGC catalyst with acetylene NGC (Shawinigan Black®) used as the support.[527, 528] The process is carried out in a 40% aqueous solution of methylamine at a temperature of 200 °C and a pressure of ~14 MPa; after 6 h, the yield of a mixture of 1,3- and 1,5-dimethyl-2-piperidones (3 : 1 ratio)

Table 21. Examples of using Pd/NGC catalysts in the hydrogenation of nitriles.

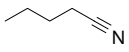
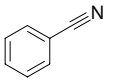
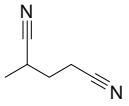
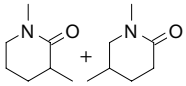
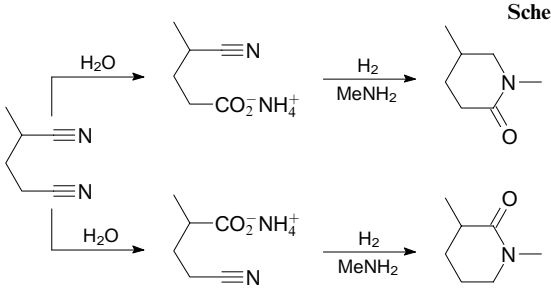
Catalyst	Substrate	Hydrogenation conditions	Substrate conversion (%)	Products	Selectivity (%)	Ref.
25% Pd–5.2% Au/ acetylene NGC (NGC grade is not specified)		AcOH, 50 °C, 0.15 MPa of H_2, 3 h	100	n-$C_5H_{11}NH_2$ $(n\text{-}C_5H_{11})_2NH$ $(n\text{-}C_5H_{11})_3N$	72 26 2	526
10% Pd/NGC (NGC grade is not specified)		Anisole, 100 °C, 0.6 MPa, 0.3 h	–	–	–	442
4.5% Pd–0.5% Pt/ Shawinigan Black®		40% aqueous solution of $MeNH_2$, 200 °C, 13.8 MPa, 6 h	–		51.7% yield	527, 528

Table 22. Catalytic properties of Pd/NGC, Au/NGC and Pd–Au/NGC samples in the liquid-phase hydrogenation of valeronitrile (AcOH, 50 °C, 0.15 MPa of H_2, 3 h).[526]

Catalyst	pH (see [a])	Fraction of the alloy in the Pd–Au system (%) (see [b])	*X* (%) (see [c])	*S*, % (see [d])		
				n-$C_5H_{11}NH_2$	$(n\text{-}C_5H_{11})_2NH$	$(n\text{-}C_5H_{11})_3N$
30% Pd/NGC	–	–	100	51	36	1
30% Au/NGC	–	–	0	–	–	–
25% Pd–5% Au/NGC	13.0	96.02	100	72	26	2
25% Pd–5% Au/NGC	8.0	12.85	100	29	34	11

[a] pH of the formaldehyde solution used for the reduction of deposited Pd and Au precursors; [b] according to XRD data of reduced catalysts; [c] valeronitrile conversion according to GC data; [d] selectivities to pentylamine, dipentylamine and tripentylamine according to GC data.

Scheme 9



reaches ~52%. These lactams are formed upon the addition of methylamine to intermediate products of hydrolysis and hydrogenation of the cyano groups in 2-methylglutaronitrile (Scheme 9).

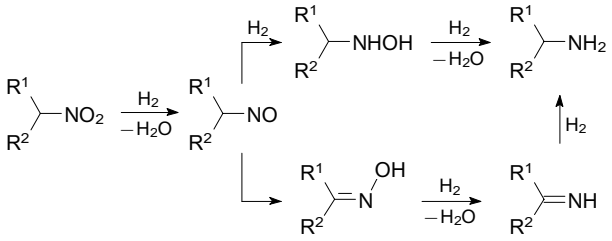
4.7. Hydrogenation of nitro compounds

Hydrogenation of nitro compounds with molecular hydrogen in the presence of metal catalysts is a well-known and widely used synthetic route to amines.[8, 529–537] Analysis of recent publications [533–537] demonstrated that the catalysts and the chemistry of hydrogenation of nitro compounds still attract a lot of attention of researchers. This may be due to both the practical significance of this process, since the resulting amines are key intermediates in organic synthesis,[529, 530, 538, 539] and the fact that the traditionally used non-catalytic reduction of nitro compounds with metallic iron, zinc or tin in acid solutions, sulfides or inorganic hydrides (such as $NaBH_4$) has considerable drawbacks.[529, 531, 532, 535, 539] The catalytic hydrogenation with gaseous hydrogen gives target products in high yields and, as a cost effective and environmentally benign method, it is more preferable for the reduction of organic compounds than chemical reduction.

According to the scheme proposed by Haber,[540] hydrogenation of aromatic nitro compounds (nitrobenzene and its derivatives) to anilines proceeds *via* a series of successive reactions and can be accompanied by condensation to give azoxy, azo and hydrazo compounds (Scheme 10). Currently, synthetic approaches for selective conversion of substituted nitrobenzenes not only to anilines, but also to partial reduction products have been proposed.[8, 536] If the hydrogenation conditions favour the transformation of the benzene ring to the cyclohexane ring, it is also possible to obtain oximes. For example, Pd/C-catalyzed liquid-phase hydrogenation of nitrobenzene in the presence of NH_2OH has been proposed as a synthetic route to cyclohexanone oxime in a yield of up to 97%.[541–543] It was shown [544–546] that hydrogenation of 1,3,5-trinitrobenzene derivatives in the presence of Pd/Sibunit gives, apart from the corresponding triamine, also cyclohexane-1,3,5-trione trioxime, the yield of which can reach 74%.

Aliphatic nitro compounds (first of all, nitroalkanes and nitrocycloalkanes) are less reactive towards the catalytic hydrogenation than aromatic nitro compounds.[8] The reductive transformations of aliphatic nitro compounds (Scheme 11) proceed *via* the intermediate formation of nitroso compounds, hydroxylamines and oximes and end in the formation of the corresponding amines.[547, 548] Under certain conditions, it is possible to attain high selectivity to the above partial reduction products; this is used in the organic synthesis practice.[8, 536]

Scheme 11



Quite a few supported catalysts containing Pt, Pd, Ru, Rh, Ni, Cu, Ag or Au have been proposed for hydrogenation of nitro compounds.[8, 531–537] Compositions of the Pd/C type are among the most demanded for this purpose, in particular, for the synthesis of amines on an industrial scale. In an industrial liquid-phase processes of nitrobenzene hydrogenation to aniline, palladium–carbon catalysts modified by platinum and iron (DuPont process [549, 550]) are used. An industrial process for aniline synthesis by gas-phase hydrogenation of nitrobenzene in the presence of lead-modified Pd/C catalysts was developed by the Bayer company.[549, 551]

A number of experimental studies [9, 73, 360, 363, 364, 391, 528, 552–569] demonstrated the application of NGC-supported palladium catalysts for hydrogenation of both aliphatic and aromatic nitro compounds (Table 23). These catalysts are often not inferior to and may even surpass the catalysts based on other carbon supports in the activity, selectivity and stability. Some of the developed bi- and polymetallic NGC-supported palladium catalysts were implemented in industrial processes for the hydrogenation of nitro compounds. For instance, Pd–Fe and Pd–Pb catalysts based on an acetylene NGC (Shawinigan Black®) are used for liquid-phase hydrogenation of nitrocyclohexane.[73, 552] They are prepared by deposition–precipitation: the carbon support is impregnated with a solution of a palladium salt (*e.g.*, $Na_2[PdCl_4]$); the subsequent addition of an alkaline reagent results in the precipitation of palladium hydroxide. The catalysts are modified by introducing iron or lead salts. These bimetallic catalysts,

Scheme 10

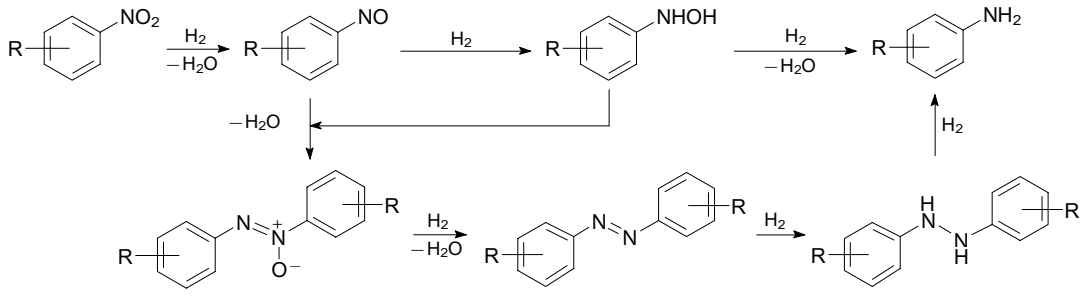


Table 23. Examples of using Pd/NGC catalysts in the hydrogenation of nitro compounds.

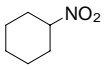
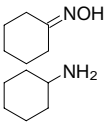
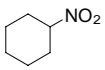
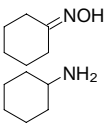
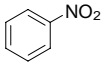
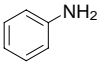
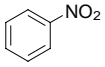
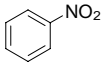
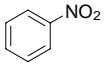
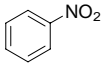
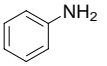
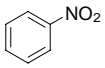
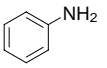
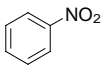
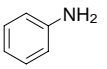
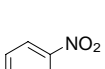
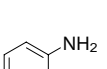
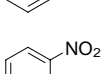
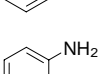
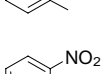
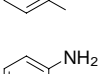
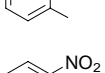
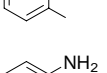
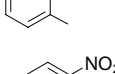
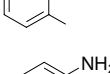
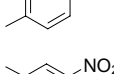
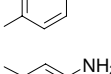
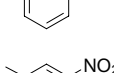
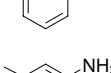
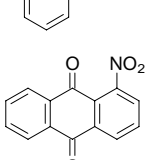
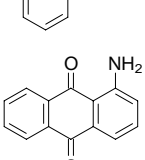
Catalyst	Substrate	Hydrogenation conditions	Substrate conversion (%)	Products	Selectivity (%)	Ref.
5% Pd – 5% Fe/Shawinigan Black®		H_2O, 75 °C, 3.4 MPa of H_2	–		71% yield	73
5% Pd – 5% Fe/Shawinigan Black®		Cyclohexylamine, 125 °C, 1.7 MPa of H_2, 1 h	100		87 13	73
5% Pd – 4% Pb/Shawinigan Black®		H_2O, 150 °C, 3.1 MPa of H_2, 1 h	–		92.1 4.3	552
5% Pd – 5% Fe/Shawinigan Black®		No solvent, 170 °C, 1.7 MPa, 1 h	> 99.9		100	73
1.75% Pd/Shawinigan Black®		$Pr^iOH - H_2O$, 30 °C, 0.1 MPa, 5 min	–	–	–	553, 554
1.75% Pd/B2 (NGC manufactured by Degussa-Hüls)		$Pr^iOH - H_2O$, 30 °C, 0.1 MPa, 5 min	–	–	–	553, 554
1.7% Pd/Vulcan® XC-72		$EtOH - H_2O$, 40 °C, 0.3 MPa	–	–	–	555
5% Pd/NGC (NGC grade is not specified)		Aniline – H_2O, 80 °C, 4.0 MPa of H_2, 9.5 min	–		–	360
4.5% Pd – 0.5% Pt/NGC (NGC grade is not specified)		Aniline – H_2O, 80 °C, 4.0 MPa of H_2, 6.5 min	–		–	360
4.5% Pd – 0.5% Pt – 5% Fe/NGC (NGC grade is not specified)		Aniline – H_2O, 80 °C, 4.0 MPa of H_2, 6.5 min	–		–	360
0.73%Pd/NGC (NGC manufactured by Micromeritics)		No solvent, 90 °C, 0.4 MPa of H_2	10 – 30		99	391
4.5% Pd – 0.5% Pt – 5% Fe/Shawinigan Black®		*o*-Toluidine – H_2O, 100 °C, 0.97 MPa of H_2	> 99.9		–	556, 557
5% Pd/Shawinigan Black®		120 °C, 3.4 MPa	–		–	528
4.5% Pd – 0.5% Pt – 5% Fe/Shawinigan Black®		120 °C, 3.4 MPa	–		–	528
1% Pd – 1% Zn/NGC (NGC grade is not specified)		AcOH, 40 °C, 0.1 MPa	100		–	558
2% Pd/acetylene NGC (NGC grade is not specified)		MeOH, 100 – 115 °C, 0.5 MPa, 4 h	99.7		94.3% yield	559
Pd – Pt – Rh/acetylene NGC (NGC grade is not specified)		MeOH, 100 – 115 °C, 0.5 MPa, 1.5 h	99.99		95.5% yield	559
5% Pd/acetylene NGC (NGC grade is not specified)		$Pr^iOH - H_2O$, NaOH, 30 °C, 0.1 MPa, ~100 min	–		94.0% yield	560

Table 23 (continued).

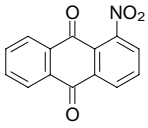
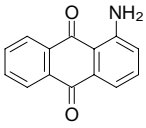
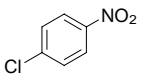
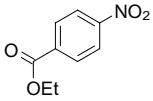
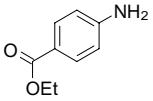
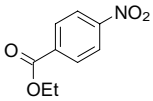
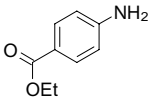
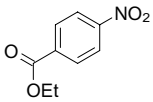
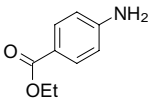
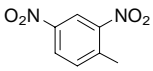
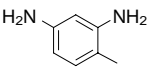
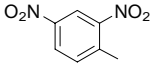
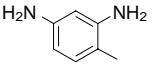
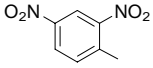
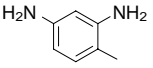
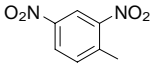
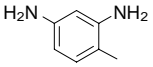
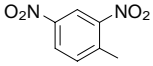
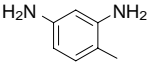
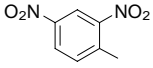
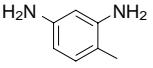
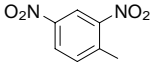
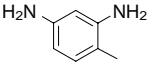
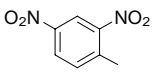
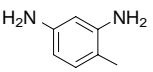
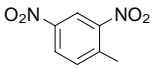
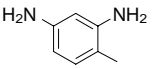
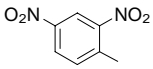
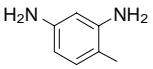
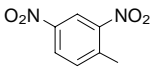
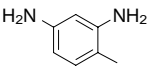
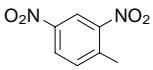
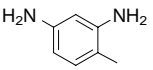
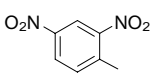
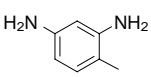
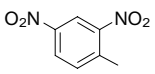
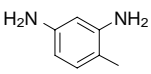
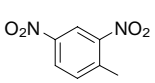
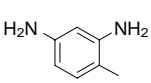
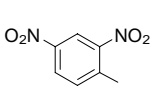
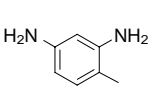
Catalyst	Substrate	Hydrogenation conditions	Substrate conversion (%)	Products	Selectivity (%)	Ref.
0.7% Pd – 0.1% Pt/acetylene NGC (NGC grade is not specified)		Pr^iOH-H_2O, NaOH, 30 °C, 0.1 MPa, ~100 min	–		97.7% yield	560
2% Pd – Pt – 3% Rh/ acetylene NGC (NGC grade is not specified)		100 – 110 °C, 0.4 – 0.6 MPa	100	–	–	561
1% Pd/P145		EtOH, 50 °C, 0.5 MPa of H_2, 1 h	> 99.9		96.2	363, 364
1% Pd/P278-E		EtOH, 50 °C, 0.5 MPa of H_2, 1 h	96.1		86.4	363, 364
1% Pd/T900		EtOH, 50 °C, 0.5 MPa of H_2, 1 h	> 99.9		> 99.9	363, 364
1.0% Pd/acetylene NGC (NGC grade is not specified)		2,4-Toluylenediamine, 90 – 110 °C, 0.7 MPa	–		–	562, 563
1% Pd – 1% Fe/acetylene NGC (NGC grade is not specified)		2,4-Toluylenediamine, 90 – 110 °C, 0.7 MPa	–		–	562, 563
4.5% Pd – 0.5% Pt – 5% Fe/ acetylene NGC (NGC grade is not specified)		2,4-Toluylenediamine, 90 – 110 °C, 0.7 MPa	–		–	562, 563
10% Pd – Fe/Shawinigan Black®		2,4-Toluylenediamine, 90 – 110 °C, 0.7 MPa	–		96% yield	563
Pd – Pt – Fe/acetylene NGC (NGC grade is not specified)		EtOH, 40 °C, 0.17 MPa of H_2	–		–	564
4.67% Pd/Vulcan® 3		MeOH, 100 °C, 1.4 MPa	–		–	565, 566
4.51% Pd/Vulcan® 3 (NGC pretreated with HNO_3)		MeOH, 100 °C, 1.4 MPa	–		–	565, 566
2% Pd – 4% Fe/NGC (NGC grade is not specified)		MeOH, 120 °C, 5.0 MPa, 40 min	100		98.2	567
1.75% Pd/Shawinigan Black®		2,4-Toluylenediamine – H_2O, 100 – 120 °C, 1.0 MPa, 27 min	100		97.8	553, 554
1.75% Pd/B2 (NGC manufactured by Degussa-Hüls)		2,4-Toluylenediamine – H_2O, 100 – 120 °C, 1.0 MPa, 0.5 h	100		98.1	553, 554
1.75% Pd – 4.2% Fe/ Shawinigan Black®		2,4-Toluylenediamine – H_2O, 100 – 120 °C, 1.0 MPa, 26 min	100		94.4	553, 554
1.6% Pd – 0.2%Pt/ Shawinigan Black®		2,4-Toluylenediamine – H_2O, 120 °C, 1.0 MPa	–		98.85	568

Table 23 (continued).

Catalyst	Substrate	Hydrogenation conditions	Substrate conversion (%)	Products	Selectivity (%)	Ref.
1.6% Pd – 0.2% Pt – 4.2% Fe/ Shawinigan Black®		2,4-Toluylenediamine – H_2O, 120 °C, 1.0 MPa	–		97.92	568
1.6% Pd – 0.2% Pt – 10.5% Ce/Shawinigan Black®		2,4-Toluylenediamine – H_2O, 120 °C, 1.0 MPa	–		99.47	568
0.77% Pd – 0.09% Pt – 0.85% Fe/acetylene NGC (NGC grade is not specified)		–	–		–	9
Pd – Fe/acetylene NGC (NGC grade is not specified)		95 – 108 °C, 0.9 – 1.2 MPa	> 99.9		> 99	569

especially 5% Pd – 4% Pb/NGC, provide high selectivity to cyclohexanone oxime in the hydrogenation of nitrocyclohexane (see Table 23); therefore, they have been used in the large-scale production of ε-caprolactam (Nixan process developed by DuPont [437]).

Quite a few supported bi- and polymetallic palladium catalysts based on acetylene type NGC (*e.g.*, Shawinigan Black®) were developed for the industrial processes of selective hydrogenation of nitrobenzene,[553, 554] 2-nitrotoluene,[528, 556, 557] 3-nitrotoluene [559] and 2,4-dinitrotoluene [9, 553, 554, 562 – 564, 568, 569] to the corresponding anilines. In particular, as a result of many years research, the companies DuPont [528] and Degussa [9] optimized the composition of trimetallic palladium-containing catalysts for the industrial hydrogenation of 2,4-dinitrotoluene to 2,4-toluylenediamine. This important product is used to prepare 2,4-toluylene diisocyanate, which is utilized in the producion of polyurethane foams and polyurethane elastomers, coatings and various other goods.[529, 530, 570] For example, it was found that the supported composition containing 1.6 wt.% Pd, 0.2 wt.% Pt and 10.5 wt.% Ce on the Shawinigan Black® NGC is very efficient in the liquid-phase hydrogenation of 2,4-dinitrotoluene (in 2,4-toluylenediamine – H_2O at 120 °C and a pressure of 1.0 MPa) and affords 2,4-toluylenediamine with a selectivity of > 99%.[568] High catalytic performance in the hydrogenation of aromatic nitro compounds was also demonstrated by the 4.5% Pd – 0.5% Pt – 5% Fe/NGC composition, which was patented by DuPont.[528, 556, 557, 562, 563] It was established that introduction of platinum into the monometallic Pd/NGC catalyst significantly increases the activity, while the subsequent addition of iron to the Pd – Pt/NGC system leads to somewhat decreasing activity; meanwhile, this prevents hydrogenation of the benzene ring in the aromatic substrate and, hence, increases the selectivity to the target amine. Möbus *et al.*[360] carried out a comparative study of the industrial 5% Pd/NGC, 4.5% Pd – 0.5% Pt/NGC and 4.5% Pd – 0.5% Pt – 5% Fe/NGC samples obtained by deposition – precipitation.[563] Using TEM, the authors found that palladium NPs in the monometallic palladium catalyst are located on the CNG surface mainly as organized aggregates strictly according to the arrangement of strong adsorption sites (see Section 3.3, Fig. 27). The introduction of platinum and iron leads to disaggregation, thus increasing the proportion of isolated NPs (Pd – Pt and Pd – Pt – Fe alloys according to their composition). According to the incoherent inelastic neutron scattering data, this leads to a pronounced decrease in the reactivity of the deposited palladium towards the formation of β-hydride (Table 24).

A study of catalysts for the liquid-phase hydrogenation of nitrobenzene (aniline – H_2O, 80 °C, 4.0 MPa of H_2) demonstrated that the increase in the relative content of isolated NPs leads to a linear increase in the catalytic activity. Thus, Möbus *et al.*[360] clearly demonstrated that the introduction of modifying metals into the Pd/NGC catalyst causes significant structural changes of the deposited particles of the active component and thus crucially affects the catalyst activity in nitrobenzene hydrogenation.

However, as has been shown earlier,[42, 43] the desired activity and selectivity of Pd/NGC catalysts can also be attained without adding modifying agents or promoters, but merely by varying the structural characteristics of the support (for example, by using an appropriate type of

Table 24. Morphology and adsorption and catalytic properties of Pd, Pd – Pt and Pd – Pt – Fe nanoparticles deposited on NGC.[360]

Catalyst	d_{av}, nm (see [a])	f_{IN} (%) (see [b])	f_{LA} (%) (see [c])	f_{SA} (%) (see [d])	I_{PdH} (rel.u.) (see [e])	Activity, mmol g_{cat}^{-1} min^{-1} (see [f])
5% Pd/NGC	2.1	10	90	0	127.0	132
4.5% Pd – 0.5% Pt/NGC	2.3	90	10	0	87.6	738
4.5% Pd – 0.5% Pt – 5% Fe/NGC	2.0	60	10	30	26.3	462

[a] Average size of primary NPs according to TEM data; [b] proportion of isolated NPs according to TEM data; [c] proportion of linear NP aggregates according to TEM data; [d] proportion of spherical NP aggregates according to TEM data; [e] integral intensity of the peak corresponding to β-PdH_x in the incoherent inelastic neutron scattering spectrum; [f] the activity was found as the ratio of the nitrobenzene hydrogenation rate to the catalyst weight.

NGC) and catalyst preparation conditions. Recently, Mironenko *et al.*[363, 364] found that monometallic Pd/NGC catalysts containing 1 or 2 wt.% palladium exhibit high activity and selectivity in the hydrogenation of aromatic nitro compounds to the corresponding anilines under mild conditions. Common commercial industrial NGC grades — P145, P278-E (furnace types) and T900 (thermal type) were used as supports to prepare catalysts. The catalysts were obtained by deposition of various palladium precursors on these carbon supports followed by reduction to palladium metal (Table 25). Hydrogenation of ethyl 4-nitrobenzoate (EtOH, 50 °C, 0.5 MPa, 1 h) was studied in most detail. It was shown that the catalytic performance of 1% Pd/NGC samples in this reaction depends both on the type of NGC and on the chemical nature of the palladium precursor used for their preparation (see Table 25). Note that many NGC-supported catalysts were more active than 1% Pd/CNTs and provided an almost 100% selectivity to ethyl 4-aminobenzoate (benzocaine) at a complete substrate conversion (see also Ref. 571). Moreover, NGC-supported catalysts were highly stable in this reaction: the activity and selectivity remained at a high level upon reuse. Therefore, 1% Pd/NGC catalysts can be considered to be fairly promising for the industrial production of benzocaine, which is used in medicine as local anesthetic.[474]

As can be seen from the data summarized in Table 25, 1% Pd/T900 catalysts were more active than 1% Pd/P145 and 1% Pd/P278-E. In the opinion of Mironenko *et al.*,[364] this can be attributed to high dispersion of palladium in the 1% Pd/T900 catalyst (see Section 3.3, Fig. 28 *b*) and also to the optimal structural characteristics of T900, which apparently ensure higher accessibility of the palladium sites to reactant molecules. The thermal NGC of the T900 grade consists mainly of single or weakly aggregated CNGs, while furnace P145 and P278-E grades consist of aggregates of tens and hundreds of nanoglobules (see Section 3.3, Table 4). During the liquid-phase reaction, NGC-supported catalysts form suspensions, the smallest particle size of which is determined by CNG aggregate (agglomerate) size. In view of the above, Mironenko *et al.*[364] assumed that catalyst particles based on furnace NGC suspended in the reaction solution had an internal porosity and clear-cut surface roughness, while the Pd/T900 particles were spherical and had a smooth surface; therefore, adsorption – desorption processes were faster in the case of Pd/T900 than for Pd/P145 or Pd/P278-E. This was favourable for high activity and selectivity of T900-based catalysts in the liquid-phase hydrogenation reactions.

Table 25. Catalytic properties of 1% Pd/C samples in ethyl 4-nitrobenzoate hydrogenation (EtOH, 50 °C, 0.5 MPa of H_2, 1 h).[363, 364]

Catalyst	Pd precursor	TOF, min^{-1} (see [a])	X (%) (see [b])	S (%) (see [c])
1% Pd/P145	$H_2[PdCl_4]$	< 30	> 99.9	96.2
1% Pd/P145	Pd PHCs	153	> 99.9	> 99.9
1% Pd/P278-E	$H_2[PdCl_4]$	< 30	96.1	86.4
1% Pd/P278-E	Pd PHCs	328	> 99.9	> 99.9
1% Pd/T900	$H_2[PdCl_4]$	253	> 99.9	> 99.9
1% Pd/T900	Pd PHCs	398	> 99.9	> 99.9
1% Pd/CNTs	$H_2[PdCl_4]$	92	> 99.9	> 99.9

[a] TOF values were calculated as the ratio of hydrogen consumption rate in the reaction to the amount of palladium in the catalyst and palladium dispersion according to CO chemisorption data; [b] ethyl 4-nitrobenzoate conversion according to GC data; [c] selectivity to benzocaine according to GC data.

The conclusions drawn by Mironenko *et al.*[363, 364] are generally consistent with the results of earlier studies by Suh *et al.*,[565, 566] according to which the absence of extensive microporosity in NGC and high degree of dispersion of palladium in Pd/NGC are favourable for high activity in the hydrogenation of 2,4-dinitrotoluene. A comparative study of the supported palladium catalysts (4 – 5 wt.% Pd) obtained using various AC grades and a furnace NGC (Vulcan® 3, Cabot) was carried out. The catalysts were prepared by alkaline hydrolysis of palladium chloride complexes carried out in the presence of carbon support and the subsequent reduction of the deposited precursor with a formaldehyde solution. The variable dispersion of palladium in the catalysts was attained by oxidative pretreatment of the support with nitric acid, hydrogen peroxide or sodium hypochlorite. It was found that oxidative treatment had no significant effect on the porosity of carbon supports, but resulted in increased concentration of oxygen-containing functional groups on the carbon surface, and, upon the subsequent deposition of palladium, in its higher dispersion, although this effect markedly depended on the carbon support and oxidant natures. It was shown that NGC-supported palladium catalysts had a markedly higher activity in the hydrogenation of 2,4-dinitrotoluene (MeOH, 100 °C, 1.4 MPa) than any Pd/AC sample. The authors attributed this result to the absence of clear-cut microporosity in NGC and accessibility of palladium NPs, which were located on the external surface of CNGs. In the case of AC, some of palladium was located in micropores; therefore, it was inaccessible for the reacting molecules. The preliminary oxidative treatment of NGC with nitric acid was favourable for increasing the dispersion of deposited palladium, which resulted in higher activity of Pd/NGC samples.

Thus, many studies demonstrated the possibility of using supported Pd/NGC compositions to catalyze the liquid-phase selective hydrogenation of a broad range of organic compounds. On the basis of the foregoing, we can distinguish the following advantages of NGC and palladium catalysts based on this carbon material over other catalysts used for liquid-phase hydrogenation.

First, NGC is cheaper and more readily available than other carbon nanomaterials, and a type of NGC, carbon black, is commercially manufactured as a wide range of grades. The variation of NGC preparation conditions and the possibility of subsequent modification make it possible to independently control the structure of particles and the physicochemical properties of CNG surface and, hence, the formation conditions and the catalytic properties of palladium-containing sites.

Second, high activity and selectivity to desired products is observed for Pd/NGC catalysts containing only 1 – 2 wt.% palladium, which is beneficial in comparison with traditionally used Pd/AC catalysts, which contain much higher amounts of this expensive metal. The Pd/NGC catalysts are prepared using simple and well-established approaches.

Third, high catalytic performance of Pd/NGC catalysts is attained under mild conditions of liquid-phase hydrogenation. In many reactions, Pd/NGC catalysts exhibit high stability, *i.e.*, they retain high activity and selectivity to the target product when reused many times.

Owing to the listed advantages, Pd/NGC compositions are fairly promising as catalysts for fine and small-scale organic synthesis in the liquid phase. These advantages are caused, in particular, by structural features of NGC such as globular morphology, abundant coordination chemistry of the surface, with the absence of clearly defined surface defects, which produce micropores, and also chemical stability to various liquid media.

However, it should be emphasized that, despite the indicated advantages, Pd/NGC compositions are still poorly studied regarding the relationship between structural features of the support and catalytic properties of palladium-containing active sites. There are virtually no data on the effect of the structure and branching of NGC aggregates on the performance of Pd/NGC catalysts in liquid-phase reactions, in which an important role is played by hydrophobic–hydrophilic interactions with the solvent in the mesoporous space of the NGC aggregate. In our opinion, elucidation of these relationships is a primary objective of future research into NGC-supported catalysts.

5. Conclusion

The first studies on the use of NGC (as carbon black) in the synthesis of Pd/NGC catalysts for the hydrogenation of organic compounds were published back in the 1950s, but only in the last decade, owing to the active development of the preparation methods and studies of properties of carbon nanomaterials and, especially, the relationship between their physicochemical and functional characteristics, researchers started to evaluate the potential and character of NGC as a promising support for metal–carbon compositions with highly uniform catalytically active sites. Below we briefly consider the most important benefits (which were noted above in the relevant parts of the review) and the existing possibilities to enhance them by studying the synthesis of Pd/NGC compositions.

1. Since the primary particles of nanoglobular carbon are spherical, the uniformity of carbon as a nanomaterial can be increased by narrowing the particle size distribution; this can be attained rather easily by changing only one parameter: the diameter of a nanoglobule. This considerably differs from the situation for carbon nanomaterials in which the primary particles have a non-spherical morphology. For example, in the case of CNTs, there will be at least three parameters: the nanotube length, diameter and wall thickness (the number of graphene layers). The independent variation of each of these parameters (in such a way that the other two parameters remain unaffected) is problematic; to our knowledge, no such examples were reported. Meanwhile, the possibility to simultaneously and selectively vary the CNG diameter, narrow the size distribution of CNG nanospheres and deliberately modify their surface is evidenced in a number of recent publications and in reviews devoted to carbon nanostructures.[572–577]

2. An important condition determining the potential of carbon materials as catalyst supports is the presence of physicochemical (ligand) properties of the carbon particle surface. These properties are needed for both the formation of active sites (starting from the precursor adsorption, subsequent transformations on the surface and generation of the active state of the catalytic component) and stabilization of the active state during the catalytic cycles. In this context, CNG is a macroligand, which not only combines the ligand functions of various carbon nanostructures, but also opens up broad prospects for targeted change in the ratio of surface concentrations of these functions and increase in their uniformity. By varying only the diameter of CNGs during the NGC synthesis, it is possible to change the ratio of the concentrations of adsorption sites located on the basal and stepped structures of graphene crystallites that make up the nanoglobule surface. A more pronounced change in the ligand properties of NGC can be attained by using surface functionalization procedures and by varying the conditions of synthesis to affect not only the structure of the CNG surface layer, but also the composition and structure of the CNG bulk (when the carbon nanoglobule is small, this will affect the physicochemical state of the surface). Among such procedures, the following can be mentioned:

— generation of carbon aerosol in a high-temperature gas flow of hydrocarbons with introduction of seeds: carbon clusters and metal clusters;

— synthesis of CNGs by plasma-chemical method in the hydrocarbon gas phase or by plasma discharge in the liquid phase of single hydrocarbons;

— preparation of NGC by chemical vapour deposition from hydrocarbons with or without catalysts;

— preparation of single CNGs with simultaneous narrowing of their size distribution by mechanochemical, ultrasonic, gravitational and flotation disaggregation of carbon black followed by surface functionalization;

— the introduction of heteroatoms into the CNG bulk by generating a plasma discharge in the liquid phase of a heteroatomic organic compound;

— structural change of the CNG bulk upon high-energy impact.

The concepts of development of these methods and their potential applications for the synthesis of NGC and the results of detailed investigation of structural changes in the CNG bulk and surface are considered in recent original papers and reviews.[125, 578–584]

3. An equally important aspect that determines the catalytic properties of Pd/NGC compositions is the development of palladium deposition methods applicable to the carbon macroligand such that the use of these methods would not decrease (due to side reactions) the initial (specified by the synthesis) uniformity of both the CNG adsorption sites and palladium compounds in solution. The solution of this challenging problem may be based on the deposition of either palladium compounds dissolved in organic solvents with a low dielectric constant or volatile palladium compounds from the gas phase. If the desired palladium compounds can be deposited only from the aqueous medium and the NGC particles are electrically conductive, the complex formation pathway (*i.e.*, the nature of the site that will interact with the palladium compound) can be controlled (chosen) by applying a certain electrical potential to the support particles and thus affecting the undesirable spontaneous palladium reduction by electrons of the carbon crystallite. High uniformity of the sites is also facilitated by depositing Pd^0/Pd^I complexes and clusters or palladium NPs (obtained by electrochemical synthesis), instead of Pd^{II} complexes. Detailed analysis of the application of cluster compounds of metals, including palladium, for the synthesis and studies of various catalytic compositions was carried out in the latest reviews.[585–592]

4. As follows from the data presented in this review, Pd/NGC compositions often demonstrate better catalytic performance in the hydrogenation of organic compounds than

supported palladium systems based on other carbon materials. These advantages may be attributable, in particular, to specific features of NGC structure (globular morphology and the absence of surface structures producing micropores). Lately, certain progress has been attained in studying the mechanisms of interaction of palladium atoms, clusters and NPs with curved carbon nanostructures (fullerene, nanotubes). However, studies at this level for CNGs the surface of which is rich in extended 2D and 3D (*e.g.*, slit-like) defects are still scarce. The research on the catalytic chemistry of Pd/NGC compositions is still at the data collection stage, with most part of the data being reported in patents. The effect of structure of NGC aggregates, especially branched ones, on the catalytic properties of deposited Pd particles is almost unexplored. It is important to understand the role of charged Pd_n states and the nature of the Pd_n/C_m contact boundary in the activation of hydrogen molecules and organic substrates and how this activation is affected by the hydrophobic–hydrophilic interactions with the solvent, occurring in the mesoporous space of NGC aggregates. Furthermore, of obvious interest is to study characteristic features and details of the variation of activity and selectivity of Pd/NGC catalysts in the following processes:

— hydrogenation of organic substrates with variable electrical potential of the catalyst;

— competitive hydrogenation of substrates with unsaturated bonds of different polarity;

— hydrogenation of substrates with variation of substituents at the unsaturated bond of the same nature;

— partial poisoning of Pd_n/C_m sites.

The concept of development of these methods and the most recent achievements in their application to palladium–carbon compositions were discussed in recent publications.[18, 593 – 597]

In conclusion, we would like to note that the interest in the development and advancement of methods for preparing NGC and other carbon nanomaterials can significantly increase in the near future due to the necessity of solving challenges of green energy production based on hydrogen. Hydrogen free from carbon dioxide can be obtained, for example, by thermal decomposition of hydrocarbons induced by plasma heating. Carbon as NGC, CNTs and other nanostructured forms can be the second valuable product of this process. Carbon nanomaterials have already proved to be commercially attractive in a number of fields such as environment protection technologies, construction industry and production of composite materials, including adsorbents and catalysts. This is an important factor that should be taken into account in the practical implementation of such a global concept as green energy production.

This review was supported by the Ministry of Science and Higher Education of the Russian Federation within the governmental order for Boreskov Institute of Catalysis (Project AAAA-A21-121011490008-3).

6. Note added in proof

While this review was prepared for publication, a number of original and review papers addressing the preparation, investigation and application of nanoglobular carbon have appeared in the scientific literature. Among them, we will mention the publications that are most important, in our opinion, regarding further development of the current trends discussed in the Conclusion.

First of all, mention should be made of the remarkable review by Martin *et al.*,[598] who gives a detailed account of inception mechanisms of carbon nanoglobules in flames based on analysis of a large body of experimental and theoretical data; the attention is focused on mechanistic details of the formation of precursor molecules and primary carbon nanoparticles from them (*i.e.*, details of system transition from the molecular zone to particle zone, which was mentioned in Section 2.1).

The researchers interest in the synthesis, investigation and application of globular carbon nanomaterials still persists. In this respect, it is necessary to note the review by Liu *et al.*,[599] who addressed modern methods for the preparation of hollow carbon nanostructures, and the review by Saini *et al.*,[600] devoted to isolation of carbon nanomaterials from soot as a part of disposal of soot as an environmental pollutant and potential application of isolated nanomaterials in biotechnology, catalysis, energy production and agriculture.

The scope of application of plasma methods for the preparation of catalysts based on nanoglobular carbon is being extended. Tipplook *et al.*[601] demonstrated the application of *in situ* solution plasma (mentioned in Section 2.3) for the synthesis of catalysts containing platinum supported on functionalized carbon nanoglobules. By applying a plasma discharge to an ethanol solution containing phenol and heteroatomic (silicon- and sulfur-containing) organic compounds as precursors of carbon nanoglobules and hydrophilic (hydrophobic) surface functional groups, respectively, and by using platinum electrodes (Pt source), the authors obtained Pt/NGC compositions, which proved to be highly efficient (in comparison with conventional Pt/C) electrocatalysts for fuel cells.

Most of recently published studies on the use of carbon in catalysis[602 – 608] still focus on such carbon materials as carbon nanotubes, nanofibres, graphene, ordered mesoporous materials and carbon–carbon composites; however, there is a trend towards increasing number of papers addressing nanoglobular carbon as a support for catalytically active components.[609 – 623] In this connection, mention should be made of several publications devoted to studying Pd/NGC compositions in the hydrogenation of vinyl derivatives,[617] alkynes,[618] furfural,[619, 620] and aromatic nitro compounds.[621 – 623] These publications demonstrated high performance (activity, selectivity) of Pd/NGC catalysts in the studied reactions. Of particular interest is the paper by Zhang *et al.*,[623] who demonstrated that, for hydrogenation of *p*-chloronitrobenzene, the inverse dependence of the selectivity to *p*-chloroaniline on the size of palladium particles supported on pre-oxidized NGC is caused by the oxygen functional groups present on the support surface, which affect the charge state of palladium in the Pd_n/C_m cluster. The results of this study are also of interest for applied purposes of development of efficient Pd/C catalysts for selective catalytic hydrogenation processes.

7. List of acronyms and designations

AC — activated carbon,
AFM — atomic force microscopy,
CNFs — carbon nanofibres,
CNGs — carbon nanoglobules,
CNTs — carbon nanotubes,
CSR — coherent scattering region,
CVD — chemical vapour deposition,

DFT — density functional theory,
EDL — electrical double layer,
EXAFS — extended X-ray absorption fine structure,
GC — gas chromatography,
GLCs — graphite-like crystallites,
GN — growth nucleus,
LAMMPS — large-scale atomic/molecular massively parallel simulation,
NGC — nanoglobular carbon,
NPs — nanoparticles,
PAHs — polycyclic aromatic hydrocarbons,
PANI — polyaniline,
PHCs — polynuclear hydroxo complexes,
PVP — polyvinylpyrrolidone,
SAXS — small angle X-ray scattering,
SMSI — strong metal–support interactions,
STEM — scanning transmission electron microscopy,
TEM — transmission electron microscopy,
TOF — turnover frequency,
TPR — temperature-programmed reduction,
XPS — X-ray photoelectron spectroscopy,
XRD — X-ray diffraction

8. References

1. L.R.Radovic, F.Rodríguez-Reinoso. In *Chemistry and Physics of Carbon*. (Ed. P.A.Thrower). (New York: Marcel Dekker, 1996). P. 243
2. F.Rodríguez-Reinoso. *Carbon*, **36**, 159 (1998)
3. P.Serp, B.Machado. *Nanostructured Carbon Materials for Catalysis*. (Cambridge: The Royal Society of Chemistry, 2015)
4. R.A.Sheldon, H.van Bekkum. *Fine Chemicals through Heterogeneous Catalysis*. (Weinheim: Wiley-VCH, 2001)
5. H.-U.Blaser, A.Indolese, A.Schnyder, H.Steiner, M.Studer. *J. Mol. Catal. A: Chem.*, **173**, 3 (2001)
6. X.Liu, D.Astruc. *Adv. Synth. Catal.*, **360**, 3426 (2018)
7. H.F.Rase. *Handbook of Commercial Catalysts: Heterogeneous Catalysts*. (Boca Raton, FL: CRC Press, 2000)
8. S.Nishimura. *Handbook of Heterogeneous Catalytic Hydrogenation for Organic Synthesis*. (New York: Wiley, 2001)
9. V.Arunajatesan, B.Chen, K.Möbus, D.J.Ostgard, T.Tacke, D.Wolf. In *Carbon Materials for Catalysis*. (Eds P.Serp, J.L.Figueiredo). (Hoboken: Wiley, 2009). P. 535
10. H.Sajiki, Y.Monguchi. In *Pharmaceutical Process Chemistry*. (Eds T.Shioiri, K.Izawa, T.Konoike). (Weinheim: Wiley-VCH, 2011). P. 77
11. W.Bonrath, J.Medlock, J.Schütz, B.Wüstenberg, T.Netscher. In *Hydrogenation*. (Ed. I.Karamé). (Rijeka: InTech, 2012). P. 69
12. I.Favier, D.Madec, E.Teuma, M.Gómez. *Curr. Org. Chem.*, **15**, 3127 (2011)
13. R.S.Oosthuizen, V.O.Nyamori. *Platinum Met. Rev.*, **55**, 154 (2011)
14. A.C.Albéniz, P.Espinet. In *Encyclopedia of Inorganic and Bioinorganic Chemistry*. (Ed. R.A.Scott). (Hoboken: Wiley, 2011)
15. I.I.Moiseev, M.N.Vargaftik. *Ros. Khim. Zh.*, **50** (4), 72 (2006)
16. J.P.Wolfe, J.J.Li. *Tetrahedron Org. Chem. Ser.*, **26**, 1 (2007)
17. H.Renner, G.Schlamp, I.Kleinwächter, E.Drost, H.M.Lüschow, P.Tews, P.Panster, M.Diehl, J.Lang, T.Kreuzer, A.Knödler, K.A.Starz, K.Dermann, J.Rothaut, R.Drieselmann, C.Peter, R.Schiele. In *Ullmann's Encyclopedia of Industrial Chemistry*. Vol. 28. (Weinheim: Wiley-VCH, 2012). P. 317
18. B.Van Vaerenbergh, J.Lauwaert, P.Vermeir, J.W.Thybaut, J.De Clercq. *React. Chem. Eng.*, **5**, 1556 (2020)
19. M.Saytzeff. *J. Prakt. Chem.*, **6**, 128 (1873)
20. G.Orlow. *Ber. Deutsh. Chem. Ges.*, **42**, 893 (1909)
21. E.Thiele. Inaugural-Dissertation zur Erlangung der Doktorwürde. Druck der Univ.-Buchdruckerei von E.A.Huth, Göttingen, 1914
22. C.Mannich, E.Thiele. *Arch. Pharm.*, **253**, 181 (1915)
23. C.Mannich, E.Thiele. *Ber. Deutsh. Pharm. Ges.*, **26**, 36 (1916)
24. C.Ellis. *Hydrogenation of Organic Substances Including Fats and Fuels*. (New York: D.Van Nostrand Company, 1930)
25. S.Berkman, J.C.Morrell, G.Egloff. *Catalysis, Inorganic and Organic*. (New York: Reinhold Publishing, 1940)
26. R.Mozingo. *Org. Synth.,* **26**, 77 (1946)
27. P.N.Rylander. *Catalytic Hydrogenation over Platinum Metals*. (New York: Academic Press, 1967)
28. A.B.Stiles.*Catalyst Supports and Supported Catalysts: Theoretical and Applied Concepts*. (Boston: Butterworths, 1987)
29. V.A.Semikolenov. *Russ. Chem. Rev.*, **61**, 168 (1992)
30. P.A.Simonov, S.Yu.Troitskii, V.A.Likholobov. *Kinet. Catal.*, **41**, 255 (2000)
31. M.L.Toebes, J.A.van Dillen, K.P.de Jong. *J. Mol. Catal.: A. Chem.*, **173**, 75 (2001)
32. A.S.Lisitsin, V.N.Parmon, V.K.Duplyakin, V.A.Likholobov. *Ros. Khim. Zh.,* **50** (4), 140 (2006)
33. B.Van Vaerenbergh, J.Lauwaert, P.Vermeir, J.De Clercq, J.W.Thybaut. *Adv. Catal.*, **65**, 1 (2019)
34. Yu.I.Yermakov, V.F.Surovikin, G.V.Plaksin, V.A.Semikolenov, V.A.Likholobov, L.V.Chuvilin, S.V.Bogdanov. *React. Kinet. Catal. Lett.*, **33**, 435 (1987)
35. V.F.Surovikin, Yu.V.Surovikin, M.S.Tsekhanovich. *Russ. J. Gen. Chem.*, **77**, 2301 (2007)
36. V.A.Likholobov, V.F. Surovikin, G.V.Plaksin, M.S.Tsekhanovich, Yu.V.Surovikin, O.N.Baklanova. *Catal. Ind.*, **1**, 11 (2009)
37. G.V.Plaksin, O.N.Baklanova, A.V.Lavrenov, V.A.Likholobov. *Solid Fuel Chem.*, **48**, 349 (2014)
38. D.S.Su. In *Nanomaterials in Catalysis*. (Eds P.Serp, K.Philippot). (Weinheim: Wiley-VCH, 2013). P. 331
39. J.Zhu, A.Holmen, D.Chen. *ChemCatChem*, **5**, 378 (2013)
40. E.Bailón-García, F.J.Maldonado-Hódar, A.F.Pérez-Cadenas, F.Carrasco-Marín. *Catalysts*, **3**, 853 (2013)
41. I.C.Gerber, P.Serp. *Chem. Rev.*, **120**, 1250 (2020)
42. R.M.Mironenko, O.B.Belskaya, V.A.Likholobov. *Russ. J. Gen. Chem.*, **90**, 532 (2020)
43. R.M.Mironenko, O.B.Belskaya, V.A.Likholobov. *Catal. Today*, **357**, 152 (2020)
44. V.Georgakilas, J.A.Perman, J.Tucek, R.Zboril. *Chem Rev.*, **115**, 4744 (2015)
45. A.Barhoum, A.E.Shalan, S.I.El-Hout, G.A.M.Ali, S.M.Abdelbasir, E.S.A.Serea, A.H.Ibrahim, K.Pal. In *Handbook of Nanofibers*. (Eds A. Barhoum, M.Bechelany, A.S.H.Makhlouf). (Cham: Springer, 2019). P. 1

46. Y.M.Manawi, Ihsanullah, A.Samara, T.Al-Ansari, M.A.Atieh. *Materials*, **11**, 822 (2018)
47. S.D.Stoica, S.Vizireanu, T.Acsente, G.Dinescu. *Plasma Chem. Plasma Process.*, **38**, 695 (2018)
48. R.Singh, R.K.Singh. *IOSR J. Appl. Phys.*, **9**, 42 (2017)
49. M.Inagaki. *Carbon*, **35**, 711 (1997)
50. P.Serp, R.Feurer, P.Kalck, Y.Kihn, J.L.Faria, J.L.Figueiredo. *Carbon*, **39**, 621 (2001)
51. N.J.Coville, S.D.Mhlanga, E.N.Nxumalo, A.Shaikjee. *S. Afr. J. Sci.*, **107**, 418 (2011)
52. Yu.G.Kryazhev, N.N.Koval', V.A.Likholobov, A.D.Teresov, V.A.Drozdov, M.V.Trenikhin. *Tech. Phys. Lett.*, **38**, 301 (2012)
53. B.P.Tarasov, V.E.Muradyan, A.A.Volodin. *Russ. Chem. Bull. Int. Ed.*, **60**, 1261 (2011)
54. J.R.Siqueira Jr., O.N.Oliveira Jr. In *Nanostructures*. (Eds A.L.Da Róz, M.Ferreira, F.de Lima Leite, O.N.Oliveira Jr.). (Amsterdam: Elsevier, 2017). P. 233
55. R.Sharma, A.K.Sharma, V.Sharma. *Cogent Eng.*, **2**, 1094017 (2015)
56. L.Stobinski, B.Lesiak, L.Kövér, J.Tóth, S.Biniak, G.Trykowski, J.Judek. *J. Alloys Compd.*, **501**, 77 (2010)
57. A.Yu, E.Bekyarova, M.E.Itkis, D.Fakhrutdinov, R.Webster, R.C.Haddon. *J. Am. Chem. Soc.*, **128**, 9902 (2006)
58. A.A.Deshmukh, S.D.Mhlanga, N.J.Coville. *Mater. Sci. Eng. R*, **70**, 1 (2010)
59. S.C.Ray, A.Saha, N.R.Jana, R.Sarkar. *J. Phys. Chem. C*, **113**, 18546 (2009)
60. J.P.Singh, T.Nandi, S.K.Ghosh, J.Srivastava, S.K.Tripathi, N.E.Prasad. *Sep. Sci. Technol.*, **53**, 2314 (2018)
61. M.Voll, P.Kleinschmit. In *Ullmann's Encyclopedia of Industrial Chemistry*. Vol. 7. (Weinheim: Wiley-VCH, 2012). P. 1
62. T.G.Gyulmisaryan, V.M.Kapustin, I.P.Levenberg. *Tekhnicheskii Uglerod: Morfologiya, Svoistva, Proizvodstvo. (Carbon Black: Morphology, Properties, Production)*. (Moscow: Kauchuk i Rezina, 2017)
63. S.Khodabakhshi, P.F.Fulvio, E.Andreoli. *Carbon*, **162**, 604 (2020)
64. T.G.Gyulmisaryan, I.P.Levenberg. *Tekhnologii Nefti i Gaza*, (3), 3 (2018)
65. C.M.Long, M.A.Nascarella, P.A.Valberg. *Environ. Pollut.*, **181**, 271 (2013)
66. A.Y.Watson, P.A. Valberg. *Am. Ind. Hyg. Assoc. J.*, **62**, 218 (2001)
67. H.Qian, F.Han, B.Zhang, Y.Guo, J.Yue, B.Peng. *Carbon*, **42**, 761 (2004)
68. C.J.Gutiérrez-García, J.M.Ambriz-Torres, J.de Jesús Contreras-Navarrete, F.G.Granados-Martínez, D.L.García-Ruiz, L.García-González, L.Zamora-Peredo, L.F.Ortega-Varela, A.Richaud, F.Méndez, L.Domratcheva-Lvova. *Physica E*, **112**, 78 (2019)
69. S.-H.Hwang, T.Okumura, K.Kamataki, N.Itagaki, K.Koga, M.Shiratani. *Diamond Relat. Mater.*, **109**, 108050 (2020)
70. J.Kang, O.L.Li, N.Saito. *Carbon*, **60**, 292 (2013)
71. K.Tamaru. *Bull. Chem. Soc. Jpn.*, **24**, 177 (1951)
72. M.Levine, S.C.Temin. *J. Org. Chem.*, **22**, 85 (1957)
73. Patent US 2823235 (1958)
74. M.Alfe, V.Gargiulo, R.Di Capua. *Eurasian Chem.-Technol. J.*, **21**, 203 (2019)
75. S.Zhong, N.Tsumori, M.Kitta, Q.Xu. *Nano Res.*, **12**, 2966 (2019)
76. M.Jametel. *L'encre de Chine. Son Histoire et sa Fabrication d'apres des Documents Chinois*. (Paris: Ernest Leroux, 1882)
77. C.A.Mitchell, T.C.Hepworth. *Inks: Their Composition and Manufacture*. (London: Charles Griffin and Company, 1904)
78. M.A.Robin. *Proizvodstvo Sazhi. (Carbon Black Production)*. (Moscow: VNIIOENG, 1967)
79. Patent US 481240 (1892)
80. G.L.Cabot. *J. Soc. Chem. Ind.*, **13**, 128 (1894)
81. I.Drogin. *Developments and Status of Carbon Black*. (Charleston: United Carbon Company, 1945)
82. Patent US 1168931 (1916)
83. R.L.Moore. *Ind. Eng. Chem.*, **24**, 21 (1932)
84. V.Yu.Orlov, A.M.Komarov, L.A.Lyapina. *Proizvodstvo i Ispol'zovanie Tekhnicheskogo Ugleroda dlya Rezin. (Production and Use of Carbon Black for Rubber)*. (Yaroslavl': Aleksandr Rutman, 2002)
85. M.Faraday. *A Course of Six Lectures on the Chemical History of a Candle*. (London: Griffin, Bohn, and Company, 1861)
86. P.A.Tesner. *Obrazovanie Ugleroda iz Uglevodorodov Gazovoi Fazy. (Formation of the Carbon from Hydrocarbons in a Gas Phase)*. (Moscow: Khimiya, 1972)
87. B.S.Haynes, H.G.Wagner. *Prog. Energy Combust. Sci.*, **7**, 229 (1981)
88. S.J.Harris, A.M.Weiner. *Annu. Rev. Phys. Chem.*, **36**, 31 (1985)
89. R.C.Bansal, J.-B.Donnet. In *Carbon Black: Science and Technology*. (Ed. J.-B.Donnet). (New York: Marcel Dekker, 1993). P. 67
90. M.Frenklach, H.Wang. In *Soot Formation and Combustion: Mechanisms and Models*. (Ed. H.Bockhorn). (Berlin: Springer-Verlag, 1994). P. 165
91. I.M.Kennedy. *Prog. Energy Combust. Sci.*, **23**, 95 (1997)
92. Z.A.Mansurov. *Combust. Explos. Shock Waves*, **41**, 727 (2005)
93. P.J.F.Harris. *Crit. Rev. Solid State Mater. Sci.*, **30**, 235 (2005)
94. M.Ozawa, E.Ōsawa. In *Carbon Nanotechnology: Recent Developments in Chemistry, Physics, Materials Science and Device Applications*. (Ed. L.Dai). (Amsterdam: Elsevier, 2006). P. 127
95. V.F.Surovikin. *Ros. Khim. Zh.*, **51** (4), 92 (2007)
96. Z.A.Mansurov. *J. Eng. Phys. Thermophys.*, **84**, 125 (2011)
97. H.Wang. *Proc. Combust. Inst.*, **33**, 41 (2011)
98. Y.Wang, S.H.Chung. *Prog. Energy Combust. Sci.*, **74**, 152 (2019)
99. M.P.Galanin, A.V.Isaev, S.A.Konev. *Institute of Applied Mathematics named after M.V. Keldysh*, 110 (2019)
100. M.Frenklach, A.M.Mebel. *Phys. Chem. Chem. Phys.*, **22**, 5314 (2020)
101. M.Gautier, V.Rohani, L.Fulcheri, J.P.Trelles. *Aerosol Sci. Technol.*, **50**, 26 (2016)
102. H.Jander, C.Borchers, H.Böhm, A.Emelianov, C.Schulz. *Carbon*, **150**, 244 (2019)
103. H.W.Kroto, K.McKay. *Nature (London)*, **331**, 328 (1988)
104. C.J.Pope, J.A.Marr, J.B.Howard. *J. Phys. Chem.*, **97**, 11001 (1993)
105. J.-B.Donnet. *Rubber Chem. Technol.*, **71**, 323 (1998)
106. V.I.Berezkin. *Phys. Solid State*, **42**, 580 (2000)

107. M.Pontier Johnson, R.W.Locke, J.B.Donnet, T.K.Wang, C.C.Wang, P.Bertrand. *Rubber Chem. Technol.*, **73**, 875 (2000)
108. V.I.Berezkin. *Phys. Solid State*, **43**, 967 (2001)
109. G.Heinrich, M.Klüppel. *Kautsch. Gummi, Kunstst.*, **54**, 159 (2001)
110. Ph.Gerhardt, S.Löffler, K.H.Homann. *Chem. Phys. Lett.*, **137**, 306 (1987)
111. A.B.Fialkov. *Prog. Energy Combust. Sci.*, **23**, 399 (1997)
112. J.B.Howard, J.T.McKinnon, Y.Makarovsky, A.L.Lafleur, M.E.Johnson. *Nature (London)*, **352**, 139 (1991)
113. J.T.McKinnon, W.L.Bell, R.M.Barkley. *Combust. Flame*, **88**, 102 (1992)
114. H.Richter, A.J.Labrocca, W.J.Grieco, K.Taghizadeh, A.L.Lafleur, J.B.Howard. *J. Phys. Chem. B*, **101**, 1556 (1997)
115. N.Pineau, L.Soulard, J.H.Los, A.Fasolino. *J. Chem. Phys*, **129**, 024708 (2008)
116. Q.Mao, A.C.T.van Duin, K.H.Luo. *Carbon*, **121**, 380 (2017)
117. J.Hernández-Rojas, F.Calvo. *Phys. Chem. Chem. Phys.*, **21**, 5123 (2019)
118. X.Mercier, O.Carrivain, C.Irimiea, A.Faccinetto, E.Therssen. *Phys. Chem. Chem. Phys.*, **21**, 8282 (2019)
119. D.Chen, K.H.Luo. *Combust. Flame*, **211**, 362 (2020)
120. G.Yang, L.Li, W.B.Lee, M.C.Ng. *Sci. Technol. Adv. Mater.*, **19**, 613 (2018)
121. J.W.Martin, R.I.Slavchov, E.K.Y.Yapp, J.Akroyd, S.Mosbach, M.Kraft. *J. Phys. Chem. C*, **121**, 27154 (2017)
122. R.Berkowitz. *Phys. Today*, **71**, 18 (2018)
123. K.O.Johansson, M.P.Head-Gordon, P.E.Schrader, K.R.Wilson, H.A.Michelsen. *Science*, **361**, 997 (2018)
124. F Schulz, M.Commodo, K.Kaiser, G.De Falco, P.Minutolo, G.Meyer, A.D'Anna, L. Gross. *Proc. Combust. Inst.*, **37**, 885 (2019)
125. J.Davis, E.Molnar, I.Novosselov. *Carbon*, **159**, 255 (2020)
126. A.Baldelli, U.Trivanovic, T.A.Sipkens, S.N.Rogak. *Chemosphere*, **252**, 126532 (2020)
127. J.W.Martin, D.Hou, A.Menon, L.Pascazio, J.Akroyd, X.You, M.Kraft. *J. Phys. Chem. C*, **123**, 26673 (2019)
128. K.Amsharov. In *From Polyphenylenes to Nanographenes and Graphene Nanoribbons*. (Eds K.Müllen, X.Feng). (Cham: Springer, 2017). P. 127
129. B.Wu, L. Jiang, Y.Luo, C.Wang. *Angew. Chem., Int. Ed.*, **132**, 3970 (2020)
130. N.Fedik, A.I.Boldyrev. *J. Phys. Chem. A*, **122**, 8585 (2018)
131. H.I.Sherazi, Y.Li. *Soot: Sources, Formation and Health Effects*. (New York: Nova Science Publishers, 2012)
132. R.D.Heidenreich, W.M.Hess, L.L.Ban. *J. Appl. Crystallogr.*, **1**, 1 (1968)
133. T.S.Totton, D.Chakrabarti, A.J.Misquitta, M.Sander, D.J.Wales, M.Kraft. *Combust. Flame*, **157**, 909 (2010)
134. M.V.Trenikhin. *Fullerenes Nanotubes Carbon Nanostruct.*, **28**, 418 (2020)
135. A.V.Krestinin. Doctoral Thesis in Physical and Mathematical Sciences, Institute of Problems of Chemical Physics of RAS, Chernogolovka, 2000
136. G.Vitiello, G.DeFalco, F.Picca, M.Commodo, G.D'Errico, P.Minutolo, A.D'Anna. *Combust. Flame*, **205**, 286 (2019)
137. A.G.Shaitanov, V.F.Surovikin. *Combust. Explos. Shock Waves*, **45**, 190 (2009)
138. O.G.Penyazkov, K.A.Ragotner. In *Shock Waves: 26th International Symposium on Shock Waves*. Vol. 2. (Eds K.Hannemann, F.Seiler). (Berlin: Springer-Verlag, 2009). P. 937
139. G.L.Agafonov, V.N.Smirnov, P.A.Vlasov. *Proc. Combust. Inst.*, **33**, 625 (2011)
140. A.V.Eremin. *High Temp.*, **51**, 673 (2013)
141. G.L.Agafonov, I.V.Bilera, P.A.Vlasov, I.V.Zhil'tsova, Yu.A.Kolbanovskii, V.N.Smirnov, A.M.Tereza. *Combus. Explos.*, **8** (1), 80 (2015)
142. G.L.Agafonov, P.A.Vlasov, O.B.Ryabikov, V.N.Smirnov. *Combust. Explos.*, **12** (4), 33 (2019)
143. M.V.Doroshko. *High Temp. Mater. Process.*, **23**, 165 (2019)
144. V.I.Ivanovskii. *Tekhnicheskii Uglerod. Protsessy i Apparaty. (Carbon Black. Processes and Apparatuses)*. (Omsk: Tekhuglerod, 2004)
145. G.I.Razd'yakonova. *Poluchenie i Svoistva Tekhnicheskogo Ugleroda. (Obtaining and Properties of Carbon Black)*. (Omsk: Izd. OmGTU, 2014)
146. J.Aihara, K.Fujiwara, A.Harada, H.Ichikawa, K.Fukushima, F.Hirota, T.Ishida. *J. Mol. Struct. (THEOCHEM)*, **366**, 219 (1996)
147. M.Singh, R.L.Vander Wal. *C – J. Carbon Res.*, **5**, 2 (2019)
148. Y.Chen, N.Shah, F.E.Huggins, G.P.Huffman. *Environ. Sci. Technol.*, **39**, 1144 (2005)
149. A.Veshkini. PhD Thesis. University of Toronto, Toronto, 2015
150. A.Veshkini, S.B.Dworkin, M.J.Thomson. *Combust. Theory Model.*, **20**, 707 (2016)
151. L.Liu, H.Xu, Q.Zhu, H.Ren, X.Li. *Chem. Phys. Lett.*, **760**, 137983 (2020)
152. L.Pascazio, J.W.Martin, K.Bowal, J.Akroyd, M.Kraft. *Combust. Flame*, **219**, 45 (2020)
153. D.Chen, T.S.Totton, J.W.J.Akroyd, S.Mosbach, M.Kraft. *Carbon*, **67**, 79 (2014)
154. C.S.Wang, N.C.Bartelt, R.Ragan, K.Thürmer. *Carbon*, **129**, 537 (2018)
155. K.Bowal, J.W.Martin, A.J.Misquitta, M.Kraft. *Combust. Sci. Technol.*, **191**, 747 (2019)
156. H.-R.Paur, W.Baumann, H.Mätzing, H.Seifert. *Nanotechnology*, **16**, S354 (2005)
157. I.P.Vereshchagin, V.I.Levitov, G.Z.Mirzabekyan, M.M.Pashin. *Osnovy Elektrogazodinamiki Dispersnykh Sistem. (Fundamentals of Electrogasdynamics of Disperse Systems)*. (Moscow: Energiya, 1974)
158. S.A.Beresnev, V.I.Gryazin. *Fizika Atmosfernykh Aerozolei. (Physics of Atmospheric Aerosols)*. (Ekaterinburg: Izd. Ural University, 2008)
159. S.Rigopoulos. *Flow Turbulence Combust.*, **103**, 565 (2019)
160. V.M.Zaichenko, I.M.Maikov. *Piroliz Uglevodorodov na Uglerodnykh Matritsakh. (Pyrolysis of Hydrocarbons on Carbon Matrices)*. (Moscow: Energiya, 2014)
161. V.I.Kasatochkin, A.T.Kaverov. *Dokl. Akad. Nauk SSSR,* **117**, 837 (1957)
162. V.I.Zheivot, V.V.Molchanov, V.I.Zaikovskii, V.N.Krivoruchko, N.A.Zaitseva, M.N.Shchuchkin. *Microporous Mesoporous Mater.*, **130**, 7 (2010)
163. M.V.Trenikhin, O.V.Protasova, G.M.Seropyan, V.A.Drozdov. *Chem. Sustain. Dev.*, **21**, 101 (2013)
164. M.V.Trenikhin, O.V.Ivashchenko, V.S.Eliseev, B.P.Tolochko, A.B.Arbuzov, I.V.Muromtsev, Yu.G.Kryazhev, V.A.Drozdov, E.Sazhina, V.A.Likholobov. *Fullerenes Nanotubes Carbon Nanostruct.*, **23**, 801 (2015)

165. K.Yehliu, R.L.Van der Wal, A.L.Boehman. *Combust. Flame*, **158**, 1837 (2011)
166. P.H.Joo, B.Gigone, E.A.Griffin, M.Christensen, Ö.L.Gülder. *Fuel*, **220**, 464 (2018)
167. M.Commodo, A.E.Karataş, G.DeFalco, P.Minutolo, A.D'Anna, Ö.L.Gülder. *Combust. Flame*, **219**, 13 (2020)
168. M.L.Botero, D.Chen, S.González-Calera, D.Jefferson, M.Kraft. *Carbon*, **96**, 459 (2016)
169. P.Verma, E.Pickering, M.Jafari, Y.Guo, S.Stevanovic, J.F.S.Fernando, D.Golberg, P.Brooks, R.Brown, Z.Ristovski. *Combust. Flame*, **205**, 206 (2019)
170. E.A.Grulke, S.B.Rice, J.C.Xiong, K.Yamamoto, T.H.Yoon, K.Thomson, M.Saffaripour, G.J.Smallwood, J.W.Lambert, A.J.Stromberg, R.Macy, N.J.Briot, D.Qian. *Carbon*, **130**, 822 (2018)
171. C.R.Herd, G.C.McDonald, W.M.Hess. *Rubber Chem. Technol.*, **65**, 107 (1992)
172. V.B.Fenelonov, A.Yu.Derevyankin, L.G.Okkel, L.B.Avdeeva, V.I.Zaikovskii, E.M.Moroz, A.N.Salanov, N.A.Rudina, V.A.Likholobov, Sh.K.Shaikhutdinov. *Carbon*, **35**, 1129 (1997)
173. H.-Y.Cheng, Y.-A.Zhu, Z.-J.Sui, X.-G.Zhou, D.Chen. *Carbon*, **50**, 4359 (2012)
174. Z.Liu, K.Suenaga, P.J.F.Harris, S.Iijima. *Phys. Rev. Lett.*, **102**, 015501 (2009)
175. L.B.Avdeeva, T.V.Reshetenko, Z.R.Ismagilov, V.A.Likholobov. *Appl. Catal., A*, **228**, 53 (2002)
176. K.B.K.Teo, C.Singh, M.Chhowalla, W.I.Milne. In *Encyclopedia of Nanoscience and Nanotechnology*. (Ed. H.S.Nalwa). (Valencia: American Scientific Publishers, 2003). P. 1
177. M.R.Axet, O.Dechy-Cabaret, J.Durand, M.Gouygou, P.Serp. *Coord. Chem. Rev.*, **308**, 236 (2016)
178. S.Yu.Troitskii, A.L.Chuvilin, D.I.Kochubei, B.N.Novgorodov, V.N.Kolomiichuk, V.A.Likholobov. *Russ. Chem. Bull., Engl. Transl.*, **44**, 1822 (1995)
179. E.O.Pentsak, A.S.Kashin, M.V.Polynski, K.O.Kvashnina, P.Glatzel, V.P.Ananikov. *Chem. Sci.*, **6**, 3302 (2015)
180. V.B.Fenelonov, M.S.Melgunov, N.A.Baronskaya. *React. Kinet. Catal. Lett.*, **63**, 305 (1998)
181. P.A.Simonov, S.V.Filimonova, G.N.Kryukova, E.M.Moroz, V.A.Likholobov, T.Kuretzky, H.P.Boehm. *Carbon*, **37**, 591 (1999)
182. K.V.Romanenko, J.-B.d'Espinose de la Caillerie, J.Fraissard, T.V.Reshetenko, O.B.Lapina. *Microporous Mesoporous Mater.*, **81**, 41 (2005)
183. P.A.Simonov, E.M.Moroz, V.A.Likholobov, G.V.Plaksin. *Bull. Acad. Sci. USSR, Div. Chem. Sci.*, **39**, 1335 (1990)
184. J.C.C.Freitas, A.G.Cunha, F.G.Emmerich. In *Chemistry and Physics of Carbon*. (Ed. L.R.Radovic). (Boca Raton, FL: CRC Press, 2013). P. 85
185. A.Fujimoto, Y.Yamada, M.Koinuma, S.Sato. *Anal. Chem.*, **88**, 6110 (2016)
186. V.Ţucureanu, A.Matei, A.M.Avram. *Crit. Rev. Anal. Chem.*, **46**, 502 (2016)
187. B.Bhattarai, D.A.Drabold. *Carbon*, **115**, 532 (2017)
188. B.Bhattarai, P.Biswas, R.Atta-Fynn, D.A.Drabold. *Phys. Chem. Chem. Phys.*, **20**, 19546 (2018)
189. C.-T.Toh, H.Zhang, J.Lin, A.S.Mayorov, Y.-P.Wang, C.M.Orofeo, D.B.Ferry, H.Andersen, N.Kakenov, Z.Guo, I.H.Abidi, H.Sims, K.Suenaga, S.T.Pantelides, B.Özyilmaz. *Nature (London)*, **577**, 199 (2020)
190. M.A.Caro, A.Aarva, V.L.Deringer, G.Csányi, T.Laurila. *Chem. Mater.*, **30**, 7446 (2018)
191. A.Knoll, M.K.Y.Chan, K.C.Lau, B.Liu, J.Greeley, L.Curtiss, M.Hereld, M.E.Papka. *Int. J. Uncertain. Quantif.*, **3**, 157 (2013)
192. A.Knoll, I.Wald, P.A.Navrátil, M.E.Papka, K.P.Geither. In *Proceedings of UltraVis 2013: 8th International Workshop on Ultrascale Visualization*. (New York, 2013). Art. No. 5
193. B.Grzyb, J.Gonzalez-Aguilar, L.Fulcheri, N.Probst. *Fullerenes Nanotubes Carbon Nanostruct.*, **19**, 210 (2011)
194. I.Sutherland, E.Sheng, R.H.Bradley, P.K.Freakley. *J. Mater. Sci.*, **31**, 5651 (1996)
195. O.A.Kokhanovskaya, V.A.Likholobov. *AIP Conf. Proc.*, **2143**, 020032 (2019)
196. G.I.Razdyakonova, O.A.Kokhanovskaya, V.A.Likholobov. *Procedia Eng.*, **113**, 43 (2015)
197. G.Lota, P.Krawczyk, K.Lota, A.Sierczyńska, Ł.Kolanowski, M.Baraniak, T.Buchwald. *J. Solid State Electrochem.*, **20**, 2857 (2016)
198. M.Ciobanu, A.-M.Lepadatu, S.Asaftei. *Mater. Today: Proc.*, **3S**, S252 (2016)
199. F.Cataldo. *J. Nanosci. Nanotechnol.*, **7**, 1446 (2007)
200. W.O'Connor, W.Schmitt, E.Moriconi. *Ind. Eng. Chem.*, **49**, 1701 (1957)
201. A.Lundstedt, M.J.Webb, H.Grennberg. *RSCAdv.*, **7**, 6152 (2017)
202. M.H.Almatarneh, E.Al-Shamaileh, Z.M.Ahmad, A.A.-A.A.Abu-Saleh, I.A.Elayan. *Acta Phys. Polonica A*, **132**, 1149 (2017)
203. A.A.Frimer. *Chem. Rev.*, **79**, 359 (1979)
204. A.G.Leach, K.N.Houk. *Chem. Commun.*, 1243 (2002)
205. X.Liu, J.Gu, J.Wightman, H.C.Dorn. *ACS Appl. Nano Mater.*, **2**, 7488, (2019)
206. T.J.Bandosz. In *Carbon Materials for Catalysis*. (Eds P.Serp, J.L.Figueiredo). (Hoboken: Wiley, 2008). P. 45
207. R.Pietrzak. *Fuel*, **88**, 1871 (2009)
208. W.Kiciński, M.Szala, M.Bystrzejewski. *Carbon*, **68**, 1 (2014)
209. A.M.Puziy, O.I.Poddubnaya, R.P.Socha, J.Gurgul, M.Wisniewski. *Carbon*, **46**, 2113 (2008)
210. M.-T.Kuo, P.W.May, A.Gunn, M.N.R.Ashfold, R.K.Wild. *Diamond Relat. Mater.*, **9**, 1222 (2000)
211. A.P.Terzyk. *Colloids Surf. A*, **177**, 23 (2001)
212. D.Leistenschneider, K.Zürbes, C.Schneidermann, S.Grätz, S.Oswald, K.Wegner, B.Klemmed, L.Giebeler, A.Eychmüller, L.Borchardt. *C–J. Carbon Res.*, **4**, 14 (2018)
213. S.E.Livingstone. *The Chemistry of Ruthenium, Rhodium, Palladium Osmium, Iridium and Platinum*. (Oxford: Pergamon Press, 1973)
214. R.F.Heck. *Palladium Reagents in Organic Syntheses*. (London: Academic Press, 1985)
215. Yu.I.Yermakov. *Catal. Rev. Sci. Eng.*, **13**, 77 (1976)
216. *Surface Organometallic Chemistry: Molecular Approaches to Surface Catalysis*. (Eds J.-M.Basset, B.C.Gates, J.-P.Candy, A.Choplin, M.Leconte, F.Quignard, C.Santini). (Dordrecht: Kluwer Academic Publishers, 1988)
217. G.V. Lisichkin, A.Yu.Fadeev, A.A.Serdan, P.N.Nesterenko, P.G.Mingalev, D.B.Furman. *Khimiya Privitykh Poverkhnostnykh Soedinenii. (Chemistry of Grafted Surface Compounds)*. (Moscow: Fizmat, 2003)

218. H.Qian, H.Huang, X.Wang. *J. Power Sources*, **275**, 734 (2015)
219. Y.Xie, S.-H.Zhang, H.-Y.Jiang, H.Zeng, R.-M.Wu, H.Chen, Y.-F.Gao, Y.-Y.Huang, H.-L.Bai. *e-Polymers*, **19**, 61 (2019)
220. P.Toth, D.Jacobsson, M.Ek, H.Wiinikka. *Carbon*, **145**, 149 (2019)
221. A.Goel, J.B.Howard, J.B.Vander Sande. *Carbon*, **42**, 1907 (2004)
222. V.F.Surovikin, A.G.Shaitanov, Yu.V.Surovikin, I.V.Rezanov, A.D.Morozov. *Dinamika Sistem, Mekhanizmov i Mashin*, (3), 234 (2012)
223. V.F.Surovikin, A.G.Shaitanov, V.A.Drozdov, I.V.Rezanov, I.V.Muromtsev. *Chem. Sustain. Dev.*, **22**, 577 (2014)
224. A.Naseri, A.D.Sediako, F.Liu, M.Barati, R.D.Baker, M.J.Thomson. *Carbon*, **156**, 299 (2020)
225. C.Fan, Y.Dong, Y.Liu, L.Zhang, D.Wang, X.Lin, Y.Lv, S.Zhang, H.Song, D.Jia. *Carbon*, **160**, 328 (2020)
226. V.F.Surovikin, A.G.Shaitanov, N.N.Leont'eva, V.A.Drozdov. *Solid Fuel Chem.*, **43**, 318 (2009)
227. Y.V.Surovikin, A.G.Shaitanov, V.A.Drozdov, I.V.Rezanov, A.D.Morozov. *Solid Fuel Chem.*, **48**, 392 (2014)
228. Y.V.Surovikin, A.G.Shaitanov, I.V.Rezanov, A.V.Syr'eva, V.A.Likholobov, A.N.Poddubnyak, K.K.Chigrin. *Russ. J. Appl. Chem.*, **90**, 1974 (2017)
229. P.E.Pavlyuchenko, G.M.Seropyan, M.V.Trenikhin, V.A.Drozdov. *Russ. J. Gen. Chem.*, **90**, 559 (2020)
230. O.V.Ivashchenko, M.V.Trenikhin, Yu.G.Kryazhev, B.P.Tolochko, V.S.Eliseev, A.B.Arbuzov, V.A.Drozdov, V.A.Likholobov. *Nanotechnol. Russ.*, **10**, 696 (2015)
231. O.L.Li, J.Kang, K.Urashima, N.Saito. *Int. J. Plasma Environ. Sci. Technol.*, **7**, 31 (2013)
232. N.Saito, M.A.Bratescu, K.Hashimi. *Jpn. J. Appl. Phys.*, **57**, 0102A4 (2018)
233. K.Hyun, T.Ueno, O.L.Li, N.Saito. *RSC Adv.*, **6**, 6990 (2016)
234. O.L.Li, Z.Shi, H.Lee, T.Ishizaki. *Sci. Rep.*, **9**, 12704 (2019)
235. P.A.Simonov. Candidate Thesis in Chemical Sciences, BIC SB RAS, Novosibirsk, 2000
236. B.A.T.Mehrabadi, S.Eskandari, U.Khan, R.D.White, J.R.Regalbuto. *Adv. Catal.*, **61**, 1 (2017)
237. P.Mäki-Arvela, D.Yu.Murzin. *Appl. Catal. A: Gen.*, **451**, 251 (2013)
238. A.S.Berenblyum, H.A.Al-Wadhaf, O.N.Shishilov, E.M.Evstigneeva, M.H.El-Hussien, V.R.Flid. *Russ. J. Coord. Chem.*, **37**, 460 (2011)
239. A.S.Berenblyum, H.A.Al-Wadhaf, E.A.Katsman, V.R.Flid. *Kinet. Catal.*, **52**, 296 (2011)
240. H.A.Al-Wadhaf, V.M.Karpov, E.A.Katsman. *Catal. Commun.*, **116**, 67 (2018)
241. S.A.Yakukhnov, E.O.Pentsak, K.I.Galkin, R.M.Mironenko, V.A.Drozdov, V.A.Likholobov, V.P.Ananikov. *ChemCatChem*, **10**, 1869 (2018)
242. N.A.Pakhomov. *Nauchnye Osnovy Prigotovleniya Katalizatorov: Vvedenie v Teoriyu i Praktiku. (The Scientific Foundations of Catalyst Preparation: An Introduction to Theory and Practice)*. (Novosibirsk: Izd. SB RAS, 2011)
243. USSR Author's Certificate 1270939; *Bull. Izobret.*, (20), 427 (1997)
244. S.Yu.Troitskii. Candidate Thesis in Chemical Sciences, BIC SB RAS, Novosibirsk, 2008
245. Patent DE 342094 (1921)
246. J.Guerra, M.A.Herrero. *Nanoscale*, **2**, 1390 (2010)
247. A.Balanta, C.Godard, C.Claver. *Chem. Soc. Rev.*, **40**, 4973 (2011)
248. J.A.Delgado, O.Benkirane, C.Claver, D.Curulla-Ferré, C.Godard. *Dalton Trans.*, **46**, 12381 (2017)
249. P.T.Witte, P.H.Berben, S.Boland, E.H.Boymans, D.Vogt, J.W.Geus, J.G. Donkervoort. *Top. Catal.*, **55**, 505 (2012)
250. USSR Author's Certificate 1188964; ; *Bull. Izobret.*, (20), 427 (1997)
251. K.I.Zamaraev. In *Perspectives in Catalysis*. (Eds J.M.Thomas, K.I.Zamaraev). (Oxford: Blackwell Scientific Publications, 1992). P. 35
252. K.I.Zamaraev. *Khim. Interesakh Ustoichivogo Razvitiya,* **1** (1), 133 (1993)
253. B.I.Peshchevitskii, A.B.Belyaev, R.L.Shchekochikhina, G.L.Mal'chikov. *Kinetika Reaktsii Zameshcheniya Ligandov v Kompleksnykh Soedineniyakh Platinovykh Metallov i Zolota. Spravochnik. (Kinetics of Ligand Substitution Reactions in Complex Compounds of Platinum Metals and Gold. Handbook)*. (Novosibirsk: Nauka, 1974)
254. F.Basolo, R.G.Pearson. *Mechanisms of Inorganic Reactions: A Study of Metal Complexes in Solution*. (New York: Wiley and Sons, 1967)
255. W.P.Griffith, S.D.Robinson, K.Swars. In *Gmelin Handbook of Inorganic Chemistry. Suppl. Vol. B2*. (Eds W.P.Griffith, K.Swars). (Berlin: Wiley and Sons, 1989)
256. B.Sahoo, N.C.Nayak, A.Samantaray, P.K.Pujapanda. *Inorganic Chemistry*. (New Delhi: PHI Learning Private, 2012)
257. A.Podborska, M.Wojnicki. *J. Mol. Struct.*, **1128**, 117 (2017)
258. J.J.Cruywagen, R.J.Kriek. *J. Coord. Chem.*, **60**, 439 (2007)
259. P.Vanýsek. In *CRC Handbook of Chemistry and Physics*. (Ed. W.M.Haynes). (Boca Raton, FL: CRC Press, 2017). P. 5
260. S.G.Bratsch. *J. Phys. Chem. Ref. Data*, **18**, 1 (1989)
261. J.-F.Boily, T.M.Seward. *Geochim. Cosmochim. Acta*, **69**, 3773 (2005)
262. N.Torapava, L.I.Elding, H.Mändar, K.Roosalu, I.Persson. *Dalton Trans.*, **42**, 7755 (2013)
263. A.Lienke, G.Klatt, D.J.Robinson, K.R.Koch, K.J.Naidoo. *Inorg. Chem.*, **40**, 2352 (2001)
264. K.J.Naidoo, G.Klatt, K.R.Koch, D.J.Robinson. *Inorg. Chem.*, **41**, 1845 (2002)
265. R.P.Matthews, G.A.Venter, K.J.Naidoo. *J. Phys. Chem. B*, **115**, 1045 (2011)
266. T.S.Hofer, B.R.Randolf, S.A.A.Shah, B.M.Rode, I.Persson. *Chem. Phys. Lett.*, **445**, 193 (2007)
267. H.Shao, Y.-C.Wu, Z.Lin, P.-L.Taberna, P.Simon. *Chem. Soc. Rev.*, **49**, 3005 (2020)
268. K.Bourikas, C.Kordulis, A.Lycourghiotis. *Catal. Rev.*, **48**, 363 (2006)
269. V.T.Nguyen, D.D.Do, D.Nicholson. *Carbon*, **66**, 629 (2014)
270. T.Horikawa, S.Tan, D.D.Do, K.-I.Sotowa, J.R.Alcántara-Avila, D.Nicholson. *Carbon*, **124**, 271 (2017)
271. L.Sarkisov, A.Centineo, S.Brandani. *Carbon*, **118**, 127 (2017)
272. X.Peng, J.M.Vicent-Luna, S.K.Jain, Q.Jin, J.K.Singh. *ACS Appl. Nano Mater.*, **2**, 7103 (2019)

273. B.Radola, L.Martin-Gondre, S.Picaud, M.-T.Rayez, J.-C.Rayez. *Chem. Phys.*, **523**, 18 (2019)
274. J.K.Brennan, T.J.Bandosz, K.T.Thomson, K.E.Gubbins. *Colloids Surf. A*, **187 – 188**, 539 (2001)
275. L.Liu, S.Tan, T.Horikawa, D.D.Do, D.Nicholson, J.Liu. *Adv. Colloid Interface Sci.*, **250**, 64 (2017)
276. J.K.Brennan, K.T.Thomson, K.E.Gubbins. *Langmuir*, **18**, 5438 (2002)
277. P.J.M.Carrott, M.M.L.Ribeiro Carrott, A.J.Estevão Candeias, J.P.Prates Ramalho. *J. Chem. Soc., Faraday Trans.*, **91**, 2179 (1995)
278. M.A.Fraga, E.Jordão, M.J.Mendes, M.M.A.Freitas, J.L.Faria, J.L.Figueiredo. *J. Catal.*, **209**, 355 (2002)
279. D.Cook, Y.Lupien, W.G.Schneider. *Can. J. Chem.*, **34**, 957 (1956)
280. D.Cook, Y.Lupien, W.G.Schneider. *Can. J. Chem.*, **34**, 964 (1956)
281. M.V.Frash, A.C.Hopkinson, D.K.Bohme. *J. Am. Chem. Soc.*, **123**, 6687 (2001)
282. W.Yuan, Y.Zhou, Y.Li, C.Li, H.Peng, J.Zhang, Z.Liu, L.Dai, G.Shi. *Sci. Rep.*, **3**, 2248 (2013)
283. S.D.Lin, Y.-H.Hsu, P.-H.Jen, J.-F.Lee. *J. Mol. Catal. A: Chem.*, **238**, 88 (2005)
284. M.Wojnicki. *Arch. Metall. Mater.*, **62**, 2405 (2017)
285. M.Wojnicki, R.P.Socha, Z.Pędzich, K.Mech, T.Tokarski, K.Fitzner. *J. Chem. Eng. Data*, **63**, 702 (2018)
286. M.Wojnicki, K.Fitzner. *React. Kinet. Mech. Catal.*, **124**, 453 (2018)
287. P.A.Simonov, A.V.Romanenko, I.P.Prosvirin, E.M.Moroz, A.I.Boronin, A.L.Chuvilin, V.A.Likholobov. *Carbon*, **35**, 73 (1997)
288. P.A.Simonov, A.V.Romanenko, I.P.Prosvirin, G.N.Kryukova, A.L.Chuvilin, S.V.Bogdanov, E.M.Moroz, V.A.Likholobov. *Stud. Surf. Sci. Catal.*, **118**, 15 (1998)
289. E.M.Moroz, P.A.Simonov, S.V.Bogdanov, A.L.Chuvilin. *Mater. Sci. Forum*, **321 – 324**, 1074 (2000)
290. P.A.Simonov, V.A.Likholobov. In *Catalysis and Electrocatalysis at Nanoparticle Surfaces*. (Eds A.Wieckowski, E.R.Savinova, C.G.Vayenas). (New York: Marcel Dekker, 2003). P. 409
291. L.I.Elding, L.F.Olsson. *J. Phys. Chem.*, **82**, 69 (1978)
292. O.B.Bel'skaya, T.I.Gulyaeva, A.B.Arbuzov, V.K.Duplyakin, V.A.Likholobov. *Kinet. Catal.*, **51**, 105 (2010)
293. E.P.Sheshin. *Struktura Poverkhnosti i Avtoemissionnye Svoistva Uglerodnykh Materialov. (Surface Structure and Field Emission Properties of Carbon Materials)*. (Moscow: Izd. MFTI, 2001)
294. H.Reiss, A.Heller. *J. Phys. Chem.*, **89**, 4207 (1985)
295. V.I.Kravtsov. *Russ. Chem. Rev.*, **45**, 284 (1976)
296. V.I.Kravtsov. *Ravnovesie i Kinetika Elektrodnykh Reaktsii Kompleksov Metallov. (Equilibrium and Kinetics of Electrode Reactions of Metal Complexes)*. (Leningrad: Khimiya, 1985)
297. Z.Zhang,T.Sun, C.Chen, F.Xiao, Z.Gong, S.Wang. *ACS Appl. Mater. Interfaces*, **6**, 21035 (2014)
298. H.Qi, P.Yu, Y.Wang, G.Han, H.Liu, Y.Yi, Y.Li, L.Mao. *J. Am. Chem. Soc.*, **137**, 5260 (2015)
299. L.S.Oliveira, J.F.G.Alba, V.L.Silva, R.T.Ribeiro, E.H.L.Falcão, M.Navarro. *J. Electroanal. Chem.*, **818**, 106 (2018)
300. K.-H.Lubert, M.Guttmann, L.Beyer. *J. Solid State Electrochem.*, **6**, 545 (2002)
301. J.B.Conant, L.F.Fieser. *J. Am. Chem. Soc.*, **46**, 1858 (1924)
302. P.S.Guin, S.Das, P.C.Mandal. *Int. J. Electrochem.*, 816202 (2011)
303. B.I.Kharisov, M.A.Méndez-Rojas, A.D.Garnovskii, E.P.Ivakhnenko, U.Ortiz-Méndez. *J. Coord. Chem.*, **55**, 745 (2002)
304. C.A.Thorogood, G.G.Wildgoose, J.H.Jones, R.G.Compton. *New J. Chem.*, **31**, 958 (2007)
305. T.Brousse, C.Cougnon, D.Bélanger. *J. Braz. Chem. Soc.*, **29**, 989 (2018)
306. G.F.Han, F.Li, W.Zou, M.Karamad, J.-P.Jeon, S.-W.Kim, S.-J.Kim, Y.Bu, Z.Fu, Y.Lu, S.Siahrostami, J.-B.Baek. *Nat. Commun.*, **11**, 2209 (2020)
307. C.Han, H.Li, R.Shi, T.Zhang, J.Tong, J.Li, B.Li. *J. Mater. Chem. A*, **7**, 23378 (2019)
308. P.Cai, K.Zou, G.Zou, H.Hou, X.Ji. *Nanoscale*, **12**, 3677 (2020)
309. A.M.Ziatdinov. *Ros. Khim. Zh.*, **48** (5), 5 (2004)
310. A.M.Ziatdinov. *Vestn. DVO RAN*, (5), 57 (2006)
311. M.F.Juarez, S.Fuentes, G.J.Soldano, L.Avalle, E.Santos. *Faraday Discuss.*, **172**, 327 (2014)
312. B.Dyatkin,Y.Gogotsi. *Faraday Discuss.*, **172**, 139 (2014)
313. R.Sharma, N.Chadha, P.Saini. *Indian J. Pure Appl. Phys.*, **55**, 625 (2017)
314. T.Tite, E.A.Chiticaru, J.S.Burns, M.Ioniţă. *J. Nanobiotechnol.*, **17**, 101 (2019)
315. T.Zhang, B.Zou, X.Bi, M.Li, J.Wen, F.Huo, K.Amine, J.Lu. *ACS Energy Lett.*, **4**, 2782 (2019)
316. O.Corduneanu, V.C.Diculescu, A.-M.Chiorcea-Paquim, A.-M.Oliveira-Brett. *J. Electroanal. Chem.*, **624**, 97 (2008)
317. R.Burgess, C.Buono, P.R.Davies, R.J.Davies, T.Legge, A. Lai, R.Lewis, D.J.Morgan, N.Robinson, D.J.Willock. *J. Catal.*, **323**, 10 (2015)
318. K.K.Maniam, R.Chetty. *J. Appl. Electrochem.*, **45**, 953 (2015)
319. K.Mech, P.Zabiński, R.Kowalik, K.Fitzner. *J. Electrochem. Soc.*, **160**, H770 (2013)
320. M.E.King, I.A.Kent, M.L.Personick. *Nanoscale*, **11**, 15612 (2019)
321. S.Gu, X.P.Wang, Y.Z.Wei, B.Z.Fang. *Sci. China Chem.*, **57**, 755 (2014)
322. A.V.Romanenko, P.A.Simonov. *Uglerodnye Materialy i ikh Physiko-Khimicheskie Svoistva. (Carbon Materials and Their Physicochemical Properties)*. (Moscow: Kalvis, 2007)
323. M.M.Olmstead, A.S.Ginwalla, B.C.Noll, D.S.Tinti, A.L.Balch. *J. Am. Chem. Soc.*, **118**, 7737 (1996)
324. S.N.Spisak, A.S.Filatov, M.A.Petrukhina. *J. Organomet. Chem.*, **696**, 1228 (2011)
325. G.Allegra, G.Tettamanti Casagrande, A.Immirzi, L.Porri, G.Vitulli. *J. Am. Chem. Soc.*, **92**, 289 (1970)
326. T.Murahashi, T.Uemura, H.Kurosawa. *J. Am. Chem. Soc.*, **125**, 8436 (2003)
327. I.I.Moiseev. *π-Kompleksy v Zhidkofaznom Okislenii Olefinov. (π-Complexes in Liquid-Phase Oxidation of Olefins)*. (Moscow: Nauka, 1970)
328. B.E.Douglas. In *The Chemistry of the Coordination Compounds*. (Eds J.C.Bailar Jr., D.H.Busch). (New York: Reinhold Publishing, 1956). P. 487
329. H.Werner. *Landmarks in Organo-Transition Metal Chemistry*. (New York: Springer Science + Business Media, 2009)

330. L.K.Shubochkin. In *Khimiya Platinovykh i Tyazholykh Metallov: Chteniya im. Akademika I.I.Chernyaeva. (Chemistry of Platinum and Heavy Metals: Readings named after Academician I. I. Chernyaev)*. (Ed. R.N.Shchelokov). (Moscow: Nauka, 1975). P. 90
331. P.Grammatikopoulos, C.Cassidy, V.Singh, M.Sowwan. *Sci. Rep.*, **4**, 5779 (2014)
332. J.Halpern, J.F.Harrod, P.E.Potter. *Can. J. Chem.*, **37**, 1446 (1959)
333. O.V.Gritsenko, A.A.Bagatur'yants, I.I.Moiseev, V.B.Kazanskii. *Russ. Chem. Rev.*, **54**, 1151 (1985)
334. P.J.Brothers. In *Progress in Inorganic Chemistry*. Vol. 28. (New York: Wiley, 1981). P. 1
335. Ya.I.Mikhailenko. *Kurs Obshchei i Neorganicheskoi Khimii. (General and Inorganic Chemistry Course)*. (Moscow: Vysshaya Shkola, 1966)
336. M.L.Blokhina, I.I.Smirnov, A.I.Blokhin. *Powder Metall. Met. Ceram.*, **28**, 505 (1989)
337. G.Neri, M.G.Musolino, C.Milone, D.Pietropaolo, S.Galvagno. *Appl. Catal, A*, **208**, 307 (2001)
338. M.Gurrath, T.Kuretzky, H.P.Boehm, L.B.Okhlopkova, A.S.Lisitsyn, V.A.Likholobov. *Carbon*, **38**, 1241 (2000)
339. G.F.Alvarez, M.Mamlouk, S.M.S.Kumar, K.Scott. *J. Appl. Electrochem.*, **41**, 925 (2011)
340. F.Wang, G.Hao, Y.Guo, X.Ma, L.Yang. *Open J. Met.*, **7** (4), 59 (2017)
341. I.Efremenko, M.Sheintuch. *J. Catal.*, **214**, 53 (2003)
342. I.López-Corral, E.Germán, A.Juan, M.A.Volpe, G.P.Brizuela. *Int. J. Hydrogen Energy*, **37**, 6653 (2012)
343. C.R.C.Rêgo, P.Tereshchuk, L.N.Oliveira, J.L.F.Da Silva. *Phys. Rev. B*, **95**, 235422 (2017)
344. T.Prasomsri, D.Shi, D.E.Resasco. *Chem. Phys. Lett.*, **497**, 103 (2010)
345. D.Duca, F.Ferrante, G.La Manna. *J. Phys. Chem. C*, **111**, 5402 (2007)
346. W.Sun, Z.Liu, C.Jiang, Y.Xue, W.Chu, X.Zhao. *Catal. Today*, **212**, 206 (2013)
347. D.I.Kochubey, V.V.Chesnokov, S.E.Malykhin. *Carbon*, **50**, 2782 (2012)
348. J.M.M.Tengco, Y.K.Lugo-José, J.R.Monnier, J.R.Regalbuto. *Catal. Today*, **246**, 9 (2015)
349. B.Zhang, D.S.Su. *ChemCatChem*, **7**, 3639 (2015)
350. L.V.Ermolov, A.A.Slinkin. *Russ. Chem. Rev.*, **60**, 331 (1991)
351. A.Schröder. Dissertation zur Erlangung des Grades Doktor der Naturwissenschaften. Universität Hannover, Hannover, 2000
352. A.Schröder, M.Klüppel, R.H.Schuster, J.Heidberg. *Kautsch. Gummi., Kunstst.*, **54**, 260 (2001)
353. A.Schröder, M.Klüppel, R.H.Schuster, J.Heidberg. *Carbon*, **40**, 207 (2002)
354. A.Schröder, M.Klüppel, R.H.Schuster. *Macromol. Mater. Eng.*, **292**, 885 (2007)
355. D.Göritz, H.Raab, J.Fröhlich, P.G.Maier. *Rubber Chem. Technol.*, **72**, 929 (1999)
356. J.B.Donnet, E.Custodéro, T.K.Wang, G.Hennebert. *Carbon*, **40**, 163 (2002)
357. A.Lapra, E.Custodero, N.Simon. *Kautsch. Gummi, Kunstst.*, **57**, 52 (2004)
358. K.Nakai, M.Yoshida, J.Sonoda, Y.Nakada, M.Hakuman, H.Naono. *J. Colloid Interface Sci.*, **351**, 507 (2010)
359. Y.Zeng, D.D.Do, D.Nicholson. *Langmuir*, **31**, 4196 (2015)
360. K.Möbus, E.Grünewald, S.D.Wieland, S.F.Parker, P.W.Albers. *J. Catal.*, **311**, 153 (2014)
361. K.Ruth, P.Albers. In *Springer Handbook of Materials Data*. (Eds W.Martienssen, H.Warlimont). (Cham: Springer, 2018). P. 931
362. S.F.Parker, H.C.Walker, S.K.Callear, E.Grünewald, T.Petzold, D.Wolf, K.Möbus, J.Adam, S.D.Wieland, M.Jiménez-Ruiz, P.W.Albers. *Chem. Sci.*, **10**, 480 (2019)
363. R.M.Mironenko, O.B.Belskaya, T.I.Gulyaeva, M.V.Trenikhin, V.A.Likholobov. *Catal. Commun.*, **114**, 46 (2018)
364. R.M.Mironenko, O.B.Belskaya, L.N.Stepanova, T.I.Gulyaeva, M.V.Trenikhin, V.A.Likholobov. *Catal. Lett.*, **150**, 888 (2020)
365. R.M.Mironenko, O.B.Belskaya, V.A.Likholobov. *Solid Fuel Chem.*, **54**, 362 (2020)
366. M.Boudart. *Chem. Rev.*, **95**, 661 (1995)
367. R.A.van Santen. *Acc. Chem. Res.*, **42**, 57 (2009)
368. H.-L.Jiang, Q.Xu. *J. Mater. Chem.*, **21**, 13705 (2011)
369. M.Sankar, N.Dimitratos, P.J.Miedziak, P.P.Wells, C.J.Kiely, G.J.Hutchings. *Chem. Soc. Rev.*, **41**, 8099 (2012)
370. A.K.Singh, Q.Xu. *ChemCatChem*, **5**, 652 (2013)
371. D.Bazin, I.Fechete, F.Garin, G.Barcaro, F.R.Negreiros, L.Sementa, A.Fortunelli. In *Nanoalloys: From Fundamentals to Emergent Applications*. (Ed. F.Calvo). (Amsterdam: Elsevier, 2013). P. 283
372. O.G.Ellert, M.V.Tsodikov, S.A.Nikolaev, V.M.Novotortsev. *Russ. Chem. Rev.*, **83**, 718 (2014)
373. E.Nowicka, M.Sankar. *J. Zhejiang Univ. Sci. A*, **19**, 5 (2018)
374. G.C.Bond. *Metal-Catalysed Reactions of Hydrocarbons*. (New York: Springer Science + Business Media, 2005)
375. Á.Molnár, A.Sárkány, M.Varga. *J. Mol. Catal. A: Chem.*, **173**, 185 (2001)
376. M.Claus, E.Claus, P.Claus, D.Hönicke, R.Födisch, M.Olson. In *Ullmann's Encyclopedia of Industrial Chemistry*. (Weinheim: Wiley-VCH, 2016)
377. Z.Xu, H.Huang, P.Wang. *Shanghai Chem. Ind.*, **Z1**, 17 (2002)
378. Patent RU 2459793 (2012)
379. N.V.Vereshchagina, T.N.Antonova, A.A.Il'in, Zh.V.Chirkova. *Petrol. Chem.*, **56**, 38 (2016)]
380. N.V.Ushakov. *Russ. J. Appl. Chem.*, **93**, 159 (2020)
381. Patent US 3400164 (1968)
382. A.Cabiac, G.Delahay, R.Durand, P.Trens, D.Plée, A.Medevielle, B.Coq. *Appl. Catal., A*, **318**, 17 (2007)
383. I.L.Simakova, O.A.Simakova, A.V.Romanenko, D.Yu.Murzin. *Ind. Eng. Chem. Res.*, **47**, 7219 (2008)
384. Patent RU 2456339 (2012)
385. A.V.Romanenko, I.N.Voropaev, R.M.Abdullina, V.A.Chumachenko. *Solid Fuel Chem.*, **48**, 356 (2014)
386. V.P.Ananikov, L.L.Khemchyan, Yu.V.Ivanova, V.I.Bukhtiyarov, A.M.Sorokin, I.P.Prosvirin, S.Z.Vatsadze, A.V.Medved'ko, V.N.Nuriev, A.D.Dilman, V.V.Levin, I.V.Koptyug, K.V.Kovtunov, V.V.Zhivonitko, V.A.Likholobov, A.V.Romanenko, P.A.Simonov, V.G.Nenajdenko, O.I.Shmatova, V.M.Muzalevskiy, M.S.Nechaev, A.F.Asachenko, O.S.Morozov, P.B.Dzhevakov, S.N.Osipov, D.V.Vorobyeva, M.A.Topchiy, M.A.Zotova, S.A.Ponomarenko, O.V.Borshchev, Yu.N.Luponosov,

A.A.Rempel, A.A.Valeeva, A.Yu.Stakheev, O.V.Turova, I.S.Mashkovsky, S.V.Sysolyatin, V.V.Malykhin, G.A.Bukhtiyarova, A.O.Terent'ev, I.B.Krylov. *Russ. Chem. Rev.*, **83**, 885 (2014)
387. Patent WO 2004/007413 (2004)
388. Patent WO 2002/20442 (2002)
389. J.S.Kim, S.-S.Hong, J.H.Kim, M.S.Lee. *Appl. Chem. Eng.*, **26**, 575 (2015)
390. J.S.Kim, J.H.Baek, Y.B.Ryu, K.H.Kim, S.-S.Hong, J.-W.Park, M.S.Lee. In *Proceedings of ISCRE 24: 24th International Symposium on Chemical Reaction Engineering*. (Minneapolis, 2016). P. 75
391. M.Ali, G.Abarca, D.Eberhardt, A.Gual, F.Bernardi, S.R.Teixeira, J.Dupont. *Tetrahedron*, **73**, 5593 (2017)
392. V.Dubois, D.Desmecht, L.Rkiouak, A.-S.Jacquet, T.Hoshinoo, K.Nakagawa, S.Hermans. *React. Kinet. Mech. Catal.*, **126**, 399 (2019)
393. L.Červený, I.Paseka, E.Fialová, V.Růžička. *Collect. Czech. Chem. Commun.*, **52**, 1015 (1987)
394. R.M.Mironenko, E.R.Saybulina, L.N.Stepanova, T.I.Gulyaeva, M.V.Trenikhin, K.S.Rodygin, V.P.Ananikov. *Catalysts*, **11**, 179 (2021)
395. J.S.Kim, J.H.Baek, M.H.Kim, S.-S.Hong, M.S.Lee. *Mater. Sci. Forum*, **804**, 149 (2015)
396. C.H.Bartholomew, R.J.Farrauto. *Fundamentals of Industrial Catalytic Processes*. (Hoboken: Wiley, 2006)
397. R.Chinchilla, C.Nájera. *Chem. Rev.*, **114**, 1783 (2014)
398. M.Crespo-Quesada, F.Cárdenas-Lizana, A.-L.Dessimoz, L.Kiwi-Minsker. *ACS Catal.*, **2**, 1773 (2012)
399. G.Vilé, N.Almora-Barrios, S.Mitchell, N.López, J.Pérez-Ramírez. *Chem. – Eur. J.*, **20**, 5926 (2014)
400. V.D.Stytsenko, D.P.Mel'nikov. *Russ. J. Phys. Chem. A*, **90**, 932 (2016)
401. C.Moreno-Marrodan, F.Liguori, P.Barbaro. *Beilstein J. Org. Chem.*, **13**, 734 (2017)
402. C.Louis, L.Delannoy. *Adv. Catal.*, **64**, 1 (2019)
403. L.Zhang, M.Zhou, A.Wang, T.Zhang. *Chem. Rev.*, **120**, 683 (2020)
404. J.A.Delgado, C.Godard. In *Recent Advances in Nanoparticle Catalysis*. (Eds P.W.N.M.van Leeuwen, C.Claver). (Cham: Springer, 2020). P. 303
405. S.A.Nikolaev, L.N.Zanaveskin, V.V.Smirnov, V.A.Averyanov, K.L.Zanaveskin. *Russ. Chem. Rev.*, **78**, 231 (2009)
406. A.J.McCue, J.A.Anderson. *Front. Chem. Sci. Eng.*, **9**, 142 (2015)
407. M.Takht Ravanchi, S.Sahebdelfar, S.Komeili. *Rev. Chem. Eng.*, **34**, 215 (2018)
408. D.V.Glyzdova, N.S.Smirnova, D.A.Shlyapin, P.G.Tsyrul'nikov. *Russ. J. Gen. Chem.*, **90**, 1120 (2020)
409. E.Joannet, C.Horny, L.Kiwi-Minsker, A.Renken. *Chem. Eng. Sci.*, **57**, 3453 (2002)
410. E.V.Pyatnitsyna, M.M.El'chaninov, A.P.Savost'yanov. *Russ. J. Appl. Chem.*, **79**, 89 (2006)
411. C.V.Rode. *J. Jpn. Petrol. Inst.*, **51**, 119 (2008)
412. Patent CN 110586081 (2019)
413. P.T.Witte, S.Boland, F.Kirby, R.van Maanen, B.F.Bleeker, D.A.M.de Winter, J.A.Post, J.W.Geus, P.H.Berben. *ChemCatChem*, **5**, 582 (2013)
414. Patent WO 2009/096783 (2009)
415. Patent US 10258967 (2019)
416. A.D.Benavidez, P.D.Burton, J.L.Nogales, A.R.Jenkins, S.A.Ivanov, J.T.Miller, A.M.Karim, A.K.Datye. *Appl. Catal., A*, **482**, 108 (2014)
417. S.Domínguez-Domínguez, Á.Berenguer-Murcia, B.K.Pradhan, Á.Linares-Solano, D.Cazorla-Amorós. *J. Phys. Chem. C*, **112**, 3827 (2008)
418. A.S.Berenblyum, H.A.Al-Wadhaf, E.A.Katsman. *Petrol. Chem.*, **55**, 118 (2015)
419. T.Yoshii, D.Umemoto, Y.Kuwahara, K.Mori, H.Yamashita. *ACS Appl. Mater. Interfaces*, **11**, 37708 (2019)
420. Z.-S.Wang, C.-L.Yang, S.-L.Xu, H.Nan, S.-C.Shen, H.-W.Liang. *Inorg. Chem.*, **59**, 5694 (2020)
421. M.Zhao. *Chem. – Asian J.*, **11**, 461 (2016)
422. M.Zhao, Y.Ji, M.Wang, N.Zhong, Z.Kang, N.Asao, W.-J.Jiang, Q.Chen. *ACS Appl. Mater. Interfaces*, **9**, 34804 (2017)
423. M.Iqbal, Y.V.Kaneti, J.Kim, B.Yuliarto, Y.-M.Kang, Y.Bando, Y.Sugahara, Y.Yamauchi. *Small*, **15**, 1804378 (2019)
424. S.Mitchell, R.Qin, N.Zheng, J.Pérez-Ramírez. *Nat. Nanotechnol.*, **16**, 129 (2021)
425. T.G.Nikiforova, Yu.V.Kabeneva, O.A.Runova. *Russ. J. Appl. Chem.*, **83**, 1001 (2010)
426. P.Weerachawanasak, O.Mekasuwandumrong, M.Arai, S.-I.Fujita, P.Praserthdam, J.Panpranot. *J. Catal.*, **262**, 199 (2009)
427. P.V.Markov, I.S.Mashkovsky, G.O.Bragina, J.Wärnå, E.Yu.Gerasimov, V.I.Bukhtiyarov, A.Yu.Stakheev, D.Yu.Murzin. *Chem. Eng. J.*, **358**, 520 (2019)
428. T.Yoshii, K.Nakatsuka, Y.Kuwahara, K.Mori, H.Yamashita. *RSC Adv.*, **7**, 22294 (2017)
429. N.Krishnankutty, M.A.Vannice. *Mater. Res. Soc. Symp. Proc.*, **368**, 81 (1994)
430. N.Krishnankutty, M.A.Vannice. *J. Catal.*, **155**, 327 (1995)
431. A.Garcia-Ortiz, J.D.Vidal, S.Iborra, M.J.Climent, J.Cored, D.Ruano, V.Pérez-Dieste, P.Concepción, A.Corma. *J. Catal.*, **389**, 706 (2020)
432. Y.Cao, S.Mao, M.Li, Y.Chen, Y.Wang. *ACS Catal.*, **7**, 8090 (2017)
433. M.P.Wiesenfeldt, Z.Nairoukh, T.Dalton, F.Glorius. *Angew. Chem., Int. Ed.*, **58**, 10460 (2019)
434. A.S.Budrian, F.G.Kokoulin, V.I.Ovchinnikov, V.R.Ruchinskii, M.S.Furman, E.I.Chechik. *Proizvodstvo Kaprolaktama. (Caprolactam Production)*. (Moscow: Khimiya, 1977)
435. M.T.Musser. *Ullmann's Encyclopedia of Industrial Chemistry*. (Weinheim: Wiley-VCH, 2012)
436. X.Kong, Y.Gong, S.Mao, Y.Wang. *ChemNanoMat*, **4**, 432 (2018)
437. J.Tinge, M.Groothaert, H.op het Veld, J.Ritz, H.Fuchs, H.Kieczka, W.C.Moran. In *Ullmann's Encyclopedia of Industrial Chemistry*. (Weinheim: Wiley-VCH, 2018)
438. K.S.Hayes. *Appl. Catal., A*, **221**, 187 (2001)
439. P.Roose, K.Eller, E.Henkes, R.Rossbacher, H.Höke. In *Ullmann's Encyclopedia of Industrial Chemistry*. (Weinheim: Wiley-VCH, 2015)
440. J.Zhong, J.Chen, L.Chen. *Catal. Sci. Technol.*, **4**, 3555 (2014)
441. Y.Wei, X.Zeng. *Synlett*, **27**, 650 (2016)
442. Patent DE 2936362 (1981)
443. P.-H.Jen, Y.-H.Hsu, S.D.Lin. *Catal. Today*, **123**, 133 (2007)
444. A.Pei, L.Ruan, J.Liao, H.Zhang, J.Wang, K.Yang, Z.Liu, L.Zhu, B.H.Chen. *New J. Chem.*, **43**, 17306 (2019)
445. J.Chen, W.Zhang, L.Chen, L.Ma, H.Gao, T.Wang. *ChemPlusChem*, **78**, 142 (2013)

446. C.R.Lee, J.S.Yoon, Y.-W.Suh, J.-W.Choi, J.-M.Ha, D.J.Suh, Y.-K.Park. *Catal. Commun.*, **17**, 54 (2012)
447. Zh.A.Boeva, V.G.Sergeyev. *Polymer Sci., Ser. C*, **56**, 144 (2014)
448. E.Eskandari, M.Kosari, M.H.D.A.Farahani, N.D.Khiavi, M.Saeedikhani, R.Katal, M.Zarinejad. *Sep. Purif. Technol.*, **231**, 115901 (2020)
449. A.Yu.Stakheev, I.S.Mashkovskii, G.N.Baeva, N.S.Telegina. *Russ. J. Gen. Chem.*, **80**, 618 (2010)
450. N.Krishnankutty, M.A.Vannice. *J. Catal.*, **155**, 312 (1995)
451. N.Krishnankutty, J.Li, M.A.Vannice. *Appl. Catal., A*, **173**, 137 (1998)
452. B.Pawelec, R.Mariscal, R.M.Navarro, S.van Bokhorst, S.Rojas, J.L.G.Fierro. *Appl. Catal., A*, **225**, 223 (2002)
453. J.Yang, Y.Fan, Z.-L.Li, Z.Peng, J.-H.Yang, B.Liu, Z.Liu. *Mol. Catal.*, **492**, 110992 (2020)
454. P.Mäki-Arvela, J.Hájek, T.Salmi, D.Yu.Murzin. *Appl. Catal., A*, **292**, 1 (2005)
455. N.Steinfeldt, K.Junge. In *Catalytic Reduction in Organic Synthesis*. Vol. 2. (Ed. J.G.de Vries). (Stuttgart: Thieme, 2018). P. 7
456. H.Surburg, J.Panten. *Common Fragrance and Flavor Materials. Preparation, Properties and Uses*. (Weinheim: Wiley-VCH, 2016)
457. F.Brühne, E.Wright. In *Ullmann's Encyclopedia of Industrial Chemistry*. Vol. 5. (Weinheim: Wiley-VCH, 2012). P. 357
458. J.T.Bhanushali, I.Kainthla, R.S.Keri, B.M.Nagaraja. *ChemistrySelect*, **1**, 3839 (2016)
459. Y.Yuan, S.Yao, M.Wang, S.Lou, N.Yan. *Curr. Org. Chem.*, **17**, 400 (2013)
460. X.Wang, X.Liang, P.Geng, Q.Li. *ACS Catal.*, **10**, 2395 (2020)
461. X.Lan, T.Wang. *ACS Catal.*, **10**, 2764 (2020)
462. M.Luneau, J.S.Lim, D.A.Patel, E.C.H.Sykes, C.M.Friend, P.Sautet. *Chem. Rev.*, **120**, 12834 (2020)
463. I.F.Bel'skii, V.M.Shostakovskii. *Kataliz v Khimii Furana. (Catalysis in Furan Chemistry)*. (Moscow: Nauka, 1972)
464. *Kontaktnye Reaktsii Furanovykh Soedinenii. (Contact Reactions of Furan Compounds)*. (Ed. M.V.Shimanskaya). (Riga: Zinatne, 1985)
465. R.Mariscal, P.Maireles-Torres, M.Ojeda, I.Sádaba, M.López Granados. *Energy Environ Sci.*, **9**, 1144 (2016)
466. X.Li, P.Jia, T.Wang. *ACS Catal.*, **6**, 7621 (2016)
467. S.Chen, R.Wojcieszak, F.Dumeignil, E.Marceau, S.Royer. *Chem. Rev.*, **118**, 11023 (2018)
468. Y.Wang, D.Zhao, D.Rodríguez-Padrón, C.Len. *Catalysts*, **9**, 796 (2019)
469. R.M.Mironenko, O.B.Belskaya, A.V.Lavrenov, V.A.Likholobov. *Kinet. Catal.*, **59**, 339 (2018)
470. R.M.Mironenko, V.P.Talsi, T.I.Gulyaeva, M.V.Trenikhin, O.B.Belskaya. *React. Kinet. Mech. Catal.*, **126**, 811 (2019)
471. R.M.Mironenko, O.B.Belskaya, V.P.Talsi, V.A.Likholobov. *J. Catal.*, **389**, 721 (2020)
472. H.Siegel, M.Eggersdorfer. In *Ullmann's Encyclopedia of Industrial Chemistry*. Vol. 20. (Weinheim: Wiley-VCH, 2012). P. 187
473. T.A.Unger. *Pesticide Synthesis Handbook*. (Park Ridge, N.J.: Noyes Publications, 1996)
474. A.Kleemann, J.Engel, B.Kutscher, D.Reichert. *Pharmaceutical Substances: Syntheses, Patents and Applications of the Most Relevant AIPs*. (Stuttgart: Thieme, 2009)
475. O.B.Belskaya, R.M.Mironenko, V.A.Likholobov. *Theor. Exp. Chem.*, **48**, 381 (2013)
476. R.M.Mironenko, O.B.Belskaya, T.I.Gulyaeva, M.V.Trenikhin, A.I.Nizovskii, A.V.Kalinkin, V.I.Bukhtiyarov, A.V.Lavrenov, V.A.Likholobov. *Catal. Today*, **279**, 2 (2017)
477. T.Harada, S.Ikeda, M.Miyazaki, T.Sakata, H.Mori, M.Matsumura. *J. Mol. Catal. A: Chem.*, **268**, 59 (2007)
478. T.Szumełda, A.Drelinkiewicz, R.Kosydar, J.Gurgul. *Appl. Catal., A*, **487**, 1 (2014)
479. M.Hu, L.Jin, Y.Zhu, L.Zhang, X.Lu, P.Kerns, X.Su, S.Cao, P.Gao, S.L.Suib, B.Liu, J.He. *Appl. Catal., B*, **264**, 118553 (2020)
480. R.M.Mironenko, O.B.Belskaya, T.I.Gulyaeva, A.I.Nizovskii, A.V.Kalinkin, V.I.Bukhtiyarov, A.V.Lavrenov, V.A.Likholobov. *Catal. Today*, **249**, 145 (2015)
481. P.M.Mironenko, O.B.Belskaya, A.V.Lavrenov, V.A.Likholobov. *Chem. Sustain. Dev.,* **23**, 645 (2015)
482. R.M.Mironenko, O.B.Belskaya. *AIP Conf. Proc.*, **2141**, 020010 (2019)
483. T.-J.Zhao, W.-J.Feng, J.-J.Zhang, B.Zhang, Y.-X.Liu, Y.-X.Lin, H.-H.Wang, H.Su, X.-H.Li, J.-S.Chen. *Appl. Catal., B*, **238**, 404 (2018)
484. R.Kosydar, D.Duraczyńska, J.Gurgul, J.Kryściak-Czerwenka, A.Drelinkiewicz. *React. Kinet. Mech. Catal.*, **126**, 417 (2019)
485. L.Ruan, H.Zhang, M.Zhou, L.Zhu, A.Pei, J.Wang, K.Yang, C.Zhang, S.Xiao, B.H.Chen. *Mol. Catal.*, **480**, 110639 (2020)
486. J.Lee, J.Woo, C.Nguyen-Huy, M.S.Lee, S.H.Joo, K.An. *Catal. Today*, **350**, 71 (2020)
487. F.Jiang, J.Cai, B.Liu, Y.Xu, X.Liu. *RSC Adv.*, **6**, 75541 (2016)
488. L.J.Durndell, G.Zou, W.Shangguan, A.F.Lee, K.Wilson. *ChemCatChem*, **11**, 3927 (2019)
489. K.Noweck, W.Grafahrend. In *Ullmann's Encyclopedia of Industrial Chemistry*. Vol. 14. (Weinheim: Wiley-VCH, 2012). P. 117
490. A.S.Berenblyum, V.Ya.Danyushevsky, P.S.Kuznetsov, E.A.Katsman, R.S.Shamsiev. *Petrol. Chem.*, **56**, 663 (2016)
491. M.A.Sánchez, G.C.Torres, V.A.Mazzieri, C.L.Pieck. *J. Chem. Technol. Biotechnol.*, **92**, 27 (2017)
492. J.Zhang, L.Jiang, H.Huang, S.Tao, H.Zhang, X.Xiao, J.Fang. *IOP Conf. Ser. Earth Environ. Sci.*, **571**, 012136 (2020)
493. A.M.Ruppert, K.Weinberg, R.Palkovits. *Angew. Chem., Int. Ed.*, **51**, 2564 (2012)
494. S.De, B.Saha, R.Luque. *Biores. Technol.*, **178**, 108 (2015)
495. X.Lia, G.Chen, C.Liu, W.Ma, B.Yan, J.Zhang. *Renew. Sustain. Energy Rev.*, **71**, 296 (2017)
496. M.Ameen, M.T.Azizan, S.Yusup, A.Ramli, M.Yasir. *Renew. Sustain. Energy Rev.*, **80**, 1072 (2017)
497. S.Kim, E.E.Kwon, Y.T.Kim, S.Jung, H.J.Kim, G.W.Huber, J.Lee. *Green Chem.*, **21**, 3715 (2019)
498. W.Jin, L.Pastor-Pérez, D.Shen, A.Sepúlveda-Escribano, S.Gu, T.Ramirez Reina. *ChemCatChem*, **11**, 924 (2019)
499. A.S.Berenblyum, V.Ya.Danyushevsky, E.A.Katsman. *Kinet. Catal.*, **60**, 381 (2019)
500. A.S.Ouedraogo, P.R.Bhoi. *J. Cleaner Prod.*, **253**, 119957 (2020)
501. V.Sharma, T.Getahun, M.Verma, A.Villa, N.Gupta. *Renew. Sustain. Energy Rev.*, **133**, 110280 (2020)

502. *Chemical Catalysts for Biomass Upgrading*. (Eds M.Crocker, E.Santillan-Jimenez). (Weinheim: Wiley-VCH, 2020)
503. L.N.Zanaveskin, V.A.Aver'yanov, Yu.A.Treger. *Russ. Chem. Rev.*, **65**, 617 (1996)
504. V.A.Yakovlev, V.I.Simagina, S.N.Trukhan, V.A.Likholobov. *Kinet. Catal.*, **41**, 25 (2000)
505. E.Lokteva, E.Golubina, V.Likholobov, V.Lunin. In *Chemistry Beyond Chlorine*. (Eds P.Tundo, L.-N.He, E.Lokteva, C.Mota). (Cham: Springer, 2016). P. 559
506. M.R.Flid, L.M.Kartashov, Yu.A.Treger. *Catalysts*, **10**, 216 (2020)
507. K.Sun, T.C.Schulz, S.T.Thompson, H.H.Lamb. *Catal. Today*, **269**, 93 (2016)
508. K.Sun. PhD Thesis. North Carolina State University, Raleigh, 2014
509. Q.Wang, H.Cheng, R.Liu, J.Hao, Y.Yu, F.Zhao. *Catal. Today*, **148**, 368 (2009)
510. Y.Amada, N.Ota, M.Tamura, Y.Nakagawa, K.Tomishige. *ChemSusChem*, **7**, 2185 (2014)
511. Patent US 2015/0298101 (2015)
512. S.A.Yakukhnov, V.P.Ananikov. *Adv. Synth. Catal.*, **361**, 4781 (2019)
513. S.A.Yakukhnov. Candidate Thesis in Chemical Sciences, Institute of Organic Chemistry, Russian Academy of Sciences, Moscow, 2019
514. J.A.Baeza, L.Calvo, J.J.Rodriguez, M.A.Gilarranz. *Chem. Eng. J.*, **294**, 40 (2016)
515. J.A.Baeza, L.Calvo, N.Alonso-Morales, F.Heras, S.Eser, J.J.Rodriguez, M.A.Gilarranz. *Chem. Eng. Sci.*, **176**, 400 (2018)
516. J.A.Baeza, L.Calvo, M.A.Gilarranz, A.F.Mohedano, J.A.Casas, J.J.Rodriguez. *J. Catal.*, **293**, 85 (2012)
517. D.B.Bagal, B.M.Bhanage. *Adv. Synth. Catal.*, **357**, 883 (2015)
518. D.B.Bagal, B.M.Bhanage. In *Catalytic Reduction in Organic Synthesis*. Vol. 2. (Ed. J.G.de Vries). (Stuttgart: Thieme, 2018). P. 375
519. J.Volf, J.Pašek. *Stud. Surf. Sci. Catal.*, **27**, 105 (1986)
520. Yu.V.Popov, S.E.Latyshev, A.O.Panov, M.Yu.Pletneva. *Izv. Volgogr. GTU*, (11), 27 (2017)
521. K.Lévay, L.Hegedűs. *Period. Polytech. Chem. Eng.*, **62**, 476 (2018)
522. K.Lévay, L.Hegedűs. *Curr. Org. Chem.*, **23**, 1881 (2019)
523. Y.Monguchi, M.Mizuno, T.Ichikawa, Y.Fujita, E.Murakami, T.Hattori, T.Maegawa, Y.Sawama, H.Sajiki. *J. Org. Chem.*, **82**, 10939 (2017)
524. S.V.Sysolyatin, A.A.Lobanova, Y.T.Chernikova, G.V.Sakovich. *Russ. Chem. Rev.*, **74**, 757 (2005)
525. D.S.Viswanath, T.K.Ghosh, V.M.Boddu. *Emerging Energetic Materials: Synthesis, Physicochemical, and Detonation Properties*. (Dordrecht: Springer, 2018)
526. Patent US 2013/0177839 (2013)
527. Patent US 5449780 (1995)
528. J.R.Kosak. In *Catalysis of Organic Reactions*. (Ed. R.E.Malz Jr.). (New York: Marcel Dekker, 1996). P. 31
529. B.E.Berkman. *Promyshlennyi Sintez Aromaticheskikh Nitrosoedinenii iAminov. (Industrial Synthesis of Aromatic Nitro Compounds and Amines*). (Moscow: Khimiya, 1964)
530. V.L.Zbarskii, V.F.Zhilin. *Toluol i ego Nitroproizvodnye. (Toluene and its Nitro Derivatives*). (Moscow: Editorial URSS, 2000)
531. H.-U.Blaser, H.Steiner, M.Studer. *ChemCatChem*, **1**, 210 (2009)
532. P.Lara, K.Philippot. *Catal. Sci. Technol.*, **4**, 2445 (2014)
533. H.Göksu, H.Sert, B.Kilbas, F.Sen. *Curr. Org. Chem.*, **21**, 794 (2017)
534. M.Orlandi, D.Brenna, R.Harms, S.Jost, M.Benaglia. *Org. Process Res. Dev.*, **22**, 430 (2018)
535. J.Song, Z.-F.Huang, L.Pan, K.Li, X.Zhang, L.Wang, J.-J.Zou. *Appl. Catal., B*, **227**, 386 (2018)
536. P.Puylaert, A.Savini, S.Hinze. In *Catalytic Reduction in Organic Synthesis*. Vol. 2. (Ed. J.G.de Vries). (Stuttgart: Thieme, 2018). P. 331
537. *Teoriya i Praktika Protsessov Zhidkofaznoi Gidrogenizatsii Zameshchennykh Nitrobenzolov. (Theory and Practice of Processes of Liquid-Phase Hydrogenation of Substituted Nitrobenzenes)*. (Ed. O.I.Koifman). (Moscow: KRASAND, 2016)
538. S.A.Lawrence. *Amines: Synthesis, Properties and Applications*. (Cambridge: Cambridge University Press, 2004)
539. A.S.Travis. In *The Chemistry of Anilines. Part 1*. (Ed. Z.Rappoport). (Chichester: Wiley, 2007). P. 715
540. F.Haber. *Z. Elektrochem. Angew. Phys. Chem.*, **4**, 506 (1898)
541. P.Rubio-Marqués, J.C.Hernández-Garrido, A.Leyva-Pérez, A.Corma. *Chem. Commun.*, **50**, 1645 (2014)
542. Patent ES 2525958 (2015)
543. L.Pietrobon, L.Ronchin, C.Sadraoui, R.Pontello, C.Tosetto, A.Vavasori. *Appl. Catal., A*, **598**, 117570 (2020)
544. O.B.Belskaya, V.P.Talsi, R.M.Mironenko, V.A.Rodionov, S.V.Sysolyatin, V.A.Likholobov. *J. Mol. Catal. A: Chem.*, **420**, 190 (2016)
545. R.M.Mironenko, O.B.Belskaya, V.P.Talzi, V.A.Rodionov, S.V.Sysolyatin, V.A.Likholobov. *Russ. Chem. Bull., Int. Ed.*, **65**, 1535 (2016)
546. O.B.Belskaya, R.M.Mironenko, V.P.Talsi, V.A.Rodionov, T.I.Gulyaeva, S.V.Sysolyatin, V.A.Likholobov. *Catal. Today*, **301**, 258 (2018)
547. J.Lehmann. In *Methoden der Organischen Chemie (Houben-Weyl). Band IV/1c. Reduktion. Teil I.* (Hrsg. H.Kropf). (Stuttgart: Thieme, 1980). S. 482
548. S.S.Novikov, G.A.Shvekhgeimer, V.V.Sevost'yanov, V.A.Shlyapochnikov. *Khimiya Alifaticheskikh i Atsiklicheskikh Nitrosoedinenii. (Chemistry of Aliphatic and Acyclic Nitro Compounds)*. (Moscow: Khimiya, 1974)
549. T.Kahl, K.-W.Schröder, F.R.Lawrence, W.J.Marshall, H.Höke, R.Jäckh. In *Ullmann's Encyclopedia of Industrial Chemistry*. Vol. 3. (Weinheim: Wiley-VCH, 2012). P. 465
550. Patent US 4185036 (1980)
551. Patent US 5304525 (1994)
552. Patent US 3457187 (1969)
553. Patent US 0077504 (2002)
554. Patent EP 1192989 (2002)
555. P.Rodriguez, F.Simescu-Lazar, V.Meille, T.Bah, S.Pallier, I.Fournel. *Appl. Catal., A*, **427**–**428**, 66 (2012)
556. Patent US 3265636 (1966)
557. Patent US 3328465 (1967)
558. Patent US 8658560 (2014)
559. PRB Author's Certificate 348321 (1983)
560. Patent JP 54046767 (1979)
561. R.Rusev, S.Pendev, K.Gramatikov. *Khim. Ind. (Sofiya)*, **55** (2), 61 (1983) [*Chem. Abstr.*, **99**, 175278 (1983)]
562. Patent US 2857337 (1958)
563. Patent US 3127356 (1964)
564. A.Sałek. *Chemia Stosowana*, **25**, 53 (1981) [*Chem. Abstr.*, **95**, 149609 (1981)]

565. D.J.Suh, T.-J.Park, S.-K.Ihm. *Ind. Eng. Chem. Res.*, **31**, 1849 (1992)
566. D.J.Suh, T.-J.Park, S.-K.Ihm. *Carbon*, **31**, 427 (1993)
567. E.Auer, M.Gross, P.Panster, K.Takemoto. *Catal. Today*, **65**, 31 (2001)
568. Patent WO 03/039743 (2003)
569. Patent CN 102952022 (2013)
570. R.A.Smiley. In *Ullmann's Encyclopedia of Industrial Chemistry*. Vol. 26. (Weinheim: Wiley-VCH, 2012). P. 617
571. P.A.Simonov, A.V.Romanenko, V.A.Likholobov. *Solid Fuel Chem.*, **48**, 364 (2014)
572. G.Speranza. *C – J. Carbon Res.*, **5**, 84 (2019)
573. A.Bianco, Y.Chen, E.Frackowiak, M.Holzinger, N.Koratkar, V.Meunier, S.Mikhailovsky, M.Strano, J.M.D.Tascon, M.Terrones. *Carbon*, **161**, 373 (2020)
574. D.Boufades, S.H.N.Mesdour, A.Moussiden, H.Benmebrouka, C.Herold, O.Kaddour. *Fullerenes Nanotubes Carbon Nanostruct.*, **28**, 716 (2020)
575. W.Kiciński, S.Dyjak. *Carbon*, **168**, 748 (2020)
576. M.R.Kholghy, G.A.Kelesidis. *Combust. Flame*, **227**, 456 (2021)
577. G.Patiño-Guillén, A.Arceta-Lozano, J.AFalcón-Montes, E.García-Díaz, J.N.DíazdeLeón, R.Vazquez-Duhalt, G.Gao, M.Á.Méndez-Rojas, J.Campos-Delgado. *Nanotechnology*, **32**, 085602 (2021)
578. M.Salamanca, M.L.Botero, J.W.Martin, J.A.H.Dreyer, J.Akroyd, M.Kraft. *Combust. Flame*, **219**, 1 (2020)
579. M.Wang, G.Sharma, H.Zhang, X.You, P.Biswas. *Fuel*, **279**, 118511 (2020)
580. T.Ishii, J.Ozaki. *Carbon*, **161**, 343 (2020)
581. J.Seebeck, P.Schiffels, S.Schweizer, J.-R.Hill, R.H.Meißner. *J. Phys. Chem. C*, **124**, 5515 (2020)
582. J.Zhu, S.Mu. *Adv. Funct. Mater.*, **30**, 2001097 (2020)
583. S.Khodabakhshi, S.Kiani, Y.Niu, A.O.White, W.Suwaileh, R.E.Palmer, A.R.Barron, E.Andreoli. *Carbon*, **171**, 426 (2021)
584. H.Chu, Y.Ya, X.Nie, F.Qiao, J.E. *Combust. Flame*, **225**, 120 (2021)
585. C.Dong, Y.Li, D.Cheng, M.Zhang, J.Liu, Y.-G.Wang, D.Xiao, D.Ma. *ACS Catal.*, **10**, 11011 (2020)
586. S.F.Yuk, G.Collinge, M.-T.Nguyen, M.-S.Lee, V.-A.Glezakou, R.Rousseau. In *Advanced Heterogeneous Catalysts*. Vol. 2. (Eds P.Sudarsanam, L.Singh). (Washington, DC: American Chemical Society, 2020). P. 1
587. Y.Du, H.Sheng, D.Astruc, M.Zhu. *Chem. Rev.*, **120**, 526 (2020)
588. R.Nandan, G.K.Goswami, K.K.Nanda. *ACS Appl. Mater. Interfaces*, **12**, 53749 (2020)
589. L.Liu, A.Corma. *Trends Chem.*, **2**, 383 (2020)
590. M.B.Gawande, P.Fornasiero, R.Zbořil. *ACS Catal.*, **10**, 2231 (2020)
591. Q.Wang, L.Zhou, Q.Chen, M.Mao, W.Jiang, Y.Long, G.Fan. *J. Hazard. Mater.*, **408**, 124456 (2021)
592. D.A.Boiko, E.O.Pentsak, V.A.Cherepanova, V.P.Ananikov. *Sci. Data*, **7**, 101 (2020)
593. C.Zhang, G.Yang, H.Jiang, Y.Liu, R.Chen, W.Xing. *Chinese J. Chem. Eng.*, **28**, 2600 (2020)
594. E.Pérez-Mayoral, I.Matos, M.Bernardo, M.Ventura, I.M.Fonseca. *Catalysts*, **10**, 1407 (2020)
595. M.A.Andrade, L.M.D.R.S.Martins. *Processes*, **8**, 1172 (2020)
596. P.Udomsap, A.Eiad-Ua, S.-Y.Chen, T.Mochizuki, N.Chollacoop, Y.Yoshimura, M.Nishi, H.Tateno, H.Takagi. *Int. J. Mol. Sci.*, **22**, 1256 (2021)
597. M.Aksoy, H.Kilic, B.Nişancı, Ö.Metin. *Inorg. Chem. Front.*, **8**, 499 (2021)
598. J.W.Martin, M.Salamanca, M.Kraft. *Prog. Energy Combust. Sci.*, **88**, 100956 (2022)
599. F.Liu, Y.Cheng, J.Tan, J.Li, H.Cheng, H.Hu, C.Du, S.Zhao, Y.Yan, M.Liu. *Front. Chem.*, **9**, 668336 (2021)
600. D.Saini, Gunture, J.Kaushik, R.Aggarwal, K.M.Tripathi, S.K.Sonkar. *ACS Appl. Nano Mater.*, **4**, 12825 (2021)
601. M.Tipplook, G.Panomsuwan, Y.Muta, N.Saito. *ACS Appl. Energy Mater.*, **4**, 5606 (2021)
602. E.Pérez Mayoral, I.Matos, M.Bernardo, C.Durán-Valle, I.Fonseca. In *Emerging Carbon Materials for Catalysis*. (Ed. S.Sadjadi). (Amsterdam: Elsevier, 2021). P. 299
603. E.García-Bordejé. In *Heterogeneous Catalysts: Advanced Design, Characterization, and Applications*.Vol. 1. (Eds W.Y.Teoh, A.Urakawa, Y.H.Ng, P.Sit). (Weinheim: Wiley-VCH, 2021). P. 57
604. S.Malik, S.Marchesan. *Nanomater.*, **11**, 2728 (2021)
605. C.Rivera-Cárcamo, I.C.Gerber, I.del Rosal, B.Guicheret, R.CastroContreras, L.Vanoye, A.Favre-Réguillon, B.F.Machado, J.Audevard, C.deBellefon, R.Philippe, P.Serp. *Catal. Sci. Technol.*, **11**, 984 (2021)
606. X.Liu, G.Lan, Z.Li, L.Qian, J.Liu, Y.Li. *Chinese J. Catal.*, **42**, 694 (2021)
607. L.R.Sassykova, A.R.Sassykova, B.T.Dossumova, M.S.Ilmuratova, N.E.Maximov, A.Y.Yerzhanov, A.A.Batyrbayeva, A.T.Raiyssov, Sh.N.Kubekova, S.M.Bazilbayev, T.S.Abildin. *RASĀYAN J. Chem.*, **14**, 1795 (2021)
608. M.A.Ali, A.Abutaleb. *Catal. Lett.*, (in the press); Published online 10 July 2021; https://10.1007/s10562-021-03714-5
609. M.Li, S.Chen, Q.Jiang, Q.Chen, X.Wang, Y.Yan, J.Liu, C.Lv, W.Ding, X.Guo. *ACS Catal.*, **11**, 3026 (2021)
610. J.Wang, K.Mu, X.Zhao, D.Luo, X.Yu, W.Li, J.Chu, J.Yang, Q.Yang. *Catalysts*, **11**, 888 (2021)
611. S.V.Belenov, V.E.Guterman, L.D.Popov, A.T.Kozakov, A.V.Nikolsky, M.V.Danilenko, O.I.Safronenko, A.Yu.Nikulin. *J. Solid State Electrochem.*, **25**, 789 (2021)
612. Y.Bu, Z.Hu, H.Li, S.Hu. *Mater. Lett.*, **305**, 130800 (2021)
613. M.Lüsi, H.Erikson, A.Treshchalov, M.Rähn, M.Merisalu, A.Kikas, V.Kisand, V.Sammelselg, K.Tammeveski. *Nanotechnol.*, **32**, 035401 (2021)
614. H.Doan, T.Morais, N.Borchtchoukova, Y.Wijsboom, R.Sharabi, M.Chatenet, G.Finkelshtain. *Appl. Catal., B*, **301**, 120811 (2022)
615. Y.Xue, Z.Lei, W.Zheng, W.Duan, L.Zhu, Z.Yan, C.Feng. *J. Environ. Chem. Eng.*, **9**, 105995 (2021)
616. D.T.González, A.Marí, J.A.Baeza, L.Calvo, M.A.Gilarranz. *J. Environ. Chem. Eng.*, **9**, 106419 (2021)
617. R.M.Mironenko, E.R.Saybulina, M.V.Trenikhin, R.R.Izmailov, K.A.Lotsman, K.S.Rodygin, V.P.Ananikov. *ChemCatChem*, **13**, 3656 (2021)
618. A.A.Khouya, H.Ba, W.Baaziz, J.-M.Nhut, A.Rossin, S.Zafeiratos, O.Ersen, G.Giambastiani, V.Ritleng, C.Pham-Huu. *ACS Appl. Nano Mater.*, **4**, 2265 (2021)
619. M.Jun, H.Yang, D.Kim, G.J.Bang, M.Kim, H.Jin, T.Kwon, H.Baik, J.-H.Sohn, Y.Jung, H.Kim, K.Lee. *Small Methods*, **5**, 2100400 (2021)
620. R.M.Mironenko, O.B.Belskaya, V.A.Likholobov. *Izv. Akad. Nauk, Ser. Khim.*, 64 (2022)

621. Á.Prekob, G.Muránszky, M.Szőri, G.Karacs, F.Kristály, T.Ferenczi, B.Fiser, B.Viskolcz, L.Vanyorek. *Nanotechnol.*, **32**, 425701 (2021)
622. F.Han, C.Hu, X.Zhang, C.Jing, T.Hu, X.Yang. *Compos. Commun.*, **23**, 100580 (2021)
623. X.Zhang, Q.Gu, Y.Ma, Q.Guan, R.Jin, H.Wang, B.Yang, J.Lu. *J. Catal.*, **400**, 173 (2021)